Modelling the hydrology of the Greenland ice sheet

Mehmet R. Karatay

Doctor of Philosophy

University of Edinburgh
School of GeoSciences

2010

Declaration

I declare that this thesis is entirely my own work, except where otherwise acknowledged. This work has never been submitted, in part or in whole, for another degree or professional qualification.

Mehmet R. Karatay
August 2010

Abstract

This thesis aims to better understand the relationships between basal water pressure, friction, and sliding mechanisms at ice sheet scales. In particular, it develops a new subglacial hydrology model (HYDRO) to explicitly predict water pressures in response to basal water production and water injection from the surface.

Recent research suggests that the Greenland ice sheet (GIS) is losing a substantial volume of ice through dynamic thinning. This process must be modelled to accurately assess the contribution of the GIS to sea-level rise in future warming scenarios. A key control on dynamic thinning is the presence of water at the ice-bed interface; Zwally et al. (2002) highlight the importance of supraglacial lakes' impact on basal ice dynamics, a process now confirmed by Das et al. (2008) and Shepherd et al. (2009).

Many studies focus on the effects of surface meltwater reaching the bed of the GIS but the underlying processes are often ignored. Geothermal, strain, and frictional melting, which evolves with basal hydrology, provide the background basal pressure profile that surface meltwater perturbates. Without understanding how these heat terms affect the background profile it is difficult to define basal boundary conditions in models and therefore difficult to model the dynamic response of the GIS to surface melting.

HYDRO tracks subglacial water pressures and the evolution of efficient drainage networks. Coupled with the existing 3D thermomechanical ice sheet model GLIMMER, model outputs include effective pressure N and the efficient hydraulic area. Defining frictional heat flux and basal traction as functions of N allow the modelling of seasonal dynamic response to randomly draining supraglacial lakes.

Key results are that frictional heat flux, as a function of N, caps potential runaway feedback mechanisms and that water converges in topographic troughs under Greenland's outlet glaciers. This leads to a background profile with low N under outlet glaciers. Therefore, outlet glaciers show a muted dynamic speedup to the seasonal surface signal reaching the bed. Land-terminating ice does not tend to have subglacial troughs and so has higher background N and consequently a larger seasonal response. This, coupled with effects of ice rheology, can explain the hitherto puzzling lack of observed seasonal velocity change on Jakobshavn Isbræ and other outlet glaciers.

Acknowledgements

Thanks to:
My supervisors Nick Hulton and Pete Nienow who came up with this project, supported my transition from pure physics to glaciology, and guided me with patience over the years. Their input was invaluable and if this thesis is worth anything this is purely due to them. I especially thank Nick for supporting me, and understanding me, when I did not feel like carrying on.

Sergei Zetsepin: for his guidance in developing the initial concept behind Hydro. He gifted me the idea of combining the conservation of mass and momentum to describe the unknown basal conditions of the Greenland ice sheet as physical conservation laws that must, in some form, hold. I also thank Sergei for our fascinating discussions about the history of science, which I wish we could have had more of.

Magnus Hagdon: for getting me started with Glimmer and for introducing me to Subversion. I cannot comprehend how I functioned without version control previously, either for writing or for coding. Steward Jamieson: for discussions, sharing of code and scripts, and for me borrowing the structure of my introduction from his thesis. Mark Naylor: for help with some difficult maths while debugging Hydro.

Gemma Richards, my fiancée: for putting up with what, at times, felt like an endless task and for the lack of support around the house, from my part, that this entailed. Also for our many discussions which helped me marshal my thoughts and ideas, her proofreading and other fiddly, last-minute contributions. My parents for their support, both emotionally and financially, throughout my university career. To Andy Hein, Kate Briggs and the many others who offered emotional support and encouragement through the years.

GeoSciences IT support: who go out of their way, without seeking recognition, to provide good infrastructure and excellent support. I've never seen an IT team that is as friendly, approachable, or willing to take time out of their day to deal with an obscure or trivial problem.

The open-source community: for developing software which I have come to rely on heavily, including: Glimmer, Kubuntu, LaTeX, Emacs, Subversion, The Gimp, Inkscape, ImageMagick, and the countless small programmes and scripts which make life easier.

This work makes use of the resources provided by the Edinburgh Compute and Data Facility (ECDF, `http://www.ecdf.ed.ac.uk`). The ECDF is partially supported by the eDIKT initiative (`http://www.edikt.org.uk`).

Contents

Figures

Tables

Symbols

Mathematical notation

Δ	Change in variable eg ΔT = change in temperature
δ	Small change in variable eg δT = small change in temperature
$\triangle$	Laplacian $\triangle = \boldsymbol{\nabla} \cdot \boldsymbol{\nabla}$
$\hat{\triangle}$	Dimensionless $\triangle$
$\boldsymbol{\nabla}$	Derivative operator $(\partial/\partial x, \partial/\partial y)$
$\hat{\boldsymbol{\nabla}}$	Dimensionless $\boldsymbol{\nabla}$
$\mathcal{F}^{(n)}$	n^{th} derivative operator
f	Arbitrary function
$\mathbb{Z}$	Set of integers
$\mathbb{R}$	Set of real numbers

Physical constants

η	1.787	Pa s	Dynamic viscosity of water
ρ_i	910	$\mathrm{kg\,m^{-3}}$	Ice density
ρ_w	1000	$\mathrm{kg\,m^{-3}}$	Water density
c_t	9.76×10^{-8}	$\mathrm{K\,Pa^{-1}}$	Temperature dependence on pressure
g	9.825	$\mathrm{m\,s^{-2}}$	Acceleration due to gravity at 70 °N
$\mathcal{H}$	335	$\mathrm{kJ\,kg^{-1}}$	Specific latent heat of fusion
k_{ice}	2009	$\mathrm{J\,kg^{-1}\ K^{-1}}$	Specific heat capacity of ice
k_{rock}	1000	$\mathrm{J\,kg^{-1}\ K^{-1}}$	Specific heat capacity of rock
R	8.314	$\mathrm{J\,mol^{-1}\,K^{-1}}$	Universal gas constant
$\mathcal{V}$	139×10^3 if $T_{\text{pmp}} \geqslant 263\,\text{K}$; 60×10^3 otherwise	$\mathrm{J\,mol^{-1}}$	Activation volume for creep

General variables

$\boldsymbol{\tau}$	Pa	Stress
φ	—	Day of the year expressed in radians from $0 \to 2\pi$
a	$\mathrm{m^2}$	Area
E_k	J	Kinetic energy
$_i$	—	Index in x direction
$\imath$	km	Step size in x direction
$_j$	—	Index in y direction
$\jmath$	km	Step size in y direction
$_k$	—	Index in time

continued

continued

l	—	Order of Taylor expansion
m	kg	Mass
$\mathcal{P}$	W	Power
Q	J	Energy
t	s	Time
$\hat{T}$	—	Dimensionless time
V	km^3	Volume
$\boldsymbol{v}$	$\mathrm{m\,a}^{-1}$	Velocity vector
$\bar{v}$	—	Relative velocity speedup
x	m	East-west model grid direction
X	—	Dimensionless variable x
y	m	North-south model grid direction
Y	—	Dimensionless variable y

Variables used by Glimmer and Hydro

h	m	Ice thickness
M	$\mathrm{mm\,a}^{-1}$	Melt rate
$\mathfrak{t}$	a	Time step

Hydro variables (basal hydrology)

α	—	Dimensionless aquifer adjustment parameter
κ	$\mathrm{m\,s}^{-1}$	Hydraulic conductivity of the bed, on a large scale
$\bar{\kappa}$	$\mathrm{m\,s}^{-1}$	Hydraulic conductivity scaling factor
$\dot{\kappa}$	—	Hydraulic conductivity spatially dependent component
μ	—	Coefficient of friction
$\mu_{\max}$	—	Maximum coefficient of friction at ice-bed interface
μ_0	—	Minimum, or residual, coefficient of friction at ice-bed interface
ϕ	a^{-1}	Source term of water
Φ	—	Dimensionless ϕ
ψ	—	Efficiency factor
ω	—	Surface to bed flux magnification factor
c_T	Pa^{-1}	Compressibility of the aquifer
d	m	Depth of aquifer
d_p	m	Depth of surface pond
$d_{p\max}$	m	Maximum depth before surface pond must drain
$d_{p\min}$	m	Minimum depth before surface pond can drain
D	$\mathrm{m}^2\,\mathrm{s}^{-1}$	Diffusivity of bed
K	m^2	Hydraulic permeability
ℓ	m	Characteristic length
N	Pa	Effective pressure
$\bar{N}$	—	Normalised effective pressure
p	MPa	Pressure of water
p_e	MPa	Equilibrium pressure
p_{hs}	MPa	Hydrostatic pressure

continued

continued

$p_{hs\max}$	MPa	Maximum hydrostatic pressure
p_{ice}	MPa	Ice overburden pressure
p_{limit}	—	p_r at which the efficiency condition is triggered.
p_r	—	The ratio of water pressure over ice overburden pressure at the bed.
p_s	MPa	Maximum seasonal pressure
p_t	MPa	Total pressure
p_0	MPa	Datum pressure
p_1	MPa	Datum defined as hydrostatic pressure
p^*	MPa	Pressure due to Darcian flow of water through a porous medium
P	—	Dimensionless pressure
P_t	—	Dimensionless p_t
P^*	—	Dimensionless p^*
$\boldsymbol{q}$	$\mathrm{m\,s^{-1}}$	Water flux
$\mathcal{T}$	$\mathrm{m^2\ day^{-1}}$	Transmissivity of bed

Glimmer variables (Ice dynamics)

β	—	Frictional heat adjustment parameter
γ	—	Basal slipperiness adjustment parameter
$\dot{\boldsymbol{\epsilon}}$	$\mathrm{a^{-1}}$	Strain rate
θ_b	—	Bed gradient, $\tan(\Theta_b)$
θ_s	—	Surface ice gradient, $\tan(\Theta_s)$
Θ_b	Radians	Bed gradient
Θ_s	Radians	Surface ice gradient
λ	°N	Latitude
λ_0	°N	Base latitude used by Eis driver
Λ	°W	Longitude
$\boldsymbol{\tau}_b$	Pa	Driving stress at the bed
a_i	—	Eis driver coefficients (also a_0, a_1, and a_2)
A	$\mathrm{Pa^{-3}\,s^{-1}}$	Flow parameter
A_0	$\mathrm{Pa^{-3}\,s^{-1}}$	Flow constant
b	m	Bed elevation
B	$\mathrm{m\,a^{-1}}$	Surface mass balance
$\flat_i$	—	Eis driver coefficients (also $\flat_0$, $\flat_1$, and $\flat_2$)
F	N	Frictional force
$\mathfrak{f}$	N	Driving force
H	$\mathrm{W\,m^{-2}}$	Generic heat flux
H_f	$\mathrm{W\,m^{-2}}$	Frictional heat flux from sliding
H_g	$\mathrm{W\,m^{-2}}$	Geothermal heat flux
H_i	$\mathrm{W\,m^{-2}}$	Heat incoming
H_o	$\mathrm{W\,m^{-2}}$	Heat outgoing
H_s	$\mathrm{W\,m^{-2}}$	Strain heat flux
k	—	Vertical temperature profile adjustment parameter
$\mathcal{L}$	°C/100 m	Atmospheric lapse rate
n	—	Flow law exponent
$\mathcal{N}$	N	Normal force on bed

continued

continued

P_{rcp}	$\text{m}\,\text{a}^{-1}$	Precipitation
s	m	Surface elevation
s_{ELA}	m	ELA elevation
s_{max}	m	Maximum prescribed ELA elevation
s_0	m	Minimum surface elevation with no summer melt
s^*	m	Vertical distance above the ELA ($s - s_{\text{ELA}}$)
S_B	a^{-1}	Gradient of accumulation rate change
S_T	$^\circ\text{C}/100\,\text{m}$	Gradient of temperature rate change
t_s	$\text{m}\,\text{a}^{-1}\,\text{Pa}^{-1}$	Basal slipperiness (Basal traction in GLIMMER documentation)
$t_{s\text{max}}$	$\text{m}\,\text{a}^{-1}\,\text{Pa}^{-1}$	Maximum basal slipperiness
T	K	Temperature
T_b	K	Basal temperature
T_s	K	Surface temperature
T_{pmp}	K	Non-adjusted pressure melting point
T^*	K	Pressure adjusted temperature
$\boldsymbol{v}_b$	$\text{m}\,\text{s}^{-1}$	Basal sliding velocity
$\boldsymbol{v}_f$	$\text{m}\,\text{s}^{-1}$	Final velocity
$\boldsymbol{v}_i$	$\text{m}\,\text{s}^{-1}$	Initial velocity
w	$\text{m}\,\text{s}^{-1}$	Vertical ice speed
W	$\text{K}\,\text{s}^{-1}$	Strain heating rate
z	m	Depth below ice surface

Other specialized variables

$\mathcal{B}$	—	Free parameter of sliding in EISMINT set-up
Υ	—	Polarity of land-marine speedup. > 1 implies that land-terminating ice is faster than nearby marine-terminating ice.
$\bar{\Upsilon}$	—	The mean polarity of all cells in a transect.
$\mathcal{C}_F$	m	Surface contour above which the bed is frozen. One method of defining a frozen bed.
d_c	m	Crevasse depth
E	m	Radial distance from centre of ice circular ice sheet at which accumulation is zero
r	m	Radius of circular ice sheet
r_{ice}	m	Outside edge of ice sheet
r_0	m	Centre of ice sheet

Abbreviations

ASTER	Advanced Spaceborne Thermal Emission and Reflection Radiometer: remote sensing satellite instrument
BHPP	Background hydraulic pressure profile
DEM	Digital elevation model
EIS	Edinburgh ice sheet: an ELA based climate driver for GLIMMER
EISMINT	European Icesheet Model INiTive intercomparison experiment
ELA	Equilibrium line altitude
GCM	Global circulation model
GLIMMER	A community ice sheet model
GLIMMER-HYDRO	The coupled GLIMMER and HYDRO model
GLINT	A GCM based climate driver for GLIMMER
GPS	Global Positioning System
GRACE	Gravity recovery and climate experiment: remote sensing satellite instrument
HYDRO	The hydrology model developed for this thesis
INSAR	Interferometric Synthetic Aperture Radar: remote sensing technique
MODIS	Moderate-resolution imaging spectroradiometer: remote sensing satellite instrument
SIA	Shallow ice approximation

Glossary

As released	GLIMMER run as it is publicly available; run without my personal modifications
Background hydraulic pressure profile	The water pressure due to only basal melting under the Greenland ice sheet, in equilibrium conditions
Balance velocity	The rate at which ice must flow to maintain mass balance, taking into account accumulation and ablation
Cold	Temperature below the pressure melting point
Effective pressure	Effective ice load on the bed, once the water has taken its share. It is defined as the ice overburden pressure minus the subglacial water pressure
Efficient	Hydrological configuration where water pressure falls as water flux increases. A stream network is efficient
Fingering	Quasi-ice streams with a longitudinal warm region sandwiched between frozen bands
Flickering	Random variation in values of a variable. New values have no bearing on old values
Frozen bed	Cold basal ice
Helheim	A fast outlet glacier on the east coast of Greenland.
Hydrofracture	Rapid downward propagation of a water-filled crevasse due to the stress differentials at the tip of the crevasse
Inefficient	Hydrological configuration where water pressure increases as water flux increases. Groundwater flow is inefficient
Interior	Areas of the ice sheet away from the margin. Specifically, areas where the overall p^* pressure gradient is towards the margin and not away from it as can be the case if the maximum in near an outlet glacier etc

continued

continued

	In a non-hydrological setting: areas away from the margin
Jakobshavn Isbræ	Greenland's fastest outlet glacier. It is on the west coast
Kangerdlugssuaq	Greenland's second fastest outlet glacier. It is on the east coast
Loose	Ice dynamics where it is easy to initiate sliding, enabling sliding to start at low speeds; the opposite of *stiff*
Mass balance	A measure of whether an ice sheet or glacier is gaining or losing net mass
Polarity of speedup	Land-terminating ice speedup amplitude divided by the marine-terminating ice speedup amplitude. Numbers greater than one show that land-terminating ice has a larger relative speedup than neighbouring marine-terminating ice
Pulsing	Rhythmic oscillation of values in a smooth manner
Relative speedup	The velocity divided by the average velocity, minus one. Positive numbers indicate a speedup and negative numbers indicate a slowdown
Shallow ice approximation	Approximating ice stresses by only calculating vertical stress components (ie ignoring longitudinal and lateral stresses) on the basis that the horizontal extent of an ice sheet is much larger than its thickness
Speedup amplitude	The amplitude of the 1 a (seasonal) peak of the Fourier transform of the relative speedup
Spring event	Sudden increase in glacial velocities due to high water pressures at the bed which occurs in the spring when surface melt water first reaches the bed
Stiff	Ice dynamics where it is difficult to initiate sliding, requiring sliding to start at high speeds; the opposite of *loose*
Swiss Camp	An area approximately 50 km from the western margin of the Greenland ice sheet. It is at an elevation of 1200 m, near the ELA
Thermomechanical	Ice dynamics and temperature evolution are functions of each other.
Uniform melt rate	A melt rate which is spatially and temporally constant
Warm	Temperature at or above the pressure melting point

Chapter 1

Introduction

> "Dynamical processes related to ice flow not included in current models but suggested by recent observations could increase the vulnerability of the ice sheets to warming, increasing future sea-level rise. Understanding of these processes is limited and there is no consensus on their magnitude."
>
> —*Fourth IPCC Assessment Report 2007,* §*Summary for Policy Makers*

The aim of this thesis is to investigate ways in which basal and surface hydrology affect the dynamic behaviour of the Greenland ice sheet. Basal hydrology strongly influences the sliding of ice and therefore the surface ice gradient, delivery of ice into the ablation zone, and it thus affects the dynamic loss of ice into the sea. Recent evidence suggests that the basal hydrology is coupled with the surface hydrology in the summer months and can lead to variation in ice velocities (eg Zwally et al., 2002; McMillan et al., 2007; Das et al., 2008; Sundal et al., 2009). For example, various studies show an increase in surface velocity in response to surface melt or draining surface lakes (Zwally et al., 2002; Van de Wal et al., 2008; Shepherd et al., 2009). This coupling provides a potential mechanism for large parts of the Greenland ice sheet to respond to changing climatic conditions more rapidly than previously thought, assuming that an increase in surface meltwater production leads to a proportional change in basal conditions. The sensitivity of this dynamic response to climate may depend on the basal conditions underneath the ice. Basal conditions evolve continually and depend on, amongst other factors, the volume and pressure of water at the bed. This, in turn, depends on basal heat sources, the structure of the subglacial drainage system, and the contribution of water from the surface.

It is very difficult to physically access the bed of a glacier, let alone an ice sheet, to determine basal conditions. Therefore, the most common methods for investigating these conditions are either remote soundings, such as radar or seismics, or by modelling. This thesis investigates, by modelling, the controls on basal hydrological conditions and basal temperatures and the consequences of these on ice dynamics with and without the effects of coupling to the supraglacial drainage system.

1.1 Rationale

The Greenland ice sheet has a major climatic influence in the northern hemisphere, affecting atmospheric circulation, North Atlantic ocean currents, and global sea-level (Clark et al., 1999). How the ice sheet will respond in a warming climate is open to debate and many important aspects of the system, such as the impact of the hydrology; calving mechanisms; and surface heat exchange and refreezing, are not yet sufficiently understood.

The Greenland ice sheet is the second largest ice sheet in the world and the only existing large ice sheet in the northern hemisphere. Climate change is likely to have a relatively minor effect on the east Antarctic ice sheet, because the vast ice sheet stabilises its own climate (eg Sugden et al., 1993; Davis et al., 2005) and its bed is largely above sea-level (Lythe et al., 2000). The west Antarctic ice sheet may become unstable because a large portion of its bed is below sea level. Both west Antarctica and Greenland may reach a tipping point, after which they may experience rapid changes as a consequence of global warming (Notz, 2009).

1.1.1 The northern hemisphere

The Greenland ice sheet affects northern hemisphere atmospheric circulation by acting as a large, cold barrier. It influences storm tracks (Hoskins and Valdes, 1990; Kageyama et al., 1999) and cyclone evolution (Kristjansson and McInnes, 1999; Petersen et al., 2004), which in turn influence northern hemisphere cloud cover and therefore temperatures (Felzer et al., 1996). Many studies investigate the impact of the ice sheet shrinking or disappearing on the northern hemisphere circulation (eg Felzer et al., 1996; Petersen et al., 2004; Dethloff et al., 2004; Junge et al., 2005) but it is difficult to focus efforts without understanding the future of Greenland in a warming world.

A sudden flux of cold freshwater from the Greenland ice sheet into the north Atlantic

has the potential to weaken, or turn off, the thermohaline circulation (Fichefet et al., 2003; Rahmstorf et al., 2005). This would result, temporarily, in a colder northern-hemisphere climate. Historically, this occurred during the demise of the Laurentide ice sheet and such an influx is the suspected cause of the 1,400-year Younger Dryas cold period (Anderson, 1997; Broecker, 2006). A key question here is whether Greenland will cause a similar abrupt climate change (Alley, 2007; Thornalley et al., 2010). Much ocean modelling work has been done to understand the influence on circulation of a large freshwater flux from Greenland entering the north Atlantic (eg Hu et al., 2004; Mu et al., 2006; Stouffer et al., 2006), but these studies lack adequate modelling of the Greenland ice sheet itself. Recent modelling studies suggest that the impact of freshwater from Greenland on Atlantic circulation may not be as large as once thought, due to the location and magnitude of the freshwater input (Driesschaert et al., 2007; Mikolajewicz et al., 2007). Nevertheless, the thermohaline system is highly non-linear with many equilibrium states (Rahmstorf et al., 2005) and therefore constraining the boundary conditions, by understanding Greenland's response to a warming climate, should greatly enhance the effectiveness of ocean models and therefore future climate projections.

If it were to disappear, the Greenland ice sheet has the potential to contribute 7 m to global sea-level rise (Alley et al., 2005a). How quickly this may happen is unknown. In the third Intergovernmental Panel on Climate Change (IPCC) assessment report, the worst-case scenario of an 8 °C warming is sufficient to remove the Greenland ice sheet in 1000 years (Gregory et al., 2004). However this study, and the later fourth IPCC report, ignore key processes which may make it easier to remove the ice sheet.

> Models currently [...] do not include full treatments of ice dynamics; thus, analyses of past changes or future projections using such models may underestimate ice flow contributions to sea-level rise, but the magnitude of such an effect is unknown. (Solomon et al., 2007)

A number of studies model the Greenland ice sheet under future climate scenarios (eg Loutre, 1995; Stocker, 1999; Huybrechts and de Wolde, 1999; Ridley et al., 2005; Pitman and Stouffer, 2006), but there is a general lack of certainty on what the dynamic response of the Greenland ice sheet to increased basal lubrication, under a warmer climate, will be. This lack of certainty led to the third and fourth IPCC reports ignoring the dynamic response altogether (Solomon et al., 2007), despite the Greenland ice sheet possibly losing up to two-thirds of its mass

dynamically (Rignot and Kanagaratnam, 2006).

The Greenland ice sheet therefore has a large influence on northern hemisphere climate and its presence and evolution is a key factor in understanding future climatic change. The next section explains why this study focuses specifically on the basal and surface hydrology of the ice sheet.

1.1.2 Dynamic response

Recent observations suggest that the Greenland ice sheet system is more complicated than previously thought. The dynamics of the ice sheet appear to be linked to surface melt and the draining of lakes which form on the ice sheet's surface in the spring (eg Zwally et al., 2002; Das et al., 2008; Shepherd et al., 2009). Although a seasonal speedup of Greenland's ice has been known for over twenty years (Andreasen, 1985b), linking this speedup to surface hydrology is more recent. Zwally et al. (2002) suggest that surface water reaches the bed of the Greenland ice sheet through moulins and crevasses where the ice is over one kilometre thick. They suggest this increases basal lubrication and sliding velocity but Zwally et al. do not explain the causal link between increased water delivered to the bed and increased sliding. Until the processes governing this link are established our ability to predict the extent of this behaviour remains unresolved. For example: how large an area can a single moulin affect; how do different basal conditions affect the speedup?

Surface lakes appear to be a key component in connecting surface and basal hydrology, providing the energy-store needed to open a connection between the surface and the bed (Weertman, 1973; Alley et al., 2005b). Once a connection is open, lakes can drain in less than one day (Box and Ski, 2007; Das et al., 2008). Ice responds quickly and both an uplift of the surface, due to higher water pressures at the bed, and an increase in surface velocity are observed (eg Zwally et al., 2002; Das et al., 2008; Van de Wal et al., 2008; Shepherd et al., 2009). Once a connection forms, subsequent diurnal ice speedup suggests that the connection remains open during the melt season and so the ice dynamics respond to the daily ablation (Van de Wal et al., 2008; Shepherd et al., 2009).

The significance of the link between hydrology and dynamics is that the Greenland ice sheet can potentially respond to climate change quicker than by simply melting. Increased sliding means that the ice sheet can lose mass dynamically through its outlet glaciers. Rignot

and Kanagaratnam (2006) find that the ice sheet loses up to two-thirds of its ice dynamically. Dynamic speedup is associated with thinning due to continuity. This means, if surface melt water injection does cause a speedup, the ice sheet will also thin and thereby bring a larger area of the ice sheet into the ablation zone, where there is a net loss of ice through surface melting (Parizek and Alley, 2004). In addition, a warming climate will raise the upper bound of the ablation zone itself, amplifying these effects.

1.1.3 Basal processes

The system is further complicated due to continually evolving basal conditions. As the volume and flux of water in the system change, the basal conditions change which affects the dynamic response of the system to a given water influx. In other words, a given flux of water entering the system will effect a different velocity change depending on the basal conditions. For Alpine and Arctic valley glaciers the seasonal evolution of the basal hydrology, an analogous process, is well documented (eg Nienow et al., 2005; Bingham et al., 2008). However, this is still a new field of research for ice sheets, where it is much harder to assess basal conditions because the ice is up to an order of magnitude thicker. A seasonal evolution does appear to occur (eg Van de Wal et al., 2008; Shepherd et al., 2009) but our understanding of the processes involved are more limited than for Alpine glaciers, despite the potential consequences being larger because of the Greenland ice sheet's influence on northern hemisphere climate.

Because Greenland is an ice sheet, some observations of seasonal evolution do not have Alpine parallels. This is mostly to do with discerning the behaviour of marine-terminating outlet glaciers and the adjacent land-terminating ice. For example, Joughin et al. (2008) find that outlet glaciers have a small seasonal speedup ($< 15\%$) compared to land-terminating ice (50–100% speedup). The lack of seasonal speedup on Jakobshavn Isbræ, a major outlet glacier on the west coast, is the focus of Echelmeyer and Harrison (1990) but a satisfactory explanation of the lack-of speedup still has not been found as of 2009 (Hughes, 2009). There are indications, however, that Jakobshavn Isbræ may be changing its flow-regime, and a distinct seasonal speedup was observed in 1995 (Luckman and Murray, 2005). Some outlet glaciers, such as those on the south-east coast of Greenland, show multi-annual increases in discharge that are not associated with a seasonal signal (Howat et al., 2007). None of

these observations are currently adequately represented in models; basal hydrology must be integrated into models for this to happen. Most ice sheet models currently do not include non-trivial basal hydrology.

The complex dynamic response of the Greenland ice sheet is a result of the basal hydrology, as subglacial water pressures are a key control on sliding velocity (Budd et al., 1979). The subglacial hydrology, in turn, is affected by a number of factors. Part of the bed of the Greenland ice sheet is probably at pressure melting point (Huybrechts, 1996; Dahl-Jensen et al., 1998; Fahnestock et al., 2001; Oswald and Gogineni, 2008). At these locations, the heat flux at the ice-bed interface is large enough to sustain melting of the ice. Heat sources are: geothermal heat flux, frictional heat, strain heat, and advection of warm ice and advection of water (Van der Veen, 1999). Geothermal heat flux varies under the ice sheet but is hard to constrain in models (Waddington, 1987). Frictional heating introduces a number of feedback mechanisms because the friction depends on lubrication which in turn affects melting and therefore the available lubrication. Strain heating and advection are reasonably well understood and included in current models (eg Hutter, 1982; Greve, 2000; Huybrechts et al., 2002; Rutt et al., 2009). However, until the interactions between all the heat sources and their subsequent effects on water pressures are understood, reproducing some observations in models will be difficult because of the lack of adequate basal boundary conditions.

1.2 Objectives

The discussion above creates a focus for this thesis on two underdeveloped areas:

- Improving the basal boundary conditions of large-scale ice sheet models, specifically the basal hydrology and its interaction with frictional heating.
- Modelling the dynamic response of the Greenland ice sheet by focusing on the physics controlling the basal hydrology, and therefore the basal boundary conditions.

Specifically, the objectives of this thesis are to:

1. Understand the relative importance of geothermal, strain and frictional heating. This will help us understand the pattern of basal melt entering the system, and so in turn the nature of the basal pressure profile in the absence of surface water inputs. Understanding the relative magnitude of the different terms will also help direct future

work; some of these heat sources may have larger influences, and therefore justify more work in constraining their values. (Chapters 3 and 4)

2. Generate estimates of how boundary conditions at the ice bed are modified by water pressure. These boundary conditions will allow more accurate modelling of the dynamic response of the Greenland ice sheet to surface water delivered to the bed. Most ice sheet models currently use proxies, such as bed temperature or basal melt rate, to control sliding. These proxies cannot account for what is happening underneath the ice, and therefore key behaviours of the ice sheets are currently missed. (Chapter 3)

3. Understand the frictional heat flux feedbacks and their consequences. Friction is an important heat source under fast-flowing ice and is inextricably linked with bed lubrication. The standard method to calculate this term in ice sheet models is simply to take the product of basal driving stress and the sliding velocity (eg Rutt et al., 2009). However, where ice is sliding quickly, water pressures are high so the frictional heat term may contribute less in these areas than current models predict. Conversely, where ice is just starting to slide, frictional heat may provide additional melt and hence the extra lubrication needed to maintain flow. (Chapter 4)

4. Investigate the behaviour of the Greenland ice sheet in response to surface hydrology, based on the resulting perturbations to the basal boundary conditions. Much recent work focuses on current observations from the Greenland ice sheet regarding the dynamic response to surface hydrology and the behaviour of Greenland's ice streams. This thesis is among the first studies to include these processes in a Greenland-wide model. (Chapter 5)

1.3 Physics of ice sheets

The goal of this thesis is to gain a better understanding of how the Greenland ice sheet dynamically responds to draining surface lakes and whether this process is likely to accelerate as climate warms. To enable this, factors affecting ice sheet evolution (eg climate, basal conditions, ice rheology) must be understood. Section 1.3.1, therefore, reviews current ice dynamics theory. Section 1.3.2 reviews glacial hydrology theory and discusses recent field

studies. Combined, I establish the framework for a new basal hydrology model, and its integration with an existing ice sheet model. The model is developed in the following chapter.

1.3.1 Ice dynamics

Ice dynamics covers a wide range of topics. Here I focus on motion of land ice and introduce convenient methods for analysing the system (pressure melting adjustment, force balance, mass balance). Most of the Greenland ice sheet is grounded, except for the tongues of some outlet glaciers (eg Reeh et al., 2001; Thomas et al., 2009). This work concentrates on grounded ice as many of the recent observations are from these areas (eg Zwally et al., 2002; McMillan et al., 2007; Das et al., 2008; Shepherd et al., 2009) and the GLIMMER ice sheet model, used in this work, only has very basic handling of calving glaciers thus far.

Pressure melting

Before starting the discussion on ice movement, it is useful to introduce the concept of pressure melting because it affects ice rheology and basal melting. The bed of an ice sheet is an extreme environment with pressures many orders of magnitude higher than encountered in everyday life. At these pressures, the temperatures at which materials change phase, for example from solid to liquid, are lower. The temperature at which melting occurs, T_{pmp}, is approximated by (Huybrechts, 1986)

$$T_{\text{pmp}} = -\rho_i g c_t z \; . \tag{1.1}$$

Here, ρ_i, g, and z are ice density, acceleration due to gravity and depth below the ice surface respectively[1]. The c_t constant defines the dependence of melting point on pressure.

To make it easy to know whether ice is at its melting point or not during data interpretation, pressure-adjusted temperature T^* is used,

$$T^* = T + T_{\text{pmp}} = T - \rho_i g c_t z \; . \tag{1.2}$$

Ice at $T^* = 0\,^\circ\text{C}$ is at pressure melting point although the actual ice temperature T may be below $0\,^\circ\text{C}$. In this work, *warm ice* refers to ice that is at, or close to, its pressure

[1] z is treated as a positive value in this thesis and therefore Equation 1.1 needs an explicit minus sign. Other work treats z as negative so the sign is absorbed by the equation (eg Rutt et al., 2009).

melting point. Conversely, *cold ice* is ice below its pressure melting point. On a model grid, two adjacent cells or nodes which have the same temperature T may have different pressure-adjusted temperature T^* due to varying ice thickness. Regardless of the actual temperature, the pressure-adjusted temperature will be zero if the ice is at pressure melting point. This simplifies data interpretation.

Glacier flow

All glacial ice, except ice on the ice-divide, moves (Raymond, 1983). An ice-divide is equivalent to the watershed of a fluvial system. It is important to understand the processes controlling the dynamics of ice if we are to predict the future of ice masses. There are three mechanisms by which glacial ice moves: internal deformation, sliding, and rafting on deforming sediments. Figure 1.1 shows these graphically. The observed surface velocity is the sum of the three simultaneous processes.

Internal deformation has been studied in detail for over fifty years and is reasonably well understood (eg Glen, 1952; Nye, 1953; Glen, 1955; Nye, 1957). Deformation occurs because of the stresses imposed on the ice by its own weight. The warmer the ice is the easier it deforms. Ice is warmest close to the bed and these regions are also under the greatest stress. Therefore, ice near the bed undergoes the most internal deformation and internal deformation drops rapidly nearer the surface, Figure 1.1. In areas where the bed is below pressure melting point, effectively all the observed surface velocity is through internal deformation.

Ice rheology can be approximated mathematically using Nye's approximation to Glen's empirical flow law (Nye, 1957; Van der Veen, 1999)

$$\dot{\boldsymbol{\epsilon}}_{iz} = A(T^*)\boldsymbol{\tau}_*^{(n-1)}\boldsymbol{\tau}_{iz}, \ _{i\in\{x,y\}}. \tag{1.3}$$

This equation describes how ice strain $\dot{\boldsymbol{\epsilon}}$ responds to a stress $\boldsymbol{\tau}$. A and n are considered constants. As stress increases, due to thicker ice or larger surface gradients, the response in strain becomes progressively larger due to Glen's empirical flow constant n. The value of n is not well constrained and may well vary from one glacier to the next. It has a suggested range of $n = 1$ (eg Doake and Wolff, 1985), for very low stress regimes, to $n = 6$ at higher stresses (Hooke, 1981) but $n = 3$ is quoted most often (Paterson, 1994). The physical mechanism by which ice may have a cubic response to stress is uncertain but this value is supported by

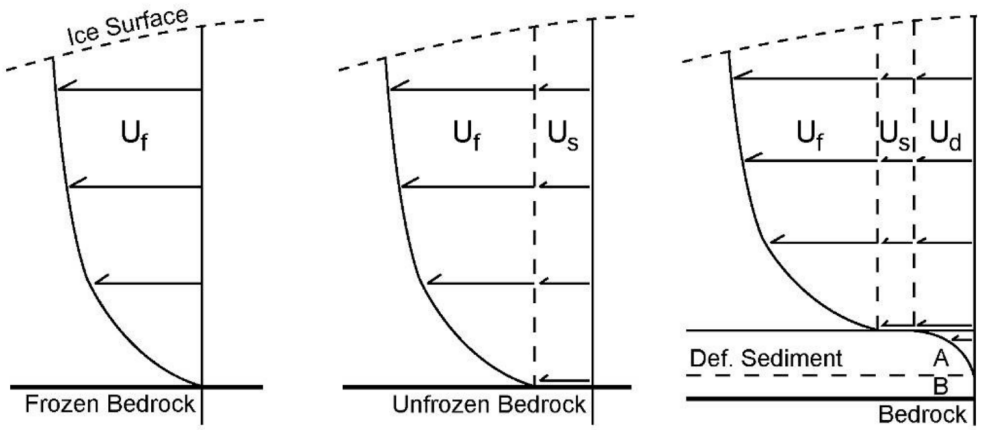

a Internal deformation b Basal sliding c Deforming sediment

Figure 1.1 Three mechanisms contribute to the surface velocity of a glacier or ice sheet. (a) Internal deformation is a result of stresses in the ice. The response to these stresses is temperature dependent. Ice near the bed is under higher stresses and closer to pressure melting point and therefore this region deforms the most. (b) If the bed is not frozen then the ice can slide over it. (c) Under appropriate conditions, basal sediment may deform under the stresses imposed by the ice. The stresses needed to deform sediment are much less than the stresses needed for internal deformation. (From Boulton, 1996b; Jamieson, 2008)

laboratory experiments and some, but not all, fieldwork (Hooke, 1981; Van der Veen and Whillans, 1990). Hooke (1981) and Budd and Jacka (1989) review the value of n in more detail. It is not the purpose of this thesis to investigate this so the widely used value of $n = 3$ is utilised.

n is key for calculating the observed surface velocity but its role in calculating basal sliding is less obvious. In some sliding models (eg Weertman, 1979), n affects the sliding rate because if affects how quickly ice deforms over a rough bed but this is difficult to model because many bed properties must be known. In the ice sheet model used in this work (Glimmer), n does not affect the treatment of basal sliding and so is of limited importance in understanding the dynamic response in the context of this work.

A reflects the hardness of the ice and varies with depth. Experiments suggest that A is determined by the Arrhenius relation which takes pressure-adjusted temperature, and therefore depth, into account (Paterson, 1994).

$$A = A_0 \exp\left(-Q/RT^*\right) \tag{1.4}$$

A_0 is usually taken to be a temperature-independent constant; Q is the activation energy for creep; and R is the universal gas constant. Theoretically, a more complete approximation for A_0 is

$$A_0 = A_0' \exp\left(-p_{hs}\mathcal{V}/RT^*\right) \tag{1.5}$$

but even the sign of the activation volume for creep $\mathcal{V}$ is unknown for ice (Paterson, 1994). p_{hs} is the hydrostatic pressure in the ice; this highlights the importance of water on internal deformation. This effect is usually ignored and will also be ignored in this thesis (Paterson, 1994) but is mentioned here for completeness.

Greenland's dynamic response to draining surface lakes is a result of increased motion at the bed (eg Zwally et al., 2002). Motion at the ice-bed interface occurs where the bed is at, or on a micro-scale very close to, pressure melting point. This motion is complicated and a number of different processes, such as sliding and regelation, may be involved. Regelation is ice moving over a bedrock obstacle by melting on the upstream side, due to the increased pressure, and refreezing on the downstream side, due to lower pressure (Weertman, 1979). The water itself probably moves over the obstacle by flowing as a thin sheet. This work focuses on large, Greenland-wide scales and therefore does not discuss small-scale motion in detail. There are many studies which do concentrate on small-scale processes; these studies are reviewed in detail by Paterson (1994) and Van der Veen (1999).

Sliding is the slipping of ice over the bed because of the presence of water. It is hard to approximate mathematically but Paterson (1994) gives

$$\boldsymbol{v}_b = k\boldsymbol{\tau}_b^{\mathfrak{p}} N^{-\mathfrak{q}} \tag{1.6}$$

as a common generic equation that is based on water pressure. The equation and the values of the positive integers $\mathfrak{p}$ and $\mathfrak{q}$ are determined empirically (eg Budd et al., 1979; Bindschadler, 1983; Lingle and Brown, 1987). k is a constant of proportionality dependent on the properties of the ice and the bed; $\boldsymbol{\tau}_b$ is the basal shear stress, which depends on ice thickness and surface gradient; N is the effective pressure of the ice on bedrock and is defined as the ice overburden pressure minus the subglacial water pressure. As N falls, sliding increases. Equation 1.6 shows the dependence, at least empirically, that water pressure has on sliding which forms the basis of this work. It is generally accepted that basal ice needs to be at pressure melting

point in order to slide (Weertman, 1979). Otherwise, the ice will be frozen to the bed and the basal drag too great. Any surface water that reaches the bed (eg Zwally et al., 2002; Das et al., 2008) can affect N and therefore velocity.

In the limit where N approaches zero, basal shear stress also approaches zero and other resistive forces, such as lateral drag, begin to dominate. In these situations, Equation 1.6 tends to infinity and becomes invalid hence another equation must be found. This adds an extra layer of complexity because the equations approximating the floating system are very different to those describing land ice, as there is no basal drag. How to treat the transition from grounded to floating ice in ice sheet models is an open, and very important, area of research (eg Schoof, 2007; Hughes, 2009; Nick et al., 2009). These equations are not treated within this thesis in order to constrain the scope of the work.

Ice rafting on basal sediment is the third component of ice motion. This is where sediments deform under the stress of the ice above, moving the ice resting on the sediments (Boulton, 1996a). When water pressure is high, the stress needed to deform sediment can be much lower than the stress needed to deform ice.

This thesis does not deal with regelation or rafting. To a limited extent, Equation 1.6 may be regarded as incorporating regelation without specifying the explicit process. Rafting, however, is not a part of the Glimmer ice sheet model at all. There is scope for it to be added — as an erosion component, which such a model would rely on, has recently been developed (Jamieson, 2008) — but this is beyond the scope of this work. These processes are not discussed further.

Force balance

Force balance is a useful concept for understanding changes to an ice sheet. When a system is in force balance all the forces acting at a point cancel out; there is no acceleration of that point (Van der Veen, 1999). When the forces change, the ice responds. For example, if the bed becomes more lubricated then there is less resistive force and the ice accelerates. Alternatively, if a floating outlet glacier retreats there is less back-force and again ice accelerates. These concepts are important because, when an acceleration is observed, the force that has changed must be determined. Chapter 5 of this thesis looks at recent accelerations in the Greenland ice sheet and attempts to understand the boundary conditions, in other words the resistive forces, that have changed to cause the observed speed-up or slow-down.

Mass balance

An ice sheet evolves towards equilibrium with its boundary conditions (Fausto et al., 2009). Determining the mass balance can give an idea whether the system is in equilibrium or not and provide a metric on the health of the system. I use this concept in Section 1.4.2 for introducing the Greenland ice sheet. *Mass balance* measures the total mass change by considering the total mass gain and loss. An ice sheet that is gaining overall mass has a positive mass balance; an ice sheet that is losing overall mass has a negative mass balance. In both cases, there is still accumulation near the centre and ablation, through melting or calving of icebergs, near the margin. Therefore, ice has to flow from the centre to the margin for the ice sheet to maintain a steady state. The ice velocities needed to maintain this steady state are known as the *balance velocities* (Benn and Evans, 2010). These can be calculated by modelling (eg Bamber et al., 2000). If observed velocities are slower than balance velocities then the system is probably gaining mass. Conversely, if balance velocities are lower than observed then the system is probably losing mass. Balance velocities are linked to the amount of ablation and accumulation. If the system has large amounts of both then the ice must flow faster to keep the ice sheet in a steady state.

The line at which there is no net melt or accumulation at the surface over a year is the equilibrium line altitude (ELA) (Paterson, 1994). This also provides a good metric for understanding glacier health and dynamics. A lower ELA suggests that the glacier (ie mass) will advance and that the mass balance is positive. A higher ELA suggests that the glacier will retreat and the mass balance is negative. The experiments in Chapter 5 use an ELA-based climate driver.

1.3.2 Glacial hydrology

The discussion so far highlights the role of basal hydrology in controlling ice dynamics. Section 1.3.1 demonstrates the link between water pressure and sliding velocity. Section 1.1 briefly discussed the potential connection between the surface and basal hydrology and the resultant dynamic response. Understanding the processes controlling this response is one of the major aims of this thesis. This subsection discusses the controls on subglacial water pressure and the observed, and theoretical, consequences of the subglacial conditions on ice dynamics.

Theory

Broadly speaking, there are two general principles to subglacial hydrology: higher water pressures result in faster ice flow and water flows down the steepest potential gradient (Shreve, 1972). This subsection examines the controls on water pressure and the nature of subglacial water flow.

Water pressure controls sliding velocity and is related to the water flux passing through the system. Under steady-state conditions, the relationship between the two depends on whether the subglacial hydraulic system is efficient or inefficient (Kamb, 1987). An *efficient* system is one where water pressure decreases as water flux increases. Conversely in an *inefficient* system, water pressure increases as water flux decreases. This is because water cannot drain from the system easily and so extra water causes back-pressure. Figure 1.2 shows a schematic of these two configurations.

There are a number of different modes of flow in each classification (Fountain and Walder, 1998). Sheet flow (Weertman and Birchfield, 1983), linked cavity systems (Kamb, 1987) and other distributed systems are examples of inefficient networks. In sheet flow, also called thin film flow, a spatially extensive, thin layer of water flows along the ice-bed interface. In a linked cavity system, water exists in pockets behind basal obstacles and these water-filled cavities connect with each other through small orifices. Inefficient flow is a stable configuration when water flux is low but as flux, and therefore water pressures, increase the system becomes less stable. For example as pressure increases, the cavities may expand or the water film may thicken; this enables the water to reorganise its flow. Eventually, a trigger is reached and an efficient channelised network, akin to a fluvial network, forms. Like a river system, a series of confluences results in larger water fluxes nearer the margin. Channels incised into the ice are known as Röthlisberger channels (Röthlisberger, 1972); channels incised into bedrock are known as Nye channels (Nye, 1976). Both are named after their proposers and, for the purpose of this thesis, exhibit similar behaviour. Channels maintain an equilibrium between closing, from creep deformation of the ice, and expanding, due to melting from the frictional heat of water flowing past the ice. When water fluxes fall therefore, channels cannot be maintained and they slowly close; the system becomes inefficient once again. Further discussion of subglacial drainage networks are found in Röthlisberger and Lang (1987), Hooke (1989), Fountain and Walder (1998), and Benn and Evans (2010).

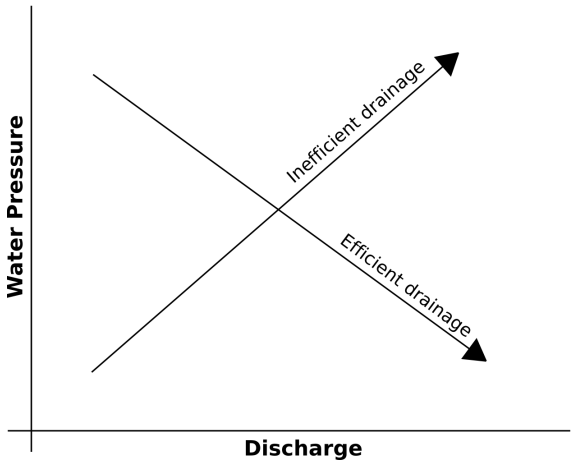

Figure 1.2 Broadly speaking, subglacial drainage can be classified as efficient or inefficient. As discharge increases, water pressure increases in an inefficient system and falls in an efficient system. Inefficient systems are more stable with less discharge and efficient systems are more stable with greater discharge. (After Kamb, 1987)

In both efficient and inefficient systems, water flows down the steepest potential gradient (Shreve, 1972). This imaginary potential surface is determined by the topography underneath the water and the ice above it. Because of the weight of the ice pressurising the water, water can flow uphill over the topography if this reduces the overall potential energy of the water. The potential surface is a key component in a Greenland-wide subglacial hydrology model; it forms the basis by which water flow is defined in the model developed for this thesis.

Observations

There is a well documented seasonal evolution in the hydrology of Alpine and Arctic glaciers. Recent work suggests that the margin of the Greenland ice sheet may undergo a similar evolution. This evolution affects the dynamics of the ice and therefore must be understood, and modelled, if the future of the Greenland ice sheet is to be predicted. This section first describes this observed seasonal evolution and then its causes. Recent observations from Greenland are discussed here but the full review of these studies is left for Chapter 5, where I attempt to reproduce Greenland's seasonal evolution through modelling.

Numerous studies show a direct correlation between water reaching the bed and a dynamic response of the ice (eg Iken and Truffer, 1997; Copland et al., 2003; Anderson et al., 2004; Nienow et al., 2005). A general pattern is described by these studies on temperate and polar glaciers. Early in the melt season surface meltwater begins to flow on the glaciers. This

water, eventually, begins to drain through moulins and reaches the bed and pressurises the system. At this point, surface velocities greater than the winter average and a lifting of the glacier surface are observed. Velocity increases and uplift correlate with diurnal melt fluctuations. The onset of high summer velocities is known as the *spring event* (Mair et al., 2003).

This behaviour is understood by considering the efficiency of the bed and the amount of water in the system. At the start of the melt season in temperate valley glaciers, the daily surface meltwater goes into inefficient networks and raises basal water pressure (Mair et al., 2003). This increased water pressure explains the associated lifting in the glacier surface. As the melt season progresses, efficient drainage networks form, first near the snout and then progressively further upglacier (Nienow et al., 1998; Mair et al., 2002). Water pressures drop in the efficient areas and so the associated spring event becomes less pronounced. At the end of the melt season, efficient networks cannot be maintained. The model used in this thesis must be able to evolve hydraulic efficiency and link the resultant effective pressures to sliding in order to reproduce this observed behaviour.

The sequence of events described is supported by various experiments. Hubbard et al. (1995) and Gordon et al. (1998) use bore-holes to show high effective pressures during maximal daily melt early in the melt season at the Haut Glacier d'Arolla, Switzerland. Dye released into the same glacier is recovered by Swift et al. (2005) over a period of hours also suggesting an inefficient system is present. Later in the melt season, Swift et al.'s (2005) dye tracing confirms the presence of efficient subglacial drainage. Efficient and inefficient systems have characteristic, but very different, peaks in the dye return signature (Hubbard and Nienow, 1997).

Copland et al. (2003) and Bingham et al. (2008) find a very similar sequence of events on the John Evans Glacier, Ellesmere Island, Canada. This glacier is a predominantly cold polythermal glacier in the high Arctic. This shows that a glacier does not have to be temperate for the hydrology to show a seasonal evolution and therefore parts of the Greenland ice sheet, which is also polythermal, may undergo similar processes. Copland et al. observe both a seasonal and diurnal response in the glacier. A diurnal response implies a rapid change in basal water pressures in response to surface melting and a seasonal response shows the evolution of the drainage network to cope with extra water.

Recent work suggests that a similar annual sequence occurs on the Greenland ice sheet. These studies are the focus of Chapter 5. Zwally et al. (2002) show, using GPS measurements at a single site, that there is a seasonal speed up at Swiss Camp, 30 km from the western margin of Greenland. Zwally et al. propose that the reason for the speed up is water reaching the bed through moulins in a region where ice is over a kilometre thick and, near the surface, below pressure melting point. Joughin et al. (2008), Van de Wal et al. (2008) and Shepherd et al. (2009) get similar results using GPS and interferometry (InSAR). Shepherd et al.'s (2009) results are especially interesting because they find both a seasonal (InSAR) and diurnal (GPS) response in the velocity which matches the evolution sequence described for non-ice-sheet glaciers. Another possible explanation for these observations is that water reaches the bed much closer to the margin and longitudinal coupling is responsible for the speedup (Price et al., 2008).

Kamb et al. (1985) provide further evidence that basal efficiency affects ice dynamics. They show that in surging years, Varigated Glacier, Alaska does not evolve an efficient drainage network, resulting in higher-than-average basal water pressures and therefore higher than average velocities. A *surging glacier* is one which periodically switches from its normal slow velocity existence to a high-velocity advance generally independent from climatic forcing (De Angelis and Skvarca, 2003; Benn and Evans, 2010). Some Greenland outlet glaciers surge and basal hydrology is probably a key mechanism (eg Joughin et al., 1996; Pritchard et al., 2005), as initially described by Kamb et al. (1985). However, this thesis does not specifically investigate surging as the focus is on seasonal dynamic response. There is overlap between the two areas and the model developed for this work could theoretically be used to investigate surge mechanisms. Surging is described here as a good example of basal conditions affecting ice dynamics.

The presence of basal water is a key component of faster motion in ice sheets. In Antarctica, where non-topographically bound ice streams exist, subglacial water appears to be a key control on Antarctica's fast-flowing ice streams (eg Engelhardt et al., 1990). The extra water supplied by subglacial volcanic eruptions near Pine Island Glacier in West Antarctica is suspected to have caused the Pine Island Glacier to accelerate in two independent events (Corr and Vaughan, 2008). Although Greenland does not have any non-topographically bound ice streams, many of its outlet glaciers start off this way before the topography

constrains them. Fahnestock et al. (2001) find that many of Greenland's outlet glaciers start in regions where basal melt rates are above average, possibly due to increased geothermal heat flux from volcanism.

In summary, this section discusses subglacial hydrology from both a theoretical and observational perspective. The nature of the subglacial drainage network, whether it is efficient or inefficient, is found to be of primary importance in controlling ice dynamics. Examples of this were given from a wide range of studies. Section 1.4 gives an overview of the Greenland ice sheet and Section 1.5 details the approach taken in this thesis for answering the objectives set out in Section 1.2.

1.4 Greenland overview

This section gives a broad overview of Greenland and its ice sheet to help define boundary conditions for the modelling and to further establish context for this work. Section 1.4.1 discusses the climate of Greenland. Climate is responsible for the presence of the ice sheet; its future evolution; and, through surface melt water generation, drives the seasonal dynamic speedup that this thesis models. Section 1.4.2 looks at the characteristics of the ice sheet such its mass balance, including how it loses and gains mass; the behaviour of the important outlet glaciers; and the ice sheet's basal conditions. This is useful for both directing the development of the basal hydrology model and for defining its boundary conditions.

Greenland lies between 60 and 83 °N and the ice sheet contains the equivalent of 7 m sea-level rise. At its thickest point, the ice is 3,367 m thick (Bamber et al., 2001b). Ice is lost both through dynamic processes and melting (Rignot and Kanagaratnam, 2006). Many outlet glaciers are retreating and therefore speeding up due to, among other factors, reduced buttressing lowering resistive forces (eg Howat et al., 2008; Joughin et al., 2008). The rate of mass loss appears to be accelerating (Velicogna, 2009).

1.4.1 Climate

The presence and behaviour of ice sheets are dependent on the climate. They form where temperatures are sufficiently low and there is sufficient solid precipitation. To model ice sheets, the model must be driven by a climate driver parametrising these conditions in some way. The climate affects accumulation and ablation. The dynamic response modelled in

Chapter 5 depends on the volume of surface water available to derive the seasonal response. This subsection therefore focuses on the climate, from which surface meltwater generation is a product.

The North Atlantic Drift brings warm water up the east of Greenland providing an east-west gradient to the climate (Van der Veen, 1999). This warm water causes a series of depressions to the south-east of the island which means the south of Greenland receives the highest precipitation each year.

The Greenland ice sheet influences its own climate both by cooling the air around it and by increasing the local surface elevation (Van der Veen, 1999). This enhances the orographic effect, the same as any large body of ice. It is unlikely that, if the ice sheet were to disappear, it would reform under present climatic conditions hence the Greenland ice sheet is often seen as a relic of the past (Van der Veen and Oerlemans, 1984; Toniazzo et al., 2004; Box et al., 2009).

The summer lapse rate is approximately $-0.6\ ^\circ\mathrm{C}/100\,\mathrm{m}$ (Hanna et al., 2005) and there is a latitudinal variation of $-0.78\ ^\circ\mathrm{C}/^\circ\mathrm{N}$ in the west and $-0.82\ ^\circ\mathrm{C}/^\circ\mathrm{N}$ in the east (Steffen and Box, 2001). The equilibrium line altitude (ELA) ranges from 1000 m in the north to around 1700 m in the south, reaching approximately 1200 m in the vicinity of Swiss Camp at $69\ ^\circ\mathrm{N}$; the inter-annual variation in the ELA is around 300 m (Van der Veen, 1999). These parameters are used by the climate driver in Chapter 5.

Over the last 100 years, Greenland has had two significant warming periods, 1919–1931 and 1994–present, with a cooling period in between, Figure 1.3 (Box et al., 2009). The cooling in the middle of the 20^{th} century is attributed to airborne sulphate aerosols, a product of emissions from coal power plants in the western hemisphere. The subsequent warming is because of an increase in greenhouse gases and a drop of sulphate emissions from power plants. The 1920s warm period was of greater magnitude than the present event but the current warming is ongoing. Generally, Box et al. (2009) find that Greenland's temperature anomalies mirror, but on average are a factor 1.6 greater than, overall northern hemisphere temperature anomalies except for an occasional decadal-scale lag. This lag is apparent at the end of the 1920s warm period and the mid-century cooling period. In the 1970s and 1980s, Greenland's temperatures continued to drop despite the northern hemisphere entering a warming period. Currently, northern hemisphere warming is greater than the average

warming on Greenland and this suggests an extra 1.0–1.6 °C warming is expected simply to reach equilibrium with the current northern hemisphere climate. This same situation occurred during the 1920s warm period (Box et al., 2009).

Continuing warming is therefore expected over Greenland simply to reach equilibrium with the present northern hemisphere climate. Increased temperatures will result in increased ablation of the ice sheet and consequently a larger volume of water, which may affect ice dynamics by reaching the bed. The key question here is whether the increased volume of water on the surface of the ice sheet will significantly affect ice dynamics or will other aspects of the system, such as basal efficiency, adapt to increased water while keeping the dynamics similar to present. The key to understanding this question is to increase our understanding of the processes controlling the spring event.

1.4.2 Ice sheet

This section briefly overviews the recent behaviour of the Greenland ice sheet. These ideas are discussed in more detail as needed in the relevant chapters.

The overall mass balance of the Greenland ice sheet appears to be negative (Rignot and Thomas, 2002; Velicogna, 2009); this means that the ice sheet is losing mass. Until the last decade, even the sign of the ice sheet's mass balance was undetermined (Bamber and Payne, 2004). Mass loss is accelerating and has increased from $104\,\mathrm{Gt\,a^{-1}}$ in 2002–2006 to $246\,\mathrm{Gt\,a^{-1}}$ in 2006–2009 (Velicogna, 2009). These values are determined using data from the GRACE satellite gravity mission. Most of the mass loss, which is more extensive in the south, appears to be through near-coastal thinning (Rignot and Thomas, 2002).

The Greenland ice sheet loses mass in two ways: through dynamic processes and through melting. Rignot and Kanagaratnam (2006) argue that the Greenland ice sheet loses two-thirds of its mass through dynamic processes. Most of this is through Greenland's outlet glaciers. These glaciers, and the drainage basins feeding them, are shown in Figure 1.5. Increased sliding leads to larger discharges by calving. Increased sliding may be due to the presence of more basal water lubricating the bed, or it may be due to a lack of buttressing as some outlet glaciers retreat along their fjords (eg Howat et al., 2008; Nick et al., 2009). Figure 1.4 shows the recent retreat of Jakobshavn Isbræ (20), one of Greenland's largest outlet glaciers and one of the fastest glaciers globally. Other important outlet glaciers include: Kangerdlugssuaq

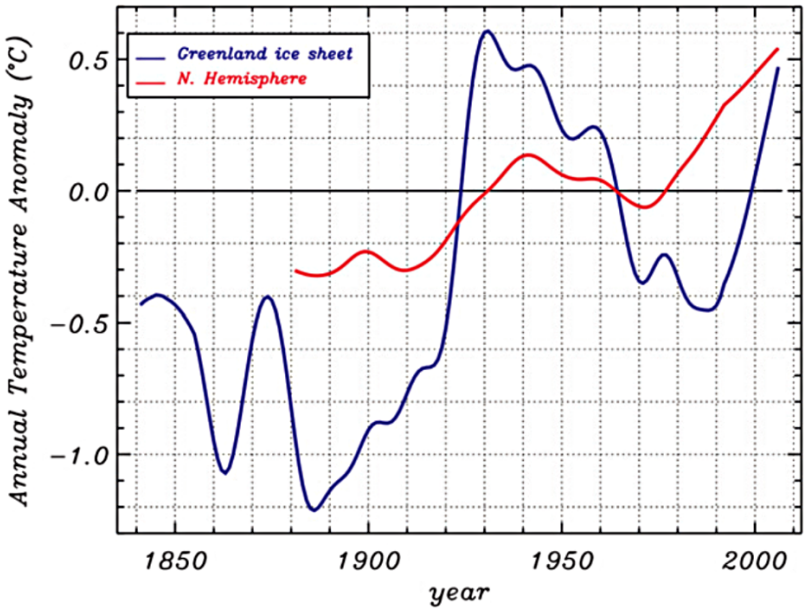

Figure 1.3 Over the last 150 years, Greenland (blue line) has undergone a number of warming and cooling periods. There was a major warming period in the 1920s followed by a cooling period. There is a phase lag between the average northern hemisphere temperatures (red line) and the average Greenland temperatures. An example of this is seen around 1970 when northern hemisphere temperatures start to rise but Greenland temperatures continue to fall. This lag suggests that an extra 1.0–1.6 °C warming is expected simply to reach equilibrium with the northern hemisphere. (Box et al., 2009)

(10), Helheim (11), Petermann (1) and the NEGIS (6). The numbers refer to the glacier's label in Figure 1.5. This figure is from Rignot and Kanagaratnam (2006), where the dynamics of the outlet glaciers are discussed further.

Figure 1.6 shows balance velocities calculated by Bamber et al. (2000) for the Greenland ice sheet. These are the velocities the ice has to flow at to maintain mass balance. Large ice streams are picked out in this map. Balance velocities match observations inland but near the margin balance velocities are lower than observed velocities, indicating a negative mass balance; compare with Figure 1.5.

Melting accounts for the remaining third of the mass loss. The classic study by Benson (1960) identified four broad zones of melt: ablation (no snow in summer), wet-snow (snowpack saturated), percolation (water refreezes in snowpack), and dry-snow (no melt). Figure 1.7 maps these zones schematically. Recent warming has increased the summer melt extent (Abdalati and Steffen, 2001; Mote, 2007), production, and duration (Box et al., 2006; Box and Ski, 2007). Melt extent has high inter-annual variability but shows an increasing trend

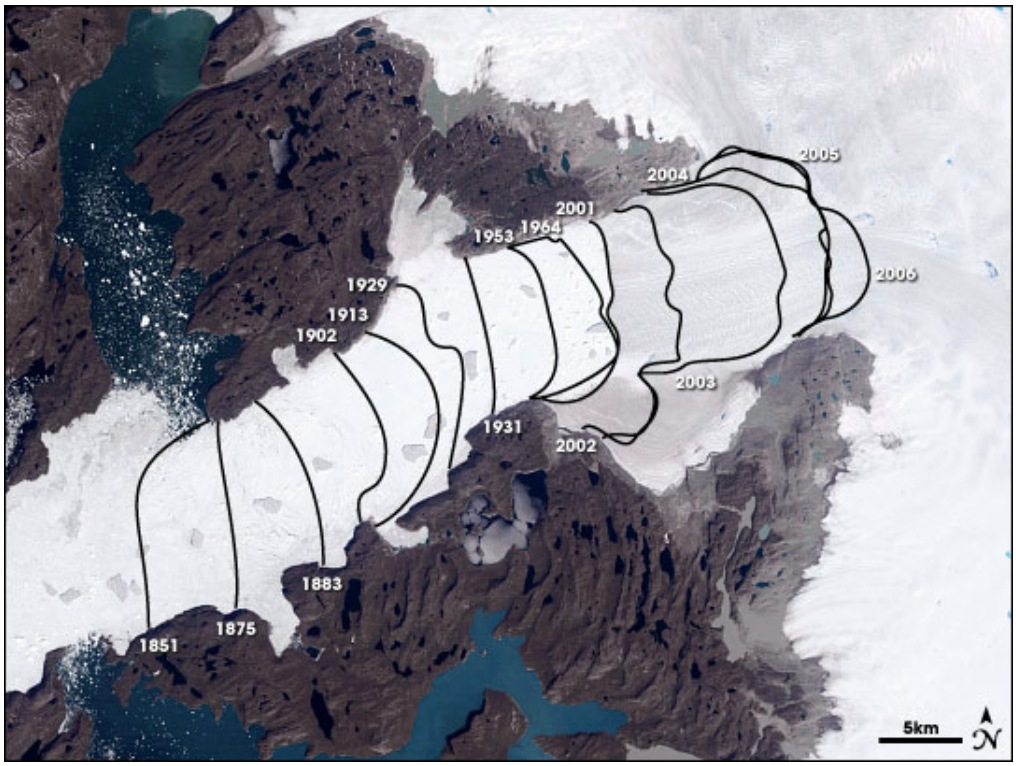

Figure 1.4 The terminus of the Jakobshavn Isbræ outlet glacier has retreated significantly since 1851. Recent terminus positions are drawn on this 2001 Landsat image. Retreat reduces the resistive forces buttressing the ice stream and so the ice stream speeds up. Jakobshavn Isbræ is one of the major outlet glaciers of the Greenland ice sheet. (Image courtesy NASA Earth Observatory)

over the last 20 years (Steffen et al., 2004). In 2007, all of the southern dome of Greenland experienced at least one day of melt (Tedesco et al., 2008). This impacts the volume of water available to the system to effect a dynamic response in ice dynamics.

A key consideration is: where does surface melt water go? Above the ELA, in the percolation zone, it mostly penetrates the snowpack and refreezes. This results in densification of the snow, but it does not affect the overall mass of the ice sheet (Parry et al., 2007), nor the volume of water that will reach the bed. Below the ELA, where the ice surface is exposed for part of the year, ponds form by surface flow converging in shallow surface depressions (McMillan et al., 2007; Sundal et al., 2009). The importance of these ponds has only just being recognised within the last decade (eg Zwally et al., 2002; Sundal et al., 2009). These periodically drain and affect the dynamics of the ice (eg Das et al., 2008), possibly leading to increased dynamic thinning (Parizek and Alley, 2004). Surface ponds, and the consequences of their draining, are reviewed in detail in Chapter 5. Very little water leaves the ice sheet

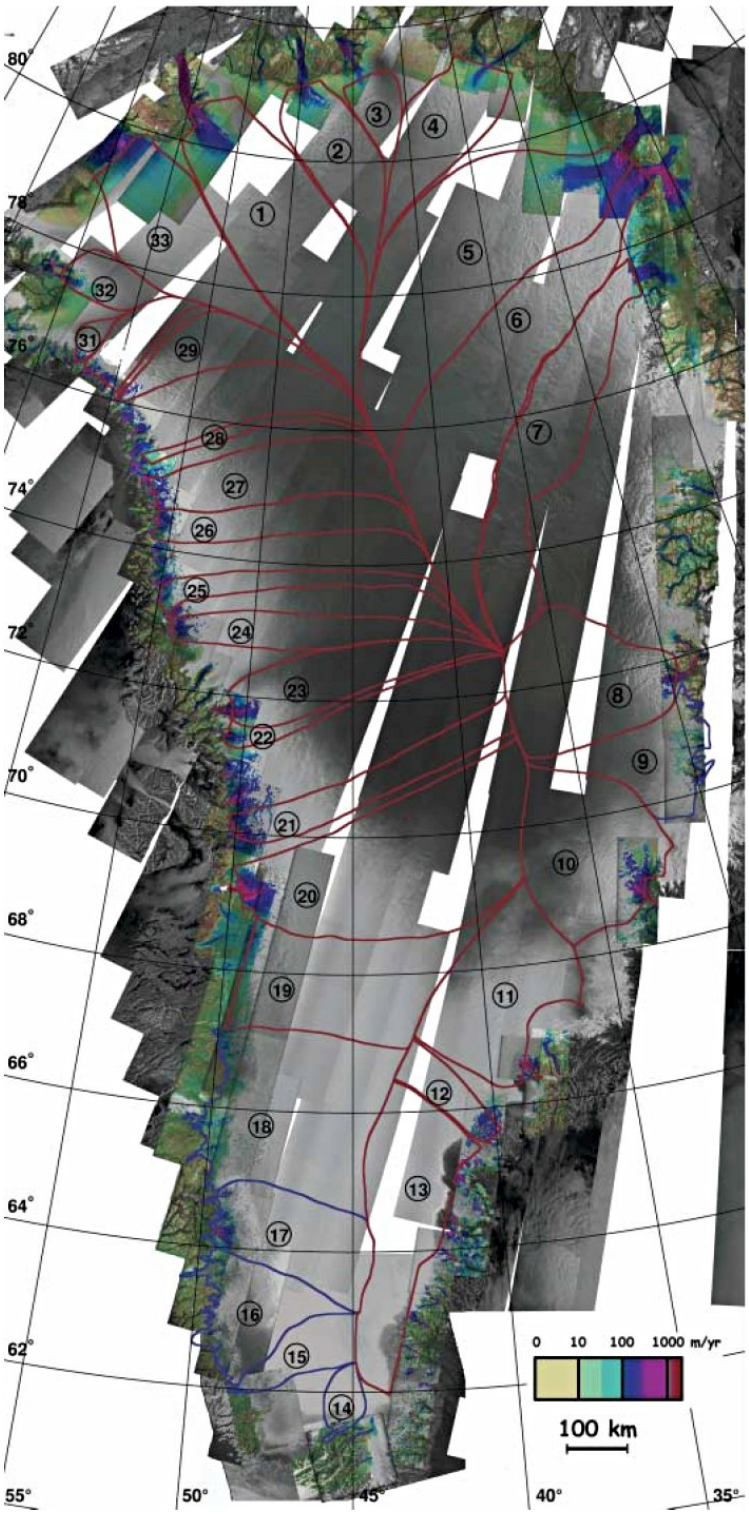

Figure 1.5 This map shows the 2004–2005 velocities of Greenland's outlet glaciers, derived from satellite interferometry. These glaciers may account for up to two-thirds of Greenland's mass loss. Significant glaciers here are: (1) Petermann, (6) North-east ice stream, (10) Kangerdlugssuaq, (11) Helheim, and (20) Jakobshavn Isbræ. A full list of names is given in Rignot and Kanagaratnam (2006), where this map is published. Extracts from this figure are used later in this thesis for comparisons.

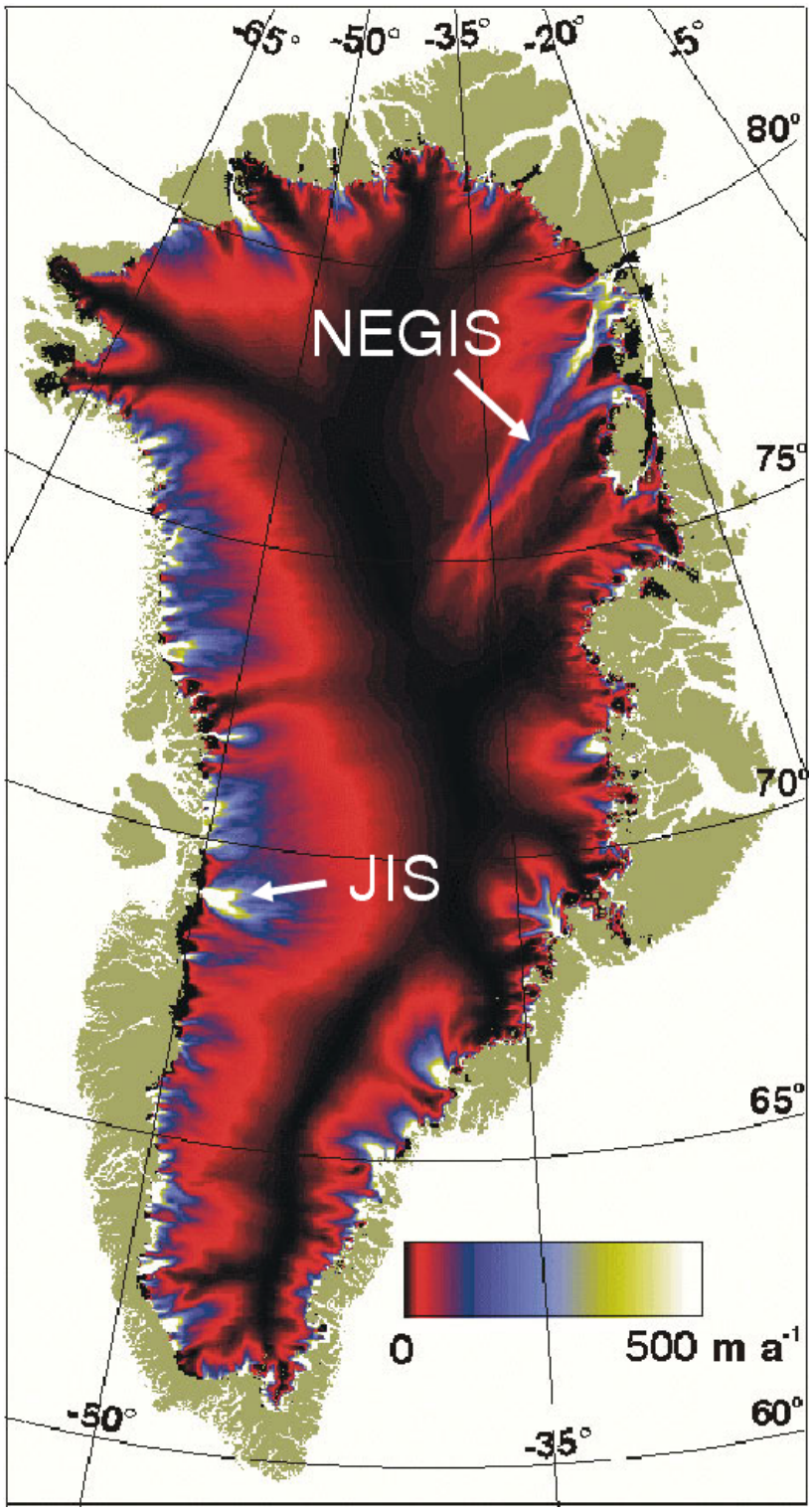

Figure 1.6 This map shows the theoretical balance velocity for the Greenland ice sheet calculated by Bamber et al. (2000). This is the velocity that ice must flow at to maintain mass balance. The values depend on accumulation and ablation rates. The outlet glaciers clearly stand out as faster flowing regions because of the topographic troughs in these areas. Where ice flows faster than the balance velocities, an overall thinning is expected. Here, JIS is Jakobshavn Isbræ and NEGIS is the north-east Greenland ice stream.

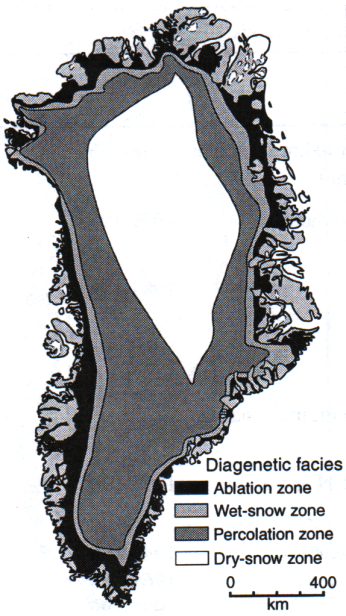

Figure 1.7 Typical schematic map of the four melt zones in increasing elevation on Greenland, from Benson (1960): ablation (no snow in summer), wet-snow (snowpack saturated), percolation (water refreezes in snowpack), and dry-snow (no melt). Over recent years, the boundaries between these zones have increased in elevation (Steffen et al., 2004); the current distribution is not shown.

on its surface; most leaves the system subglacially showing that the majority of water must reach the bed (Ahlstrøm et al., 2005).

The basal conditions of the ice sheet, the focus of Chapter 3, also need discussing to complete this broad picture of Greenland. These form the boundary conditions acting on the ice sheet and therefore play a large part in its dynamics. The bed of the Greenland ice sheet is generally below sea-level because of isostatic adjustment to the weight of the ice (Bamber et al., 2001b). The bed is also largely frozen (Huybrechts, 1996). A frozen bed has too much resistance to slide and is impermeable to water. Basal temperatures affect the nature of the subglacial hydrology by removing basal water by freezing, limiting the area where basal water can exist, and limiting the area where basal melt occurs. The basal conditions of present-day ice sheets are determined by a range of methods including: ice cores (eg Dahl-Jensen et al., 1998) ground penetrating radar surveys (eg Winebrenner et al., 2003; Carter et al., 2009), seismic surveys (eg Smith, 1997), or modelling (eg Huybrechts, 1996). A new concept-technology that is currently being pioneered is to embed sensors in ice and have the device transmit information wirelessly (BBC, 2009). Modelling remains the only way to understand basal conditions on Greenland-wide scales at a reasonable resolution,

but other methods are very useful in defining the boundary conditions that models need to function.

1.5 Approach

The goal of this thesis is to model, and better understand, a realistic response of the Greenland ice sheet to seasonal surface melt and to compare the results to observations. The key to doing this is to build a good understanding of the basal boundary conditions by using a physically-based model. The approach taken is to develop a new basal hydrology model, Hydro, that can run independently or couple with the open-source community ice sheet model Glimmer. Hydro is used to study the controls on the basal boundary conditions which then allows the seasonal response to be investigated. The goal is not to predict the Greenland ice sheet's future or to assess the impact of its loss, but to understand the processes involved to enable others to incorporate these processes when investigating the ice sheet's future.

Hydro tracks the evolution of basal water pressure over large spatial scales based on a simple Darcian expression. The model represents areas of efficient and inefficient flow by modifying the overall basal hydraulic conductivity as a function of water pressure. Thus, basal hydraulic conductivity serves as a simple large-scale proxy to the development of basal water conduits without explicit specification of the system. Areas where the bed is frozen are impermeable. Model inputs are basal temperature, basal and surface melt rates, ice thickness, and bed topography which are usually calculated by Glimmer.

Glimmer is a thermomechanical three-dimensional ice sheet model which is based on the shallow ice approximation (Rutt et al., 2009). One of the reasons it is chosen for this project is because it has a free, open source license and is therefore freely extendible, with a growing userbase and support network. The model has a long history, stretching back to a 1986 model by Huybrechts (1986) (Jamieson, 2008). Of importance in the context of this work, Glimmer calculates ice velocities, temperatures, basal and surface melt rates and ice thickness. The basal sliding velocities are based on a linear sliding law with the *basal slipperiness* parameter defined as a constant of proportionality. This work extends Glimmer by defining basal slipperiness as a function of water pressure, data not available without Hydro. Glimmer's calculation of frictional heat flux from sliding is also modified to take

water pressure into account; where there is more lubrication less heat is produced for a given sliding velocity.

When required, a surface ponding algorithm in HYDRO deals with the surface to basal hydrology connection. This algorithm is used to control the volume of water entering the subglacial hydrological system as a result of surface ponds draining stochastically. Crucially, no explicit assumptions, except that the connection is formed by instantaneous hydrofracture, are made when determining the response of the ice sheet to extra basal water. Any behaviour is a direct consequence of the broad-scale physics included in the coupled GLIMMER-HYDRO model.

1.6 Thesis structure

The thesis structure is based on developing a new model and using this model in progressively more complicated scenarios. The initial focus is the basal boundary conditions. This is followed by investigating the Greenland ice sheet's seasonal evolution and dynamic response.

Chapter 2: *Model Development* describes the community ice sheet model GLIMMER and explains the modifications added for this project. The chapter later focuses on basal hydrology. Existing basal hydrology models are reviewed and the need for a new model is established. This is followed by a formal introduction to the HYDRO model.

One of the objectives of this thesis is to establish reasonable basal boundary conditions for ice sheet models; this is a reason for developing HYDRO. Before HYDRO is used however, it is instructive to understand the various heat sources at the bed and therefore the resulting basal melt patterns. Chapter 3: *Strain and Geothermal Heating* compares analytically calculated strain heating rates at the bed to geothermal heat flux from ice-cores. These values are later compared to frictional heat flux values in Chapter 4. Chapter 3 focuses on establishing the equilibrium pressure profile, and understanding the factors affecting it, by running HYDRO independently for increasingly complicated scenarios. This chapter aims to demonstrate that the nature of the equilibrium profile can explain some of the ice dynamics observed on Greenland.

Chapter 4: *Friction and Sliding* investigates the feedbacks between basal hydrology and frictional heat flux. The chapter reviews the current understanding of ice friction and conceptually develops the friction model used by the coupled GLIMMER-HYDRO model. This

is an important step in understanding the evolution of boundary conditions under ice sheets. The approach here is to build an understanding of the different components of the feedback by gradually increasing the complexity of the system. Initially a circular ice sheet is used to introduce elements of the friction model in a piecemeal fashion.

Chapter 5: *Dynamic Response to Draining Surface Ponds* shifts the focus from basal boundary conditions to Greenland's surface melting and the connection between the surface and basal hydrology. The chapter reviews current observations regarding Greenland's surface ponding and its dynamic response to draining lakes. The chapter also reviews work studying the connection mechanisms between the surface and basal hydrological systems. The surface ponding algorithm is introduced and then used with the Glimmer-Hydro model. This chapter demonstrates and provides an explanation for the hitherto unexplained observation that outlet glaciers show a muted season speedup compared to land-terminating glaciers (eg Echelmeyer and Harrison, 1990; Joughin et al., 2008)

The final chapter brings the ideas discussed together and reviews them critically. Areas where the work can be improved are highlighted and areas for future research are set out.

Chapter 2

Model Development

> "Models currently [...] do not include full treatments of ice dynamics; thus, analyses of past changes or future projections using such models may underestimate ice flow contributions to sea-level rise, but the magnitude of such an effect is unknown."
>
> —*Fourth IPCC Assessment Report 2007,* §*TS 3*

Capturing the dynamic response of the Greenland ice sheet, and hence improving our understanding of its future, requires ice sheet models to include a basal hydrology component. Chapter 1 introduced the link between basal hydrology and ice dynamics and the fact that in some cases ice dynamics can be linked to surface hydrology during Greenland's melt season. Existing hydrology models are not capable of reproducing the coupling between hydrology and dynamics at ice-sheet scales (Section 2.4). Therefore, a new hydrology model is needed in order to meet the objectives of this thesis. This chapter formally introduces the Hydro model developed for this project in Sections 2.5 and 2.6. Hydro is coupled with the existing community ice sheet model Glimmer. Section 2.1 overviews general ice sheet modelling and Section 2.2 overviews Glimmer in order to establish current limitations and thereby demonstrate the function that Hydro must perform.

2.1 Ice sheet modelling

Ice sheets evolve slowly and so observation alone cannot help us understand the processes that control them. Observations can tell us what is currently happening to an ice sheet and some of what has happened to an ice sheet (for example by landforms, past sea-levels and

past climate), but observations are limited in their ability in telling us why ice sheets behave the way they do and so what they may do in future. Ice sheet modelling fills this niche. Ice sheet models also play an important part in modelling the integrated earth system (which includes the geosphere, hydrosphere, cryosphere, atmosphere, and biosphere) by providing surface elevation data, albedo data, and water storage for these models in return for data needed to drive the ice sheet models (Hagdorn, 2003).

2.1.1 Framework

The behaviour of the ice sheet system can be approximated by mathematical equations, within the bounds of our current understanding. Many of these equations become complex very quickly and cannot be solved analytically (Hooke, 2005). These equations can, however, be simplified and solved numerically as an ice sheet model. Each model, by its very nature, has to make assumptions and simplifications about the system it is modelling. Often, the analytic assumptions and simplifications chosen exert a much larger influence on model behaviour than the numerical methods employed. As long as the models are applied to systems where these assumptions hold, and the results are interpreted within the bounds of these assumptions, much knowledge can be gained (Van der Veen, 1999).

There are three general uses of ice sheet models: experimentation, explanation, and prediction (Paterson, 1994). Experimentation helps us to understand the controls on the ice sheet, within the bounds of the model set-up; the sensitivity of the ice sheet to physical parameters; and how the ice sheet responds to external forcing. Models can provide an explanation of observed behaviour, but here ice sheet models are least reliable. It is possible for the model to be set up to provide correct behaviour for incorrect reasons (Paterson, 1994). Understanding the assumptions and simplifications used when defining the model may help. Alternatively, at best we gain an understanding of what might be possibly causing the observed behaviour, if certain conditions hold and if certain assumptions are true (Hooke, 2005). Finally, ice sheet models can be used to predict the past and future evolution of ice sheets. For this to work well, the model must be tuned using data from observations. The tuned model must then be validated using independent data. It is crucial to avoid using all available data for the tuning process so that some can be retained for validation. Only at this stage can the model be used to predict past or future evolution on the major assumption

that the tuning parameters chosen remain valid over the relevant time domain (Paterson, 1994; Van der Veen, 1999).

Even if models do not reproduce observed behaviour, we still gain valuable information on where further observation or improved theoretical understanding is needed (Paterson, 1994). When these deficient processes are better understood, or advances in computing power allow them to be modelled (if already understood), they can then be incorporated into the next generation of models and the cycle repeated.

2.1.2 Application

Ice sheet models numerically integrate their governing equations. This numerical integration is done on discrete nodes, set by the user, to cover the ice sheet domain. This domain may be a two-dimensional flow-line (eg Reeh, 1988; Parizek and Alley, 2004; Pattyn, 2006) or the full three-dimensional ice sheet (eg Letréguilly et al., 1991; Huybrechts et al., 2004; Rutt et al., 2009), depending on the goals of the study.

The first three-dimensional ice sheet models were created in the 1970s, with Jenssen (1977) being to first to thermomechanically couple ice flow and ice temperature in such a model (Van der Veen, 1999). Thermomechanical coupling is now standard practice in three-dimensional ice sheet models and is very important for obtaining correct ice behaviour. Letréguilly et al. (1991) run a thermomechanical ice sheet model for Greenland through a full glacial cycle. They produce a good approximation of present-day ice thickness, but their model does not include any sliding. Huybrechts et al. (1991) use the same model to make predictions of the evolution of the Greenland ice sheet for future climatic scenarios.

2.1.3 Current development

As part of the model development cycle there will always be areas which can be improved. With the current generation of models areas needing improvement are (Lipscomb et al., 2008): higher-order physics; calving laws; ice shelves and grounding lines; and hydrology (surface, englacial, and basal) and sliding. Here, I review each of these with a view of demonstrating where the model-development contribution of this thesis fits.

Higher-order physics

Each point in an ice sheet is under stress from various directions. The degree to which these stresses and directions are calculated determine the 'order' of the model. Many ice sheet models use the so-called Shallow Ice Approximation (SIA), which only calculates vertical shear stresses on the basis that the surface slope and bed rock slopes are small (Fowler and Larson, 1980; Hutter, 1983). In effect it is valid when the ice sheet has a much larger area than its thickness (Hooke, 2005). It greatly simplifies calculations, but cannot model fast flowing ice, areas with steep surface gradients, or regions where ice decouples from the bed.

Models which calculate the stresses at each point more fully are known as higher-order ice sheet models. Such models exist (eg Colinge and Blatter, 1998; Pattyn, 2003; Marshall, 2005; Pattyn et al., 2008) but are not freely available for use or modification. Other established models (perhaps which handle thermomechanical coupling well or are easily extensible) need to be improved to make use of higher-order physics while retaining their other benefits and often significant work that has gone into them.

There are elements of this thesis, which focus on fast-flowing outlet glaciers or regions with low effective pressure, that would work much better with a higher-order model. The results presented must be interpreted with this simplification in mind. HYDRO can theoretically couple with higher-order models. Work is currently in progress to add higher-order physics to GLIMMER[1], the ice sheet model used in this thesis. When this next version of GLIMMER is available, the added functionality provided by HYDRO should transfer with minimal effort. This is a continuation of the model development cycle.

Calving laws

Calving affects the dynamics of outlet glaciers by controlling the amount of back-pressure and therefore potentially their velocity (Howat et al., 2008). There are many complex feedbacks to investigate and increased velocity may lead to increased calving but conversly increased calving may lead to increased velocity (Benn et al., 2007). Currently, many models (including GLIMMER) handle calving in a very simplistic manner; ice is lost if it approaches floating. This stops ice sheets from extending beyond their land-mass, but does not help understand how calving affects the evolution of ice sheets. Developing a good, physically-based calving

[1] See `http://glimmer-cism.berlios.de/` and Lipscomb et al. (2008).

law is an active area of research (eg Meier and Post, 1987; Van der Veen, 2002; Benn et al., 2007; Alley et al., 2008) and will, hopefully, lead to improved ice sheet models. Calving is not directly relevant to this thesis, except that it may affect the dynamics of the outlet glaciers studied to some extent.

Ice shelves and grounding lines

Ice shelves are large floating extensions of ice sheets which are present around the coast of Antarctica. Ice tongues are floating extensions to glaciers which are present around both Antarctica and Greenland. Both of them appear to significantly slow down outlet glaciers through a buttressing effect (Dupont and Alley, 2005; Howat et al., 2008). Understanding ice shelves, and their potential break-up, is very important for predicting future sea-level changes and the future ice dynamics of Antarctica.

Ice shelves can be modelled reasonably well with current techniques, including some higher-order physics (eg MacAyeal et al., 1996; Walker and Holland, 2007; Pollard and DeConto, 2009; Gagliardini et al., 2010). Two major areas for work are the parametrisation of melting and freezing beneath floating ice and the coupling of ice shelf models to ice sheet models across the grounding line (Lipscomb et al., 2008; Gagliardini et al., 2010). The grounding line is the line where ice becomes decoupled from the bed and starts to float.

Effective handling of ice flux and physics across the grounding line is proving to be a major obstacle (eg Vieli and Payne, 2005; Gladstone et al., 2010). The grounding line problem needs to be solved before ice shelves can usefully be incorporated into ice sheet models. The handling of the grounding line may affect the dynamics of outlet glaciers in Greenland, but due to the simplistic calving law used in many models, including Glimmer, this effect is often ignored by necessity.

Hydrology and sliding

Basal hydrology is known to significantly affect basal sliding rates and so ice dynamics. Surface and englacial hydrology control where water is injected into the bed. Also, englacial hydrology affects ice temperatures and so ice rheology. Thermomechanical models can couple temperature and ice dynamics calculations well but they are not yet at the stage where external influences, such as englacial water, are considered.

Two general improvements to calculating basal sliding are currently needed: the inclusion of different basal regimes, such as bed rock or glacial till, and coupling sliding to water pressure. Currently, the only distinction many ice sheet models make is whether the bed is frozen or not, but glaciological evidence suggests that the mechanisms of sliding are different over hard bedrock or over soft till (Paterson, 1994). One obstacle to this is the need to model which regions are bedrock and which regions are till. Recent advances (eg Jamieson et al., 2008; Jamieson, 2008) in modelling subglacial erosion on the ice sheet scale may help.

The contribution of this thesis is to develop a basal hydrology model and a basic surface hydrology model. Basic surface hydrology is included to drive the basal model, but explicit modelling of the englacial connection is not considered because this is assumed to only have a limited impact on the basal processes investigated. Englacial hydrology affects ice temperatures and so ice rheology and may affect where water reaches the bed from the surface. However as a first-order approximation this link can be considered to be vertical through the process of hydrofracture. This potential link and how it may form is discussed in detail in Section 5.2. In this thesis, basal hydrology is linked to basal sliding in a moderately simple manner once basal water pressures are known, but even this is a large improvement on the current handling of basal sliding in models.

2.2 Glimmer ice sheet model

This thesis uses the Glimmer (General Land Ice Model with Multiply Enabled Regions) ice sheet model (Rutt et al., 2009) to model ice dynamics and to couple with Hydro, which is developed to improve Glimmer's basal boundary conditions. Glimmer is an open-source, fully thermomechanical ice sheet model with a long history. An earlier version of it (Payne and Dongelmans, 1997) performed well in the published Eismint-2 experiments (Payne et al., 2000); current versions still meet this benchmark. This section first discusses why Glimmer is used in this thesis and then gives an overview of the model. This is not a full description of the model, as it is well documented elsewhere (Hagdorn et al., 2007; Rutt et al., 2009), but simply an overview of the key components that impact upon this work.

Glimmer is released under the Gnu public license which means anyone can obtain, modify, distribute, and profit from the source code as long as they give the same rights to others (Free Software Foundation, 1991). This is important because no existing model

captures the subglacial hydrology and links it to ice dynamics in a suitable fashion for this project's aims (Section 2.4). Therefore an existing model must be chosen that can be extended in order to avoid duplicating work unnecessarily. Given GLIMMER's license and growing user base, and therefore support network, GLIMMER is a good choice for this project.

This section introduces the GLIMMER model as it is available to the community. This project uses version 1.5.1 of the CVS[2] development branch of GLIMMER. The model can be obtained from `http://glimmer-cism.berlios.de/`.

2.2.1 Ice and temperature evolution

A key question regarding any ice sheet model is how it calculates the evolution of ice through time t. GLIMMER does this using a continuity equation

$$\frac{\partial h}{\partial t} = -\boldsymbol{\nabla} \cdot (\bar{\boldsymbol{v}} h) + B \tag{2.1}$$

where h is ice thickness, $\bar{\boldsymbol{v}}$ is the vertically averaged ice velocity and B is the mass balance. This equation is solved using the shallow ice approximation which ignores normal stress components of the stress tensor on the basis that the surface slope and bed rock slopes are small (Hutter, 1983). The evolution of ice thickness is important to a hydrology model because it will help determine where the basal water flows by influencing the pressure gradients at the bed.

Strain rates of glacial ice $\dot{\boldsymbol{\epsilon}}$ are dependent on the stress $\boldsymbol{\tau}$ as well as temperature T,

$$\dot{\boldsymbol{\epsilon}} = A \boldsymbol{\tau}^n \ . \tag{2.2}$$

Here $\boldsymbol{\tau}_*$ is the effective shear stress and T^* is the temperature corrected pressure melting. GLIMMER fully solves the heat equation for ice sheets. The equation is[3]:

$$\frac{\partial T}{\partial t} = \frac{k}{\rho_i k_{\text{ice}}} \boldsymbol{\nabla}^2 T - \boldsymbol{v} \cdot \boldsymbol{\nabla} T + \frac{H}{\rho_i k_{\text{ice}}} + w \frac{\partial T}{\partial z}. \tag{2.3}$$

[2] Concurrent Versioning System (CVS) is a revision control system. It allows code developers to track changes and to develop different features without affecting each other's work or the production version of the code. Any previous version of the code can be accessed. It is strongly recommended that a revision control system is used for any coding or writing.

[3] The GLIMMER manual defines z as distance above the ice bed, not depth below ice surface, so the sign of the last term is reversed.

The individual terms represent vertical diffusion, horizontal advection, internal heat generation due to friction and vertical advection of heat respectively.

The two boundary conditions of this heat equation are the ice surface temperature and the basal heat flux. The ice surface interacts with the climate driver so is not directly coupled to HYDRO. The basal boundary has a direct impact on basal meltwater generation and therefore the water input into HYDRO. GLIMMER, as released, never allows basal ice temperatures to go above the pressure melting point of the ice; any extra heat present is used to generate meltwater. In cases where GLIMMER knows the ice is floating the basal ice temperature is kept constant.

2.2.2 Sliding laws

Sliding influences melt water generation through frictional heating and water pressures influence sliding velocities (Section 1.3.1). The dynamic response of Greenland to seasonal melting is a consequence of sliding due to basal water at the ice-bed interface.

Models must reduce sliding to a mathematical equation which approximates known behaviour. GLIMMER, as released, does this by using a simplified version of Equation 1.6. GLIMMER uses $\mathfrak{p} = 1$ but simplifies the equation further by defining a *basal slipperiness*[4] parameter, $t_s = kN^{-\mathfrak{q}}$, which reduces the sliding law to

$$\boldsymbol{v}_b = t_s \boldsymbol{\tau}_b. \tag{2.4}$$

Basal slipperiness has units of metres per Pascal per year. Thus basal sliding increases with basal slipperiness.

The user chooses the equation used to calculated basal slipperiness at run time. The option chosen affects sliding velocity and therefore ice evolution. The following options are available to GLIMMER by default:

1. zero everywhere
2. constant everywhere
3. constant where ice is melting

[4] This is referred to as *basal traction* in the GLIMMER documentation. This phrase is misleading and is therefore not used here: basal slipperiness is proportional to velocity.

4. function of basal water

5. function of basal melt rate

Option 1 turns sliding off. Options 2 and 3 only set a constant basal slipperiness so sliding velocity is directly proportional to shear stress; Option 3 only allows sliding if the bed is warm. A constant basal slipperiness value is supplied by the user. This does not capture the important fact that sliding is proportional to effective pressure. For example, the bed can be wet but the effective pressure may be very high. The model will not treat this any different to the effective pressure being zero.

In an attempt to remedy this situation, Options 4 and 5 are provided. In the first case, basal slipperiness, and hence sliding velocity, is directly proportional to the volume of water at the bed. This is a reasonable approximation if we believe that effective pressure is proportional to the inverse of basal water volume. This is likely to be the case in an inefficient hydrological regime; Option 4 does not allow for the presence of an efficient system.

Option 5 makes the basal slipperiness, and hence sliding velocity, proportional to the melt rate. This proxy, again, assumes an inefficient system as water pressure rises (effective pressure falls) as more water enters the system. This option has the advantage that water is not allowed to build up. GLIMMER has no method to transport basal water.

It is apparent that GLIMMER has a reasonable method to estimate sliding velocities if basal slipperiness is known. A method to calculate basal slipperiness explicitly, ideally from effective pressure, is an obvious potential enhancement to the model.

2.2.3 Basal water

Water input is essential for any subglacial hydrology model. GLIMMER calculates both basal and surface melt rates. GLIMMER has basic basal water depth routines but these are overridden by the HYDRO model.

Surface melt is calculated from interaction with the climate, usually using a positive degree-day model. This is then used as the surface mass balance component of the ice evolution equation, Equation 2.1. GLIMMER has no surface water tracking routines.

Basal melt rate is an important component that needs to be calculated to couple GLIMMER with HYDRO. This will be HYDRO's main source of water. GLIMMER uses basal melt in

simple basal water calculations. Basal water, in turn, is used to calculate the thermal and mechanical basal boundary conditions.

How basal melt interacts with the mechanical basal boundary condition (ie sliding) has already been discussed (Section 1.3.1). Basal melt affects the thermal basal boundary condition by dictating basal temperatures. If water is present then the bed must be at pressure melting point T_{pmp}. If it were higher there would be no ice and if it were lower there would be no water (Hagdorn et al., 2007). If there is no water present then the thermal boundary condition is set equal to the geothermal heat flux (Hagdorn et al., 2007).

Glimmer calculates basal melt by solving the heat balance equation when the bed is at pressure melting point. Otherwise, the basal melt rate is automatically set to zero. Basal melt rate M is calculated by looking at the difference between the incoming, H_i, and outgoing, H_o, heat fluxes. Any excess heat is used to melt the ice as opposed to raise ice temperatures further. The equation for M is

$$M = \frac{H_o - H_i}{\rho_i \mathcal{H}} \tag{2.5}$$

where $\mathcal{H}$ is the specific latent heat of fusion,

$$H_o = H_{\text{outgoing}} = -k_{\text{ice}} \left.\frac{\partial T}{\partial z}\right|_{z=h}, \tag{2.6}$$

and

$$H_i = H_{\text{incoming}} = -k_{\text{rock}} \left.\frac{\partial T}{\partial z}\right|_{z=h} + \boldsymbol{v}_b \cdot \boldsymbol{\tau}_b + \begin{cases} \rho_i M/\mathcal{H} & \text{when } M < 0 \\ 0 & \text{otherwise} \end{cases}. \tag{2.7}$$

Positive M is defined as melt. Heat is lost into the ice above the ice-bed interface; this flux is determined by the temperature gradient at the interface. The temperature gradient, in turn, is calculated from Equation 2.3. The incoming heat flux consists of geothermal heat (first term of Equation 2.7), frictional heat (second term), and the latent heat released by melting ice (third term).

Basal water depth is approximated from the basal melt rate. Basal water depth affects the sliding rates calculated by Glimmer in certain run-time configurations. It has no further effect on any other part of the model. When coupled with Hydro, all of these options are overridden and the basal water depth is supplied by Hydro. Because of this, the

implementation of how basal water is calculated by GLIMMER by default is not discussed in detail.

The basal water tracking algorithms in GLIMMER are very basic. Most do not allow for any movement of water, but simply remove a set percentage or set amount over time without any further explanation to simulate water loss from flow. There is a basic flow calculation where water is driven by the hydrostatic gradient at a constant rate. Only basal water depth is traced, not water pressure. Further details about these algorithms are found in Rutt et al. (2009).

2.2.4 Climate drivers

The ice dynamics module in GLIMMER is driven by a climate module. The role of the climate module is to determine the surface mass balance, B, used in Equation 2.1. The surface mass balance determines where new ice forms and also where surface ice is lost, thereby controlling the size and evolution of the ice sheet. Climate is parametrised by a range of methods ranging from accurate data from the recent past to mathematical abstraction. A number of climate modules come with GLIMMER and others can be easily coupled to the model. Three climate drivers, of increasing complexity, are used in this thesis: EISMINT, Edinburgh Ice Sheet (EIS), and GLINT.

Eismint

When developing models, it is important to be able to gain faith that the model is behaving as expected. This is impossible with complex geometries and climates. To remedy the situation, the ice sheet modelling community uses a series of model intercomparison experiments with simple climates and topographies. There are standard results for these experiments. When modifying GLIMMER and validating GLIMMER-HYDRO these predefined model runs will be used to understand how the new changes or the coupled model is behaving.

From 1996 onwards the European Ice Sheet Model INiTiative (EISMINT) intercomparison experiments were run (Huybrechts and Payne, 1996). The experiments generally used simple climate drivers and topographies that could be solved analytically. There were three levels of complexity to the experiments: EISMINT-1, -2 and -3. At each level a number of different experiments were run. For details of the set-up of EISMINT-2 see Payne et al. (2000); for

details of the set-up of EISMINT-3 see Ritz (1997). EISMINT-1 experiments are not discussed as they are not used in this project.

EISMINT-2 uses a radially symmetric climate resulting in a circular ice sheet. The margin of the ice can either be fixed or moving. The EISMINT-2 climate is parametrised to be radially symmetric:

$$B(x,y) = \min\left[B_{\max}, S_B\left(E - \sqrt{\left[(x-\hat{x})^2 + (y-\hat{y})^2\right]}\right)\right] \tag{2.8}$$

$$T(x,y) = T_{\min} + S_T\sqrt{\left[(x-\hat{x})^2 + (y-\hat{y})^2\right]} \tag{2.9}$$

where B is the ice accumulation or ablation rate, $B_{\max}$ is the maximum specified B, S_B is the gradient of accumulation rate change, S_T is the gradient of temperature rate change and $(\hat{x},\hat{y})$ is the centre of the circular ice sheet. E is the radial distance from the centre at which accumulation is zero.

Experiment H of EISMINT-2 is used for testing GLIMMER-HYDRO. This experiment allows basal sliding and therefore the testing of how HYDRO affects GLIMMER's dynamics. In experiment H sliding is parametrised as (Payne et al., 2000)

$$\boldsymbol{v}_i(h) = \begin{cases} -\mathcal{B}\rho_i g h \frac{\partial s}{\partial i} & \text{if} \quad T(h) = T_{\text{pmp}} \\ 0 & \text{if} \quad T(h) < T_{\text{pmp}} \end{cases}, \; i = x, y \tag{2.10}$$

where $\mathcal{B}$ is a free parameter, ρ_i is ice density, g is acceleration due to gravity, h is ice thickness, s is ice surface elevation, and T_{pmp} is the pressure melting point of the ice.

The standard topography for an EISMINT-2 run can either be a flat bed, mounds or a single trough, Figure 2.1. Hulton and Mineter (2000) and Jamieson et al. (2008) find that a slightly rough bed removes dependence on the numerical grid when the topography is flat. Therefore, in this project the standard EISMINT-2 topographies have been modified by the addition of white noise with a uniform distribution between -1 and 1 m. All EISMINT-2 runs in this work will have this roughness.

The EISMINT-3 experiment set models the Greenland ice sheet, which cannot be solved analytically. EISMINT-3 is not used in this thesis in preference to the more complicated EIS and GLINT drivers, which offer better control of the climate.

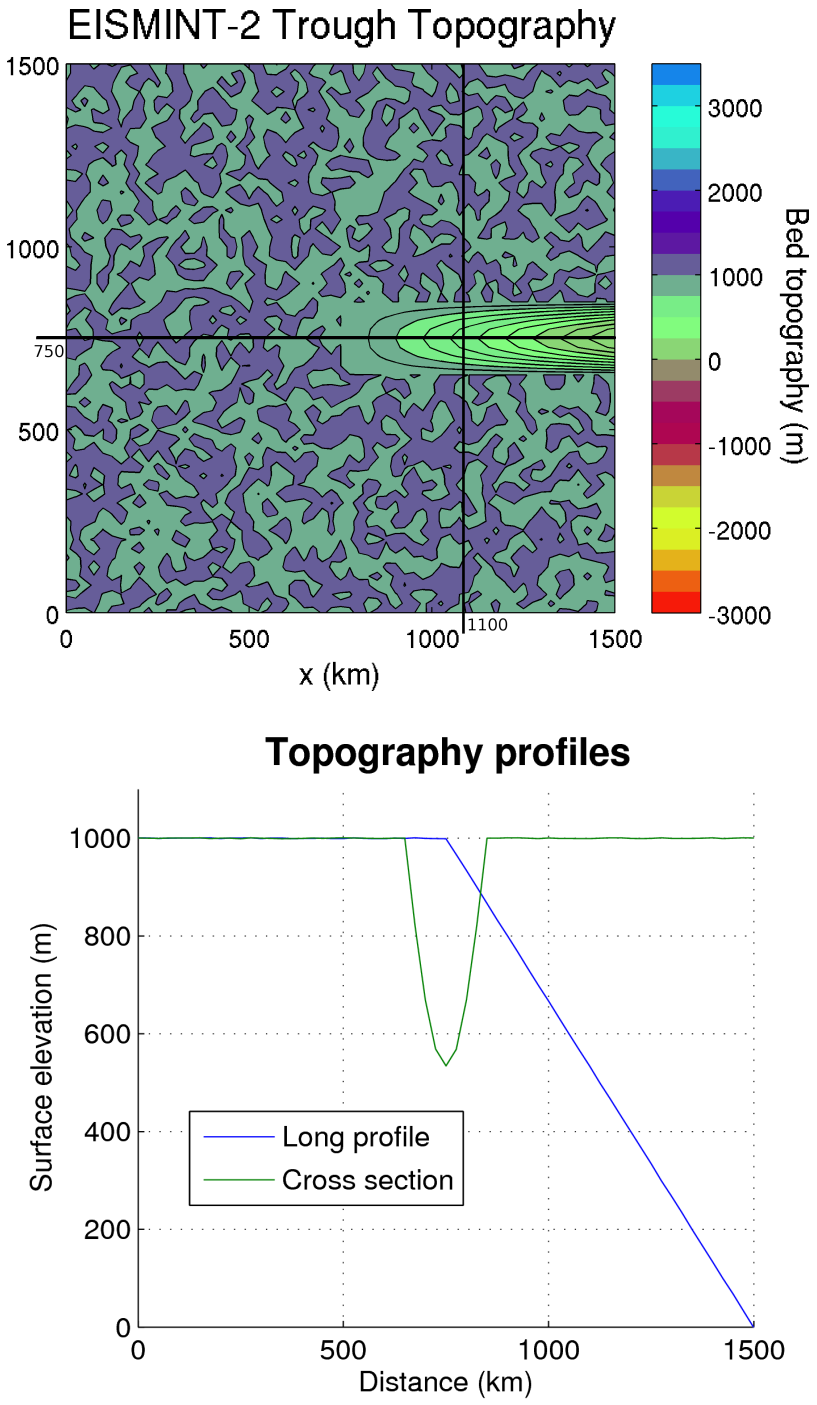

Figure 2.1 (a) Eismint trough topography, marking transect locations (b) Topography profile along transects. There are three standard topographies defined for the EISMINT-2 experiments. Of these, this thesis uses the trough. This is defined as a 1000 m plateau with a parabolic cross-section and linear long-profile, 0 m at its lowest point. A random ± 1 m variation is applied to the topography to increase stability (following Hulton and Mineter, 2000; Jamieson et al., 2008).

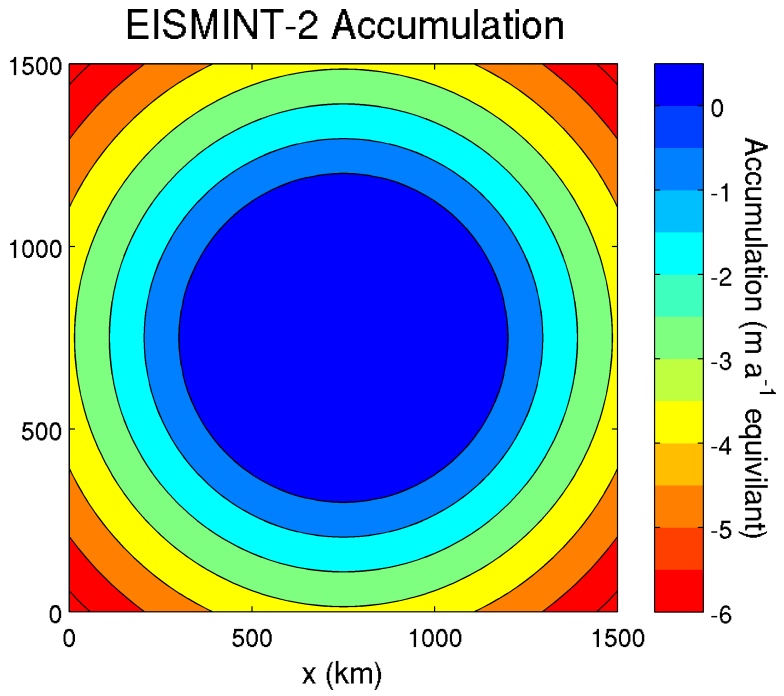

Figure 2.2 The EISMINT-2 climate is parametrised to produce a radially-symmetric climate, Equation 2.8. This thesis uses maximum mass balance $B = 0.5\,\mathrm{m\,a^{-1}}$ to produce the accumulation pattern mapped.

Edinburgh Ice Sheet

EISMINT is useful for model verification, but it is hard, if not impossible, to use it for useful experiments involving real ice sheets. A step up in complexity is to define climate based on latitude, longitude and altitude. All of these can still be defined mathematically, but they can also be used to simulate past, present and future ice sheets.

The Edinburgh Ice Sheet climate driver (EIS) is based on the parametrisation of the equilibrium line altitude (ELA) (Hagdorn, 2003). It is an established driver that has been used to model the Antarctic (eg Jamieson, 2008; Jamieson et al., 2010), Feno-Scandanavian (eg Boulton et al., 1995b; Hagdorn, 2003), and the Patagonian (eg Hulton and Sugden, 1995, 1997) ice sheets. In this work, the EIS driver is used to simulate seasonal variation of the Greenland ice sheet for investigating the effect of surface ponding.

The ELA is defined as the elevation at which there is no overall accumulation or ablation of the ice surface, as measured relative to the old surface over the course of a year. The ELA is usually seen as a function of: temperature, precipitation, latitude, continentality, and elevation (Benn and Evans, 2010). In transient states, the ELA is a proxy of the mass balance

of an ice sheet. The lower the ELA is, the larger the area of accumulation so the higher the chance that the overall mass balance will be positive. In steady states, by definition, the mass balance will be zero as the ice sheet will be in equilibrium with its environment.

The EIS parametrises the ELA s_{ELA} based on latitude λ, longitude Λ, and time t,

$$s_{\text{ELA}} = a_0 + a_1\lambda + a_2\lambda^2 + \Delta s_{\text{ELA}}(t, \Lambda) \; . \tag{2.11}$$

This is used to calculate mass balance B,

$$B = \begin{cases} 2B_{\max}\left(s^*/s_{\max}\right) - B_{\max}\left(s^*/s_{\max}\right)^2 & \text{for} \quad s^* \leqslant s_{\max} \\ B_{\max} & \text{for} \quad s^* > s_{\max} \end{cases} \; , \tag{2.12}$$

where $s^* = s - s_{\text{ELA}}$ is the vertical distance above the ELA. Temperature is also defined to depend on latitude. This is parametrised as an exponential function

$$T(t) = \flat_0 + \flat_1 \exp\left(\flat_2\left(\lambda - \lambda_0\right)\right) \; . \tag{2.13}$$

The time dependence and the coefficients a_i and $\flat_i$ are defined by the user at run time. The EIS driver can account for continentality if required but this is not used in this thesis. See Hagdorn (2003) and Hagdorn et al. (2007) for further details of the EIS driver.

Glint

There are high quality climate data available to drive ice sheet models. Two sources of this climate data are measurements from global instruments over the past few decades and modern Global Circulation Models, GCMs. Both of these data sources can be used to drive GLIMMER (Rutt et al., 2009).

GLINT is a module of GLIMMER that provides an interface between GCMs and the ice sheet model (Hagdorn et al., 2007). GLINT can take the temporally high resolution output of a GCM, or real global data, and use it to drive the climate in GLIMMER. GLINT requires the input of a temperature field and precipitation field from a GCM. This can either be local values for the latitude and longitude range that GLIMMER is working with or the global fields.

GCMs typically have a resolution of around $5^\circ \times 5^\circ$, resulting in 12 grid cells covering

Greenland while GLIMMER usually operates at a much finer $20 \times 20\,\mathrm{km}^2$ ($\sim 4\,000$ cells) or $10 \times 10\,\mathrm{km}^2$ ($\sim 16\,000$ cells) resolution. Because GLINT's typical input and output is much coarser than GLIMMER's, GLINT needs to interpolate the data taking into account the effects of the ice sheet on local climate, continentality, and orographic effects (Hagdorn et al., 2007).

The integral of precipitation over the finer grid is equal to the original GLINT input. Higher cells on the finer grid have more precipitation than lower cells. A problem with this method is that if the higher cells are, in reality, drier then ice can easily grow in areas that are in fact arid (D. Sugden, P. Comm., August 2008). Some other ice sheet models also expand present day ice on these mountains (eg Greve and Otsu, 2007).

2.2.5 Summary

In summary, GLIMMER is a fully thermomechanical ice sheet model that currently uses the shallow ice approximation (SIA). Within this scope, it handles internal ice and temperature evolution well and the model accounts for a number of complex interactions between different processes. There are a variety of climate drivers available and each is suited for a different purpose.

Basal sliding is handled by proxy and, as released, is not linked to basal hydrology. At best, basal melt rate is used as a proxy but this does not directly equate to effective pressure. Also, sliding friction, a major heat source, is handled in a very simplistic manner, common to many ice sheet models. It is defined to increase linearly with sliding velocity. This is not realistic because if extra water drives faster sliding, then this extra water will also reduce the perceived roughness of the bed and so reduce frictional heat generation.

The main advantage of GLIMMER is that the code is continually developing and the model is easily extendible by third parties. Sliding is parametrised in a useful way so once effective pressure data are available, linking these to sliding will fit within GLIMMER's current framework. The following section introduces the modification needed to make GLIMMER a suitable choice for coupling with the basal hydrology model HYDRO. The combined model will then be suitable to meet the objectives of this thesis: understanding basal boundary conditions due to hydrology and investigate Greenland's dynamic response.

2.3 Modifications to Glimmer

The rationale behind the Glimmer-Hydro project is to modify Glimmer as little as possible to enable it to couple with Hydro. Glimmer has a number of limitations which must be addressed before this coupling can take place. The modifications now described are not part of the standard Glimmer distribution; they have been created specifically for this project.

The two modifications are: a function to calculate basal slipperiness based on effective pressure and a function to calculate frictional heat from sliding based on effective pressure. Both modifications are enabled at run time and the model can still run as before if desired. These two functions will enable the Glimmer-Hydro model to meet the objectives of this thesis. The modifications to Glimmer are written to a generic interface so they can be used with any model that supplies effective pressure data. Previously, Glimmer did not consider effective pressure except through the proxies of basal water and basal melt rate.

2.3.1 Sliding laws and basal slipperiness

Glimmer has no method to calculate effective pressure explicitly, but knowing effective pressure will enable basal slipperiness to be calculated from a more realistic proxy than, for example, basal melt rate. This will improve Glimmer's calculated sliding velocities and introduce the physics needed to model a dynamic response to surface melt. This is one of the key benefits of having a hydrology model that can calculate effective pressure.

To enable coupling in Glimmer-Hydro, two new effective pressure variables are added to Glimmer: effective pressure and normalised effective pressure. These values are supplied by an external model, in this case Hydro. Effective pressure is useful for result interpretation and is one of the variables Glimmer can now output. Normalised effective pressure is useful for calculations because we are usually interested in how close the ice is to floating, not the actual value of the pressure. I define normalised effective pressure at a location (x, y) as

$$\bar{N}(x, y) = \frac{N(x, y)}{\rho_i g h(x, y)} \tag{2.14}$$

where N is the effective pressure and $\rho_i g h$ is the localised pressure of grounded ice on the bed. If the ice is entirely grounded $\bar{N} = 1$; if the ice is entirely floating $\bar{N} = 0$. $\bar{N}$ is unitless and must be within the range $[0, 1]$.

If GLIMMER is asked to use effective pressure and it is not supplied then it is set to be maximum; the ice is considered fully grounded. A new subroutine calculates basal slipperiness from effective pressure. The rest of the code is modified to accept basal slipperiness directly from an external model if desired.

The following two options are added to the basal slipperiness list introduced in Section 2.2.2:

6. set by external model

7. proportional to effective pressure

Option 6 simply lets an external model calculate and set basal slipperiness. GLIMMER uses this value but does not concern itself with how it has been obtained. The external model needs to supply its own routines to calculate basal slipperiness. The advantage of this is that the developer of the external model does not have to modify GLIMMER's code if they do not agree with GLIMMER's supplied basal slipperiness calculations.

Because GLIMMER now has access to effective pressure data, it makes sense to introduce a subroutine which enables it to calculate basal slipperiness from them. Option 7 provides this functionality. GLIMMER calculates basal slipperiness using

$$t_s = \begin{cases} t_{s\max}\left(1-\bar{N}\right)^{\gamma} & \text{for} \quad \bar{N} < 1 \\ t_{s\max} & \text{for} \quad \bar{N} = 1 \end{cases} \tag{2.15}$$

where $t_{s\max}$ and γ are supplied by the user at run time. Figure 2.3 shows the effect γ has on the scaling. When γ is small, there is a fast response in basal slipperiness for high effective pressures. Conversely, when γ is large, there is a delayed response in basal slipperiness. Physically, a delayed response could be because protrusions at the bed are a signifiant source of basal resistance and water has to build up before these are overcome noteciablly.

Another advantage of knowing effective pressure is that frictional heat from sliding can be calculated more accurately; this is the focus of the next subsection.

2.3.2 Frictional heat generation from sliding

An important process to consider in an ice sheet model, is friction generating extra melt from sliding over a rough bed and the interaction of this with basal hydrology. This can

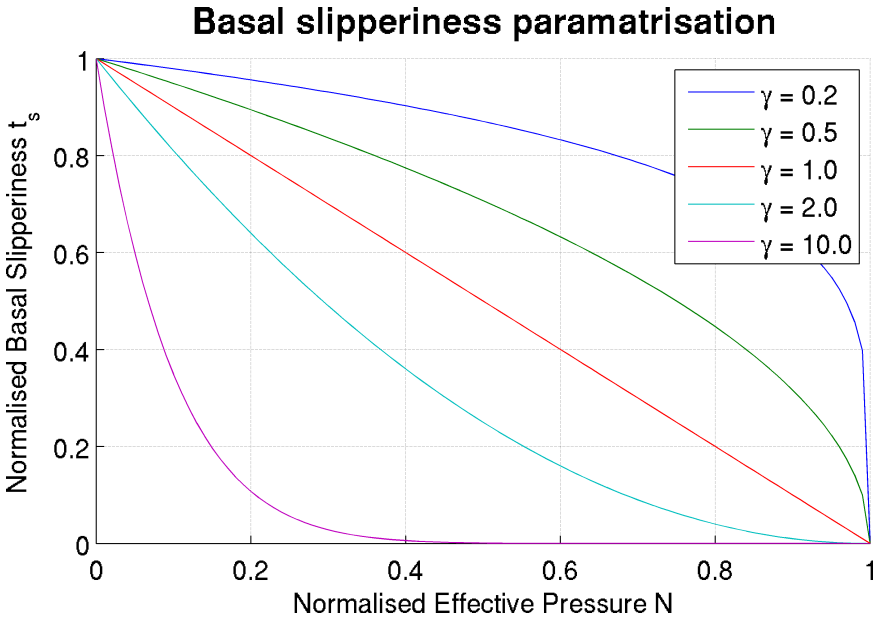

Figure 2.3 The sliding velocity depends on the basal traction which can be calculated from effective pressure using Equation 2.15. The scaling changes depending on whether $0 < \gamma < 1$, $\gamma = 1$ or $\gamma > 1$.

When γ is small, there is a fast response in basal slipperiness for high effective pressures. Conversely, when γ is large, there is a delayed response in basal slipperiness. Physically, a delayed response could be because protrusions at the bed are a signifiant source of basal resistance and water has to build up before these are overcome noteciablly.

potentially lead to feedback mechanisms where the extra melt increases subglacial water pressure which reduces friction, which then reduces the extra melt from friction. As most sliding laws incorporate effective pressure, sliding velocities are affected which in turn also affects the extra melt due to friction, completing the loop. Where ice flows quickly, such as in the major ice streams that drain the Greenland ice sheet, this effect may potentially be very important.

Currently Glimmer does not take effective pressure, and thus the associated reduction in friction, into account when calculating the frictional heat term. The calculation is simply based on ice velocity and basal shear stress using the second term of Equation 2.7: $\boldsymbol{v}_b \cdot \boldsymbol{\tau}_b$. When effective pressure is included in Glimmer's calculations, this term will be ignored and a replacement heat term used. This new heat term is now derived from first principles.

1d Derivation

Many factors affect the feedback between friction and melt. Whether the subglacial environment is hard or soft affects the amount of resistance, and hence heat, the bed can provide. The roughness of the bed affects how the coefficient of friction scales with effective pressure. The subglacial hydrological regime, such as efficient or inefficient flow, determines how extra water from frictional melting affects the rest of the system. The bed topography and the force-balance of the system must also be considered.

The coupled system can be modelled using four equations:

$$\boldsymbol{v}_b = \mathrm{f}_1(N), \quad N = \mathrm{f}_2(H), \quad H_f = \mathrm{f}_3(\boldsymbol{v}_b, \mu), \quad \mu = \mathrm{f}_4(N). \tag{2.16}$$

$\boldsymbol{v}_b = \mathrm{f}_1(N)$ is simply a sliding law based on effective pressure N, where $\boldsymbol{v}_b$ is basal sliding velocity. $N = \mathrm{f}_2(H)$ calculates the effective pressure from the heat flux H. HYDRO is responsible for the solution of this equation using melt input from GLIMMER. Finally, $H_f = \mathrm{f}_3(\boldsymbol{v}_b, \mathrm{f}_4)$ and $\mu = \mathrm{f}_4(N)$ are the friction-dependent portion of the coupling. These equations calculate the frictional heat flux from basal sliding velocities and effective pressure.

To get a first-order approximation for $H_f = \mathrm{f}_3(\boldsymbol{v}_b, \mathrm{f}_4)$, a number of simplifications need to be made. Let us assume the forces are in balance so there is no acceleration of the ice. This is an approximation often used in ice sheet models due to the slow velocities of ice (Van der Veen, 1999). Let us also assume that the bed is reasonably smooth locally so that the coefficient of friction scales directly with effective pressure. When effective pressure is maximum (water pressure is minimum), the friction is maximum. When there is no effective pressure (water pressure is equal to ice overburden pressure), the friction is minimal due to residual bumps touching the ice in places across the model grid square.

The basal shear stress of a column of ice is approximated by $\mathfrak{f} = mg \sin \theta_s$ where m is the mass of the ice column, g is the acceleration due to gravity, and θ_s is the ice surface gradient (Hooke, 2005). As the forces are assumed to be balanced the resistive forces acting on the column of ice must equal the driving stress. If the overly-simplistic assumption is made that all the energy dissipated by these resistive forces is lost as heat at the bed then an upper bound on the extra heat flux at the bed is calculated. Figure 2.4 shows a schematic of this set-up.

The conservation of energy is used to calculate the frictional heat flux. The change in

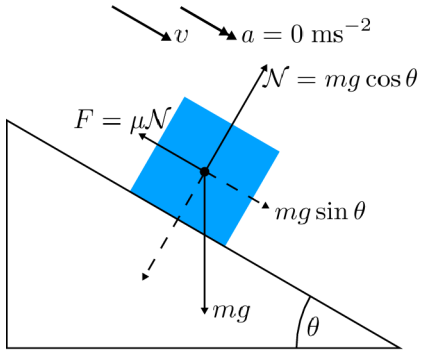

Figure 2.4 A column of ice is sliding over an idealised rough surface of gradient θ_b. The coefficient of friction is μ. The column is in force balance when all the forces acting on it are equal. The resistive forces are assumed to be entirely frictional and equal to the driving stress; there is no acceleration. It is further assumed that all the energy dissipated by friction is available for heating, giving an upper bound for the frictional heat flux.

kinetic energy that would result if the friction were removed is the amount of energy that must be dissipated from the system for the acceleration to remain zero. As we are assuming that all this energy is available as heat at the bed, this change in kinetic energy ΔE_k is equal to the frictional heat over a time t.

$$\begin{aligned}
\Delta E_k(t) &= E_{k_{\text{final}}} - E_{k_{\text{initial}}} && (2.17)\\
&= \frac{1}{2}m\left(\boldsymbol{v}_f^2 - \boldsymbol{v}_i^2\right) && (2.18)\\
&= \frac{1}{2}m\left(\left(\boldsymbol{v}_i + \frac{\mathfrak{f}}{m}t\right)^2 - \boldsymbol{v}_i^2\right) && (2.19)\\
&= \frac{1}{2}m\left(\boldsymbol{v}_i^2 + 2\boldsymbol{v}_i\frac{\mathfrak{f}}{m}t + \frac{\mathfrak{f}^2}{m^2}t^2 - \boldsymbol{v}_i^2\right) && (2.20)\\
&= \boldsymbol{v}_i\mathfrak{f}t + \frac{1}{2}\frac{\mathfrak{f}^2}{m}t^2 && (2.21)
\end{aligned}$$

To get the frictional heat flux H_f in $\mathrm{W\,m^{-2}}$, as opposed to the energy in J, we need to take the time derivative of Equation 2.21 per unit area a.

$$H_f = \frac{1}{a}\frac{\partial}{\partial t}\Delta E_k(t) = \frac{1}{a}\left(\boldsymbol{v}_i\mathfrak{f} + \frac{\mathfrak{f}^2}{m}t\right) \qquad (2.22)$$

$\mathfrak{f}$ has the same magnitude as the frictional force F and causes the acceleration of the ice when friction is removed. However, there is friction so Equation 2.22 is only of interest at time $t = 0$. This is the rate at which energy is being dissipated from the system per unit

area to prevent the ice accelerating.

$$H_f = \frac{1}{a}\frac{\partial \Delta E_k(t=0)}{\partial t} = \frac{\boldsymbol{v}_i \mathfrak{f}}{a} \tag{2.23}$$

The frictional force F, illustrated in Figure 2.4, is usually taken to be the normal force on the bed $\mathcal{N}$ times the coefficient of friction μ. As this normal force reduces with larger water pressures at the ice–bed interface the friction is defined as

$$F = \mathrm{f}_4(N)\mathcal{N} = \bar{N}\mu_{\max} mg\cos\theta_b \ . \tag{2.24}$$

The function $\mu = \mathrm{f}_4(N)$ determines how friction scales with effective pressure. The simplest case, used in this example, is to define $\mathrm{f}_4(N) = \mu_{\max}\bar{N}$ where $\bar{N}$ is the normalised effective pressure. When $\bar{N} = 1$ the ice is fully grounded and therefore experiencing maximum friction $\mu_{\max}$. When $\bar{N} = 0$ the water pressure equals the ice overburden pressure and so is only experiencing residual friction from bedrock protrusions over the grid cell. Numerically, the effective pressure is normalised for each grid square individually.

$\cos\theta_b$ is present because the friction should be a maximum when the bed is horizontal because the load on the bed is a maximum. If the traditional driving stresses at the bed are used to calculate friction, as Glimmer does by default[5], then friction will not be a function of the normal force at the bed and so will not depend on the bed angle. I argue that a flat bed is when the most heat from friction is generated for a given velocity if the effects of water pressure are, temporarily, ignored.

For Glimmer it makes sense to couple the coefficient of friction μ with the basal slipperiness t_s introduced in Section 2.2.2. To do this, a maximum coefficient of friction $\mu_{\max}$ and the residual coefficient of friction μ_0 are defined by the user. μ is then scaled as

$$\mu = (\mu_{\max} - \mu_0)\left(1 - \frac{t_s}{t_{s\max}}\right) + \mu_0. \tag{2.25}$$

If basal slipperiness t_s is scaled using effective pressure N, as in Equation 2.15, then the basal slipperiness terms cancel giving

$$\mu = \mathrm{f}_4(N) = (\mu_{\max} - \mu_0)\left(1 - \left(1 - \bar{N}\right)^{\gamma}\right) + \mu_0. \tag{2.26}$$

[5] By default Glimmer calculates sliding friction as $\boldsymbol{\tau}_b \cdot \boldsymbol{v}_b = mg\sin\theta_s \cdot \boldsymbol{v}_b$.

When effective pressure is minimum, and therefore sliding is maximum, the coefficient of friction experienced by the ice is a minimum. In this project, $\mu_0 = 0$ is used for simplicity but on the scale that HYDRO operates at it will not be zero in reality due to basal undulation touching the ice even if water pressure is at ice overburden pressure.

Combining Equations 2.23, 2.24, 2.26 and mass $m = \rho_i a h$ gives

$$\begin{aligned} H_f &= \boldsymbol{v}_i \mu \left(\bar{N}, \gamma\right) \rho_i g h \cos\theta_b \\ &= \boldsymbol{v}_i \mu_{\max} \left(1 - \left(1 - \bar{N}\right)^{\gamma}\right) \rho_i g h \cos\theta_b \end{aligned} \tag{2.27}$$

where h is the thickness of the ice column. Note that this equation has the same units as the standard $\boldsymbol{\tau}_b \cdot \boldsymbol{v}_b$ used in GLIMMER as released. The differences are the dimensionless μ term and the replacement of $\sin\theta_s$ with $\cos\theta_b$. For the small gradients typically associated with ice sheets, the scaling of $\mu\cos\theta_b$ keeps the equation roughly at the same order of magnitude as $\sin\theta_s$. The processes involved in the calculation are, however, different so the equation will produce spatially different results to GLIMMER's default behaviour.

The derivation so far assumes that all resistive forces are frictional and so Equation 2.27 actually calculates the upper bound on frictional heat flux. As GLIMMER does not have higher-order physics, it is difficult to know how large the other resistive forces are. This situation is improved by defining a scaling factor β, in the range $[0, 1]$, so that Equation 2.27 becomes

$$H_f = \beta \boldsymbol{v}_i \mu_{\max} \left(1 - \left(1 - \bar{N}\right)^{\gamma}\right) \rho_i g h \cos\theta_b \,. \tag{2.28}$$

β is either explicitly set by the user or, when higher order physics become available, can be calculated from longitudinal forces and lateral shear stress.

2d Derivation

When this problem is solved in two dimensions, an extra step needs to be added to the derivation. We must consider the magnitude of the gradient. In other words, friction is independent of the flow direction. The reason for this is that frictional force is a function of the normal force on the ice and the coefficient of friction, which is a scalar. The normal force is the same whether the ice is flowing down the steepest slope or perpendicular to it along a contour line.

If the bed elevation is given by a function $b = \mathrm{f}(x, y)$ then the magnitude of the gradient is given by

$$|\boldsymbol{\nabla}\mathrm{f}(x,y)| = \left(\frac{\partial^2}{\partial x^2}\mathrm{f}(x,y) + \frac{\partial^2}{\partial y^2}\mathrm{f}(x,y)\right)^{\frac{1}{2}}. \tag{2.29}$$

Equation 2.27 is a function of θ_b; θ_b is given by

$$\theta_b = \arctan(|\boldsymbol{\nabla}\mathrm{f}(x,y)|). \tag{2.30}$$

The assumption used in Section 2.3.2 regarding the force balance still holds. If the ice is flowing parallel to the contour line, then this is the same as a flat bed. As the ice is assumed to be flowing at a constant velocity, as compared to the time scales involved for this effect, there must be a driving stress that is equal to the resistive forces. The remainder of the derivation is the same.

Implementation

The implementation of the new frictional heat term in the GLIMMER code must be discussed because there is no other documentation of the changes. Minimal changes have been made to GLIMMER to introduce the frictional heat flux calculation: GLIMMER has a basic friction term that does not rely on effective pressure which needs to be disabled; the new term needs to be calculated; the new term needs to be introduced into the existing equations. In this discussion, it is assumed that effective pressure data are available.

Many features in GLIMMER are controlled at run time through configuration files. The new frictional heat flux calculation is no exception. Depending on the configuration file choice, either the old frictional heat term or the new one is used. If the new one is used and there is no effective pressure data then the effective pressure is assumed to be maximum.

The frictional heat flux term is calculated in the new subroutine `calc_fheatflx` in `glide_temp.F90`. This subroutine is only called from `glide_temp.F90` and only if an appropriate configuration option is selected. It solves Equation 2.28 and saves the effective coefficient of friction (Equation 2.25) and the heat flux H_f to the `friction` and `fheatflx` variables defined in `glide_types.F90`. If frictional heat flux is not calculated then the two new variables are set to zero everywhere. Both new variables are defined on the regular,

non-staggered, grid[6].

Frictional heat flux and basal heat flux have the same units, $\mathrm{W\,m^{-2}}$. Both heat fluxes act on the same boundary and so the ice sheet cannot tell where the heat is coming from. The logical way to introduce the new frictional heat flux term into the equations is to add it to basal heat flux. In `glide_temp.F90`, `bheatflx` has been replaced with `(bheatflx + fheatflx)` whenever it is used. As `fheatflx` $= 0$ by default, the model runs as before if the old heat term is used.

2.4 Subglacial hydrology modelling

I now review methods for modelling subglacial hydrology. The aim is to highlight the possible approaches to developing a new model. Model scale is very important in ice sheet modelling because it defines some of the assumptions needed and the DEM data available. The detail and realism at which processes are modelled are also highly dependent on scale.

The first focus is the valley-glacier scale to show what is possible in subglacial hydrological modelling. Next, I look at the ice sheet scale and give examples of the generalisations that must be made and the general approaches taken at this scale. One aim is to highlight the current level of subglacial hydrology incorporation in contemporary models. Finally, I begin to discuss the approach used in this project.

2.4.1 Valley-glacier scale

Valley-scale models tend to be able to capture more interacting processes and realism due to the limited size of the domain and the availability of high-resolution input data. The approaches range from abstract, theoretical models to highly-detailed realistic models.

Iken (1981) models the effect of subglacial water pressure on sliding for an idealised glacier with a wavy bed. Iken defines the bed as a mathematical function and defines the governing equations of the cavity system, which she solves for water pressure using an idealised numerical model. The aim is to investigate generic basal processes and the model is not, in fact cannot be, glacier specific.

[6] GLIMMER uses two grids, staggered by half a grid square, for its calculations. This is for stability. Ice thickness and associated variables are on one grid; velocity and associated variables are on the other. See Rutt et al. (2009) for more details.

A clever, semi-abstract representation of the subglacial system is defined by Clarke (1996). Clarke models the hydrological system as analogous to an electrical circuit. By using *Lumped-element analysis* it is possible to define the behaviour of individual elements of the system such as: different water sources and sinks, channels, cavities, sheet flow etc. This approach allows a detailed analysis to be made of various hydrological feedbacks. It is hard to apply this method to real glaciers but it is very useful for understanding the feedbacks and resonance in the system.

Flowers and Clarke (2002a) develop an alternate model based on the planar coupling of four independent hydrological systems. These systems are: surface, englacial, subglacial and subsurface hydrology. Governing equations are developed for each system. This model is based on work by Flowers (1994). The equations are initially solved for different idealised valley glacier domains. No ice dynamics feedbacks are included, but could potentially be added in future. This model is also applied to Trapridge Glacier, Canada where it predicts the seasonal evolution of the hydrology well. The entire spring event, from the evolution of an efficient system to its demise, is captured (Flowers and Clarke, 2002b).

Finally, realistic modelling of specific glaciers is also possible. This needs high-resolution data sets and very specific boundary conditions and tuning parameters supplied by field data. Hubbard et al. (1995) and Arnold et al. (1998) use this approach to model the subglacial hydrology of the Haut glacier d'Arolla, Switzerland. They have high resolution bed DEMs and high resolution field data available. The results they produce are impressive for their realism and the detail they capture, but the models are not necessarily transferable from one glacier to another. This approach is good for understanding processes about specific glaciers.

2.4.2 Ice sheet scale

Ice sheet scale models, by their nature, have to make larger assumptions about the system. This section discusses how the effects of hydrology are currently modelled and establishes a baseline for my approach, which is discussed in Sections 2.4.3 and 2.5.

Upscaling models to the larger ice sheet scale is problematic. A high resolution DEM of valley glaciers is often obtainable using ground penetrating radar. This is much harder on the ice-sheet scale. The best bed DEM that is currently available for the entire Greenland ice sheet has a resolution of 5 km (Bamber et al., 2001b), although 1 km DEMs do exist for some

individual basins near the margin and for the surface (Bamber et al., 2001a). Even the 5 km DEM is heavily reliant on interpolation of available data. At a 5 km scale it is meaningless to solve equations for individual channels, of which there may be many with in a model grid square (Alley, 1996).

When working at the ice sheet scale, with the extra unknowns that this entails, assumptions have to be made or the domain made simpler. Common approaches are to model either specific processes (eg Alley, 1996); specific basins (eg Breemer et al., 2002; Ahlstrøm et al., 2005), flow lines (eg Nick et al., 2009), or ice streams (eg Lingle and Brown, 1987); or to use very broad assumptions, such as assuming the entire ice sheet lies on deformable sediment (eg Shoemaker, 1986). It is simply not possible to know what is happening at the bed near the centre of the Greenland ice sheet, except for a few point observations at drill sites. Marshall (2005) reviews recent subglacial ice-sheet hydrology models.

Flow lines

Flow lines allow detailed modelling of specific glaciers or processes without a large computational cost. Boulton et al. (1995a) and Boulton et al. (1996) use a one-dimensional flow-line model to predict groundwater flow under the past Feno-Scandinavian ice sheet. Their model is based on the assumption that on a large scale, the bedrock underneath the ice sheet is permeable enough to allow ground water flow. With this assumption, they find that subglacial water pressures remain low because water can evacuate through the bed rock. No ice dynamics is modelled.

Nick et al. (2009) apply a one-dimensional flow line model to the Helheim glacier in eastern Greenland. The flow line stretches from the ice divide, along the outlet glacier, to its terminus. This model is defined to linearly increase basal slipperiness towards the margin, starting 15 km upglacier. This acts as a proxy for basal hydrology in order to investigate its effects on dynamics but it does not model the hydrology explicitly. This approach does not help us understand the basal processes responsible for the speedup and a large part of the results are dependent on the model formation.

Surface draining lakes have a large influence on ice dynamics. This is modelled by Parizek and Alley (2004) in a thermomechanical flow line model which includes a basic basal hydrology component[7]. Their model contains a basal slipperiness parameter that is defined

[7] The Parizek and Alley (2004) model is discussed further in Section 5.3.3.

as a function of basal water injection. This study tunes the model to fit Zwally et al.'s (2002) data but ignores the key subglacial process of hydraulically efficient areas forming, which will change the nature of the response to water injection.

Flow line studies are useful for gaining an understanding of specific glaciers or processes and are relatively simple to implement, but even so the current studies often miss key hydrological processes.

Two-dimensional ice sheets

Lewis and Smith (2009) use a geographic information system to study the subglacial drainage basins of the Greenland ice sheet. The drainage basins depend on both bed topography and ice thickness (Paterson, 1994) and so are non-trivial. This is a broad-scale hydrological assessment and not a study of subglacial processes. From the piezometric surface, based on the Bamber et al. (2001b) DEM, they identify 293 distinct hydrological basins and correlate this with observed outlet locations along the ice sheet perimeter. This study does not explicitly model water flow or pressure and so cannot couple with an ice sheet model.

Johnson and Fastook (2002) couple a subglacial hydrology model with a map-plane finite element model, based on Johnson (2002). They assume that most of the water flows through efficient channels and calculate the effective pressure from the ice velocity. This is the opposite of what this project aims to do. Here, my goal is to calculate effective pressure using a physically-based hydrology model in order to drive ice dynamics instead of determining effective pressure from ice dynamics. Both approaches are useful depending on the aims of the study.

Three-dimensional ice sheet

There are a number of models that couple physically based, two-dimensional ice sheet models to three-dimensional thermomechanical ice sheet models. All of these models need to make broad-scale assumptions of the system they are modelling.

Flowers et al. (2005) simplify the valley glacier model used in Flowers and Clarke (2002a) and apply it to Vatnajökul, Iceland. The simplified model has two coupled hydrology levels, subglacial and subsurface, but no capability to simulate an efficient regime. Unlike their 2002a work, this model includes ice dynamics. Marshall et al. (2005) use this model to attempt to introduce longitudinal stresses into the ice dynamics by perturbing the shallow

ice approximation solution. The hydrology and the dynamics are coupled asynchronously with the assumption that the hydrology regime would remain mostly constant for five year periods. They find that incorporating hydrology increases orographic precipitation feedbacks and thus the sensitivity to climate.

Greve and Otsu (2007) attempt to model the consequences of the speedup mechanism proposed by Zwally et al. (2002). Their model does not include a hydrology model, but in areas they feel subglacial hydrology is important, such as the north-east Greenland ice stream (NEGIS), they artificially increase the bed slipperiness by a factor of three[8]. They also account for surface meltwater reaching the bed by directly coupling the surface melt rate to their basal slipperiness parameter.

Brocq et al. (2009) couple a subglacial hydrology model with GLIMMER and apply this to the Ross Sea sector of the West Antarctic ice sheet. The model is a thin-film flow model which is run both to look at a steady state solution and a time-dependent solution. They couple basal slipperiness, and so ice dynamics, to basal water depth, based on the parametrisation by Budd and Jenssen (1987). The model does not account for hydraulic efficiency, mainly due to the thin water depths (order of mm) involved. I argue for Greenland, where much more water is known to enter the subglacial system (eg Zwally et al., 2002; McMillan et al., 2007; Das et al., 2008) that efficiency is important. In an efficient system water depth is not a good proxy for basal sliding due to the inverse flux relationship described by Kamb (1987). Instead, basal slipperiness should be a function of water pressure.

Arnold and Sharp (2002) develop a good hydrology model to simulate the dynamic response of the palaeo Feno-Scandinavian ice sheet to water, based on an earlier model by Arnold and Sharp (1992). Their model accounts for evolving hydraulic efficiency, warm- and cold-based basal regimes, and surface melt water input if surface melt rates are high. They assume a hard bed and couple sliding to effective pressure. They use a three-dimensional ice sheet model but it is not thermomechanical. They couple frictional heat generation to sliding but do not account for the extra hydraulic lubrication in calculating this term. The model is applied to the Scandinavian ice sheet with a goal of understanding the processes and dynamic feedbacks. The model does not aim for realism. Of the models reviewed, this is the most suited for the current project.

[8] Greve and Otsu (2007) find the NEGIS an important control on Greenland's dynamics after explicitly defining it to be so. This paper did not pass review and was withdrawn because of this circular argument. It is still worth discussing here because it highlights a contemporary approach to modelling subglacial hydrology.

2.4.3 Present approach

One of the aims of this thesis is to understand how basal heat sources and basal water input (from basal melting and surface injection) affect the basal boundary of ice sheets and so the dynamic response of ice sheets. The goal is to make this as physically self-regulating as possible instead of, for example, manually tweaking the basal slipperiness where I deem it is important. The physics of the model should drive the adjustment of basal slipperiness instead, taking into account the evolving basal efficiency, and resultant drop in water pressure, and the influence of a frozen bed. This should enable a true dynamic response of the Greenland ice sheet to be modelled. Of the models reviewed, only Arnold and Sharp (2002), and arguably Brocq et al. (2009), use models with similar capabilities.

My approach, therefore, is to construct a model similar to Arnold and Sharp's (2002) but with some key differences:

1. use a finer grid to improve water routing and resolve troughs under outlet glaciers,
2. couple to a fully thermomechanical ice sheet model for better basal melt rate calculations,
3. link basal hydrology to frictional heat generation (more water should mean less frictional heat) for better basal melt rate calculations and to investigate related feedbacks, and
4. use a ponding algorithm to simulate realistic basal water delivery to study Greenland's dynamic response.

This model will, like all models, have its own limitations but these will be compatible with the goals of this project. The model will be able to run either independently if investigating simple hydrological processes as done by a number of authors above, asynchronously when seasonal evolution isn't important and fully synchronously, as Arnold and Sharp (2002) do, when investigating dynamic feedbacks.

2.5 Hydro subglacial hydrology model

The need for a subglacial hydrology model to couple with existing ice sheet models to better determine subglacial boundary conditions has now been established. Some subglacial

hydrology models exist, but Section 2.4 shows that these do not meet the needs of this project.

HYDRO is developed to provide a basal hydrology component for GLIMMER. The rationale behind HYDRO is to modify GLIMMER as little as possible, by providing a stand-alone hydrology model that couples with it. The advantage of this modular approach is that HYDRO is able to couple easily with other ice sheet models and can be tested and used independently. The coupled model is referred to as GLIMMER-HYDRO. When GLIMMER or HYDRO are referred to individually no coupling is implied.

2.5.1 Hydro conceptualisation

HYDRO models the evolution of subglacial hydraulic pressure through time. I now describe the model conceptually, explain the key assumptions I make, and use this to describe the basic behaviour of the system that results. This is then used as the basis for developing the mathematical model in the remainder of Section 2.5. The numerical solutions of the equations are discussed in Section 2.6.

Assumptions

The model derivation initially assumes that water is flowing through a layer of till sitting on almost impermeable bedrock. This derivation is then developed by using some of the model parameters as a proxy for other subglacial hydrological regimes. The model is based on the coupling between two conservation laws: the conservation of mass and the conservation of momentum. These are two general conservation laws and must hold regardless of the specifics of the system. This is a good starting point, but the specifics of the system, when taken into account, will change the results they produce.

To understand the model conceptually, it is easiest to think of a one dimensional ice sheet. The system I am modelling can be thought of a hose that is filled with till and saturated with water. Along the length of the hose I can inject water at different rates. Each end of the hose is open and water can flow out freely. When the total volume of water injected into the hose matches the volume of water leaving the hose at the end I say the system is in *equilibrium*.

This state can be reached with the hose lying on a flat plane as long as water is being

injected in. Due to the inefficient nature of flow through till, there is resistance to the flow and so water pressure increases as the water flux increases. This water pressure drives the water outwards when the hose is horizontal. As long as the hose is strong enough there is no limit on the water pressure in the hose at this stage; the water pressure at the centre of the hose will be the highest so that a pressure gradient towards the margin exists at equilibrium.

Topography and ice

The next level of complexity that I introduce are the effects of topography and ice overburden pressure. Each is introduced independently of the other before the combined system is considered.

To visualise the effects of topography, simply consider the hose lying on an inclined surface. The ends of the hose are open so water will flow down the hose until it is free of the system. If only a little water is entering the system then the incline of the hose may be enough for the system to be in equilibrium; water pressure will simply be determined by topography and will be zero at the end of the hose. As more water enters the system the incline may not be enough to evacuate all the water so the water pressure in the hose will increase. The total pressure in the hose from this increase and potential gradient from the incline will determine when equilibrium is reached. The increase of water pressure from the flow will be less than the flat case because gravity is doing some of the work.

Next consider the case where the topography is a shallow parabola with the middle of the hose at the lowest point. This is similar to the bed of an ice sheet, where the centre of the bed has depressed due to isostatic adjustment to the weight of the ice. At equilibrium there must be an overall potential gradient outward from the centre. This means the maximum pressure at the centre of the hose must be greater than in the flat scenario to override the topographic potential gradient driving water towards the centre.

Now consider ice overburden pressure. Again, imagine the hose lying on a flat surface. This time, a weight is place near the centre of the hose. This pressurises the water and creates a potential gradient acting outwards. Therefore less water pressure needs to build up inside the hose for equilibrium to be reached. Depending on the weight resting on the hose, some water pressure will be needed, but it is not as high as the flat, no-weight case.

Saturation

There is, however, a large assumption that has been made: the hose is assumed to be saturated with water. If the hose is not saturated the topography will behave the same, but some of the weight placed on the hose will be taken by the till. It will not all go to pressurising the water. In the limit where there is no water, all the weight will be taken by the till. As the water pressure increases it gradually becomes more aware of the weight until the till is fully saturated and the water is supporting all of the weight.

This can be likened to the inclined topography. Instead of a weight, another way to think of ice overburden pressure is the hose with no water lying on the topography. As the hose fills the incline of the surface gradually increases until the hose is saturated. At this stage, the incline of the hose is the incline of the topography plus 0.9 of the ice thickness.

Efficiency

When water flux is large, and so in our so-far-inefficient model water pressure is large, the system typically becomes efficient as discussed in Section 1.3.2. We make the hose efficient by changing the properties of the till to allow water to flow through it more easily. For example, by changing the till from sand to pebbles there is less resistance to flow. In glacial systems, this typically occurs near the ice margin. Therefore if the end of the hose is filled with pebbles instead of sand, the water pressure in its interior can be lower as it only has to drive the water until it reaches the pebbles instead of the end of the hose. We are effectively shortening the length of the hose[9].

Notice that with this set-up we have not made the hose efficient near its ends by introducing channels, but rather by changing the bulk-properties of the till. If the hose were entirely filled with pebbles, the system would still be inefficient and water pressures would build as already discussed. The key process enabling efficiency is the change from one basal system to another.

Practically, the reason for this is because the effects of the efficient bed need to be averaged over what will become a grid cell in the model. These cells are much larger than the size of channels so it is difficult to account for channels directly. Instead, the bulk-effect

[9] Actually, this is an oversimplification. The water pressure is higher than atmospheric pressure at the pebble-sand boundary so water pressure in the interior is higher than if the hose was shorter. However, the water pressure at the boundary is lower than if the hose was only full of sand and so the water pressure at the centre of the hose is also lower.

of the efficient bed is worked into the model to study the processes that result and not the processes that cause the system to be efficient.

Frozen bed

Finally, ice sheets typically have frozen centres due to the advection of cold ice near the ice divide. A frozen bed will not allow the flow of water. This is equivalent to plugging an end of our one-dimensional hose so no water can escape. Now at equilibrium, the highest water pressure will be at the closed end of the hose as there must be an overall potential gradient to the open end. If, however, the hose becomes a two-dimensional plane then the highest water pressure will not necessarily be at the border of the frozen bed as water may be able to flow towards the warm-cold boundary and then along it as the easiest path.

If both ends of the one-dimensional hose are closed then the water pressure in the hose will continue to rise in an unrealistic manner as long as water is being injected. In the numerical model, a warm area completely surrounded by a frozen bed, if it were to exist, would therefore cause instability.

Summary

To summarise, the key outcomes of this conceptual model are:

1. water can control its own flow direction,
2. water experiences ice overburden pressure gradually,
3. water can flow uphill without ice overburden pressure due to its own pressure,
4. water can over-pressurise,
5. changing the diffusivity can act as a proxy for efficiency, and
6. a frozen bed acts as a barrier to water flow and may cause instability.

2.5.2 Coupling with Glimmer

Before describing the specifics of Hydro, I will describe the key model inputs and outputs and how these are dealt with when coupling to Glimmer to form Glimmer-Hydro. Figure 2.5 shows a flow diagram visualising the interaction between the two models.

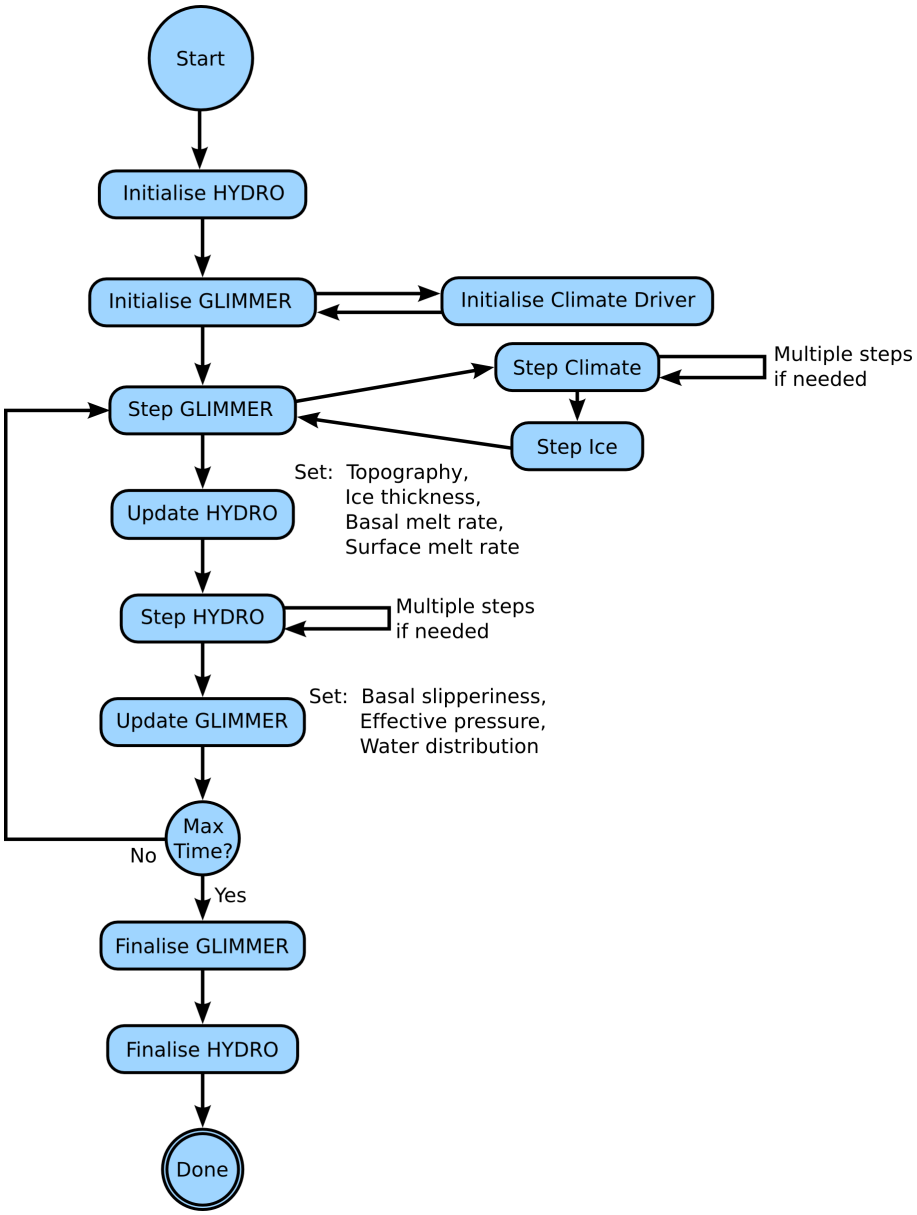

Figure 2.5 The coupling algorithm for GLIMMER-HYDRO. The climate, ice dynamics, and basal hydrology can all use different time steps, ideally an integer factor of each other. For each of GLIMMER's time steps HYDRO gets updated topography, ice thickness, and basal and surface melt rates. GLIMMER gets basal slipperiness, effective pressure, and water distribution from HYDRO. The climate driver used depends on the experiment. Three climate drivers (EISMINT, EIS, and GLINT) are provided with GLIMMER.

As Section 2.3 describes, GLIMMER can now accept effective pressure and basal slipperiness as model inputs to calculate basal sliding and frictional heat flux. HYDRO, in turn, requires: topography, ice thickness, basal melt rate, surface melt rate and basal temperature data. Topography and ice thickness are used to determine potential gradients affecting water flow. Basal and surface melt rates are water sources and basal temperature determines where the bed is frozen.

The two models are coupled asynchronously so that each model does its required iterations before passing its outputs to the next model. HYDRO and GLIMMER can use different time steps. For example, HYDRO may have a time step of one month and GLIMMER may have a time step of one year in the same GLIMMER-HYDRO run. In practice, I use a time step of one month for both in this thesis.

2.5.3 Mathematical basis

The mathematical basis of the model, based on the conceptualisation in Section 2.5.1, is now introduced. Two conservation laws form the core of HYDRO: the conservation of mass and the conservation of momentum. I now introduce the model mathematically, starting with the coupling between these two laws.

The conservation of mass is expressed through the continuity equation. One method of writing this is as conservation of volume in terms of pressure. The equation then becomes:

$$c_T \frac{\partial p}{\partial t} + \boldsymbol{\nabla} \cdot \boldsymbol{q} = \phi. \tag{2.31}$$

c_T is the compressibility with units one over pressure, p is the pressure of water and t is time. $\boldsymbol{\nabla} = (\partial/\partial x, \partial/\partial y)$ is the gradient operator, in this case defined on the Cartesian co-ordinate system. $\boldsymbol{q}$ is the volumetric flux defined as the volume of water through a unit cross-section per unit time (Stauffer, 2006). ϕ is the source term, accounting for water entering and leaving the system away from the ice margin. ϕ accounts for basal melt and freezing and any water input from other sources such as the surface.

Compressibility measures the change in volume V of an aquifer in response to an applied pressure p (Bear, 1988)

$$c_T = -\frac{1}{V}\frac{\partial V}{\partial p}. \tag{2.32}$$

This shows that the first term of Equation 2.31 relates to the change of volume of water in the aquifer with time

$$c_T \frac{\partial p}{\partial t} = -\frac{1}{V}\frac{\partial V}{\partial p}\frac{\partial p}{\partial t} = -\frac{1}{V}\frac{\partial V}{\partial t} \ , \tag{2.33}$$

using the chain rule.

The flux $\boldsymbol{q}$ is calculated using Darcy's law,

$$\boldsymbol{q} = -\frac{K}{\eta}\boldsymbol{\nabla} p, \tag{2.34}$$

which is an expression of the conservation of momentum. K is the hydraulic permeability of the aquifer and η is the dynamic viscosity of water. Experimentally, hydraulic transmissivity $\mathcal{T}$, not permeability K, is traditionally measured in field work (AWWA, 2003).

$$K = \frac{\mathcal{T}\eta}{\rho_w g d} \tag{2.35}$$

relates the transmissivity $\mathcal{T}$ to the permeability K with dimension $[L^2]$ (Bear, 1988). ρ_w is the density of water, g is the acceleration due to gravity and d is the thickness of the aquifer. Permeability is used so a mathematical diffusivity term is produced by the coupling. The quantity $\kappa = \mathcal{T}/d$ is the hydraulic conductivity with dimension $[L/T]$. Note that with its current level of development, HYDRO uses a constant thickness aquifer for the entire ice sheet.

Substituting Darcy's law, Equation 2.34, into the continuity Equation 2.31 completes the coupling.

$$c_T \frac{\partial p}{\partial t} = \frac{K}{\eta}\boldsymbol{\nabla}\cdot\boldsymbol{\nabla} p + \phi \tag{2.36}$$

The negative sign of Darcy's law has been lost because the diffusion term, $\boldsymbol{\nabla}\cdot\boldsymbol{\nabla} p$, has been moved to the right hand side. This equation can be rewritten by dividing through by c_T and by defining

$$D = \frac{K}{c_T \eta} = \frac{\mathcal{T}}{c_T \rho_w g d} \ . \tag{2.37}$$

This gives

$$\frac{\partial p}{\partial t} = D\boldsymbol{\nabla}\cdot\boldsymbol{\nabla} p + \frac{\phi}{c_T}. \tag{2.38}$$

D has dimension $[L^2/T]$ and so can be referred to mathematically as diffusivity (Griffiths and

Smith, 1991). From D, the characteristic time and length of the system can be determined. A perturbation at a given time and location will affect an area $[L^2]$ when a time $[T]$ has passed.

The source term ϕ, which has dimension $[T^{-1}]$, is defined as

$$\phi = \frac{M}{d} \tag{2.39}$$

where M is the water flux entering the system and d is the depth of the aquifer, as before. d is necessary for the dimensions to balance. It controls how quickly the system will respond to a perturbation in M.

2.5.4 Potential gradients

The next level of complexity that needs to be added is potential gradients, from the topography and ice overburden pressure driving flow. As discussed in the model conceptualisation (Section 2.5.1), this will have a large impact on the water pressures calculated. Water flows down the steepest potential gradient and calculating flow direction is an important element of a hydrology model. Before we can measure the potential gradient, a datum must be defined.

The piezometric surface drives the flux $\boldsymbol{q}$. To express this mathematically a few assumptions must be made. A datum surface p_0 is defined in the model to have zero pressure at mean sea-level. In order for the topographic term to have physical meaning, it must be assumed that all the bedrock above sea-level is saturated with water. This bedrock can be assumed to have a very low porosity and transmissivity so in the time scales of the model, the water in the bedrock does not affect the solution (S. Zetsepin, P. Comm., September 2006). Figure 2.6 represents these terms visually.

The piezometric surface is then defined as (Van der Veen, 1999)

$$p_{\text{total}} = p_t = p_0 + \rho_w g b + \rho_i g h + p^*. \tag{2.40}$$

ρ_i is the density of ice, h is the elevation of the ice above the datum, and b is the bed elevation. The expression therefore gives the thickness of ice. p^* is the pressure of the water

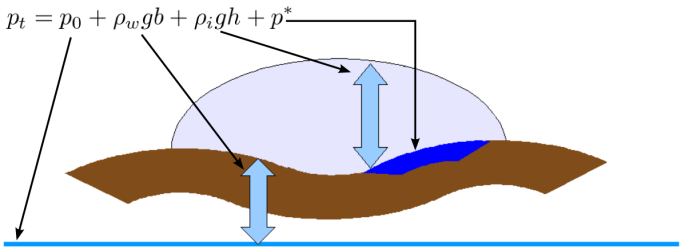

Figure 2.6 Two datums are used to measure pressure. p_0 is used to measure topographic and ice overburden pressure; the sum of p_0 and the two overburden pressures is used to measure the pressure due to Darcian flow, p^*.

at the bottom of the aquifer; it is measured in relation to a second datum surface defined by

$$p_1 = p_0 + \rho_w g b + \rho_i g h. \tag{2.41}$$

p^* is the pressure due to the flow of water through a porous medium. If Darcy's law was solved without any coupling on a flat bed without any ice present, p^* is the pressure that would be calculated. It is caused by water not being able to leave the system freely and is analogous to the inefficient flow regime shown by Kamb in Figure 1.2.

This means that as the water builds up, and thus the water pressure builds up the water can influence its own flow direction. If water builds up in a trough, and p^* increases because of it, then the water will eventually be able to flow against the topographic gradient even if there is no ice overburden pressure. A key concept to understand for this to make sense is that even though the ice overburden pressure is zero, for the sake of discussion, we cannot allow the water to leave the porous medium, by forming a lake for example. It can only flow along the medium.

At this stage, a potential problem must be dealt with before we go further. If p_t is substituted directly into Equation 2.38 then a constraint must be added (solve the equation only where there is water) to keep the equation physical. Otherwise, water is mathematically forced to flow even if there is no water present to flow; this is not a problem when there is no potential gradient acting on the system.

$$\frac{\partial p_t}{\partial t} = \frac{\partial p^*}{\partial t} = D\boldsymbol{\nabla} \cdot \boldsymbol{\nabla} p_t + \frac{\phi}{c_T}, \tag{2.42}$$

as only the p^* term of p_t has time dependence on timescales relevant to HYDRO. However, if $p_t = 0$ for all space initially and $\phi = 0$ for all time and space, ie there is no water present, then $\partial p^*/\partial t = 0$ but $D\boldsymbol{\nabla} \cdot \boldsymbol{\nabla} p_t \neq 0$ but as $\partial p^*/\partial t = D\boldsymbol{\nabla} \cdot \boldsymbol{\nabla} p_t$ there is a contradiction $0 = 1$.

This is resolved by introducing a dimensionless factor, which physically equates to the till saturation discussed in the model conceptualisation (Section 2.5.1)

$$\alpha(p^*) = \begin{cases} 0 & \text{for} \quad p^* \leqslant 0 \\ p^*/\rho_w g d & \text{for} \quad 0 < p^* \leqslant \rho_w g d \\ 1 & \text{for} \quad p^* > \rho_w g d \end{cases} \tag{2.43}$$

where $\rho_w g d$ is the pressure at the bottom of the aquifer just as it reaches saturation. It is measured in relation to the p_1 datum surface. α is the ratio of the water level in the aquifer to the depth of the aquifer. It has to be defined for $p^* > \rho_w g d$ as when the aquifer is saturated, the water pressures can continue to increase. In effect there is a layer of water between the aquifer and the ice.

Consider Equation 2.38 without the source term ϕ. The source simply dictates the volume of water entering or leaving the system regardless of what is happening in the system. The ratio α will not affect it. Equation 2.38 is multiplied by α to give

$$\alpha(p^*)\frac{\partial p^*}{\partial t} = \alpha(p^*) D\boldsymbol{\nabla} \cdot \boldsymbol{\nabla} p_t. \tag{2.44}$$

The source term is reintroduced and the equation divided by α to give

$$\frac{\partial p^*}{\partial t} = D\boldsymbol{\nabla} \cdot \boldsymbol{\nabla} p_t + \frac{\phi}{\alpha(p^*) c_T}. \tag{2.45}$$

As the water in the aquifer falls, α becomes large; the source term will dominate. The pressure in thinner aquifers increases faster than thicker aquifers for a given melt rate M as the pressure change is proportional to M/d. The α term simply reduces the effective thickness of the aquifer when needed. This effect means that the situation of the aquifer being empty, and so the contradiction, is never reached. The equation compensates for the situation as $\phi \to 0$ and the equation is only now valid if either $p^* > 0$ or $\phi > 0$.

2.5.5 Boundary conditions

A number of boundary conditions are imposed on the equations to enable them to be solved. The water flux pressure p^* is maintained at zero where there is no ice. This is equivalent to saying the total pressure is maintained at the hydrostatic pressure where there is no ice. In effect, once the water leaves the ice sheet it is assumed to flow fluvially, unpressurised. Physically, water may flow through till and so may cause back-pressure at the margin if the system is not efficient, but HYDRO does not consider this. There is potential to couple the runoff calculated by HYDRO to other models if desired in future.

Water input and output from the system is calculated from the source term. Where this is negative, water is removed by freezing onto the bed of the ice, resulting in lower water pressure.

Where the ice is frozen to the bed there cannot be any liquid water present and water cannot flow into these areas but must build up against it. The frozen bed is defined at run time, by the user, as either areas where the bed is below pressure melting point, or areas where basal melt rat rate $M \leqslant 0\,\mathrm{mm\,a^{-1}}$.

2.5.6 Efficient flow

The system described so far does not consider hydraulic efficiency, despite this having a large effect on water pressures (Section 1.3.2) and therefore ice dynamics (Section 1.3.1). Broadly speaking, two possible hydrological regimes exit. Ignoring the details of how they come about, these are efficient and inefficient. HYDRO must be able to simulate the two different responses of water pressure to water flux. The model developed so far describes Darcian flow which is inefficient. In this case, as water flux increases so does the pressure. An efficient system is now introduced.

GLIMMER and HYDRO both operate on a large, ice sheet scale. The grid resolution ranges from $5 \times 5\,\mathrm{km}^2$ to $20 \times 20\,\mathrm{km}^2$. At these scales it is impossible to directly resolve channels using the equations in Röthlisberger (1972) or Nye (1976). However, the effect of efficiency is clear. In an efficient system, as water flux increases the water pressure decreases (Kamb, 1987). A method must be found, therefore, which reduces water pressures when water flux becomes large. One could work on finding a method to upscale the effects of channels to the grid-cell area, or simply find a proxy for the bulk effect of the channels. The solution for

HYDRO is to simply say the bed becomes more efficient without explaining the processes driving it. The aim is to model the results of the efficiency, not the causes.

The conductivity κ is the key to enabling areas of efficient flow. No matter what value is chosen for conductivity, the flow is inefficient if κ is uniform. It is important to note that if κ is uniform and the system is allowed to reach equilibrium, the final pressure is relatively insensitive to the value of κ when κ has reasonable values. The main sensitivity of the system to conductivity is the time taken for equilibrium to be reached. However, if certain areas are given a higher conductivity than others, these areas will drain quicker and so the system will display the behaviour of an efficient system and the water pressure will drop. In this case the pressure begins to depend on the conductivities used.

The creation of areas of higher conductivity is one method that can be used to include the overall effects of channels on the ice sheet system. As the equations are being solved over a large area, individual channels cannot be calculated realistically, but their overall effect can be estimated.

Having a dual conductivity regime means Equation 2.45 must be modified as conductivity κ now has spatial dependence. To begin, I define $\kappa = \bar{\kappa}\dot{\kappa}(x, y)$ where the old κ is split into its dimensionless, spatially-dependent component $\dot{\kappa}$ and a scaling factor $\bar{\kappa}$. Equation 2.45 can now be rewritten

$$\frac{\partial p^*}{\partial t} = D\boldsymbol{\nabla} \cdot \dot{\kappa}\boldsymbol{\nabla} p_t + \frac{\phi}{\alpha(p^*)c_T}, \tag{2.46}$$

with the diffusivity redefined to be

$$D = \frac{\bar{\kappa}}{c_T \rho_w g} \, . \tag{2.47}$$

This equation reinforces the fact that the equation should only be solved if water is present, ie $p^* > 0$, as otherwise the gradient in the conductivity will cause the apparent build up of pressure even though there is no water.

An efficiency condition is defined for the bed to become efficient.

2.5.7 Model drivers

The source term ϕ is the primary driver of HYDRO. This is made up of the basal melt rate M but also consists of any surface melt that is passed to the bed. The specific driver used

is chosen at run time. It is important to understand how HYDRO deals with this input when running on its own or coupled with another model. The method chosen will affect any seasonal response that HYDRO exhibits.

When the coupled GLIMMER-HYDRO model is running, GLIMMER calculates the basal and surface melt rates. When HYDRO is run independently, it must either read the melt rate from a file or supply its own. Even when GLIMMER-HYDRO is running, HYDRO can add a seasonal signal to GLIMMER's calculated melt if desired. Alternatively, GLIMMER may be able to supply a seasonal signal if an appropriate climate driver has been chosen.

When running independently, HYDRO can supply the following melt regimes: a uniform basal melt rate, two uniform melt rates in concentric circles, a single time slice read in from a file and a sequence of melt rates read in from a file. A seasonal signal can be superimposed on any of these regimes.

The seasonal signal is calculated using

$$\phi = \phi_{\text{basal}} + \begin{cases} 0 & \text{for} \quad \cos(\varphi) \geqslant 0 \\ -\phi_{\max}\cos(\varphi) & \text{for} \quad \cos(\varphi) < 0 \end{cases} \tag{2.48}$$

where φ is the day of the year as expressed in radians in the range $0 \rightarrow 2\pi$. This gives six months of increased melt every year. This is superimposed on any basal melt present, if requested.

When HYDRO is coupled with GLIMMER, GLIMMER calculates the basal and surface melt rates as discussed in Section 2.2.3. The basal malt rates are a direct input into HYDRO. If GLIMMER calculates the basal melt rate to be negative, then water will be removed from the system. If HYDRO is told to include the surface melting calculated by GLIMMER, then there are two options. One, a user defined proportion of this is passed directly to the bed. Two, a ponding algorithm (introduced in detail in Section 5.4) supplied with HYDRO can pond surface water and drain the ponds in a stochastic manner, simulating observations on Greenland (eg McMillan et al., 2007; Das et al., 2008). These are both based on the assumption that on the grid size that GLIMMER operates at there will be moulins in most grid squares.

2.6 Numerical scheme of Hydro

The assumptions and simplifications set out in Sections 2.5.1 and 2.5.2 are defined mathematically in the remainder of Section 2.5. This section takes that mathematical model and details how it is solved numerically. The numerical methods used affect the ease of programming, the accuracy of the solution, and the speed of calculation (Press et al., 1992). While these factors are important, they are of secondary importance to model behaviour compared with defining the initial governing equations (Van der Veen, 1999).

The approach taken for the HYDRO model was to initially choose an easy to programme yet relatively accurate solution driver. Once the model is established, then this driver can be replaced with a more accurate and faster one. The Newton method using a finite difference regime is used to solve the differential equations and the convergence of the solution is demonstrated in Chapter 3. The derivation of the difference equations will be demonstrated and the rationale behind other choices, such as making the equations dimensionless, will be discussed.

Some extra boundary conditions for the HYDRO model will also be introduced. These extra boundary conditions are needed to deal with issues raised from the numerical scheme chosen.

2.6.1 Dimensionless equation

Dimensionless equations have several benefits and so for the calculations in the model Equation 2.45 will be used in dimensionless form. When an equation is dimensionless, everything is scaled near the range between 0 and 1. This is the most accurate range for numerical calculation. It also has the benefit that when looking at individual terms it is immediately obvious which term dominates, if any, and this helps develop an intuitive understanding of the equations.

The dimensionless parameters, following Griffiths and Smith (1991), are defined to be

$$X = \frac{x}{\ell}, Y = \frac{y}{\ell}, P = \frac{p}{p_{hs_{\max}}}, \hat{T} = \frac{Dt}{\ell^2} \tag{2.49}$$

where ℓ is the characteristic length, $p_{hs_{\max}}$ is the maximum pressure from ice and topography ($\rho_w g b + \rho_i g h$) at the start of the model run. The factor ℓ^2/D is the characteristic time of

the equation. This is the time taken for a single perturbation to the system to diffuse back to the equilibrium solution.

Formally, X and Y must be differentiated to derive the dimensionless form of the gradient operator, $\boldsymbol{\nabla}$. By the chain rule this gives,

$$\frac{\partial}{\partial x} = \frac{\partial}{\partial X}\frac{\partial X}{\partial x} = \frac{\partial}{\partial X}\frac{\partial}{\partial x}\left(\frac{x}{\ell}\right) = \frac{1}{\ell}\frac{\partial}{\partial X}\ , \tag{2.50}$$

and similarly,

$$\frac{\partial}{\partial y} = \frac{1}{\ell}\frac{\partial}{\partial Y}. \tag{2.51}$$

Substituting these into the gradient operator $\boldsymbol{\nabla}$, the dimensionless version $\hat{\boldsymbol{\nabla}}$ is given by

$$\boldsymbol{\nabla} = \left(\frac{\partial}{\partial x}, \frac{\partial}{\partial y}\right) = \frac{1}{\ell}\left(\frac{\partial}{\partial X}, \frac{\partial}{\partial Y}\right) = \frac{1}{\ell}\hat{\boldsymbol{\nabla}}\ . \tag{2.52}$$

The time derivative becomes

$$\frac{\partial}{\partial t} = \frac{\partial}{\partial \hat{T}}\frac{\partial \hat{T}}{\partial t} = \frac{\partial}{\partial \hat{T}}\frac{\partial}{\partial t}\left(\frac{Dt}{\ell^2}\right) = \frac{D}{\ell^2}\frac{\partial}{\partial \hat{T}}. \tag{2.53}$$

Substituting $p^* = p_0 P^*$, $p_t = p_0 P_t$ and equations 2.52 and 2.53 into Equation 2.46, the dimensionless equation becomes

$$\frac{p_0 D}{\ell^2}\frac{\partial}{\partial \hat{T}}P^* = \frac{p_0 D}{\ell^2}\hat{\boldsymbol{\nabla}}\cdot\dot{\kappa}\hat{\boldsymbol{\nabla}}P_t + \frac{\phi}{\alpha(p_t)c_T}. \tag{2.54}$$

Dividing through by Dp_0/ℓ^2 reduces the equation to

$$\frac{\partial P^*}{\partial \hat{T}} = \hat{\boldsymbol{\nabla}}\cdot\dot{\kappa}\hat{\boldsymbol{\nabla}}P_t + \frac{\phi\ell^2}{\alpha(p^*)c_T D p_0}\ . \tag{2.55}$$

Now let

$$\Phi = \frac{\phi\ell^2}{c_T D p_0}\ , \tag{2.56}$$

and Equation 2.55 reduces to

$$\frac{\partial P^*}{\partial \hat{T}} = \hat{\boldsymbol{\nabla}}\cdot\dot{\kappa}\hat{\boldsymbol{\nabla}}P_t + \frac{\Phi}{\alpha(p^*)}. \tag{2.57}$$

Note that compressibility is no longer a component of the, now dimensionless, source term. The dimensionless diffusivity is simply unity. $\alpha(p^*)$ and $\dot{\kappa}$ are already dimensionless and are therefore not affected.

2.6.2 Numerical scheme

An appropriate numerical scheme must be employed to solve Equation 2.57. The details of how this equation is broken down to be solved computationally is now discussed. HYDRO uses the discrete element method.

A Newtonian scheme is used as opposed to the more accurate Crank-Nicolson scheme. The primary controls on the processes are the definitions and assumptions of the mathematical model in Section 2.5 and not the choice of numerical integration method (Van der Veen, 1999). Although the Crank-Nicolson scheme is more accurate and more stable, the Newtonian scheme is faster to develop. The Newtonian scheme also has the advantage of being able to apply the various boundary conditions during the calculation as opposed to before or after the calculation of each time step. In future, switching the model to use the Crank-Nicolson scheme is desirable for increased stability but the aims of this thesis are not affected by this choice.

Theoretically, the Newtonian scheme is stable as long as

$$\frac{D\delta t}{\delta x \delta y} \leqslant \frac{1}{2}\,, \tag{2.58}$$

where D is the diffusivity (Press et al., 1992). In practice the accuracy of the integration begins to break down at a lower threshold than the theoretical one, but it is obvious when the solution is inaccurate.

The dimensionless equation we are solving is

$$\frac{\partial P}{\partial \hat{T}} = \hat{\boldsymbol{\nabla}} \cdot \dot{\kappa} \hat{\boldsymbol{\nabla}} P + \frac{\Phi}{\alpha(p^*)}. \tag{2.59}$$

First order and second order difference equations are used to solve Equation 2.59. The first order difference is used in the time dimension, while the two spatial dimensions both use second order difference.

$P(x_i, y_j, t_k)$ will be expressed as $P_{i,j,k}$ and the time step as $\mathfrak{t} = \hat{T}_{i+1} - \hat{T}_i$. The first order

finite difference equation is then given by

$$\begin{aligned}
P_{i,j,k+1} &= \mathfrak{t}\,\ell^2 \left(\frac{\partial \dot{\kappa} \partial P_{i,j,k}}{\partial x^2} + \frac{\partial \dot{\kappa} \partial P_{i,j,k}}{\partial y^2} + \dot{\kappa} \boldsymbol{\nabla} \cdot \boldsymbol{\nabla} P_{i,j,k} + \Phi_{ij} \right) + P_{i,j,k} \\
&= \mathfrak{t}\,\ell^2 \left[\frac{1}{4\imath^2} (\dot{\kappa}_{i+1,j} - \dot{\kappa}_{i-1,j})(P_{i+1,j,k} - P_{i-1,j,k}) \right. \\
&\quad + \frac{1}{4\jmath^2} (\dot{\kappa}_{i,j+1} - \dot{\kappa}_{i,j-1})(P_{i,j+1,k} - P_{i,j-1,k}) \\
&\quad + \dot{\kappa}_{ij} \left(\frac{1}{\imath^2} (P_{i+1,j,k} + P_{i-1,j,k} - 2P_{i,j,k}) \right. \\
&\quad \left. \left. + \frac{1}{\jmath^2} (P_{i,j+1,k} + P_{i,j-1,k} - 2P_{i,j,k}) \right) + \Phi_{ij} \right] + P_{i,j,k}
\end{aligned}$$

where $\imath = x_{i+1} - x_i$ and $\jmath = y_{j+1} - y_j$. Note that the actual finite differences used for the spacial dimensions are identical and that the ℓ^2 term appears due to the dimensionless $\hat{\boldsymbol{\nabla}} = \ell \boldsymbol{\nabla}$ factor.

The substitutions used are as follows:

$$\begin{aligned}
\frac{\partial \dot{\kappa}_{ij}}{\partial x} &= \frac{1}{2\imath} (\dot{\kappa}_{i+1,j} - \dot{\kappa}_{i-1,j}) \\
\frac{\partial \dot{\kappa}_{ij}}{\partial y} &= \frac{1}{2\jmath} (\dot{\kappa}_{i,j+1} - \dot{\kappa}_{i,j-1}) \\
\frac{\partial P_{i,j,k}}{\partial x} &= \frac{1}{2\imath} (P_{i+1,j,k} - P_{i-1,-j,k}) \\
\frac{\partial P_{i,j,k}}{\partial y} &= \frac{1}{2\jmath} (P_{i,j+1,k} - P_{i,j-1,k}) \\
\frac{\partial^2 P_{i,j,k}}{\partial x^2} &= \frac{1}{\imath^2} (P_{i+1,j,k} + P_{i-1,j,k} - 2P_{i,j,k}) \\
\frac{\partial^2 P_{i,j,k}}{\partial y^2} &= \frac{1}{\jmath^2} (P_{i,j+1,k} + P_{i,j-1,k} - 2P_{i,j,k}) \ .
\end{aligned}$$

2.6.3 Solving for hydrostatic pressure

Due to the treatment of pressures in the numerical scheme described in Section 2.6.2, the hydrostatic pressure needs specific treatment to be physically valid. This can be thought of as an extra boundary condition imposed by the numerics.

The problem is that Equation 2.59 cannot tell the difference between pressure due to water and pressure from the hydrostatic pressure. Therefore the equation diffuses both as it is solved in time. In other words, the topography and ice attempt to diffuse and become flat due to the numerics. This is unphysical; the hydrostatic pressure should simply increase and

direct the flux away from a cell, but not contribute to it itself. To avoid this, the diffusion that would result is calculated and subtracted from the solution of Equation 2.59 every time step.

For the purpose of this discussion Equation 2.59 will be simplified to

$$\frac{\partial p}{\partial t} = \boldsymbol{\nabla} \cdot \boldsymbol{\nabla} p + \phi \; . \tag{2.60}$$

The conductivity κ is not important because there will only be a conductivity gradient if water is present. This is due to the way new conductivities are calculated.

p in this case is the total pressure p_t, given by

$$p_t = p^* + p_{hs}$$

where p^* is pressure due to water flux from Darcy's equation, and the hydrostatic pressure p_{hs} is the sum of the pressures due to topography and ice overburden. In the time scales that this equation is integrated over

$$\frac{\partial p_{hs}}{\partial t} = 0$$

as the topography and ice thickness are considered to be constant. Substituting p_t into Equation 2.60, and cancelling out the $\partial p_{hs}/\partial t$ term we get

$$\frac{\partial p^*}{\partial t} = \boldsymbol{\nabla} \cdot \boldsymbol{\nabla} \left(p^* + p_{hs} \right) + \phi$$

to represent the hydrostatic time dependent solution.

Unfortunately this equation has the following problem:

1. With $p^* = 0$ and $\phi = 0$ for all time, $\boldsymbol{\nabla} \cdot \boldsymbol{\nabla} p_{hs} = 0$ which is not the case, unless the topography is flat.

2. A consequence of this follows for numerical solutions. If $p^* = 0$ at the first time slice, and $\phi = 0$ for all time, then it follows that

   $$p^* > 0 \text{ for } t > 0,$$

   due to the non-zero hydrostatic term $\boldsymbol{\nabla} \cdot \boldsymbol{\nabla} p_{hs}$ when in fact p^* *should equal* 0 for all

time.

These problems are dealt with during the solution of the equation by setting $p_{hs} = 0$ if $p^* = 0$. The equations are not physically valid in the limit $\phi \to 0$ so are only where $\phi > 0$. If this wasn't done, hydrostatic pressure would be set each time GLIMMER updates HYDRO, but extra water would be entering the system through numerical artifacts.

2.6.4 Implementing boundary conditions

A number of HYDRO's boundary conditions have already been introduced. How these are implemented numerically are now considered.

The boundary conditions are applied to the calculation at every time step. The boundary conditions used are:

1. the current bed topography and ice thickness,
2. zero pressure where there is no ice,
3. adjusting for efficient areas,
4. no water flux where the bed is frozen,
5. no water generation due to the numerical artifacts,
6. only solving the equations where water or melt is present, and
7. limiting water pressure.

HYDRO stores the current bed topography and ice thickness in two arrays. Depending on how HYDRO was invoked, these arrays may be updated every time step. The hydrostatic pressure derived from these data is stored in a separate array. All pressure arrays, except the hydrostatic, are set to zero where there is no ice every time step. Efficient areas are removed when no longer under ice using the same subroutine. Where there is ice, a different subroutine introduces and removes efficiency.

Each cell calculates the water that it will gain and lose individually. This means that if a cell calculates it will lose water, this water will not automatically be added to the down-slope cell. When it is that cell's turn, then it will realise water needs to be added. This due to the difference equations derived in Section 2.6.2. The advantage of this approach is that a cell

will only start a calculation if conditions 4 and 6 allow it. If a warm cell is bounded by a frozen cell, water flow into the frozen cell is prevented by temporarily setting the pressure in the frozen cell equal to the warm cell. This is a numerical trick and has no physical basis.

Because the model cannot distinguish between hydrostatic pressure and water flux pressure, the equations attempt to diffuse the hydrostatic pressure so, if they were allowed, the bed and ice sheet would eventually become flat. This numerical artifact is dealt with by subtracting the numerical diffusion that would result from the solution every time step.

As demonstrated in the model conceptualisation (Section 2.5.1), there is no inherent limit on water pressure and the system can easily over-pressurise. This happens in efficient areas due to the definition of the efficiency condition ($p_r > 0.9$). To stop the model becoming unstable, I artificially limit the pressure ratio so that $p_r \leqslant 10$. This value is larger than 1 to enable water flow gradients to be calculated, which helps evacuate water. The efficient areas are defined simply to remove water as fast as possible, so this boundary condition agrees with the conceptual model.

2.7 Summary

One of the key missing processes in the current generation of ice models is the handling of basal hydrology and its link to ice dynamics (Lipscomb et al., 2008). This chapter develops Hydro, a subglacial hydrology model, to address this. Hydro is coupled with a modified Glimmer ice sheet model to produce Glimmer-Hydro.

Figure 2.7 summarises the key equations, and their interaction, of the Glimmer-Hydro model. Hydro calculates basal water pressures, driven by melt supplied by Glimmer. This is used by Glimmer to calculate basal sliding and frictional heat generation, both processes that depend on basal water but which Glimmer, as released, is unable to account for. Hydro treats hydraulic efficiency in a semi-physical manner and accounts for the frozen bed underneath an ice sheet. An efficient bed is defined to be more diffusive and so evacuates water more easily, lowering water pressures. This enables Glimmer-Hydro to adapt the basal conditions to melt water input dynamically. Many contemporary basal hydrology models do this by proxy, if at all, and therefore cannot model a truly physical response in ice dynamics in relation to surface melt water input.

The next chapter introduces the capabilities of Hydro in a piecemeal fashion. The

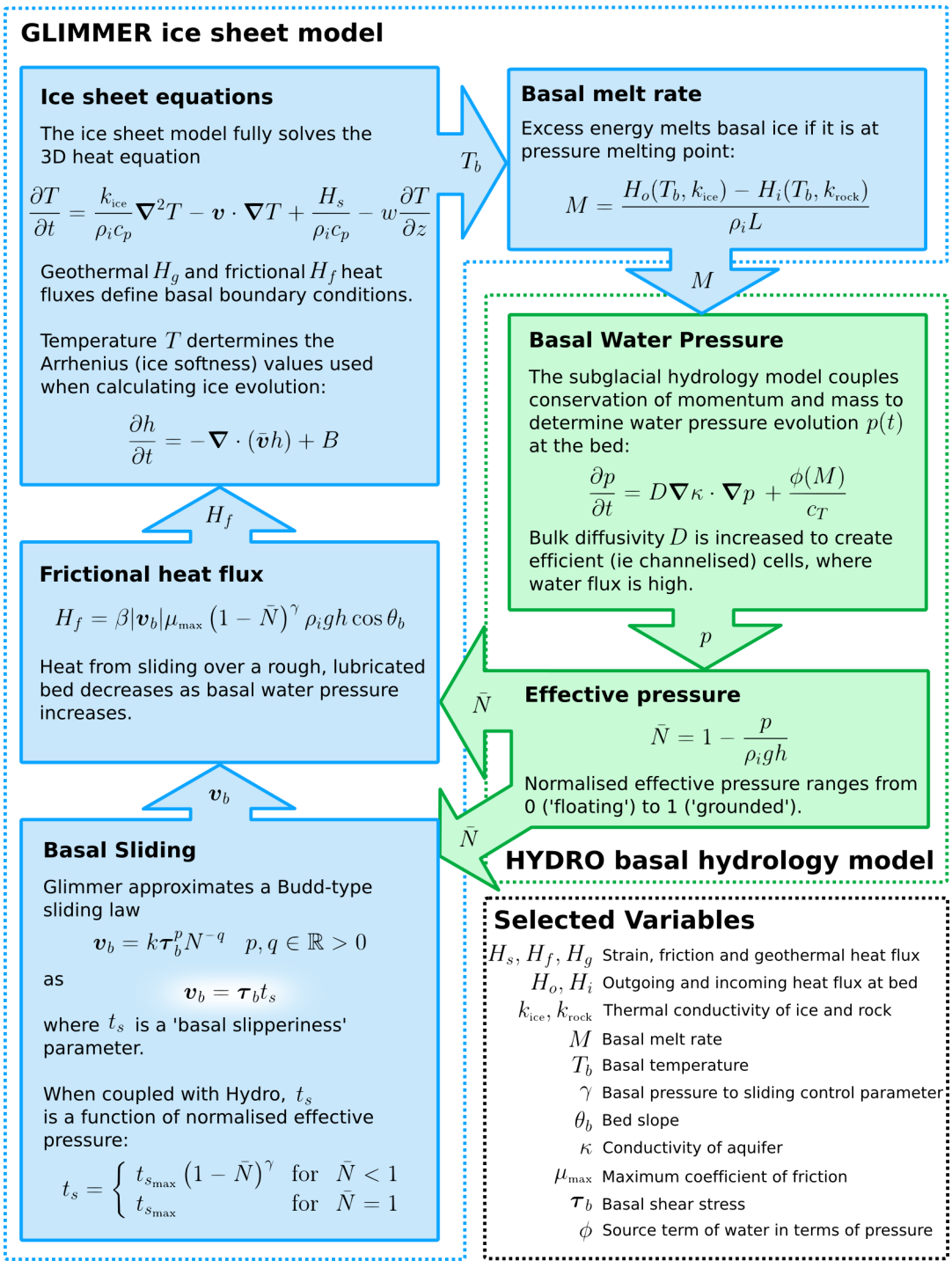

Figure 2.7 Summary of the key equations defining the coupling between GLIMMER and HYDRO. GLIMMER is modified to calculate basal sliding and frictional heat flux using effective pressure from HYDRO. HYDRO is driven by melt rates calculated by GLIMMER. The coupling of secondary features, such as ice thickness and bed topography, are not displayed.

coupled Glimmer-Hydro model is first used in Chapter 4. Chapter 5 introduces a new surface-ponding driver for Hydro, which is beyond the scope of this chapter.

Chapter 3

Strain and Geothermal Heating

> "Limited knowledge of basal processes [...] leads to large uncertainties in the understanding of ice flow processes and ice sheet stability."
>
> —*Fourth IPCC Assessment Report 2007,* §*TS 6.2.2*

This chapter investigates the importance of geothermal and strain heating on melting under the Greenland ice sheet and uses this to understand controls on the background hydraulic pressure profile (BHPP). I define *background hydraulic pressure profile* as the water pressure p^* due only to basal melting under the Greenland ice sheet, in equilibrium conditions.

In order to understand the background hydraulic pressure profile, the basal water sources must be known. While this can be read from model output (eg GLIMMER), heat sources need to be analysed to understand the processes responsible for the basal melt rates calculated. Section 3.3 analyses strain heating rates at the base of the Greenland ice sheet and compares this to geothermal heat flux in order to understand the heat flux distribution that is responsible for basal melting.

To establish the pressure profile under the Greenland ice sheet, Section 3.4 uses uniform, and more complicated basal melt rates to drive HYDRO. The effects of hydraulically efficient areas and a frozen, impermeable bed on the Greenland-wide scale are investigated. Friction also provides an important basal heat source. The interaction of this term with hydrology is complex and is the focus of Chapter 4 and so is not dealt with here. It is necessary to understand the effects of all these on the steady-state solution, with only basal melting, before the effects of surface water reaching the bed can be considered in Chapter 5.

First, however, I discuss the general set-up of the models used in this chapter. Experiment specific configuration is discussed as needed.

3.1 General model setup

The model set-up in this section applies to all runs in this chapter. This chapter uses both HYDRO and GLIMMER, but the two models are not coupled. Section 3.3 uses GLIMMER runs with varying geothermal melt rates. Section 3.4 uses HYDRO to model the background pressure and later uses GLIMMER to provide the initial conditions for HYDRO runs.

3.1.1 Digital elevation models

The experiments use two ice and bed DEMs. The first is based on the 5 km ice thickness and bed elevation data set by Bamber et al. (2001b). Figure 3.1 shows the ice thickness, basal topography and surface topography for the area around Greenland. These data only cover terrestrial Greenland, so to allow the potential expansion of the ice sheet and to calculate isostatic adjustment in later work, they are stitched together with 2 minute Gridded Global Relief Data(NOAA, 2006). The second DEM is a 10 km subset of the first.

The 5 km DEM offers better resolution of the outlet glaciers, and thus the hydrology in these regions. The coarser subset is more stable and so is used with GLIMMER runs. High bed gradients in the 5 km DEM reduce stability when calculating ice deformation and sliding, but hydrology calculations are less affected.

3.1.2 Run times and equilibrium profiles

All mapped output in this chapter is the equilibrium profile of the run. The run is driven with a temporally-constant driver and as there are no feedback mechanisms to consider there is no interesting behaviour except the spatial distribution. Depending on the model and its set-up, reaching equilibrium requires different length runs. HYDRO runs typically reach hydraulic equilibrium within 5–50 ka, depending on basal melt rates. GLIMMER runs take much longer to reach thermal equilibrium because this is a 100 ka process (Hindmarsh, 1990).

To calculate thermal equilibrium, the temperature of the entire ice column is set to the surface ice temperature, where temperatures are coldest. If initial basal temperatures are

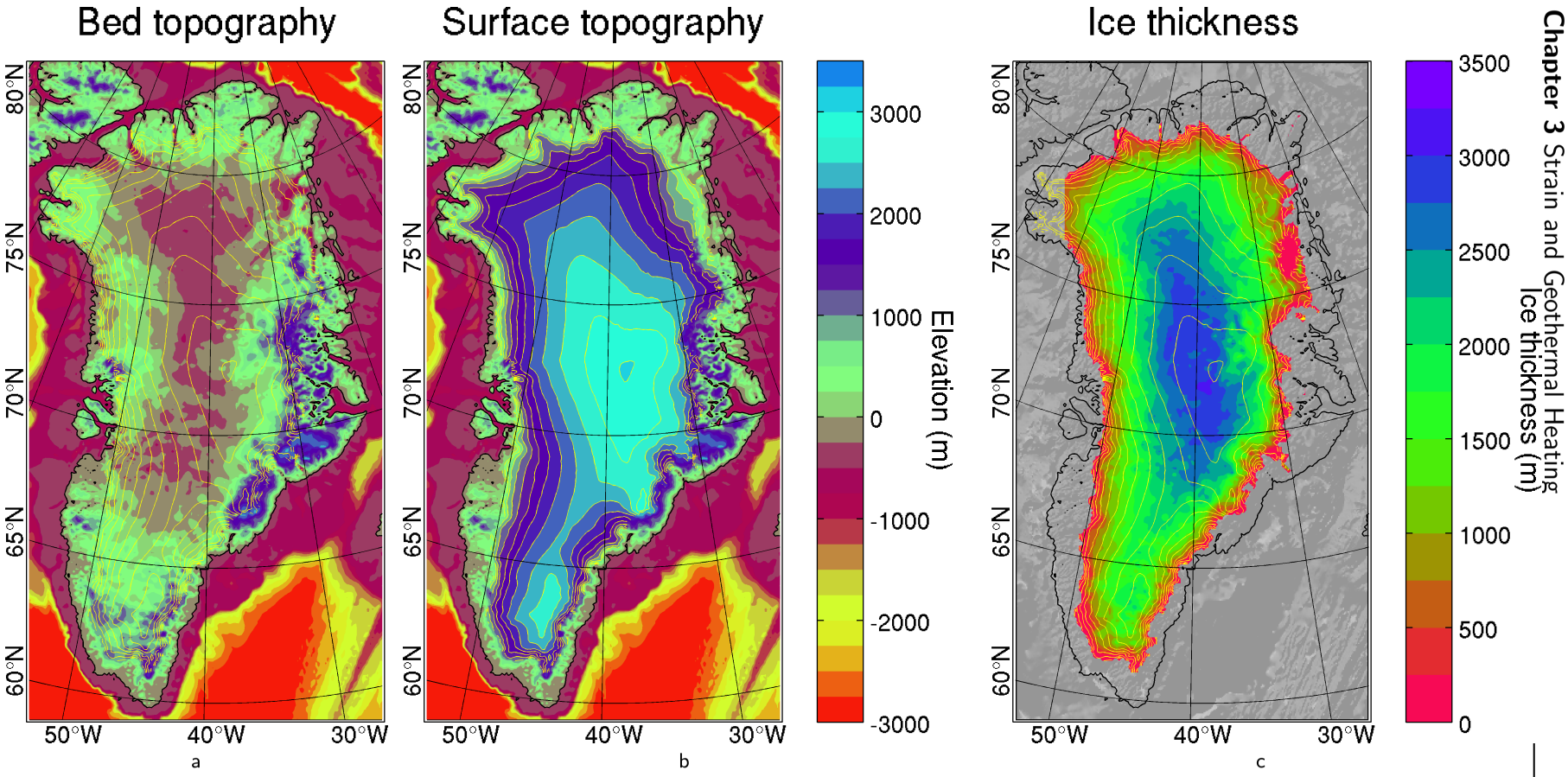

Figure 3.1 This thesis uses a 5 km and 10 km Greenland DEM. This figure shows the (a) bed topography, (b) surface elevation, and (c) ice thickness in the 10 km data set. The 5 km ice data from Bamber et al. (2001b) are stitched together with 2 minute Gridded Global Relief Data (NOAA, 2006) to provide bathymetry. Irregularities in the bed are masked by the ice thickness to provide, at this resolution, a smooth ice surface. In this DEM, the Greenland ice sheet's summit is at 3277 m and the maximum ice thickness is 3353 m.

All maps in this thesis show land surface (grey background), the land margin (black line), and 250 m surface elevation contours (yellow lines).

too high then GLIMMER significantly over-predicts ice temperatures. The model is run for at least 100 ka. The time to reach equilibrium increases as the basal heat flux increases because more ice needs to be heated. The GLIMMER runs start with present day ice thickness and topography with the entire ice sheet set to the surface temperature.

3.1.3 Models drivers

The model runs in this chapter do not use the coupled GLIMMER-HYDRO model. GLIMMER and HYDRO are run independently until equilibrium because for the first experiments reaching a true, time-independent equilibrium removes potential complications when interpreting the BHPP. HYDRO is driven either with prescribed uniform melt rates or with non-time-dependent GLIMMER output. GLINT drives the GLIMMER model using data from the National Oceanic and Atmospheric Administration's Climate Prediction Centre that comes with GLIMMER. The goal is to run GLIMMER to equilibrium and this is simplified by using data averaged over a year to provide a constant climate.

Figure 3.2 shows the ice thickness and surface elevation calculated by GLIMMER at equilibrium. This is the ice sheet that the later HYDRO runs (H105–109) use in this chapter. The climate driver used does not support current conditions long-term. The ice sheet extent reaches Greenland's coast, Figure 3.2. This is probably due to an over estimation of accumulation. For the purpose of this thesis this is not a significant problem because the focus is basal processes and not prediction. The increased extent does, however, make the ice sheet look unusual when looking at data from these runs.

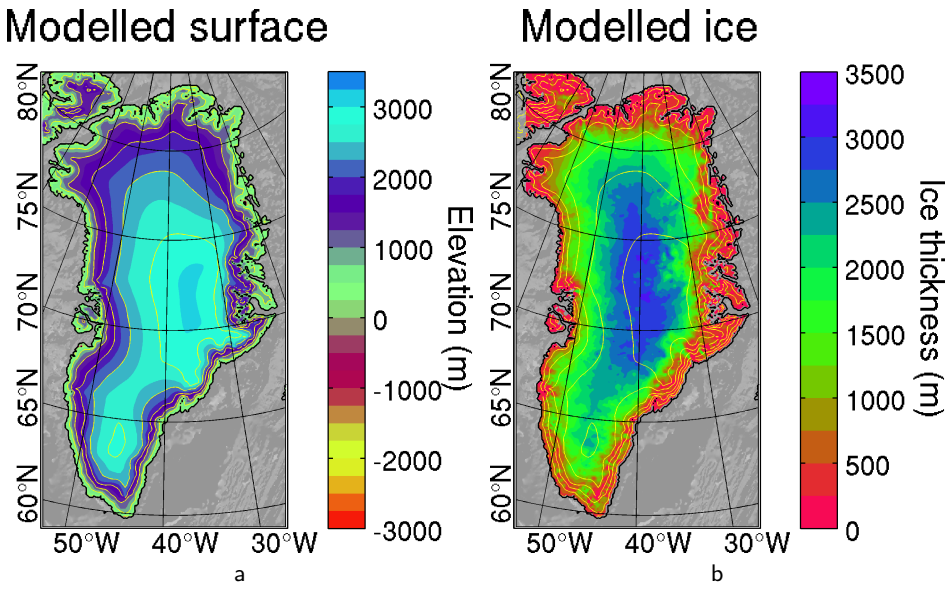

Figure 3.2 The climate driver used by GLIMMER (Runs G1–5 and) overestimates ice thickness and extent. This modelled ice surface is used in runs H105–109. Section 3.3 also uses this run to define basal ice temperatures, but in that instance the data are cropped to present day ice. While overestimating ice thickness is not ideal, the nature of the background hydraulic pressure profile, and the processes which control it, can still be studied.

3.2 Subglacial troughs

Subglacial troughs affect ice dynamics and, arguably, determine the location of outlet glaciers. Many of the processes described in this chapter, and this thesis, are dependent on the location and influence of subglacial troughs. This section briefly examines the interaction between ice dynamics and troughs.

An important research topic, well beyond the scope of this thesis, is the feedbacks driving fjord formation. These feedbacks include subglacial water, erosion, and driving stresses. The key observation at the moment is that subglacial troughs tend to form under outlet glaciers, and conversely, where there is a deep subglacial trough there tends to be fast-flowing ice. These areas are potentially problematic for GLIMMER because of its use of the shallow ice approximation (SIA). The SIA works well in low-stress regimes by ignoring higher-order physics including longitudinal stress. The behaviour of fast-flowing ice, on the other hand, is dominated by longitudinal stresses. This leads to GLIMMER poorly handling the physics in outlet glaciers.

Greenland's outlet glaciers are typically marine-terminating tidewater glaciers which

become increasingly decoupled at the bed towards the terminus. When there is little resistive force at the bed ice does not shear in the same way as grounded ice. In outlet glaciers, the main resistive force is lateral shear and this leads to the fastest velocities in the centre of the trough with most of the ice column travelling at the same velocity. Glimmer incorrectly keeps basal shear high at the bed and ignores lateral shear. Because the troughs lead to thick ice high basal shear is calculated. This leads to Glimmer calculating fast surface ice velocities, as observed, but through incorrect physics.

In this thesis, I often refer to outlet glaciers or subglacial troughs. The key factor in the processes I discuss is the trough and not the fact that these troughs happen to contain marine-terminating outlet glaciers through fjord-creating feedbacks. In these regions Glimmer overestimates strain rates due to the weight of the ice, but lateral and longitudinal strain is not calculated at all so high strain is still appropriate. Incorrect strain calculation leads to overestimating basal melt and underestimating basal sliding. These issues are discussed further in the relevant sections.

3.3 Strain heating

As ice deforms, the internal friction of the ice generates heat. At the bed of an ice sheet, this may be enough to melt ice. This section looks at strain heating analytically and compares the importance of this heat source to geothermal flux. I take an analytical approach, as opposed to reading strain heating rates from Glimmer, to gain an understanding of what controls the strain heating rate.

It is important to study these terms so the processes controlling basal melt rates, and therefore the background hydraulic pressure profile, can be understood. By understanding the relative importance of strain and geothermal heat sources in different regions, future work can be directed. Despite the focus of the results on Greenland, the principles apply to any ice sheet.

Section 3.3.1 derives the equation I use to calculate basal strain heat flux. The sensitivity of the equation is discussed in Section 3.3.2. Section 3.3.3 plots the strain heat flux map for Greenland and compares these values to geothermal heat flux. The basal ice temperatures, for a variety of geothermal heat fluxes, are mapped to discuss the combined effect of the two heat sources.

3.3.1 Equation derivation

Due to the non-Newtonian nature of ice dynamics, the equations for calculating the strain heat flux are non-trivial. Here, I derive an approximate equation for this as a function of depth below the ice surface. This must have the same units as geothermal heat flux to enable a valid comparison.

To derive the term I have called *strain heat flux* H_s, I start with the rate of temperature change in ice due to strain. To match the units with geothermal heat flux, I convert this temperature change to an energy change and then convert that to power per area.

Van der Veen (1999, pg 184) approximates the rate of temperature change in $\mathrm{K\,s^{-1}}$, at a depth z below the ice surface, to be

$$W(z) = \frac{2A(z)}{\rho_i k_{\mathrm{ice}}} \left(\frac{z}{h}\right)^4 \tau_{dx}^4 \,. \tag{3.1}$$

$A(z)$ is determined by the Arrhenius relation, Equation 1.4. It is a function of the pressure adjusted ice temperature T^*, which is a function of depth:

$$T^*(z) = T(z) + \rho_i g c_t z \,. \tag{3.2}$$

For a mass dm, the energy entering the system for a given temperature change is

$$Q = k_{\mathrm{ice}} \Delta T \; dm \,. \tag{3.3}$$

Dividing this equation by time t and area a converts it into power per area ($\mathrm{W\,m^{-2}}$):

$$\frac{\mathcal{P}}{a} = \frac{Q}{at} = \frac{1}{at} k_{\mathrm{ice}} \Delta T \; dm \,. \tag{3.4}$$

The change in temperature is given by $\Delta T = W(z)t$ and the mass can be expressed as $dm = \rho_i a \; dz$. Substituting these two equations into Equation 3.4 cancels the time and area terms from the right hand side. Integrating the resulting equation over z gives an equation

for the strain heat flux H_s,

$$H_s(z) = \frac{P(z)}{a} = \rho_i k_{\text{ice}} \int W(z)\, dz \tag{3.5}$$

$$= \frac{2\tau_{dx}^4}{h^4} \int z^4 A(z)\, dz\ . \tag{3.6}$$

The equation for $A(z)$, the flow constant as a function of depth, is complex and depends on the temperature profile of the ice column. This must be defined before the integration can take place. Weertman (1968) shows a temperature profile for Camp Century in Greenland. I have approximated the general shape of the curve using

$$T(z) = (T_b - T_s)\left(\frac{z}{h}\right)^k + T_s \tag{3.7}$$

where T_b and T_s are the non-pressure corrected bed and surface temperature of the ice and k controls the shape of the curve. Figure 3.3 gives a visual representation of this equation for a range of k. In order for the shape of Equation 3.7 to remain realistic the surface temperature must remain below the bed temperature. This seems a reasonable assumption for Greenland. In reality, the lowest ice temperature is often a little below the ice surface (Van der Veen, 1999); Equation 3.7 does not take this into account. The approximation seems reasonable in the context of this work.

Combining Equations 3.6, 1.4, 3.2 and 3.7 results in an integrand that cannot easily be evaluated analytically:

$$H_s(z) = \frac{2A_0\tau_{dx}^4}{h^4} \int z^4 e^{-Q/R(T(z)+\rho_i g c_t z)}\, dz \tag{3.8}$$

$$= \frac{2A_0\tau_{dx}^4}{h^4} \int z^4 e^{-Q/R\left[(T_b-T_s)(z/h)^k+T_s+\rho_i g c_t z\right]}\, dz\ . \tag{3.9}$$

I overcome this problem by performing a Taylor expansion about $h/2$ of Equation 1.4 with the pressure corrected temperature profile substituted in. Equation 3.6 becomes

$$H_s(z) = \frac{2\tau_{dx}^4}{h^4} \int z^4 \sum_{n=0}^{30} \frac{\mathcal{F}^{(n)}A(h/2)}{n!}(x - h/2)^n\, dz\ , \tag{3.10}$$

where 30 is the order of expansion and $\mathcal{F}^{(n)}$ is the n^{th} derivative operator. This integration is performed analytically using the software package *Mathematica*® (Wolfram Research,

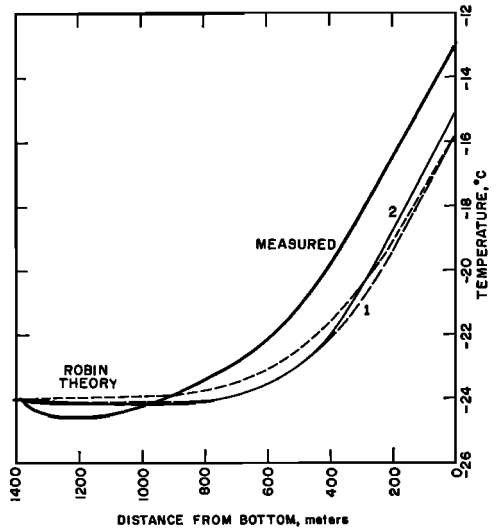

a Greenland temperature profile

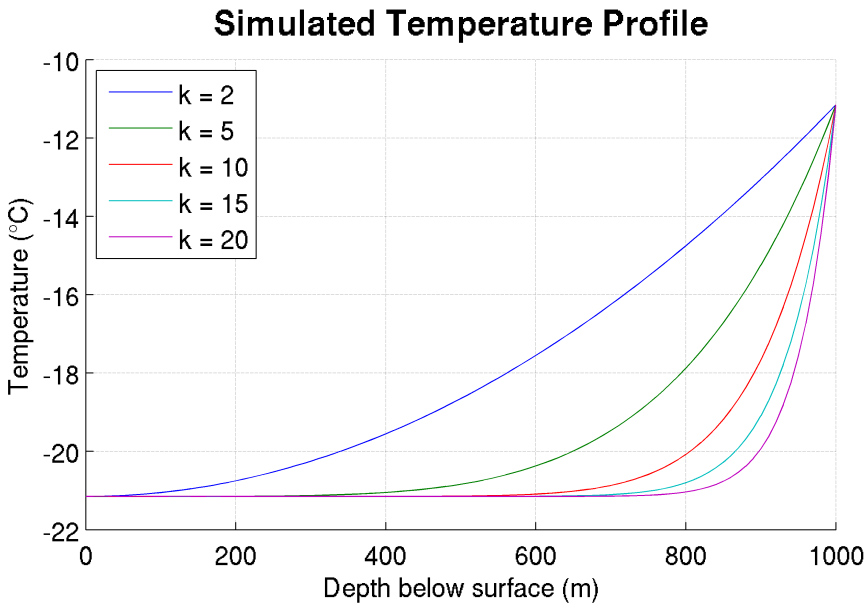

b Simulated temperature profile

Figure 3.3 (a) The vertical temperature profile at Camp Century in Greenland (Weertman, 1968). The location of Camp Century is plotted in Figure 3.8. b) The evaluation of Equation 3.7 for a range of the controlling parameter $k = \{2, 5, 10, 15, 20\}$. The value $k = 10$ is used to calculate the strain heat flux because its shape is closest to the same of the measured curve in (a).

Inc, 2008). A 30^{th} order expansion converges over the desired depth range and allows a margin of error in case varying the parameters affects the convergence. The integration is not reproduced here due to its size. The result is expressed as the function

$$H_s(z, h, \theta_s, T_b, T_s, k) \; . \tag{3.11}$$

θ_s is the surface gradient and is a component of the shear stress $\tau_{dx} = -\rho_i g h \theta_s$. Due to this equation's many variables, I only refer to it by the variables that are changing as long as the meaning is unambiguous. Figure 3.4 plots $H_s(z, 1000, 0.01, 262, 252, 10)$ against z to show a sample depth profile produced by the function.

3.3.2 Sensitivity

Equation 3.11 is sensitive to the temperature profile $T(z)$. For a given ice thickness of 1000 m and surface gradient of 0.01, Figure 3.5 plots the range of basal strain heat flux as T_b and T_s vary when $k = 10$. This variation is a consequence of the non-Newtonian nature of ice dynamics. For constant h, θ_s, and k, strain heat flux $H_s(T_b, T_s)$ at the bed is more sensitive to T_s than T_b, but the sensitivity to T_b increases close to the pressure melting point.

In my derivation, the variable k, used to modify the shape of the temperature profile, controls the relative sensitivity of the system to T_s and T_b. As k increases, larger proportions of the ice column are closer to the surface temperature than the bed temperature. Changing the surface temperature therefore has a larger affect on the integration than the bed temperature. This sensitivity to T_s comes from the overall variation of the flow parameter A through the ice column. Varying T_s shifts the large, low-gradient portion of the curve near the surface. This produces a large change in area under the graph, compared to varying T_b by the same magnitude. Because strain heat flux depends on basal ice temperatures, they also depend on geothermal heat flux. This is a small effect due to the relative insensitivity on T_b demonstrated.

Interestingly, because strain heat flux depends on the temperature of the whole ice column, it also depends on past ice history. This implies that past climate, for example, may influence strain heating fluxes. It also leads to a feedback mechanism whereby ice heated by strain heating has higher strain heating rates. If the system is in thermal equilibrium, both these effects are removed but real ice sheets are not likely to be in thermal equilibrium (Hindmarsh,

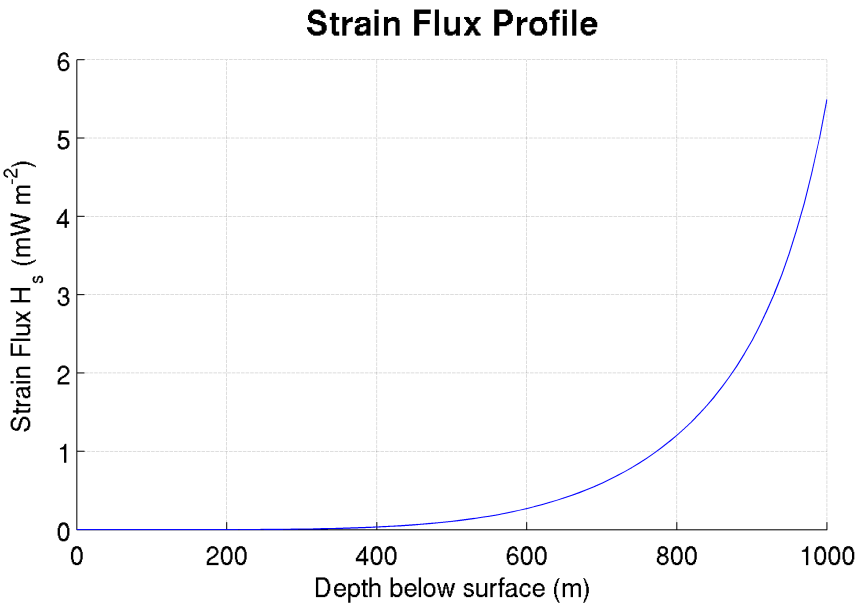

Figure 3.4 The strain heat flux through a vertical ice column of 1000 m with a 0.01 surface gradient. In this plot: $T_b = 262$, $T_s = 252$, $k = 10$. In this instance, the strain heating at the bed is calculated to be one less order of magnitude than the usual geothermal flux assumed for Greenland, $H_g = 42\,\mathrm{mW\,m^{-2}}$ (Lee, 1969; Greve, 1996; Johnsen et al., 2002).

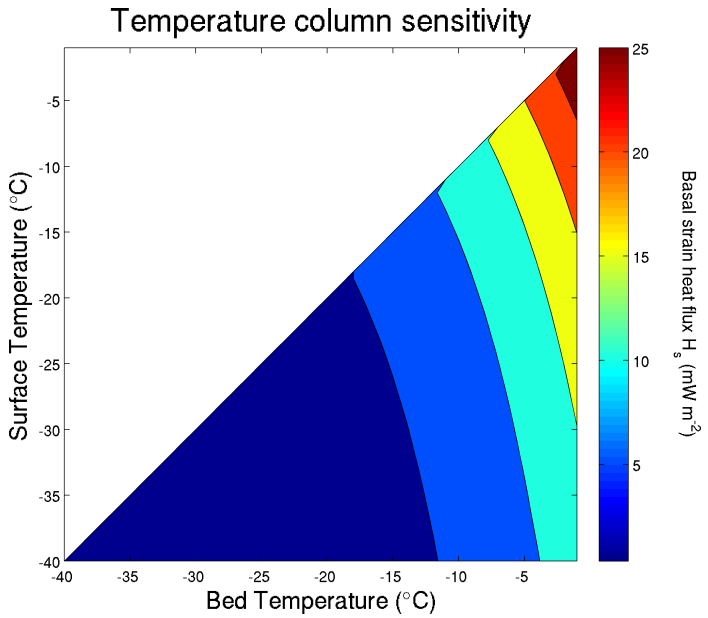

Figure 3.5 The strain heat flux H_s is sensitive to the temperature profile. This plot shows the variability of $H_s(T_b, T_s)$ in the domain $T_s < T_b$. Other variables are set as $h = 1000$ m, $dh/dx = 0.01$, $k = 10$. The system is more sensitive to surface temperature than bed temperature, although the degree of sensitivity changes with k and h.

1990). In this thesis, these effects are adequately dealt with by GLIMMER's temperature handling. They do not impact on understanding the response to surface-draining lakes beyond controlling the background hydraulic pressure profile so are not dealt with further.

Strain heat flux H_s is also sensitive to ice thickness h and surface gradient Θ_s. Due to the stresses in ice sheets the largest surface gradients are near the margin where ice is thin. Conversely, where ice is thick surface gradients tend to be low. The exception to this is where there are deep subglacial troughs. As discussed in Section 3.2, if these areas are presumed not to slide (as in this discussion) then larger surface gradients can exist with thicker ice leading to large H_s. Figure 3.6 plots the mathematical surface of basal H_s for a range of h and Θ_s, but without any implied coupling. Only values less than $H_s = 1000\,\mathrm{mW\,m^{-2}}$ are plotted. The basal strain heat flux is generally below the often cited value[1] for Greenland ($42\,\mathrm{mW\,m^{-2}}$, dashed contour) implying that in the majority of areas under the ice sheet geothermal heat flux dominates. However H_s does cross the $42\,\mathrm{mW\,m^{-2}}$ contour with reasonable h, Θ_s combinations. Where H_s dominates it is likely to be one to two orders of magnitude more important than H_g.

3.3.3 Greenland maps

I now apply these equations to Greenland and compare the basal strain heat flux H_s to typical geothermal heat flux H_g values.

Setup

The basal strain heat flux equation (3.10) depends on surface and basal ice temperatures, as well as surface gradients, Figure 3.7. For Greenland, surface temperature data are available but basal temperature data are harder to find. One solution is to run GLIMMER to calculate basal temperatures, but these do not equate to present day ice thicknesses and depend on the initial model configuration to some extent.

Other options include defining arbitrary basal temperatures based on the pressure melting point or interpolating from the few ice core data available. Defining temperatures based on pressure melting point does not take the advection of cold ice in the interior of the ice sheet into account. There are too few ice core data to produce a reasonable interpolation.

[1] Discussed in the following section.

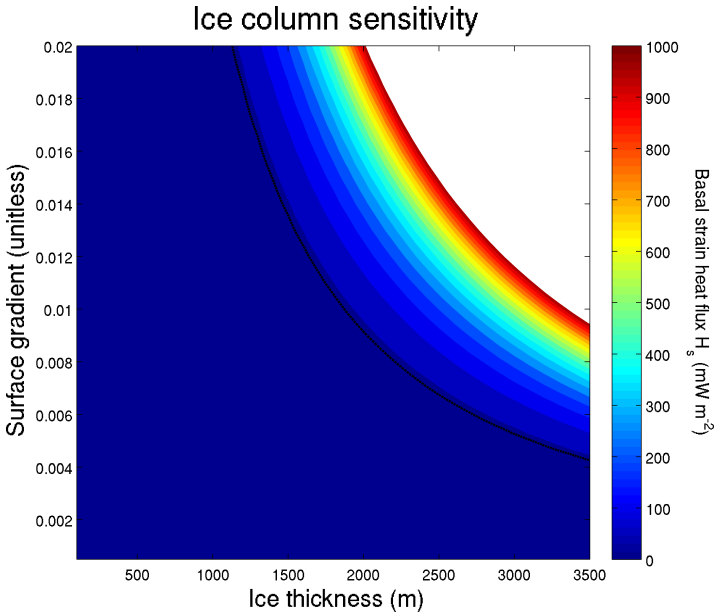

a Varying h and Θ_s

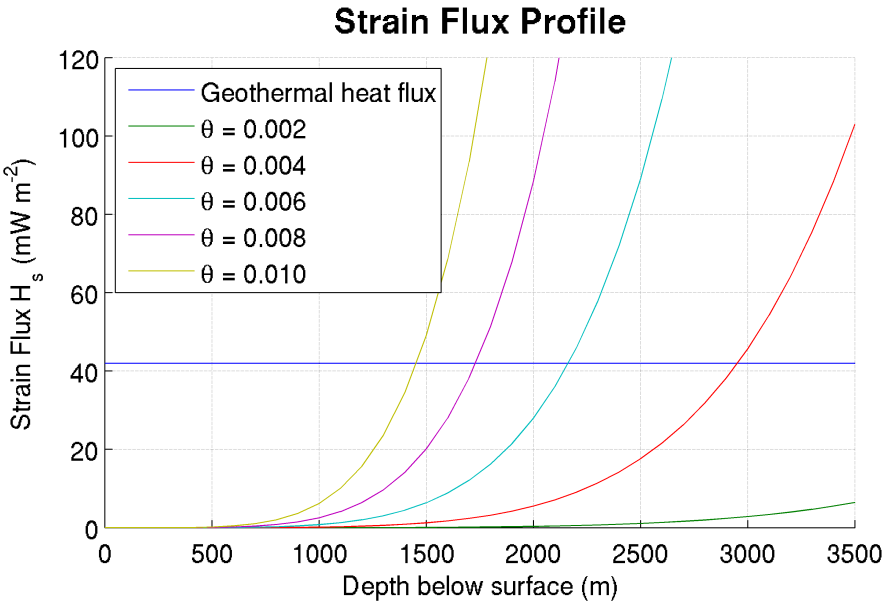

b Varying Θ_s with constant $h = 1000\,\mathrm{m}$

Figure 3.6 Strain heat flux at the bed is sensitive to both surface gradient Θ_s and ice thickness h. (a) A mathematical surface of basal strain heat flux H_s with varying h and Θ_s. Values larger than $1000\,\mathrm{mW\,m^{-2}}$ are omitted. The dashed contour line represents $H_g = 42\,\mathrm{mW\,m^{-2}}$, the geothermal heat flux often quoted for Greenland. (b) basal H_s curves as ice thickness increases, for range of surface gradients $\Theta_s = (0.002, 0.004, 0.006, 0.008, 0.010)$. These plots wrongly assume no correlation between h and Θ_s to allow a comparison.

Theoretically, strain heat flux H_s at the bed ranges from less than geothermal heat flux (dashed contour in (a), blue line in (b)) to much larger than it. In the interior of ice sheets, H_g dominates and near the margin H_s dominates.

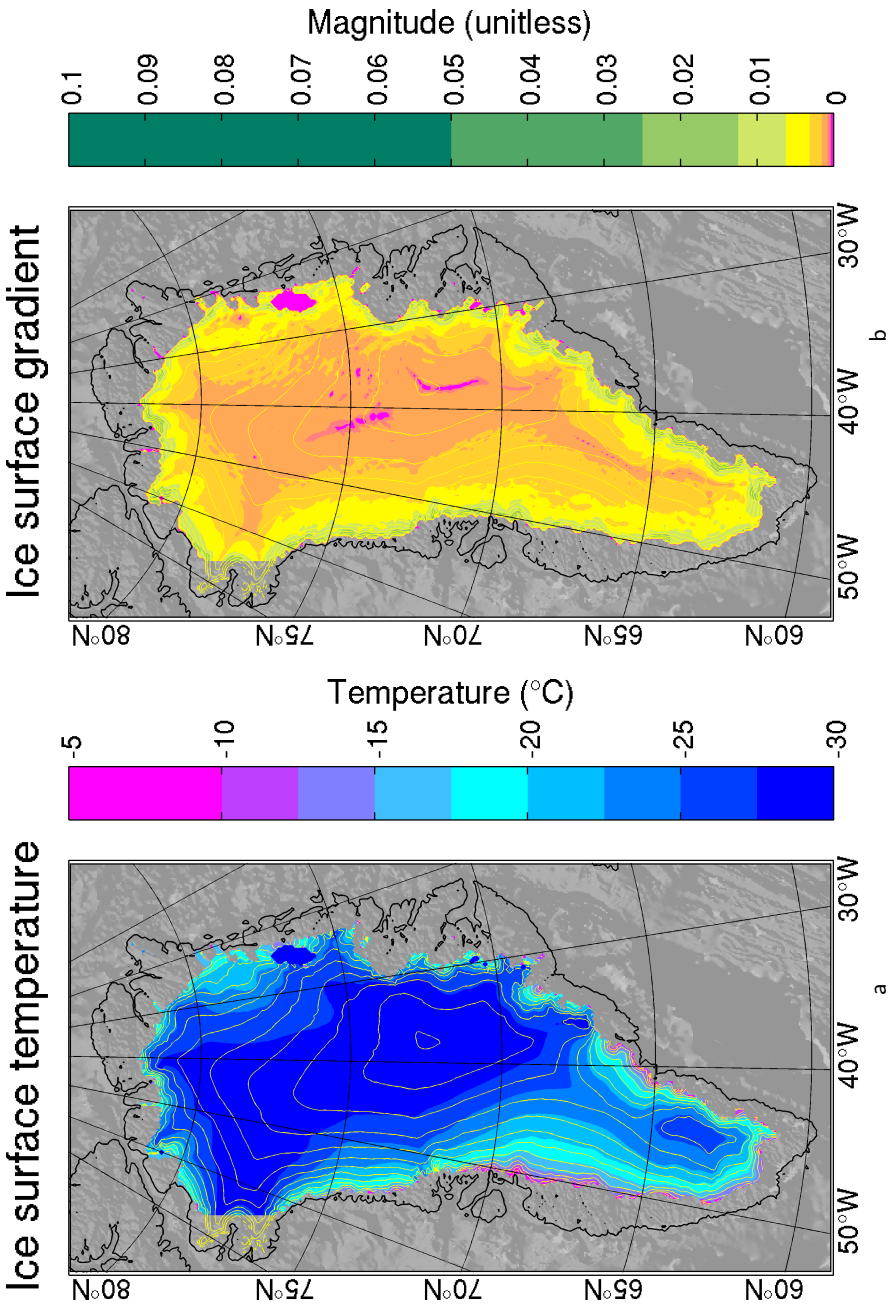

Figure 3.7 (a) Average present day ice surface temperatures (calculated by GLINT using NOAA Climate Prediction Centre data) are used to provide the upper boundary conditions for calculating strain heat flux at the bed. Strain heat flux H_s is more sensitive to surface ice temperature than basal ice temperature due to the integration of the term through the ice column.

(b) Surface gradients are an important control on strain heat flux H_s. The colour scale is adjusted to emphasises low values. High values at the margin are not plotted to constrain the range.

Overall, modelling is a good solution in this context. The relative insensitivity of H_s to T_b means that if the basal temperatures are not that accurate, it does not affect the result too much. However, because basal temperatures depend on geothermal heat flux, I still run GLIMMER for each H_g value to generate estimated basal temperature.

I prefer to use present day ice for calculating H_s because it is easier to relate to. GLIMMER produces ice that is more spatially extensive than present day Greenland, but the cold-based centre is well within the bounds of present day ice. At the margin, the ice is at pressure melting point and so the bed temperature is a direct function of the ice thickness. The only place where calculated values become important is where the ice is cold, ie the interior. This means that cropping the calculated basal ice temperatures to present-day Greenland does not affect the results significantly.

Geothermal heat flux

As the results from this experiment depend on, and are compared to, geothermal heat flux H_g, it is worth diverging for a short discussion about this heat source. Geothermal heat comes from two main sources. Approximately 80% of the heat comes from radioactive decay in the Earth's core. The remainder is residual heat from the formation of the planet (Turcotte and Schubert, 2002). The geothermal heat flux for Greenland is often cited to be $42\,\mathrm{mW\,m^{-2}}$ (Lee, 1969; Huybrechts and Payne, 1996; Greve, 1996; Johnsen et al., 2002). Greve and Otsu (2007) publish a contour map of geothermal heat flux for Greenland based on model data from Pollack et al. (1993) tuned with measurements from four ice-core sites, Figure 3.8. The data presented by Greve and Otsu (2007) is heavily influenced by the four measurement points making the data away from these points questionable. For example, even at the Dye 3 core, H_g is only constrained between 30 and $45\,\mathrm{mW\,m^{-2}}$ (Dahl-Jensen and Johnsen, 1986; Hooke, 2005). Instead of using their map directly, I simply use the range of values to constrain the range of geothermal heat fluxes.

Strain heat flux does not affect geothermal heat flux, but geothermal heat flux affects basal ice temperature T_b and therefore the strain heat flux. Figure 3.9 shows the bed temperatures calculated by three GLIMMER runs[2] at 100 ka using uniform geothermal heat fluxes of $H_g \in \{0, 50, 100\}\,\mathrm{mW\,m^{-2}}$. GLIMMER was run as released and its solution includes

[2] These runs are discussed in further detail in Section 3.4.2 where they are used to supply the initial conditions for HYDRO runs.

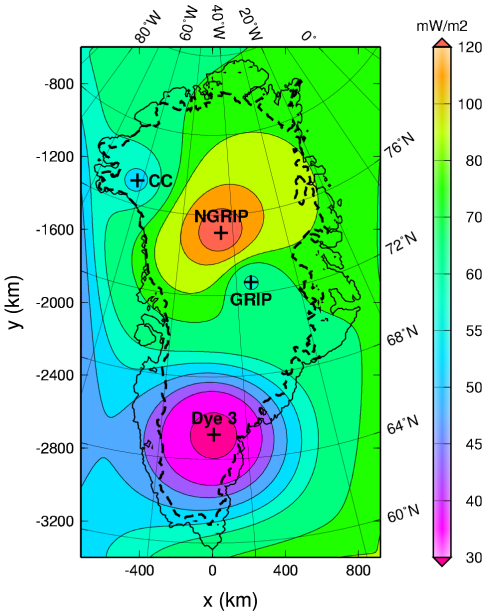

Figure 3.8 Geothermal heat flux map from Greve and Otsu (2007), based on data from Pollack et al. (1993) and ice-core sites: GRIP, NGRIP, Camp Century and Dye 3 (Greve and Otsu, 2007). Due to the sparse interpolation of data I believe this map, while providing a useful upper and lower bound, is not accurate enough to be useful in this thesis. Nevertheless, it highlights that the uniform geothermal heat flux used is an oversimplification.

strain heating, advection, diffusion and simple sliding friction heat terms. The cold bed ($T_b < T^*$) has not reached equilibrium but the warm regions ($T_b = T^*$) have. The ice sheet expands early in the run due to the climate but the extent is then constant.

When $H_g = 0\,\mathrm{mW\,m^{-2}}$, the only heat source in the interior of the ice sheet is from strain heating. Figure 3.9 (b) shows that when there is no geothermal heat, a large proportion of the bed is cold. The cold region of the bed is centred on the ice divide and the location of this does not change throughout the run. This gives me faith that the bed temperatures may approximate the temperature pattern obtained with present day ice for different heat fluxes. As geothermal heat flux increases, the area of the bed that is warm and the minimum temperatures, in the interior, increase. This shows that geothermal heat flux helps counter the advection of cold ice whereas strain heating on its own cannot. Geothermal heat flux does not act on its own however because as the ice warms the strain heat flux increases as well.

There is a final effect which warrants mention. Topography affects the distribution of geothermal heat flux, where the flux intensifies in valley bottoms and attenuates near valley

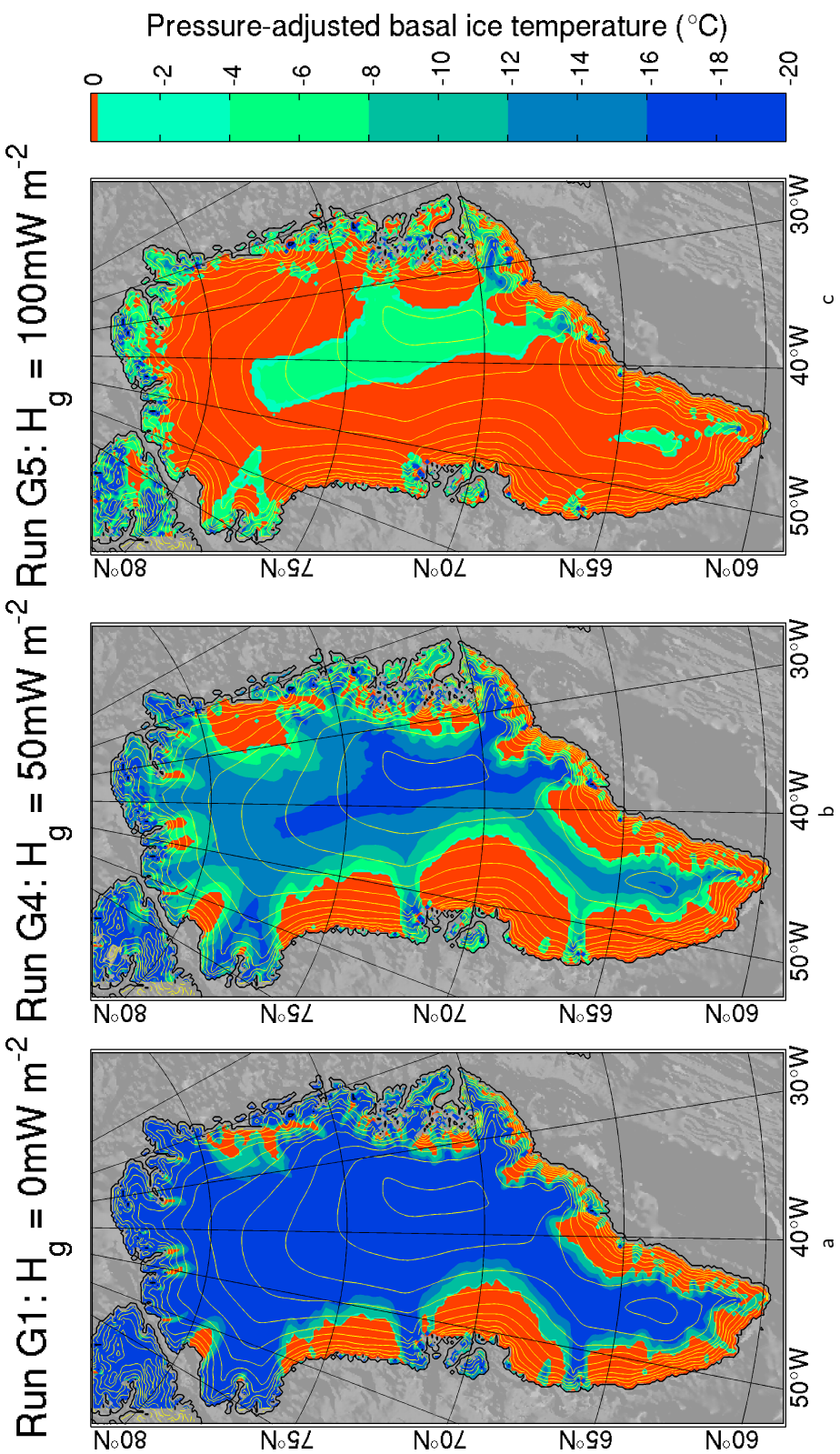

Figure 3.9 Pressure-adjusted basal ice temperatures calculated by GLIMMER using uniform geothermal heat flux (a) $H_g = 0$, (b) 50, and (c) 100 mW m^{-2} are used to define the basal boundary for calculating strain heat flux at the bed. The model runs used (G1–5) are defined in Section 3.4.2. The non-frozen bed is shown as orange. This area is highly dependant on the value of H_g used. The ice temperature drops to −33 °C in (a) but values below −20 °C are not displayed.

tops. Van der Veen et al. (2007) find, using ground penetrating radar, that this may double local geothermal heat flux under Jakobshavn Isbræ. However, this effect is localised and the DEMs used in this project are too coarse for resolving it.

Heat flux to melt rate

Before taking this discussion further, let me look at how heat fluxes translate into melt. This helps translate the heat fluxes presented into a potentially more familiar basal melt rate term, assuming all the energy melts ice.

For a given energy input, if all energy melts ice, then the mass of ice melted is $m = Q/\mathcal{H}$, where $\mathcal{H}$ is the enthalpy of fusion. Dividing the mass by $\rho_w a$ gives the melt rate in $\mathrm{m\,a^{-1}}$. The total energy entering the system for an area a over a time t is $Q = Hat$. Combining, the melt rate for a heat flux H is

$$M = \frac{Ht}{\mathcal{H}\rho_w} \,. \tag{3.12}$$

For water, $\mathcal{H} = 333,500\,\mathrm{J\,kg^{-1}}$ (Lide, 2004). A heat flux of $1\,\mathrm{mW\,m^{-2}}$ therefore produces a melt rate of $0.946\,\mathrm{mm\,a^{-1}}$, or roughly $1\,\mathrm{mm\,a^{-1}}$, when all energy goes to melting.

Maps

Figure 3.10 shows the basal strain heat flux maps for Greenland with basal ice temperature defined from $H_g \in \{0, 50, 100\}\,\mathrm{mW\,m^{-2}}$ and $T_b = T^*$. Strain heat flux values are largest near the margin due to steeper surface gradients. The final value for T_b provides an upper limit on basal ice temperature. The maximum strain heat flux is the same for all the runs. This is expected because the highest strain rates are near the margin where there is fast flowing ice and the bed is at pressure melting point.

The strain heat flux shows good correlation with surface ice velocities. This is due to the shallow ice approximation used in the derivation and is not physical. The basal ice is assumed to not slide and so has high deformation due to the thick ice in outlet glaciers (deep troughs in basal topography), coupled with high surface gradients near the margin. In real outlet glaciers, lateral strain is more important than basal strain but, overall, the frictional energy of the deformation must release somewhere. It is doubtful whether this will be near the bed as assumed here. Nevertheless, the strain heat maps give a good indication of the heat sources used in this thesis. Possibly even, results that are approximately correct are

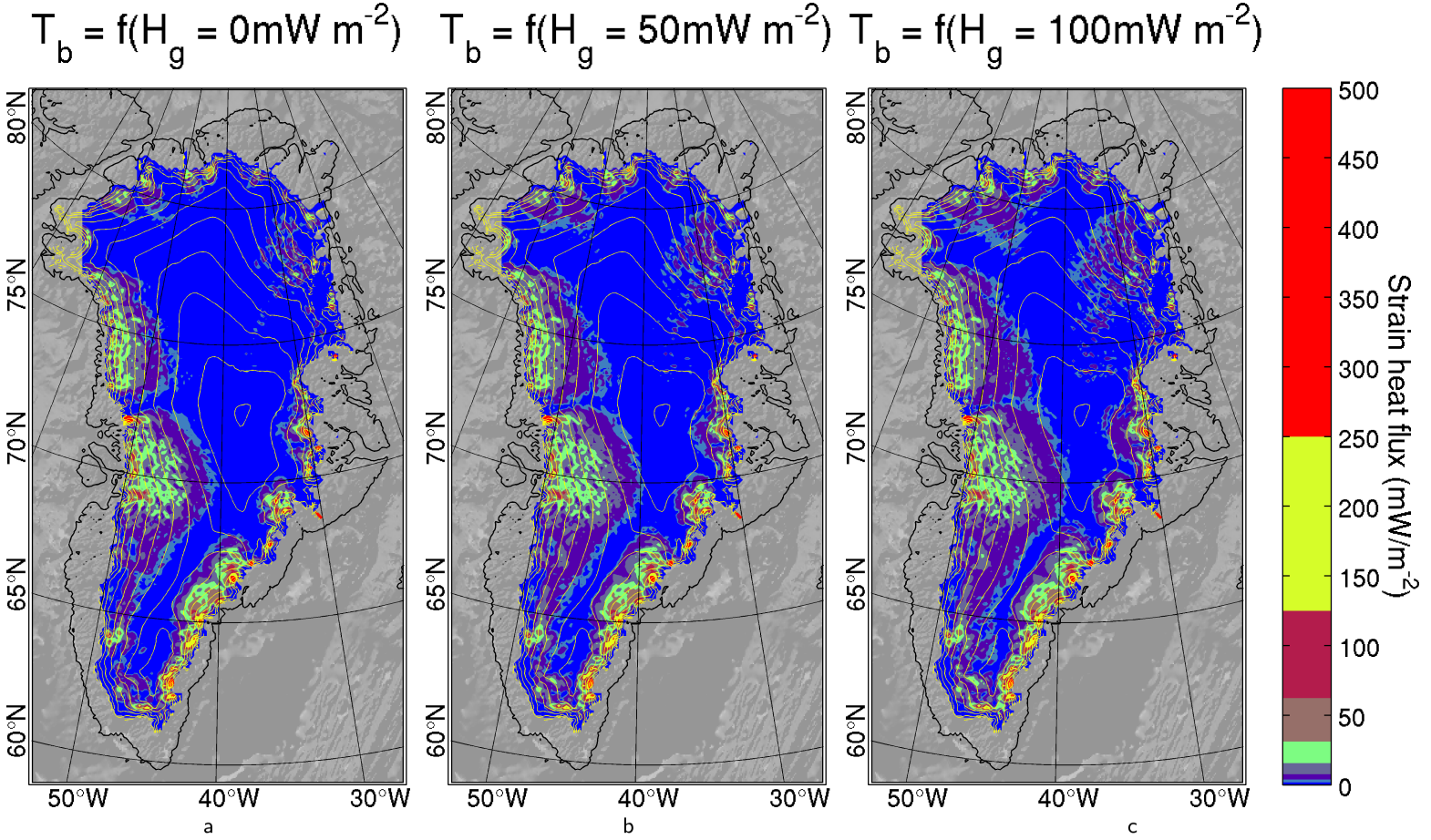

Figure 3.10 Strain heat flux maps for Greenland. The basal ice temperature are calculated from (a) $H_g = 0\,\mathrm{mW\,m^{-2}}$, (b) $H_g = 50\,\mathrm{mW\,m^{-2}}$, and (c) $H_g = 100\,\mathrm{mW\,m^{-2}}$. The values of cells at the margin are not plotted because the surface gradient gets steep. The colour mapping is adjusted to emphasise the low values; values above 500 $\mathrm{mW\,m^{-2}}$ are not shown. The highest values is around $1500\,\mathrm{mW\,m^{-2}}$ in all runs.

Notice that: H_s increases in the vicinity of the NEGIS as H_g increases; values near the margin are independent of H_g because surface gradient dominates; and the area near the ice divide with low H_s shrinks with increasing H_g. This is noticeable in the south and the ice surface ridge around 72 °N on the western margin.

obtained from incorrect physical reasons.

3.3.4 Summary

These data suggest the following conclusions:

1. Strain heat flux is insignificant near the ice divide, even if the bed is at pressure melting point.

2. For the majority of the bed (purple and light blue in Figure 3.10; max H_s = $100\,\mathrm{mW\,m^{-2}}$) geothermal heat flux is at least an order of magnitude larger than strain heat flux.

3. There are significant areas (yellow; max $H_s = 50\,\mathrm{mW\,m^{-2}}$) where strain and geothermal heat fluxes are of similar importance. This is the case near Jakobshavn Isbræ.

4. Areas of high strain heat flux (dark red; max $H_s = 500\,\mathrm{mW\,m^{-2}}$ and red; max $H_s = 1500\,\mathrm{mW\,m^{-2}}$) correlate well with the locations of the outlet glaciers.

In summary, strain heat flux is less important than geothermal heat flux in the interior. Towards the margin, its importance increases until the strain heat flux becomes the dominant of the two terms. It is especially important in the outlet glaciers. Geothermal heat is important in the interior, without which, large areas of the bed would remain frozen. Strain heating depends on temperature pre-conditions and so strong feedbacks and coupling exists.

3.4 Background hydraulic pressure profile

The remainder of this chapter investigates the controls on the background hydraulic pressure profile produced by basal melting. The goal is to establish basal boundary conditions for the coupled Glimmer-Hydro model and to establish a framework to discuss surface melt water perturbation in Chapter 5.

To avoid ambiguity, I now define terms commonly used in this chapter. A *uniform melt rate* is spatially and temporally constant. A *variable melt rate* is spatially variable, but in this chapter, temporally constant. In *warm* regions water can flow anywhere under the ice and the bed is at pressure melting point. *Cold* regions (below the pressure melting point) are impermeable. A *frozen bed* contains cold basal ice.

3.4.1 Research questions

HYDRO is run to equilibrium for a variety of model set-ups to determine the influence of melt rate, basal diffusivity, hydraulic efficiency, and an impermeable frozen bed. These are all factors which potentially affect the behaviour of HYDRO on a Greenland-wide scale and must therefore be determined before the model can be used to investigate more complicated processes. Key questions are:

1. What is the pressure distribution when a uniform basal melt rate is used? How does this distribution change with melt rate? What processes control this?

2. Does allowing an efficient bed affect the system? How sensitive is the system to choice of the efficiency factor ψ, an abstract concept in HYDRO?

3. How sensitive is the system to size and shape of the frozen bed? How accurately must this be modelled by GLIMMER to produce reasonable input for HYDRO?

3.4.2 Experimental set-up

The experiment is performed in four stages, each building on the previous: uniform basal melt (1), with hydraulic efficiency (2), with a frozen bed (3), and basal melt calculated by GLIMMER with efficiency and a frozen bed (4). HYDRO is run, without GLIMMER, to equilibrium using the 5 km DEM for Stages 1–3 and the 10 km DEM for Stage 4. Table 3.1 shows the model runs used in each experiment stage.

Experiment stages

The experiment uses four stages because this builds an intuitive understanding of the processes controlling the model. A single process (eg diffusion, efficiency, frozen bed) can be examined before the next is introduced. By using a uniform melt rate, one can look at where water converges (low effective pressure) as a result of the flow and not the increased melt in these regions. Water tends to converge in subglacial troughs, but these areas also tend to have fast flowing ice and therefore high basal melt rates due to increased strain heating and possibly sliding friction. This extra complexity is ignored until Stage 4, by which time the effects of diffusion, efficiency, and the frozen bed are known.

Pressure profile model runs

Stage	Run	Variable	Values	ψ
1	H1–13	M	$M \in \{0.5, 1, 2, 3, 4, 5, 6, 7, 8, 9, 10, 50, 100\}\,\mathrm{mm\,a^{-1}}$	1
2	H14–17	ψ	$\psi \in \{10, 25, 50, 100\}$, $M = 100\,\mathrm{mm\,a^{-1}}$	—
	H18–30	M	M as H1–13	10*
3	H31–67	$\mathcal{C}_F \times M$	$\mathcal{C}_F \in \{1500, 2000, 2250, 2500, 2750, 3000\}\,\mathrm{m}$	1
	H68–104	$\mathcal{C}_F \times M$	$\times\ M \in \{1, 3, 5, 7, 10, 100\}\,\mathrm{mm\,a^{-1}}$	10*
4	G1–5	H_g	$H_g \in \{0, 30, 40, 50, 100\}\,\mathrm{mW\,m^{-2}}$	—
	H105–109	M	M from G1–5 output	100

Table 3.1 Summary of model runs in this chapter: H denotes HYDRO runs and G denotes GLIMMER runs.

Each stage increases the complexity of the experiment. Stages 1–3 use a uniform basal melt rate M. Stage 1 uses a warm and inefficient ($\psi = 1$) bed. Stage 2 introduces efficiency ($\psi = 10$) for all melt rates and varies the efficiency factor ψ for a single melt rate. Stage 3 introduces a frozen bed. It has two sets ($\psi \in \{1, 10\}$) of 36 runs each, varying both the frozen area (defined off surface contours $\mathcal{C}_F$) and melt rate. Stage 4 uses a spatially varying, but temporally constant, basal melt rate calculated by runs G1–5; the bed is defined as frozen where $M = 0\,\mathrm{mm\,a^{-1}}$.

*$\psi = 100$ for $M \geqslant 50\,\mathrm{mm\,a^{-1}}$

Stage 4 (runs G1–5) uses the 10 km DEM as GLIMMER is not stable with the 5 km DEM. The run is very nearly to thermal equilibrium, as described in Section 3.1. The runs are not to full equilibrium, because the runs take a long time and equilibrium is achieved asymptotically so increasingly lengthy runs are needed for little extra gain. Once the size of the frozen bed appears quasi-stable, I terminate the run. Runs G1–5 use strain heating and basic sliding friction heating for calculating the basal melt rate for geothermal heat fluxes $H_g \in \{0, 30, 40, 50, 100\}\,\mathrm{mW\,m^{-2}}$. Frictional heat generation is considered in much more detail in Chapter 4.

Stage 1: Uniform melt with warm bed

The uniform basal melt rates are chosen to go from unrealistically low to unrealistically high to understand the parameter space and to understand the process controlling subglacial water pressure. In Section 3.3.3, the majority of the strain heat flux is shown to be below $50\,\mathrm{mW\,m^{-2}}$ and the maximum geothermal heat flux is $120\,\mathrm{mW\,m^{-2}}$ in a region where strain is low (NGRIP core). I define uniform basal melt rates 1 to $10\,\mathrm{mm\,a^{-1}}$, in $1\,\mathrm{mm\,a^{-1}}$ increments.

To cover an extra low scenario I use $0.5\,\mathrm{mm\,a^{-1}}$. I use $100\,\mathrm{mm\,a^{-1}}$ to overestimate[3]. The high and low values help determine the limits of behaviour. The range is concentrated around $1\text{–}10\,\mathrm{mm\,a^{-1}}$ because this is the order of magnitude that GLIMMER predicts (runs G1–5). It also agrees with the values of other studies; Buchardt and Dahl-Jensen (2007) calculate a basal melt rate of $6.1\,\mathrm{mm\,a^{-1}}$ at NGRIP.

The bulk diffusivity, a function of hydraulic conductivity κ, is defined by $\kappa = 3.0 \times 10^{-3}\,\mathrm{m\,s^{-1}}$. This number is loosely based on the value of conductivity through subglacial till (eg Heigold et al., 1979; Boulton and Zatsepin, 2006; Boulton et al., 2007), but is arbitrary because it is impossible to determine it for the majority of the Greenland ice sheet because of the inaccessibility of the subglacial system. Halving or doubling it results in unstable HYDRO runs due to steep gradients (doubled) or lack of flow (halved). The important distinction, within a non-physical modelling context, is the difference in κ between efficient and inefficient regions. With an inefficient bed, or with a high efficiency factor ψ, the final equilibrium profile does not vary with a $\pm 10\%$ change of κ. Only the time taken to reach equilibrium is affected. Because I only consider equilibrium profiles in this chapter, I do not vary the value of κ until Chapter 5 when time-dependent effects become important.

Stage 2: Hydraulic efficiency

In Stages 2–4, efficient areas are allowed anywhere $p_r > 0.9$. This value is, to an extent, arbitrary but for any value in the region close to 1, the principles demonstrated are the same. 0.9 is chosen because efficient areas likely form before $p^* = p_{\mathrm{ice}}$ for the entire 5 km or 10 km cell. It would be better to run the experiment with a range of values, but there are practical limits to how many variables can be used and how many model runs can be undertaken. Using a value of 0.9 seems to be a reasonable approximation to keep the experiment manageable.

To keep the model stable, different efficiency factors are used for the 5 and 10 km DEMs and for the higher melt rates ($M \geqslant 50\,\mathrm{mm\,a^{-1}}$). The standard efficiency factor is $\psi = 10$. However, this is ineffective with the 10 km DEM and with high melt rates. In these cases, $\psi = 100$ is used. For a given uniform melt rate, the effect of ψ reaches a limit as ψ increases. The Stage 2 results discuss this further. As long as ψ is sufficiently large, the actual value

[3] $H_g = 120\,\mathrm{mW\,m^{-2}}$ is the maximum value Greve and Otsu (2007) give for Greenland, but this is a spot measurement, I am using $100\,\mathrm{mW\,m^{-2}}$ applied uniformly over all of Greenland.

chosen makes no difference to the run unless it is too high, in which case steep gradients cause instability.

Stage 3: Uniform melt with frozen bed

Stages 3 and 4 introduce a frozen bed because the centre of the Greenland ice sheet is known to be cold-based (eg Huybrechts, 1996).

Stage 3 determines the frozen bed using the ice surface contours. Regions where the surface elevation is above the $\mathcal{C}_F$ contour are defined to have a frozen bed. Figure 3.11 maps the frozen area for $\mathcal{C}_F \in \{1500, 2000, 2250, 2500, 2750, 3000\}$ m. These values are chosen to provide basal conditions ranging from mostly cold to mostly warm. Table 3.2 gives the percentage of warm basal ice present with these contours. $\mathcal{C}_F < 1500$ m results in isolated warm cells along the margin which HYDRO does not handle well. Each $\mathcal{C}_F$ value is run with the same uniform melt rates as Stage 1. Water is only allowed to enter the system where the bed is warm.

Stage 4: Geothermal and strain melting

Stage 4 uses variable melt rate output from the GLIMMER runs G1–5. These runs have reached quasi-thermal equilibrium and model output contains the frozen area. HYDRO sets the bed to be frozen where $M = 0\,\mathrm{mm\,a^{-1}}$.

For this run GLIMMER was used without any of my modifications. Uniform geothermal heat flux values of 0, 30, 40, 50 and 100 $\mathrm{mW\,m^{-2}}$ are used. There is a cluster around 40 because the standard geothermal heat flux for Greenland is often quoted to be 42 $\mathrm{mW\,m^{-2}}$.

Warm bed percentage

Contour	Warm area
1500 m	16.9%
2000 m	24.7%
2250 m	47.1%
2500 m	61.6%
2750 m	77.2%
3000 m	91.3%

Table 3.2 The warm (red) areas in Figure 3.11 are expressed as a percentage of the area covered by ice.

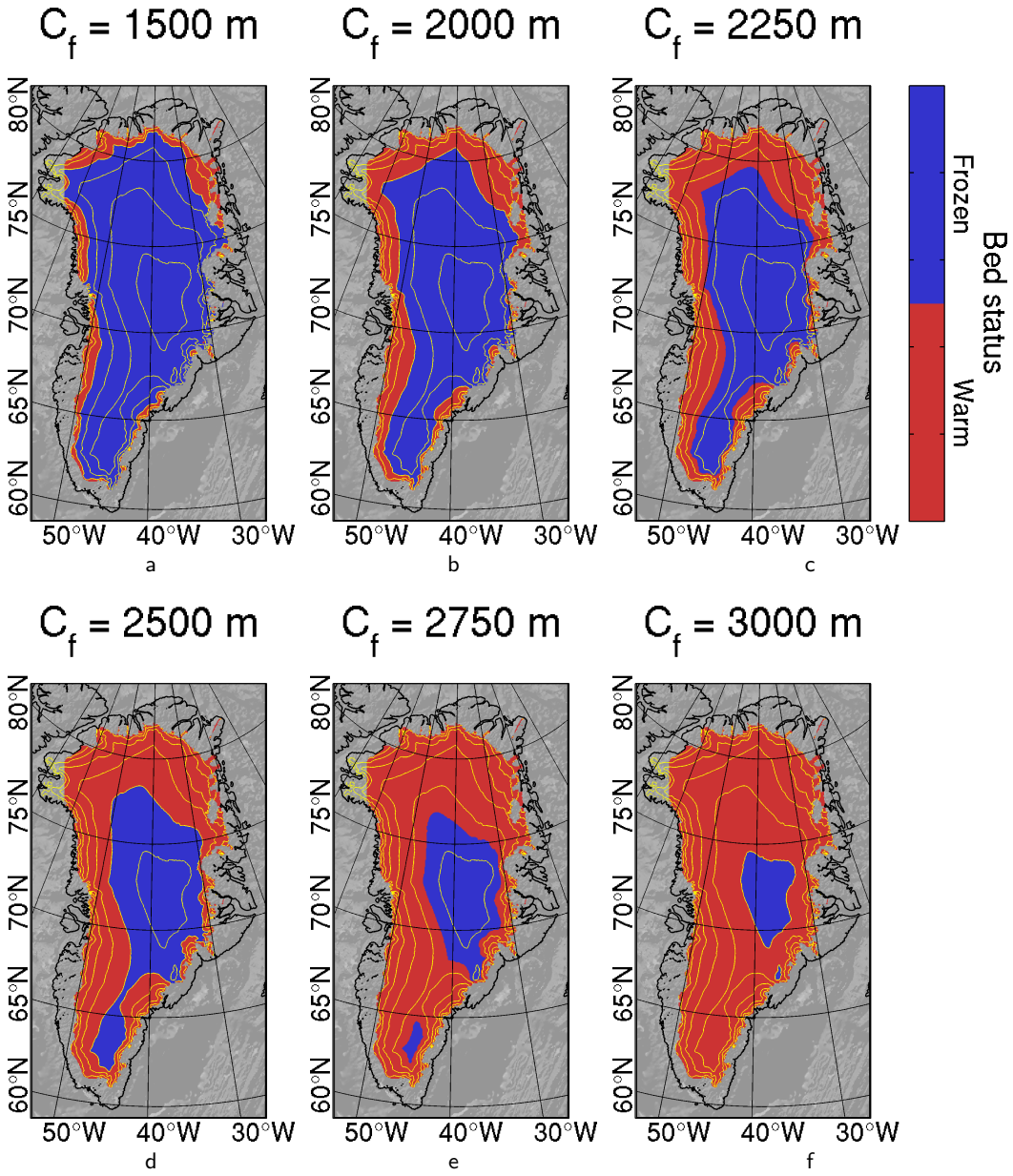

Figure 3.11 The frozen bed (blue) for Stage 3 is defined using surface elevation, a reasonable first approximation. Stage 3 uses a range of uniform basal melt rates where the bed is warm (red). Stage 4 uses GLIMMER for more realistic melt rates and the frozen area definitions (Figure 3.9).

Greve and Otsu (2007) give 120 mW m^{-2} as the maximum in the north of Greenland, at a single location, so 100 mW m^{-2} over all of Greenland is used as an upper bound.

The varying geothermal heat flux pattern proposed by Greve and Otsu (2007) (Figure 3.8) is not used to define any runs because I do not feel those data are reliable. The contour plot produced is highly dependent on measurements from four sites which have been interpolated over the domain. A range of geothermal heat fluxes proposed by that work is used here and, for the observations that I am making from these model runs, I feel this is sufficient.

3.4.3 Results

Results are presented by experiment stage. Key observations are discussed within each stage to enable full understanding of the following stages. Section 3.5 consolidates these discussions and identifies key processes affecting the background hydraulic pressure.

Stage 1: Uniform melt with warm bed

The top row of Figure 3.12 maps the water pressure p^* equilibrium profiles for different uniform melt scenarios with a warm, inefficient bed (runs H1–13). Runs with similar results are omitted from the figure. The maximum overall pressure raises linearly with the melt rate. The bottom row of Figure 3.12 maps normalised effective pressure $\bar{N}$ (range $[0, 1]$) at equilibrium. Where $\bar{N} = 0$, water pressure is at ice overburden pressure.

For lower melt rates ($M < 4\,\mathrm{mm\,a^{-1}}$), topography determines water location. Water converges in the troughs and as the pressure rises, effective pressure falls. The water diffusion is effectively smoothing out irregularities in the hydrostatic surface. As the melt rate increases, the pressure distribution becomes less dependent on the topography. Water pressure begins to overwhelm the topographic signal, especially away from the margin where the ice is thick. Ridges in the pressure ratio surface still correlate well with the location of outlet glaciers, near the margin.

An entirely inefficient bed, as used in Stage 1, is unrealistic. The inability of the water to flow freely causes a pressure back log and drives up maximum water pressure. Figure 3.12 shows that the majority of the bed is at ice overburden pressure for high melt rates, a highly unlikely scenario. Efficient areas remedy this situation by allowing water to escape (Stage 2).

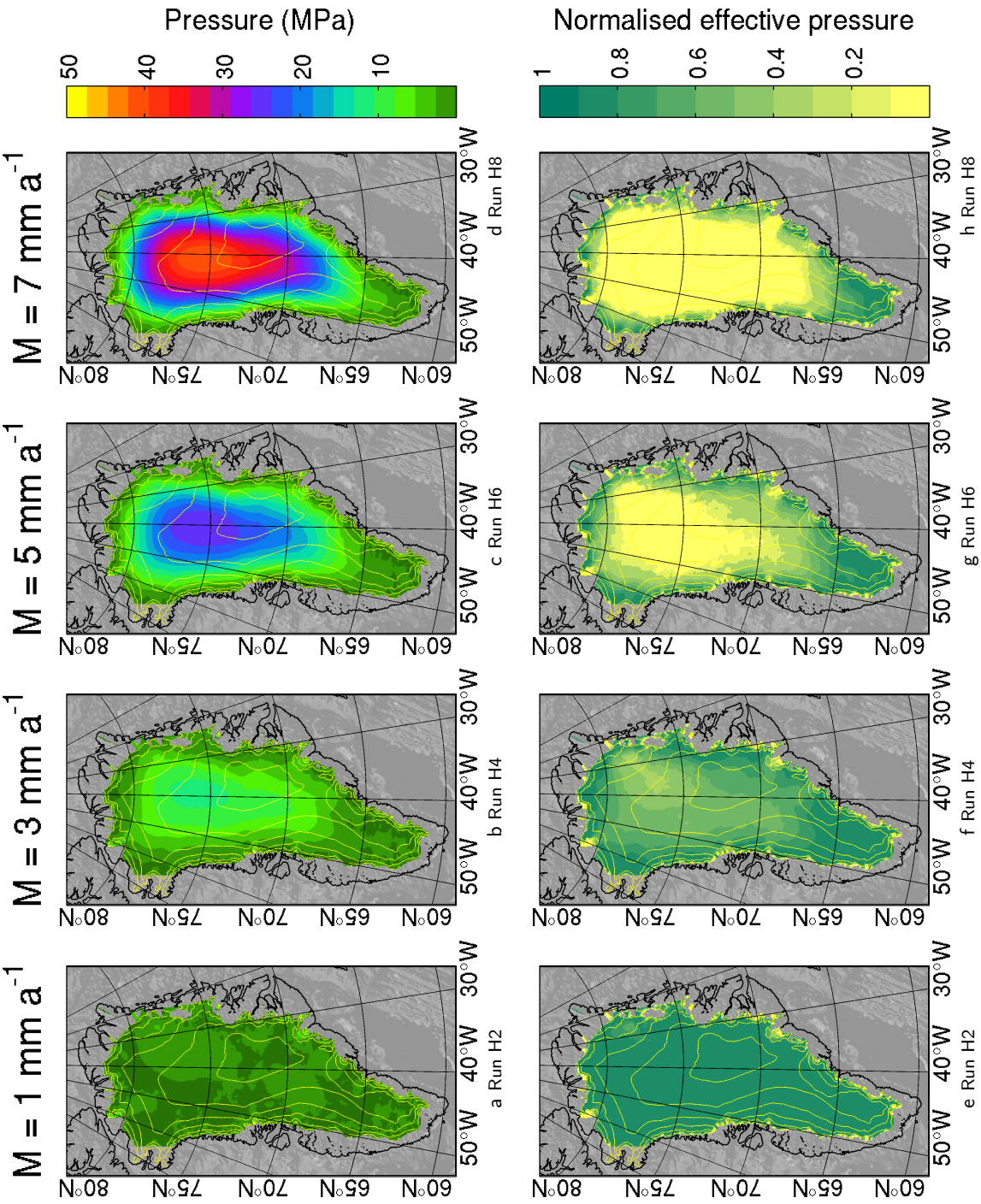

Figure 3.12 Top row (a–d): Equilibrium water flux pressures, p^* for selected uniform basal melt with a fully temperate, inefficient bed. Bottom row (e–h): Normalised effective pressure $\bar{N}$ of the same data. The range of melt covered ($M \in \{1, 3, 5, 7\}$ mm a^{-1}) covers the transition from the topography-dominated regime to the topography-overwhelmed regime. Values less than 1 MPa use finer contours to show detail.

Stage 2: Hydraulic efficiency

The Stage 2 experiment is presented in two parts. First, I look runs H13–17 to demonstrate the effect of increasing the efficiency factor ψ. Next, I show the effect of efficiency on the pressure profile from different melt rates (runs H18–30).

Efficiency factor ψ

As the efficiency factor ψ increases, water passes through, or along, the bed easier in efficient areas. This reduces hydraulic back-pressure and overall maximum water pressures drop. Figure 3.13 plots the maximum water pressure of runs H13–17 against ψ. The limit of the efficiency influence is apparent. This limit is present because once the system is efficient enough to remove the total water that is entering it, it cannot remove it any easier if efficiency is increased. If the water entering the system increases, then an increasing ψ may be appropriate.

Runs H13–17 use a melt rate of $M = 100\,\mathrm{mm\,a^{-1}}$ because this shows the effect very clearly. However, this effect is present for smaller melt rates as well. The maximum pressure and the point at which the limit is reached varies with the melt rate used. With high melt ($M = 100\,\mathrm{mm\,a^{-1}}$) the maximum pressure is highest, and larger ψ is needed before the plateau is reached.

I take a value well into the plateau in Figure 3.13 so that the efficient areas have maximum effect. With low M, $\psi = 10$ meets this requirement; with higher M, $\psi = 100$ is needed. In physical channels, which ψ acts as a proxy for, water pressures are very low. However, channels take up very little physical space and the average water pressure over a 5 or 10 km cell is larger. The Hydro model works by diffusion, so even in efficient areas once the capacity of the system to evacuate all water every time step is surpassed, water pressure will rise with increasing flux. The difference is, it will start to raise later than in inefficient areas.

Background profile

Figure 3.14 maps the water pressure p^* and normalised effective pressure $\bar{N}$ for uniform melt runs with a warm, efficient bed (runs H18–30). Efficient areas are highlighted in blue and enlarged to make them more apparent.

The key result is that the overall maximum pressure has decreased significantly, compared to Stage 1. This is especially noticeable for the $\bar{N}$ maps (Figure 3.14, bottom row) as the majority of the interior is now below ice overburden pressure. Areas of low effective pressure

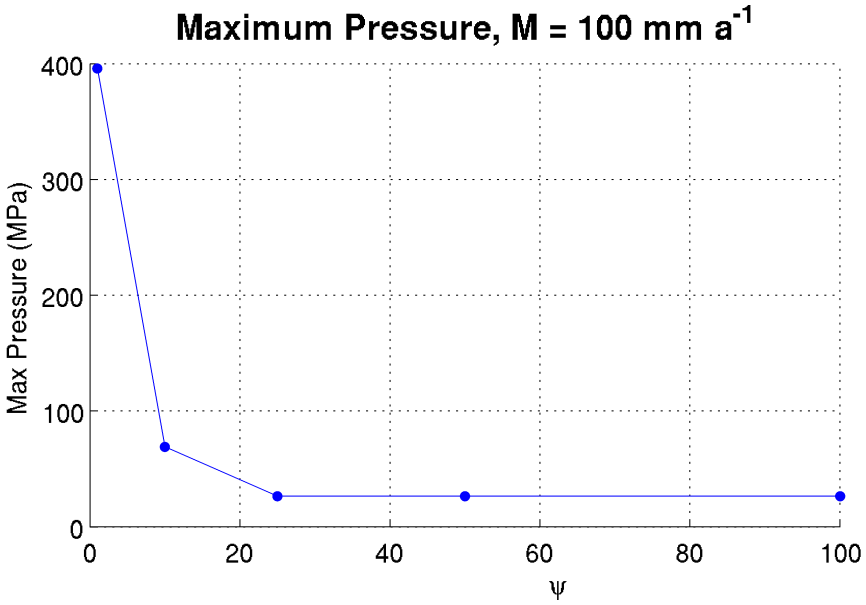

Figure 3.13 The efficiency factor ψ is defined at run-time. It determines how easy efficient areas find it to transmit water.

Each data point represents the maximum equilibrium pressure p^* from a single run. A limit in the factor's influence is reached as ψ increases. The value needs to be chosen with care: if it is too low it has little effect, if it is too high the model becomes unstable. The melt rate is high ($M = 100\,\mathrm{mm\,a^{-1}}$) to make the effect more obvious, but it is present whenever water overwhelms the topography.

correlate well with fast flowing ice and the water pressures are more reasonable.

The maximum pressure and the percent of the bed that is at pressure melting point at equilibrium are plotted in Figure 3.15 for both efficient (runs H18–30) and inefficient (runs H1–13) beds. This shows that pressure increases approximately linearly if the bed in inefficient, but when efficient areas are allowed the maximum pressure is capped. The percentage of the bed at ice overburden pressure increases rapidly if the system is inefficient, but remains at approximately 1.6% when efficient areas are present.

The percentage of the bed that is efficient remains small; the capping effect is provided by approximately 1.5%–3.5% of the bed being defined as efficient. This figure is larger than the area at ice overburden pressure because the efficiency condition in these runs is set to 0.9 of the overburden pressure. Figure 3.16 shows the variation in efficient area as melt rate changes.

When the entire bed is warm, I conclude that efficient areas are important in keeping the water pressure in the interior realistic even with low melt rates. With higher melt rates they

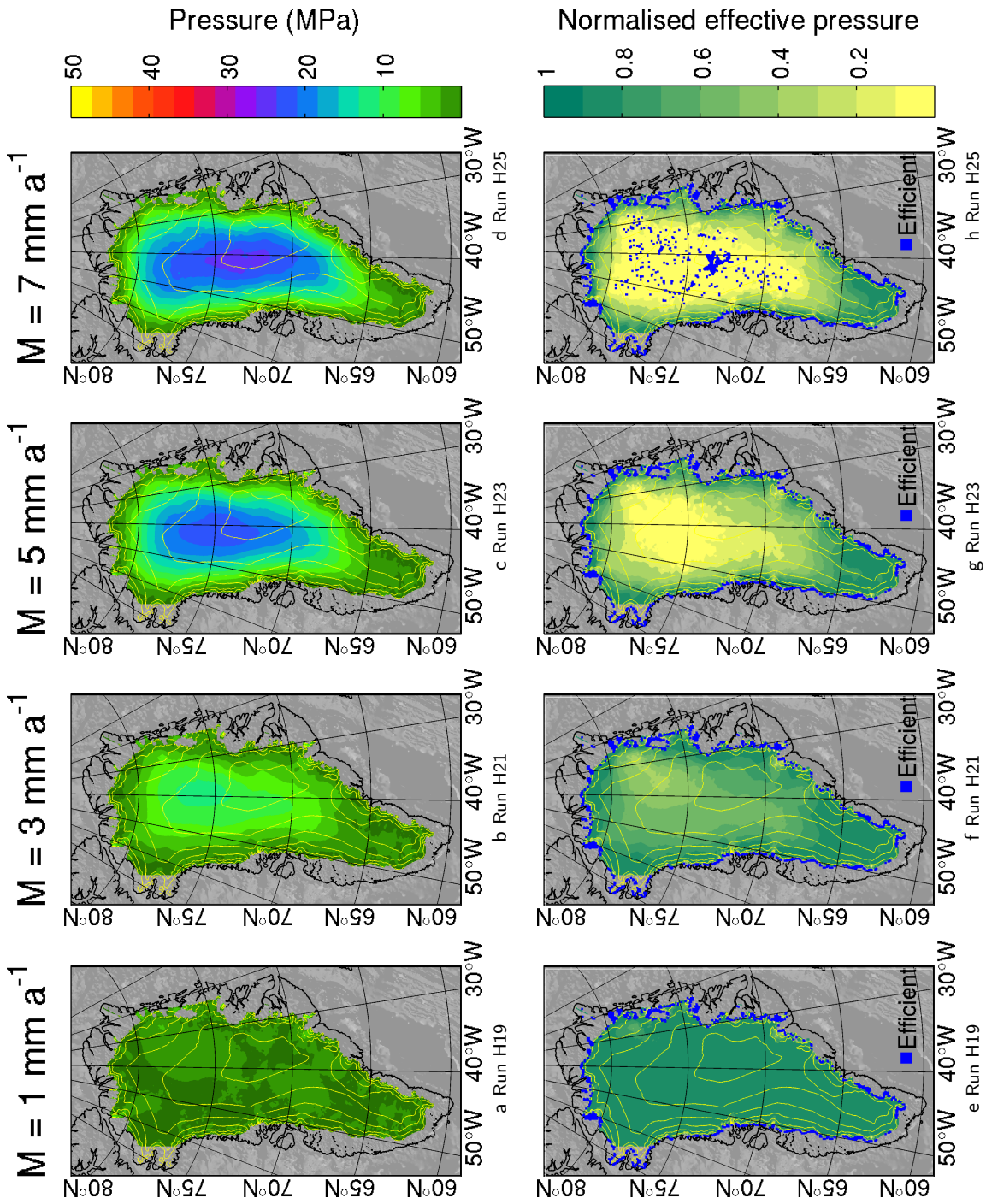

Figure 3.14 Figure as Figure 3.12 but with an efficient bed where $\bar{N} < 0.1$. Note that having only a small portion of the bed efficient (blue: most noticeable in the north-east of $\bar{N}$ maps) the maximum water pressure is much lower than the inefficient case (Figure 3.12).

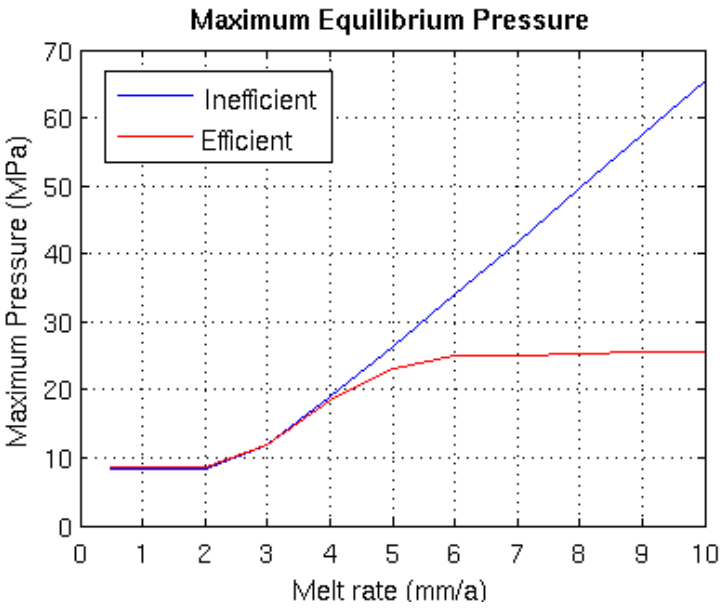

a

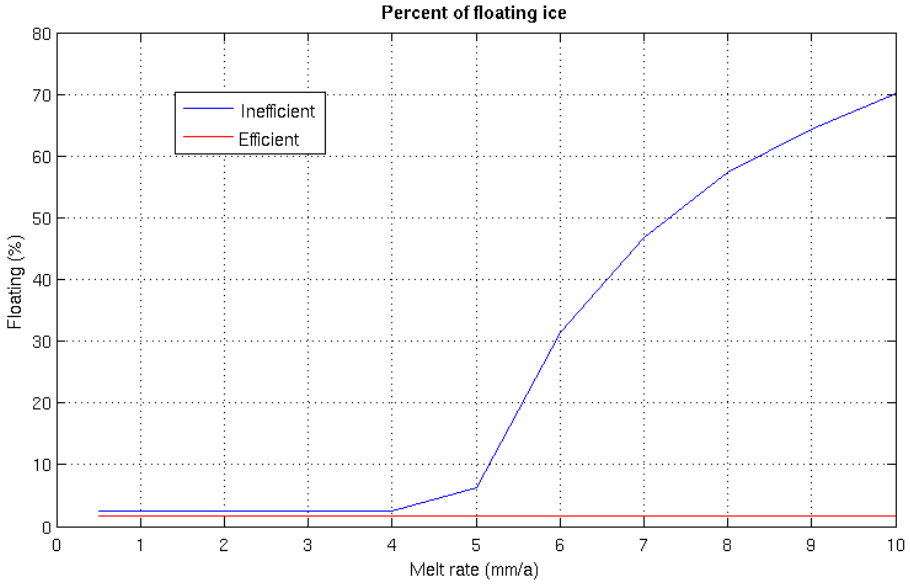

b

Figure 3.15 (a) Efficient areas cap the maximum water pressure p^* that is reached as melt rates increase. When there is no efficiency, the rise is linear and makes the model unstable when it becomes too large. The point at $2\,\mathrm{mm\,a^{-1}}$ is when the pressure begins to overwhelm the hydrostatic (due to topography and ice) surface.

(b) The percentage of the bed that is at ice overburden pressure is reduced to realistic figures. There is a slight increase with M, as expected, but this is not noticeable at the scale shown.

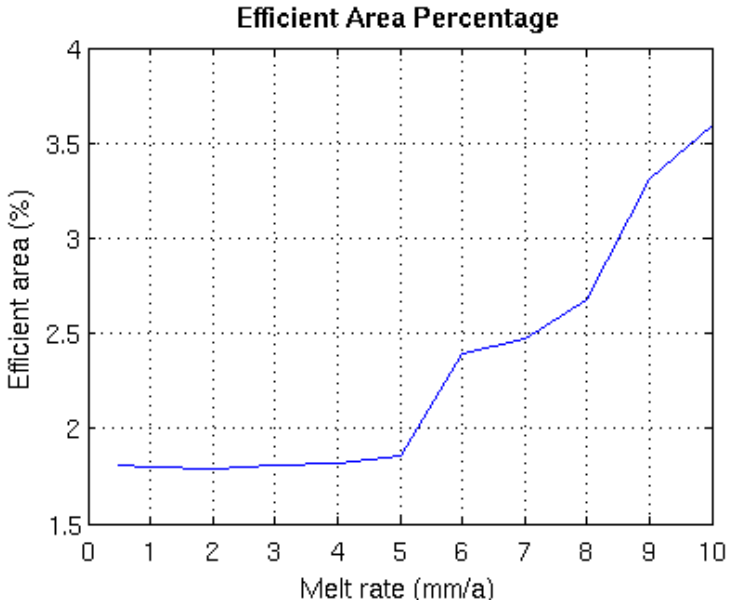

Figure 3.16 The capping in Figure 3.15 is achieved by only a small proportion of the bed being defined as efficient. In these runs, an efficient area is defined where water pressure reached 0.9 of the ice overburden pressure.

are even more important. Only a small proportion of the bed has to be efficient in order to drain large areas of the ice sheet.

Stage 3: Uniform basal melt with frozen bed

Stages 1 and 2 ignore the fact that the centre of the Greenland ice sheet is cold-based in order to introduce two important concepts: low melt rates can create high water pressures in outlet glaciers and a small efficient area can drain large areas inland. Stage 3 investigates how a partially frozen bed affects these results.

Model runs from the Stages 1 and 2 are repeated with different percentages of bed set to be frozen. As before, the equilibrium profiles of inefficient (runs H31–67) and efficient (H68–104) runs are compared. It is not practical to display these two sets of 36 model runs as presented in the earlier stages. Figures 3.17 and 3.18 map a selection of these runs ($\mathcal{C}_F \in \{2250, 2750\}$) to enable a comparison to the data of the previous section. Further data are presented in a more concise form. Key things to note from Figures 3.17 and 3.18 are that:

1. effective pressures are low near the outlet glaciers,

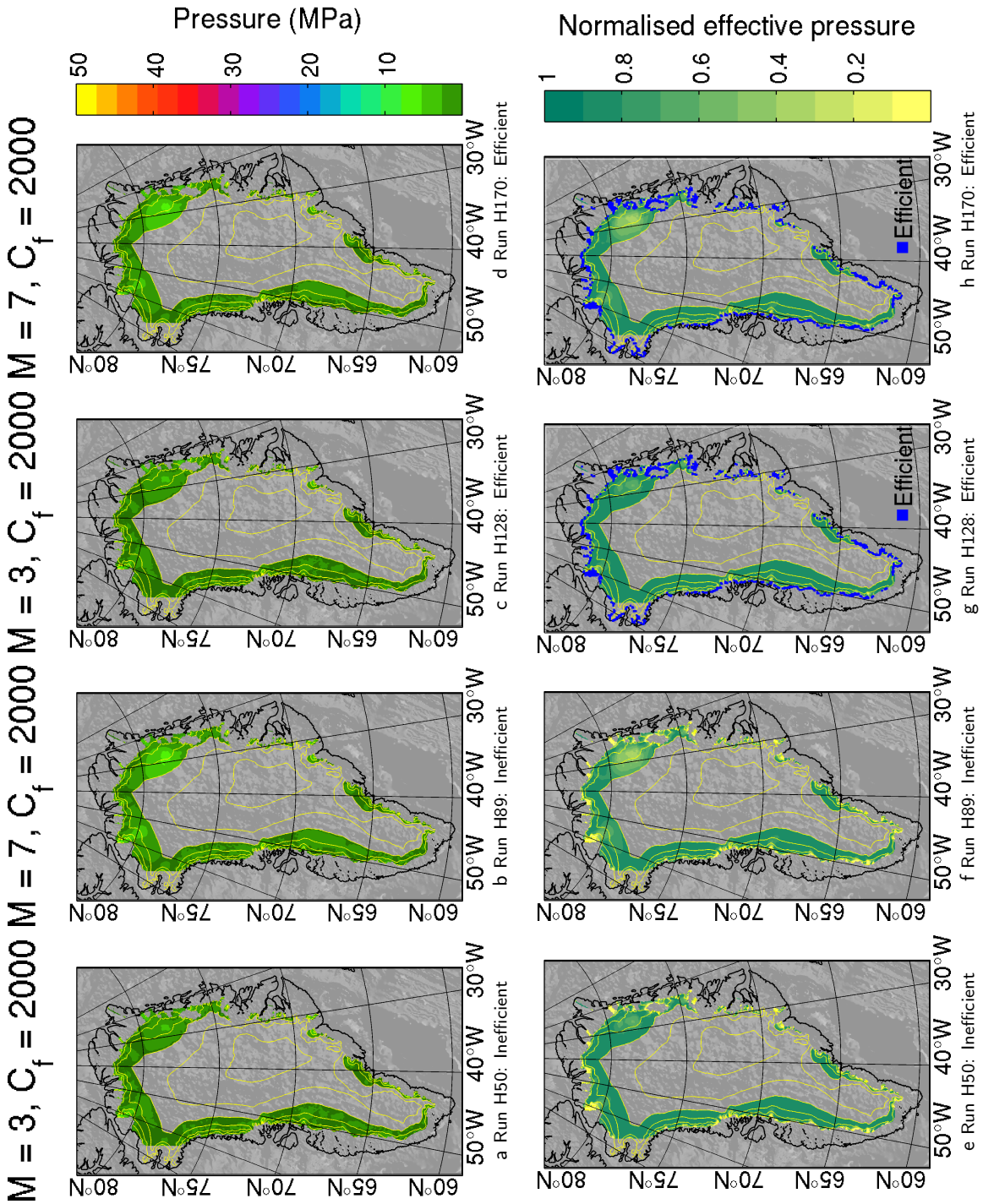

Figure 3.17 Stage 3 runs ($M \in \{3, 7\}$ mm a^{-1}) with the bed defined to be frozen where the surface elevation > 2000 m. Both inefficient (left two columns) and efficient (right two columns) runs are presented. Top row: water pressure p^*. Bottom row: normalised effective pressure $\bar{N}$ with the efficient bed highlighted (blue, enlarged for emphasis).

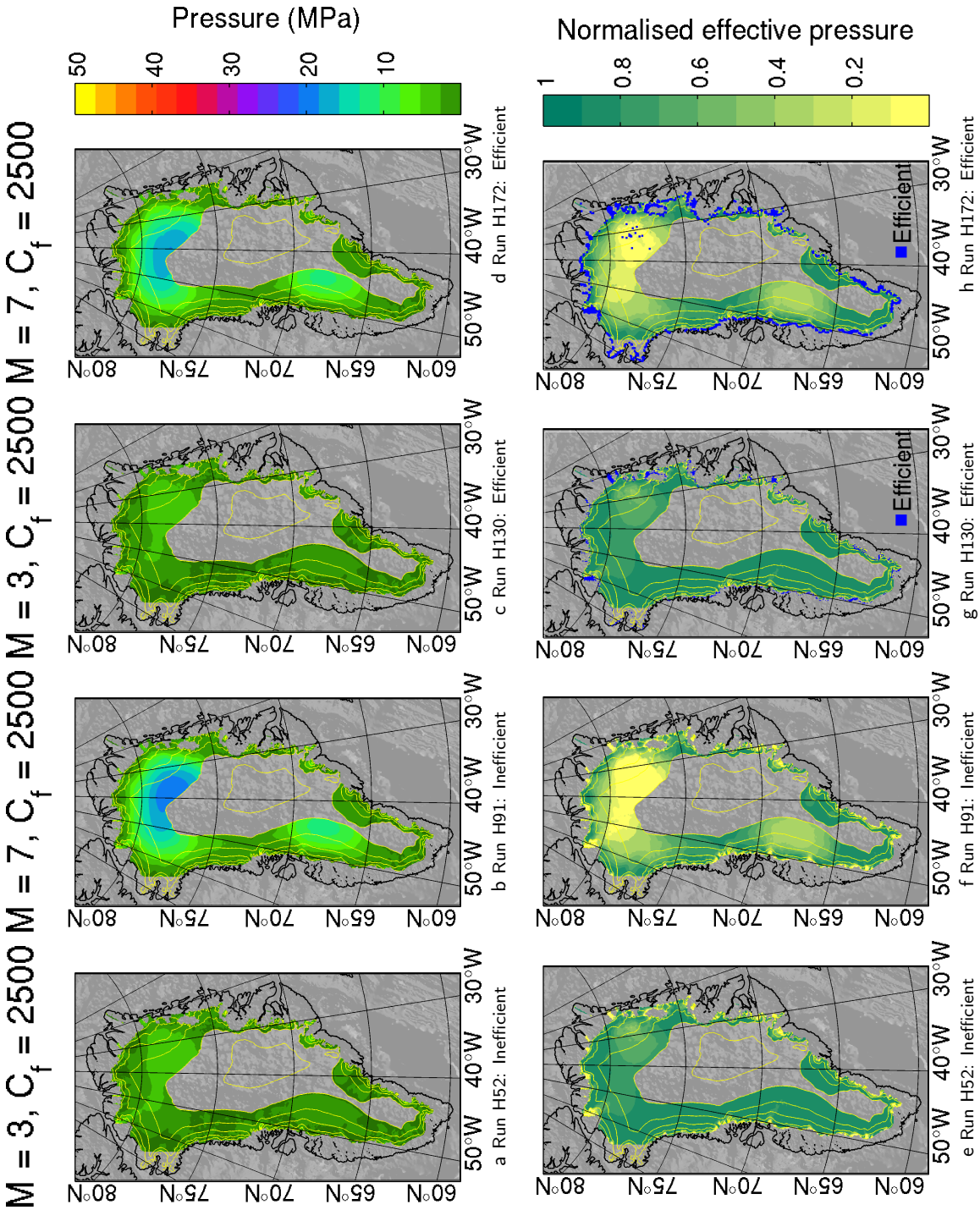

Figure 3.18 As Figure 3.17, but with the frozen bed defined as > 2500 m. The larger warm bed enables more water to enter the system leading to higher water pressure p^* (lower $\tilde{N}$). Slightly more of the bed becomes efficient (blue, enlarged for emphasis).

2. with higher melt rates, efficient areas still play an important role in lowering water pressure,

3. there is little difference between efficient and inefficient results with low melt, but the results diverge as melt increases. This is also the case with a fully warm bed.

The correlation between high water pressure and surface ice velocities observed in Stages 1 and 2 still holds. Although there is less water, the convergence of water near the outlet glaciers is still sufficient to offer an explanation for the high ice velocities observed there for all experiment runs H31–67. This holds for all the warm bed area and melt rate combinations used in this experiment.

Figure 3.19 plots a surface showing the percentage of the bed at ice overburden pressure as basal melt rate and the warm-bed area varying over different model runs. Both efficient (runs H31–67) and inefficient (runs H68–104) data sets are shown. Figure 3.20 plots four slices of data through both surfaces for easier comparison. Figures 3.21 and 3.22 plot a similar surface, and four slices, for the maximum water pressure in the interior of the ice sheet of the same runs. These figures also show a similar variation with melt rate, warm-bed area, and efficiency. In most cases, the maximum water pressure occurs near the head of the NEGIS, because of the subglacial trough combined with thick ice enabling large pressures before ice overburden is reached.

When melt rate and warm-bed area are small the solutions of both efficient and inefficient runs are similar. As either of these increase, a threshold is reached where the solutions begin to change rapidly for a given change in melt rate or warm-bed area. The inefficient runs change at a much faster rate than the efficient runs; both cases still show this change however. The threshold is the point at which the water pressure begins to overwhelm the hydrostatic surface, as discussed for Stage 1.

As expected, as the melt rate increases this threshold is reached sooner as there is more water in the subglacial system. As the warm-bed area increases the water in the system also increases so again the threshold is reached sooner. For example, the threshold has not been reached with $3\,\mathrm{mm\,a^{-1}}$ melt, it is around the 80% warm-bed level with $5\,\mathrm{mm\,a^{-1}}$, 50% warm-bed level with $7\,\mathrm{mm\,a^{-1}}$ and the solution diverges for all the warm-bed levels used with a melt rate of $10\,\mathrm{mm\,a^{-1}}$. While an increase in maximum pressure may be explained by back pressure increasing pressures as the warm area migrates further from the margin, the

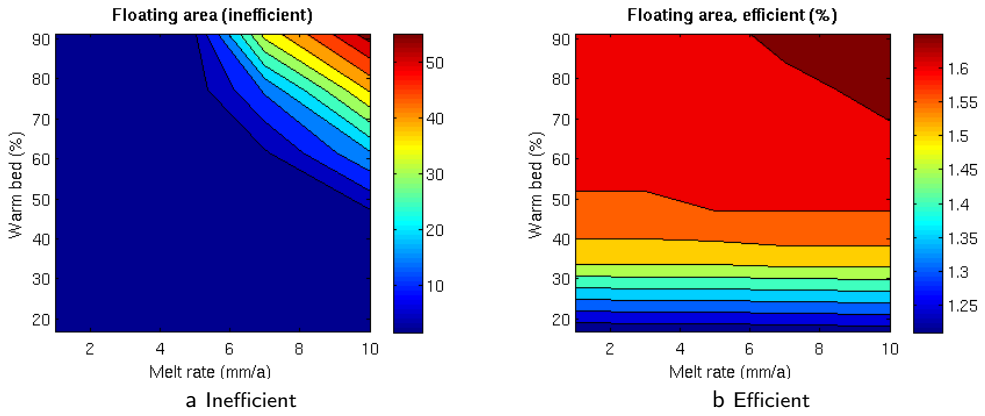

a Inefficient b Efficient

Figure 3.19 Surface plots of basal area at ice overburden pressure for runs H31–67 (a) and runs H68–104 (b). Each surface consists of 36 data points. Table 3.2 shows the association between warm bed percentages and the frozen bed definition contour C_F. The two plots use different colour scaling to highlight the shape of the efficient surface. The variation in (b) is small, but important, and is not noticeable with a global colour scaling.

There is a threshold value, which varies with the warm area and the melt rate, where efficient areas become increasingly important. Below the threshold, efficient areas lower the water pressures but the overall distribution of the water is not affected. Above the threshold, the distribution of water and its behaviour differs greatly between efficient and inefficient runs.

increase in efficient area cannot be explained in this manner. More water must be reaching the margin which is reasonable as there is more water in the system. Crucially, Figures 3.17 and 3.18 show that the increased efficient areas form under outlet glaciers. This supports my conclusion that water converging in subglacial troughs is responsible for the low effective pressures in these regions.

In summary, the results from Stages 1 and 2 are still valid but the frozen region affects where the results for lower and higher melt diverge. With a frozen bed, the overall interior water pressures are lower because there is less back pressure through the inefficient bed to clear. Efficient areas are still needed to keep the water pressures in the interior low. Small areas of efficiency still help to drain large areas of the bed. Because the solution, and especially the location and proportion of efficient bed, depends on the size of the frozen area, it is important to model basal temperatures accurately to predict the background hydraulic pressure profile which the rest of the thesis is based on.

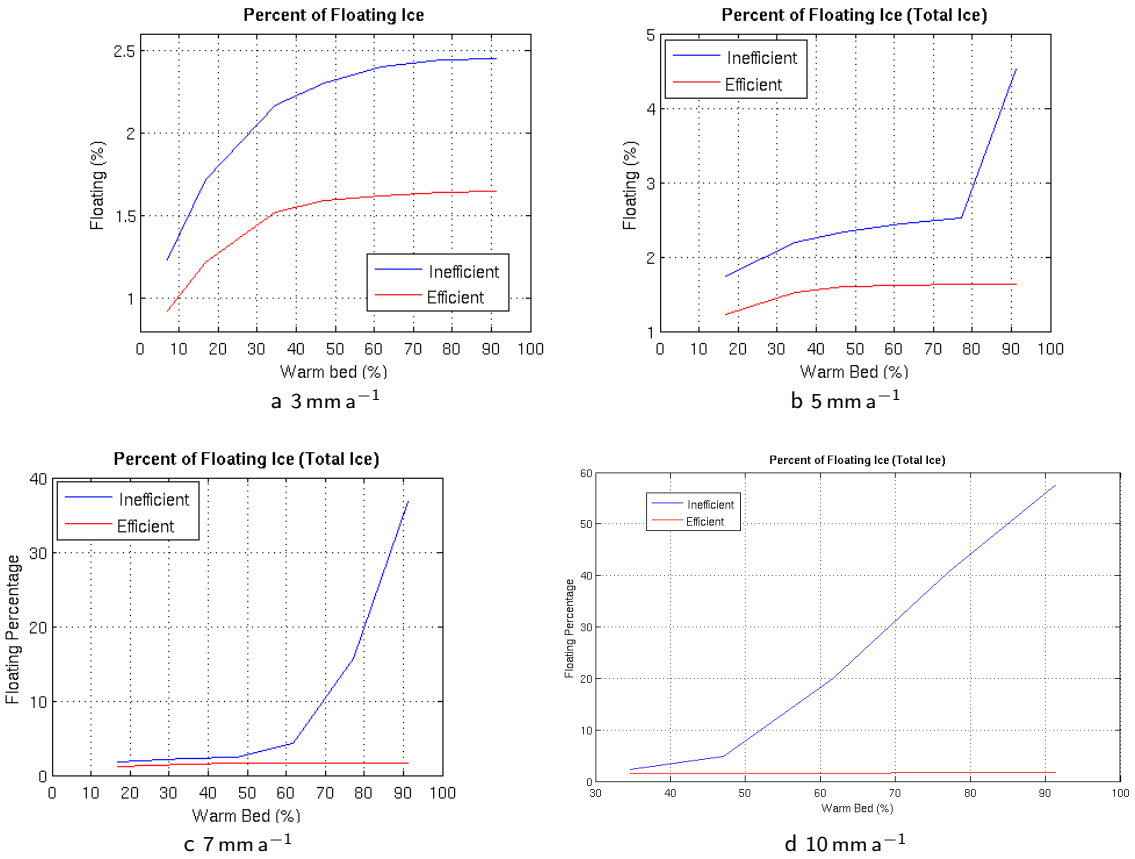

Figure 3.20 Slices through surfaces in Figure 3.19 for $M = 3$ (a), 5 (b), 7 (c), and 10 mm a^{-1} (d) showing the area of the bed at ice overburden pressure with increasing warm basal area.

As more water enters the system (increasing M or warm area) larger areas reach ice overburden pressure with an inefficient bed, but the values is mostly constant with an efficient bed (with sufficiently large efficiency factor ψ). The the threshold where the solutions diverge is clear and moves to smaller warm basal area as melt increases.

Stage 4: Geothermal and strain melting

A variable melt rate adds extra complexity. This section first looks at the melt rates predicted by GLIMMER for a range of geothermal heat fluxes ($H_g \in \{0, 30, 40, 50, 100\}$) and then looks at the background hydraulic pressure profile produced by these melt rates.

Melt rate maps

Figure 3.23 maps the basal melt rates calculated by GLIMMER in runs G1–5. Basal melt rates typically increase towards the margin due to increased strain and frictional heating from sliding. Close to the margin much larger values are obtained than I have considered so

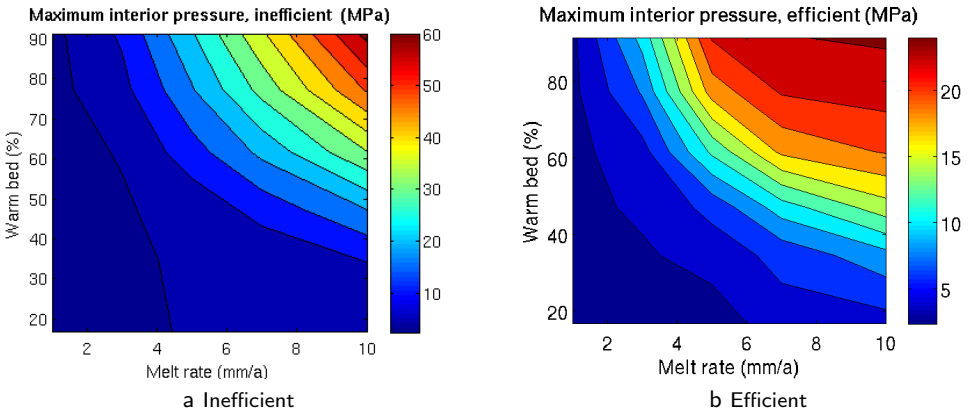

Figure 3.21 Surface plots of the maximum pressure of efficient runs H31–67 (a) and inefficient runs H68–104 (b). Each surface consists of 36 data points. Table 3.2 shows the association between warm bed percentages and the frozen bed definition contour C_F.

Maximum pressure increases with both M and warm basal area because the system has to evacuate increasing volumes of water. The maximum pressure in (b) plateaus due to a sufficient portion of the bed becoming efficient to cope with the extra water entering the system. This plateau is where the two solutions begin to diverge significantly.

far. This is especially true under outlet glaciers due to the very high strain rates in these regions.

Under outlet glaciers, the melt rate is effectively independent of geothermal heat flux H_g. The maximum melt rate with $H_g = 0\,\mathrm{mW\,m^{-2}}$ (run G1) is $3626\,\mathrm{mm\,a^{-1}}$ and with $H_g = 100\,\mathrm{mW\,m^{-2}}$ (run G5) is $3642\,\mathrm{mm\,a^{-1}}$; a $16\,\mathrm{mm\,a^{-1}}$ or 0.44% difference. Excluding the outlet glaciers, the melt rate then increases to around $500\,\mathrm{mm\,a^{-1}}$ at the margin. Further inland, as H_g increases the low basal melt rates and the warm basal area significantly. The melt rate at the western edge of the $H_g = 0\,\mathrm{mW\,m^{-2}}$ frozen area (around 70 °N) with $H_g = 0\,\mathrm{mW\,m^{-2}}$ is $3\,\mathrm{mm\,a^{-1}}$, with $H_g = 50\,\mathrm{mW\,m^{-2}}$ is $10\,\mathrm{mm\,a^{-1}}$, and with $H_g = 100\,\mathrm{mW\,m^{-2}}$ is $15\,\mathrm{mm\,a^{-1}}$. The pattern of melt remains similar but the frozen area at the centre becomes smaller. This is reasonable because the geothermal heat flux is applied to GLIMMER uniformly. The extra heat changes some of the bed from cold- to warm-based but does not affect the pattern of existing melt rates. Table 3.3 shows the percentage of the warm bed at thermal equilibrium for varying H_g.

Background hydraulic pressure profile

Figure 3.24 maps water pressure p^* and normalised effective pressure $\bar{N}$ calculated by HYDRO using variable melt rates.

Extra water from the increased melt rates drives $\bar{N}$ to be much lower and the efficient bed area increases. The interior of the ice sheet is still below ice overburden pressure, as expected. Stage 3 demonstrates that changing low melt over a large area and changing warm basal area affects water convergence under outlet glaciers. Varying H_g affects both these parameters. As expected, HYDRO runs using melt from a higher H_g show more extensive

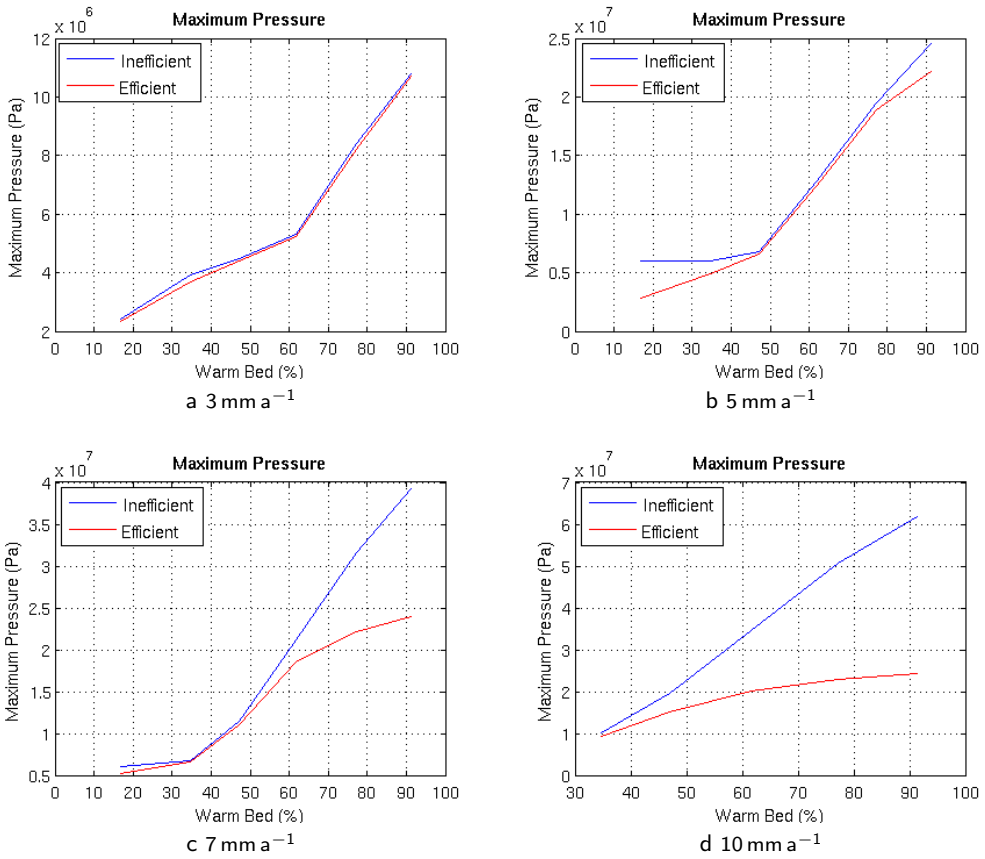

Figure 3.22 Slices through the maximum pressure surfaces in Figure 3.21 are shown for melt rates $M = 3$ (a), 5 (b), 7 (c), and 10 mm a^{-1} (d).

There is a divergence in behaviour as M and warm basal area increase. The plateau discussed in Figure 3.21 is noticeable. I cannot explain the divergence for the low warm bed area in (b).

areas of low $\bar{N}$ and a more efficient bed. The effect is not large, but may make a difference to the calculated dynamic speedup when draining surface lakes are included in the model.

Fast ice still correlates with low $\bar{N}$ but the correlation is not as good as before because extra water can overwhelm shallow subglacial troughs in the DEM and start spreading the low $\bar{N}$ area outwards from the trough. This is partially due to scale issues with the 10 km DEM[4] and partly due to the increased water. In the deeper troughs (eg Kangerdlugssuaq, Helheim) the correlation remains good. Notice especially the low $\bar{N}$ that forms under the area of the NEGIS. The deep subglacial troughs are present due to the erosion of outlet glaciers under the ice. In the DEM these are not always as apparent when the ice sheet expands to the extent it

[4] Stages 1–3 use a more detailed 5 km DEM but this is not stable in GLIMMER.

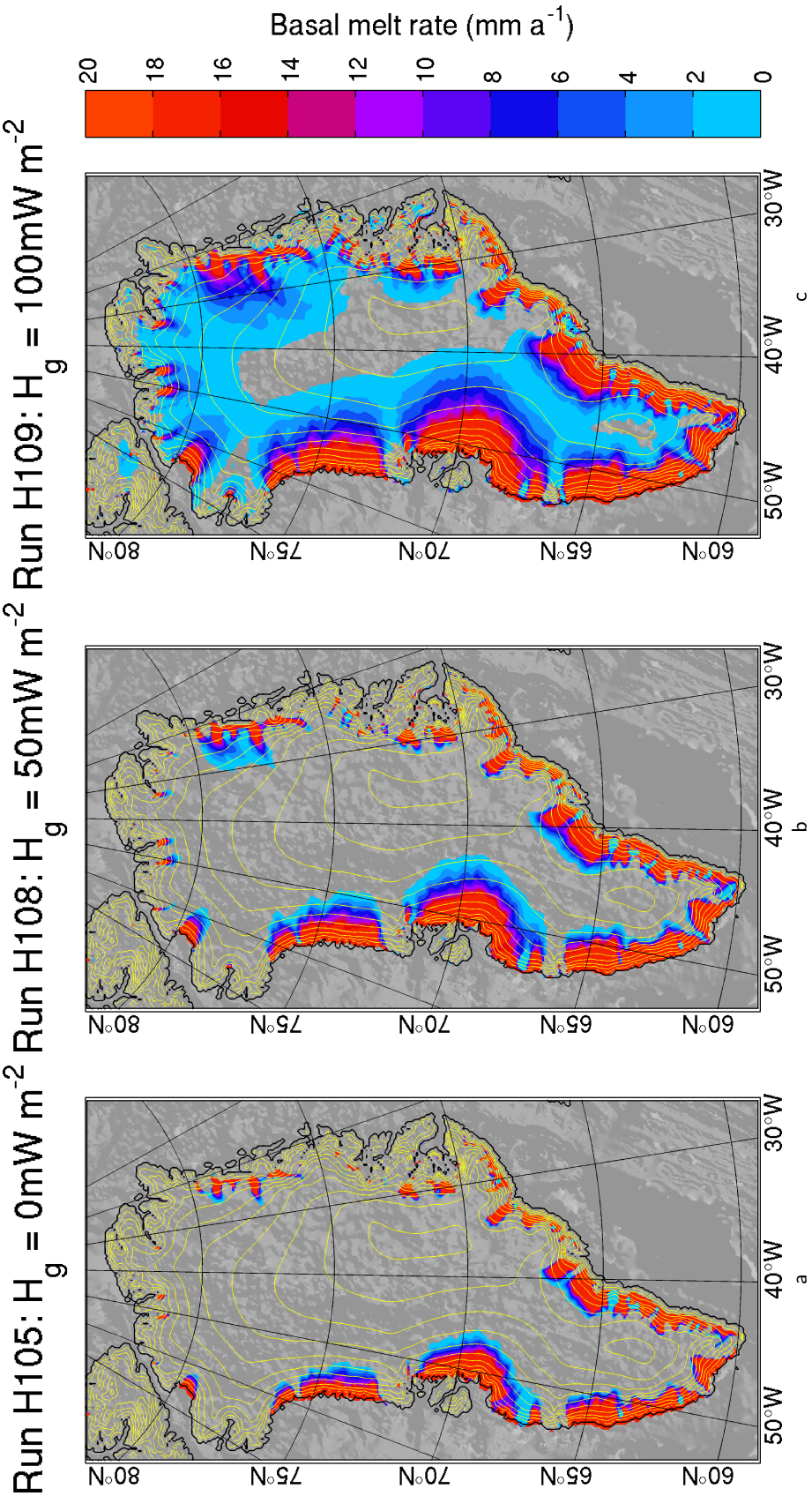

Figure 3.23 Basal melt rates calculated by GLIMMER (runs G1–5) are used to derive HYDRO runs H105 and 109. These plots show the melt rates at thermal equilibrium for (a) $H_g = 0\,\mathrm{mW\,m^{-2}}$, (b) $H_g = 50\,\mathrm{mW\,m^{-2}}$, and (c) $H_g = 100\,\mathrm{mW\,m^{-2}}$. The central transparent area is the frozen bed.

As geothermal heat flux H_g increases, both the melt rate in the interior and the size of the warm bed increase leading to a significant increase in the total water entering the subglacial system. The melt rate at the edge of the frozen area (around 70 °N) with $H_g = 0\,\mathrm{mW\,m^{-2}}$ is $3\,\mathrm{mm\,a^{-1}}$ (a), with $H_g = 50\,\mathrm{mW\,m^{-2}}$ is $10\,\mathrm{mm\,a^{-1}}$ (b), and with $H_g = 100\,\mathrm{mW\,m^{-2}}$ is $15\,\mathrm{mW\,m^{-2}}$ (c).

The maximum melt rate in each case is (a) $3.63\,\mathrm{m\,a^{-1}}$, (b) $3.63\,\mathrm{m\,a^{-1}}$, and (c) $3.64\,\mathrm{m\,a^{-1}}$ showing that the higher melt rates are not sensitive to geothermal heat flux. High values only occur in small areas so on values up to $20\,\mathrm{mm\,a^{-1}}$ are mapped.

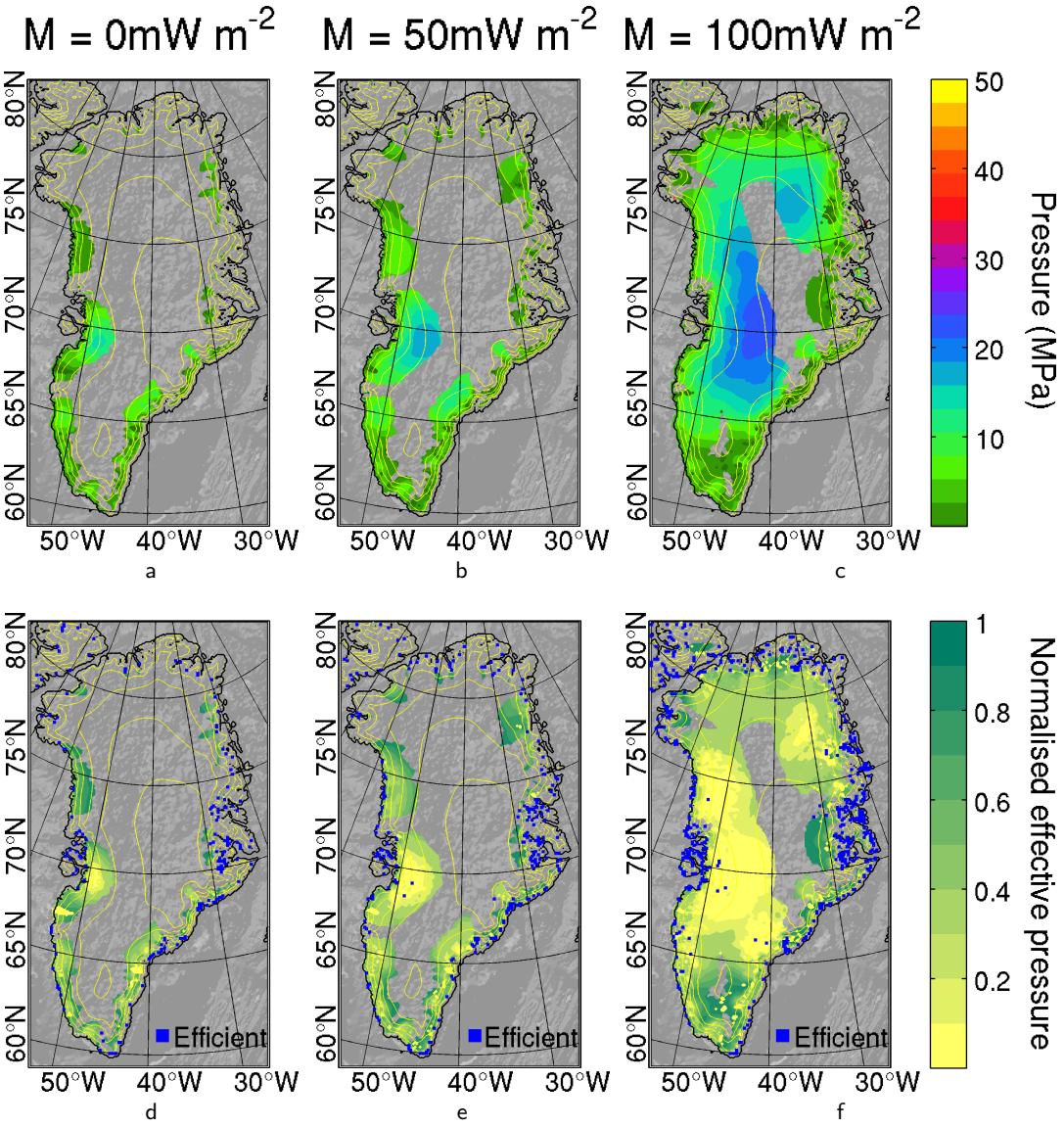

Figure 3.24 Equilibrium profiles of water pressure for varying basal melt patterns based on (a) $H_g = 0\,\mathrm{mW\,m^{-2}}$, (b) $H_g = 50\,\mathrm{mW\,m^{-2}}$, and (c) $H_g = 100\,\mathrm{mW\,m^{-2}}$. Top row: water pressure p^*. Bottom row: normalised effective pressure $\tilde{N}$ with the efficient bed highlighted (blue, enlarged for emphasis).

does. In reality there are fjords, but the 10 km DEM does not always resolve them well.

3.5 Discussion

I now discuss the subglacial processes identified in Sections 3.3 and 3.4 and their implications on the background hydraulic pressure profile (BHPP). Section 3.5.1 looks at the processes and their interaction with each other. Section 3.5.2 then discusses the features of the BHPP and their potential implications on ice dynamics.

3.5.1 Processes

The key factors controlling the BHPP are the volume and distribution of melt entering the system and the evolution of an hydraulically efficient bed. The melt volume, in turn, is a product of the basal heat sources.

Water input

Experiment Stages 1–3 show that the volume of water entering the subglacial system is an important control on the BHPP. The distribution of the water (Stage 4) is also important but extra water near the margin is dealt with by a larger efficient bed. Water from the increased melt rate near the margin escapes the system quickly so has a lesser effect that it might further inland.

Varying both the basal melt rate (M) and the frozen area affects the hydraulic efficiency of the bed. More water in the system means that a larger proportion of the bed is efficient. Because of the dependence even on minor changes in M and frozen area it is important to model ice temperatures accurately. Both the melt rate and frozen area depend on calculating basal ice temperatures. When the basal ice temperature is at the pressure melting point, excess heat is used by GLIMMER to melt ice.

There is a threshold where the nature of the BHPP varies dramatically. This is due to the basal water beginning to overwhelm the hydrostatic pressure surface. The hydrostatic pressure surface is a function of the bed topography and ice thickness and is given by Equation 2.41. This surface has many hollows and ridges, although far less than the bed topography or ice thickness display individually. Water initially flows off the ridges and converges in these hollows, raising water pressures. This convergence occurs even with the lowest melt rate ($M = 0.5\,\mathrm{mm\,a^{-1}}$, run H18) used in Stage 2. Run H18 picks up the location of the Petermann glacier and the NEGIS as a cluster of efficient grid cells. A single efficient

cell may be due to very thin ice, but when a few cells are next to each other and that cluster is perpendicular to the margin then it is significant.

The water pressures on the ridges remain low. As these hollows fill the pressure surface becomes smooth and the threshold is reached. After this, water pressures rise everywhere and the nature of the BHPP stops reflecting the imperfections of the hydrostatic surface. At this point efficiency becomes increasingly important in keeping water pressures below ice overburden pressure for the majority of the bed.

Efficiency

Hydraulic efficiency strongly controls the BHPP. Stages 2–3 demonstrate that if efficient areas are not allowed then large areas of the bed reach ice overburden pressure, regardless of the size of the frozen area. When efficient areas are allowed, less than 5% of the bed usually becomes efficient in the model runs, but this is sufficient to drop water pressures over a large area of the interior of the ice sheet.

Numerically, the value of the efficiency factor ψ is important. To simulate the behaviour of R-channels and N-channels, which on a very small scale (smaller than the model scale) can be seen as infinitely efficient, I set this as high as possible. As long as the efficiency factor ψ is large enough, the BHPP does not change with increasing ψ. The efficiency factor ψ cannot be set arbitrarily large as steep gradient causes model instability. I therefore choose ψ in subsequent chapters to make the bed as efficient as possible while maintaining numerical stability.

There is a slight rise in efficient area and maximum pressure as the melt rate or the warm-basal area increases. Although this could be because ψ is not sufficiently large, I do not believe this is the case. As both variables increase, it makes sense for both maximum pressure and the efficient area to increase slightly as the system has to evacuate more water. When ψ is not adequately large, such as with $\psi = 10$ with uniform $M = 100\,\mathrm{mm\,a^{-1}}$ then increase in total efficient area is much more pronounced. Despite ψ being a reasonable method to proxy an efficient bed, it is still modelled as a diffusive process which is in effect inefficient according to Kamb's (1987) definition. As water flux increases in efficient areas near the margin, water pressure rises and the resultant back-pressure increases pressures in the interior. The efficiency factor simply makes the bed more efficient than its surroundings.

Nevertheless, simple tests should be performed before setting up each experiment in

subsequent chapters to test the ψ value used. This is done before defining model runs in Chapter 4 and Chapter 5.

Heat sources

Basal heat sources include geothermal heating, strain heating, sliding friction and advection of ice. Section 3.3 demonstrates that geothermal heat is dominant in the interior with strain heating becoming increasingly dominant towards the margin. At the margin, away from fast flowing ice, strain heating is typically an order of magnitude stronger than geothermal heating. In the subglacial troughs, where the fast-flowing outlet glaciers are, strain heating is two orders of magnitude larger than geothermal. This is partially due to incorrect physics in Glimmer due to thick ice in these troughs, and steep surface gradients, leading to such large values, as discussed in Section 3.2. However, strain rates will be higher in troughs because of increased strain rates from lateral shear, which the analysis in Section 3.3 and Glimmer ignore, possibly justifying the large values.

Geothermal heat flux exerts a strong influence on model behaviour because it controls the volume of basal melt entering the system by affecting both the size of the frozen area and the low, interior basal melt rate over a large area. Experiment Stage 3 demonstrated the sensitivity of the system to these two variables. When there is no geothermal heat flux (run G1), the only heat sources at the bed, away from the margin, are from strain heating and advection. Both of these heat terms are small in the interior and so the bed remains primarily frozen (82% frozen). Near the ice-divide, advection does not bring in heat but rather acts as a heat sink due to cold ice arriving from the surface. As H_g increases, both the size of the warm area and the low basal melt rate also increase. With geothermal heat flux unnaturally high (run G5, $H_g = 100\,\mathrm{mW\,m^{-2}}$) the bed is primarily warm-based (28% frozen). There is a significant increase in the area experiencing low melt rates, Figure 3.25. The average melt rate in this area also increases (Figure 3.23), lowering the effective pressure of the background pressure profile.

From this discussion it is clear that it is important to calculate heat sources accurately to model any potential dynamic response of the Greenland ice sheet. Glimmer is a fully thermomechanical ice sheet model so handles these temperature calculations well, within the constraints of the shallow ice approximation, provided its thermal boundary conditions are set appropriately. Glimmer fully calculates strain heating and advection although, as discussed

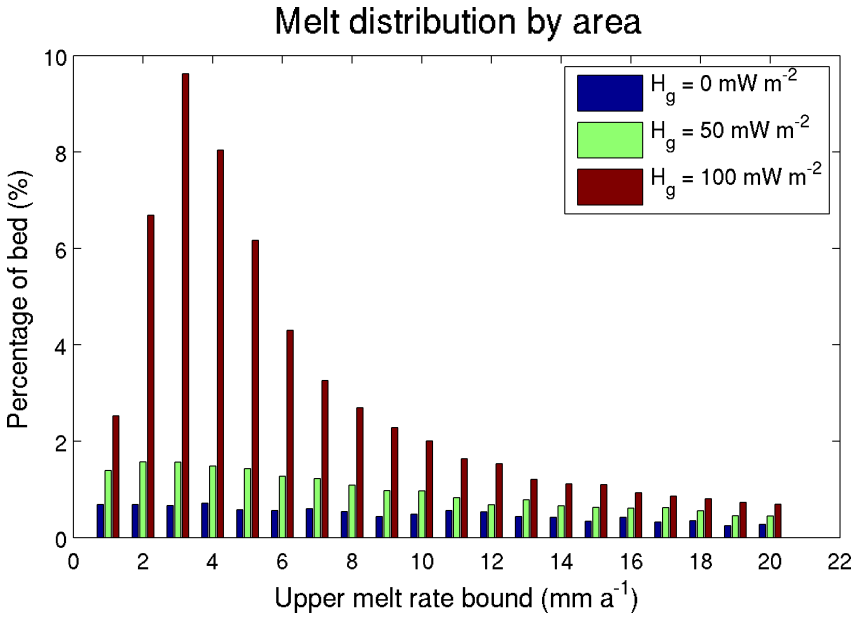

Figure 3.25 Histogram of basal area divided by melt rate M in $1\,\mathrm{mm\,a^{-1}}$ intervals for M calculated by GLIMMER (runs G1, 3, 5) using geothermal heat flux $H_g \in \{0, 50, 100\}\,\mathrm{mW\,m^{-2}}$. Each grouping around M shows the range $(M-1)-M$. Only values $M \leqslant 20$ are plotted.

There is a significant increase in the area experiencing low melt rates with increasing H_g. This area is more than doubled, compared to the lower H_g value plotted, for $2 \leqslant M \leqslant 9$. Higher melt rates show less dependence on geothermal heat flux.

in Section 3.3, basal shear is overestimated and lateral shear is ignored in fast-flowing outlet glaciers. Setting the thermal boundary conditions requires defining geothermal heat flux H_g accurately and dealing with friction from sliding.

Unfortunately, while geothermal heat flux is relatively easy to deal with numerically in models, it is difficult to determine the actual values to use. Sparse data are available from various drill sites (Greve and Otsu, 2007) and there is some input from earth heat flow models (eg Pollack et al., 1993) but interpolating a handful of data points over an area as large as Greenland is tantamount to guessing the pattern and it is difficult to set the boundary conditions of the earth heat-flow model itself under Greenland. Coarse interpolation may introduce variation and behaviour in model runs which have no physical basis and so confuse the analysis for no gain. I therefore choose to use the standard $42\,\mathrm{mW\,m^{-2}}$ applied uniformly to Greenland for consistency with other studies, but accept that this is not an ideal solution. When better data become available, ice sheet models will be able to incorporate them without much effort.

The final major heat term contributing to the thermal basal-boundary conditions is from sliding friction. This is a complicated area that is not dealt with adequately by most ice sheet models because models lack the necessary hydrology calculations. Water is key for enabling sliding, but the extra lubrication it provides also limits the frictional heat released by sliding friction. These feedback mechanisms are complex and are the focus of the next chapter.

3.5.2 Background hydraulic pressure profile

The background hydraulic pressure profile (BHPP), which I define as the equilibrium hydraulic subglacial pressure p^* due to only basal melting, affects Greenland's dynamic response to draining surface lakes. The previous section discusses processes responsible for the modelled BHPP, I now look at the BHPP's key features and propose how these may affect ice dynamics.

The BHPP is highly dependent on the model setup. The wide variety of the BHPPs mapped in this chapter show this. Melt rate and distribution, the size of the frozen area, and hydraulic efficiency all affect HYDRO's calculation of the BHPP. Therefore, a single BHPP cannot be calculated once and used in all model runs. The BHPP calculation is an integral part of each model run's evolution. There are, however, common features to all the BHPPs mapped. These are:

1. Low effective pressure $\bar{N}$ in subglacial troughs,
2. Presence of efficient areas around the margin and especially in the subglacial troughs,
3. Highest water pressures in the interior, but not the lowest $\bar{N}$ due to the weight of the ice, and
4. Increasing maximum water pressures and efficient area with increasing basal melt rate and warm area.

Of these, the most influential on ice dynamics are the first two points: low effective pressures in subglacial troughs and the resultant efficient areas. Water converges in subglacial troughs, as discussed in Section 3.5.1, and causes both the low effective pressure and the increased efficiency in these regions.

Ice sliding appears to be a function of effective pressure $\bar{N}$ (Paterson, 1994) and therefore

ice is expected to slide faster in areas with low $\bar{N}$. This is how the coupling the GLIMMER-HYDRO model is set up in Chapter 2.

3.6 Summary

This chapter establishes the basic model set-up used in subsequent chapters by studying the sensitivity and nature of the background hydraulic pressure profile (BHPP) for Greenland. The melt rate pattern and distribution are found to be key controls on the BHPP. The chapter also investigates the relative importance of the geothermal and strain heating terms to establish controls on the basal melt rate distribution and the size of the frozen area at the centre of the Greenland ice sheet's bed.

Key results are:

1. Strain heating dominates near the margin, where deformation is highest; geothermal heating dominates in the interior.

2. Geothermal heat flux is the primary control on the size of the frozen central area and the low interior basal melt rate.

3. The BHPP is sensitive to the low interior basal melt rate and the frozen area and is therefore sensitive to the geothermal heat flux.

4. Water converges in subglacial troughs which results in low effective pressure and increased efficiency in these regions.

5. Efficient areas ($< 5\%$ of bed) drain subglacial water from large areas of the ice sheet.

The basal melt rate is a key control on the BHPP and therefore on ice dynamics. To calculate it accurately the ice sheet model (GLIMMER) must know the geothermal heat flux and must calculate strain heating and frictional heating. Strain heating is handled well by GLIMMER, within the constraints of the shallow ice approximation. Frictional heating is the focus of the next chapter. Geothermal heat flux is more elusive. It is a relatively simple heat term to handle numerically, but it is difficult to determine a precise value. This chapter demonstrates the hydraulic system is sensitive to the value of geothermal heat flux. It is the dominant heat term in the interior of the ice sheet (Result 1) and affects the size of the frozen area and the basal melt rate there (Result 2). Both of these variables appear to be

primary controls on the BHPP (Result 3) and therefore on ice sliding, at least when surface melt water input is ignored.

The BHPP correlates well with Greenland's surface velocities calculated by Rignot and Kanagaratnam (2006). Water appears to converge in subglacial troughs (Result 4), which also happen to be where the marine-terminating outlet glaciers are. These areas have low effective pressure and therefore fast flowing ice. Using the shallow ice approximation, GLIMMER predicts outlet glaciers to have high strain rates which lead to high surface velocities. In reality, vertical strain rates in ice streams are low and most of the velocity appears to be due to decoupling at the bed (eg Bindschadler, 1983). The convergence of water in subglacial troughs, even with low basal melt rates, may explain this decoupling.

I propose that because water purely from basal melting converging in subglacial troughs is sufficient to make water pressures approach ice overburden pressure ($\bar{N} \rightarrow 0$), these regions will not show a significant response to seasonal surface melt water injection. The converse of this is that subglacial ridges, where water does not converge and therefore $\bar{N}$ is higher, will show a much larger seasonal response than the troughs for the same melt water input. Before I can investigate this further in Chapter 5, I need to understand how frictional heat flux interacts with basal hydrology and ice dynamics.

Chapter 4

Friction and Sliding

"Rapid basal motion requires that the basal temperature be raised to the melting point by heat from the Earth's interior, delivered by melt water transport, or from the 'friction' of ice motion."

—Fourth IPCC Assessment Report 2007, Box TS 3

This chapter examines the complex feedbacks between sliding, friction, and melt water generation. Friction from sliding is an important heat source at the bed of ice sheets and leads to a number of feedback mechanisms that affect the stability of ice flow. Frictional heat causes increased melting, which in turn causes faster ice by lowering effective pressure. In turn, reducing the effective pressure reduces friction and so produces less heat for the same sliding velocity. In effect, the same velocity is permitted but because the bed is more slippery there are two possible conceptual end-number states — high friction, low velocity and high velocity, low friction — which can lead to similar magnitudes of basal heat production. Most ice sheet models do not include this full feedback mechanism and instead rely on various proxies to estimate portions of it. This chapter attempts to model the full mechanism.

Friction is an elusive quantity and hard to quantify experimentally—especially in a glaciological setting. Section 4.1 reviews studies investigating the value of the coefficient of friction and the processes that control its evolution. I work this understanding into a conceptual model of friction in Section 4.2, where I describe how I envision friction and its various feedbacks to behave under an ice sheet. Section 4.3 looks at typical values of frictiona heat fluxes adn compares these to geothermal and strain heat terms. Finally, Section 4.4 investigates the effect these feedbacks have on a standard circular EISMINT-2 ice sheet run

and the sensitivity of the system to various parameters.

4.1 Coefficient of friction

The coefficient of friction μ is a ratio between the maximum frictional force during sliding and the normal force to a surface. The friction of ice is an order of magnitude lower than everyday objects and the reason for this has been the cause of much debate. Understanding what values μ has, and how this affects basal heat generation is important to understanding the structure and stability of ice sheets.

The derivation for frictional heat flux in Section 2.3.2 assumes that the maximum possible coefficient of friction $\mu_{\max}$ is known. This is not the case. Attempts have, however, been made to determine this elusive value for ice in contact with various materials.

At the 10–20 km grid scales that Glimmer-Hydro uses, it is useful to make a distinction between small scale friction and large scale friction. By this, I mean friction of pure ice over a small area and the friction of debris carrying ice over large areas where bed undulations, as well as surface roughness, impact upon the effective friction of the entire area. First, however, I review what gives ice its unusual properties.

4.1.1 Why is ice slippy?

In essence the coefficient of friction μ quantifies the slipperiness of ice. In general it is an order of magnitude lower than other crystalline solids (Bowden, 1953). The reasons for this are not completely understood. The slipperiness of ice is usually attributed to the presence of a liquid film of water on its surface; the problem is understanding where this film comes from. Four processes, possibly working together to various degrees, are contenders (Barnes et al., 1971; Slotfeldt-Ellingsen and Torgersen, 1983):

1. water from pressure melting,
2. water from frictional heating,
3. water from vapour, and
4. impurities lowering the melting point.

Mills (2008) also suggests the rotation of ice molecules on the surface of the crystal due to the lack of hydrogen bonds at the surface, instead of a water film, as a possible explanation for the slipperiness of ice.

Bowden and Hughes (1939) first suggested that frictional heat may account for some of the water on the ice surface. Before this, pressure melting alone was thought sufficient to account for the water (Rosenberg, 2005). In a glaciological setting, Hooke (1977) states that the amount of frictional heat is often estimated as proportional to velocity times basal shear stress. This is not useful in the present context, however, because this does not account for the various feedbacks involving basal meltwater.

4.1.2 Controls on the coefficient of friction μ

Laboratory experiments to determine the coefficient of friction μ for ice in contact with steel, granite and other metals are common. Many of these experiments are performed for winter sports (eg Slotfeldt-Ellingsen and Torgersen, 1983) or road safety (eg Ivanovic et al., 2006). At least one experiment has been done at the Svartisen Subglacial Laboratory in northern Norway (Iverson et al., 2003; Cohen et al., 2005) in a glaciological context.

Before I summarise the values of μ obtained, I want to review what μ seems to depend on for ice. The specific heat capacity of each material, whether it is an insulator or a conductor, and the overall temperature gradient through the interface affect the friction (Marmo et al., 2005). These factors influence whether the frictional heat is dissipated away or whether it remains to generate lubricating meltwater. μ is often seen as a function of load, speed, pressure, temperature and contact geometry (Liang et al., 2003). In a laboratory, pressure can be controlled independently of load but under a glacier they are effectively the same variable. Marmo et al. (2005) find in their experiments of steel on ice that μ does not vary for loads of 2.10 N to 4.20 N over a constant area of 1.6 cm^2; this is much less than loads at the bed of a glacier which are of the order of 1×10^3 N for 1000 m of ice over 1 cm^2 of bed. Measuring the load over a constant area is, in effect, a proxy for pressure. Because it is defined as a ratio, μ should not depend on the contact area. However, Barnes et al. (1971) find that their results do depend on this. A possible explanation could be as the area changes the contact geometry changes. While this experiment is only for small areas, this highlights the fact that when we discuss friction under glaciers there is a difference between

localised friction and friction on larger scales.

In real situations, μ depends on velocity and temperature because velocity and temperature affect frictional melting. It thus constantly evolves. This is the process that I am attempting to capture in Glimmer-Hydro, on a larger scale, by linking basal slipperiness to frictional heat generation and, in turn, to water pressure. Experimentally this is observed as a decrease in μ, both at large scales and at localised scales. The processes defining friction do not scale but the general concept of water lubricating the bed in some way to reduce bulk friction do. At the large scale that Glimmer-Hydro operates at, there will always be irregularities in the bed which create a residual friction even where effective pressure is zero. On a first-order level, I ignored this residual friction ($\mu_0 = 0$) but the mechanism for dealing with it is incorporated into Equation 2.26. To use it adds an extra degree of complexity to the system and requires the user to define the value of μ_0 in some way.

For this project, I want a maximum reasonable value for μ, which I call $\mu_{\max}$. $\mu_{\max}$ is the coefficient of friction when the ice just begins to slide because it is no longer frozen; the water present at the ice-bed interface is the minimum necessary for sliding. At this stage, I envision the ice to have just reached pressure melting point and for there not to be any extra energy available for melt. As more water becomes available, Glimmer-Hydro calculates a lower value for μ from $\mu_{\max}$ as needed. In other words, Glimmer-Hydro accounts for the decrease in μ observed in experiments dynamically.

4.1.3 Review of experimental values for μ

The ideal experiments of interest look at cases where ice friction is at its maximum, at the limit of sliding. Experimentally, once sliding begins the measured value of friction is lower (Budd et al., 1979). One of the reasons for this is that melting lubricates the interface. On a large scale, this is incorporated in the model equations. Therefore the model can calculate the reduction needed, based on a sliding adjustment parameter $t_{s_{\max}}$, but needs the maximum value as a parameter. The ideal experiments also look at how the coefficient of friction changes as the variables vary. This helps determine a suitable value for $t_{s_{\max}}$.

Most relevant experiments focus on the contrast between steel or granite and ice. The coefficient of friction calculated by a variety of authors is summarised in Table 4.1.

Barnes et al. (1971) find that there are three different regimes of friction for sliding at

Coefficeint of friction values for ice

Material	Temperature	Coefficient μ	Author
Granite (limit of sliding)	-11.75 °C	0.05–1.2	Barnes et al. (1971)
Concrete (limit of sliding)	$\sim T_{\mathrm{pmp}}$	0.2	Budd et al. (1979)
Concrete (10 & 13 km a^{-1}) with $N = 10$ bar	$\sim T_{\mathrm{pmp}}$	0.09	Budd et al. (1979)
Concrete (10 & 13 km a^{-1}) with $N = 30$ bar	$\sim T_{\mathrm{pmp}}$	0.04	Budd et al. (1979)
Shale (limit of sliding)	$\sim T_{\mathrm{pmp}}$	0.3	Budd et al. (1979)
Pebbles (limit of sliding)	$\sim T_{\mathrm{pmp}}$	0.4	Budd et al. (1979)
Coarse bedrock (limit of sliding)	$\sim T_{\mathrm{pmp}}$	0.5	Budd et al. (1979)
Granite (limit of sliding)	$\sim T_{\mathrm{pmp}}$	0.6	Budd et al. (1979)
Bedrock	—	0.7	Piotrowski and Tulaczyk (1999)
Bedrock	—	0.05	Iverson et al. (2003)
Rock	—	0.6	Cohen et al. (2005)
Steel	-11.75 °C	0.05	Barnes et al. (1971)
Steel pin	—	0.06–0.1	Liang et al. (2003)
Steel	—	0.042–0.170	Marmo et al. (2005)
Steel	-5 °C	0.02–0.04	Mills (2008)
Stainless steel	-7 °C	0.05–0.15	Kietzig et al. (2010)
Steel (M2)	-7 °C	0.06–0.07	Kietzig et al. (2010)
Steel (P20)	-7 °C	0.04–0.2	Kietzig et al. (2010)
Brass	-11.75 °C	0.25	Barnes et al. (1971)
Silicon	—	0.6	Liang et al. (2003) citing Bluhm et al. (2000)
Ice skates	-17 °C	0.005 minimum	Wettlaufer (2006)
Cobalt-chromium alloy	-7 °C	0.04–0.15	Kietzig et al. (2010)
Polyethylene	—	0.08–0.12	Slotfeldt-Ellingsen and Torgersen (1983)
Oxidised polyethylene	—	0.09–0.14	Slotfeldt-Ellingsen and Torgersen (1983)
Glass	-11.75 °C	0.3	Barnes et al. (1971)

Table 4.1 Summary of the coefficient of friction at the ice-material interface. Most experiments are controlled laboratory experiments, but those where the temperature are at pressure melting point (T_{pmp}) are performed in a subglacial laboratory.

low velocities: creep; plastic flow with fracture; and frictional heating with melt lubrication. Their experiments look at ice on brass, steel, glass and granite. The dependence of μ on sliding speed changes with each material; however the overall profile of the dependence for a single material is roughly constant. Figure 4.1 reproduces their results for granite. The three regimes observed are where the gradient of the plotted curves are positive, near zero and negative. Barnes et al.'s work (1971) does not use a high load. In an ice sheet, where the load is much higher and extra heat sources, such as strain and geothermal heating, are present, sliding occurs where the ice is close to pressure melting. In their work, they found the coefficient of friction hard to measure as the temperatures approached the melting point. Despite this, at a temperature of $-0.25\,^{\circ}\mathrm{C}$ they calculate a maximum friction of $\mu = 0.25$ for ice on granite (Figure 4.1). This may be a reasonable realistic upper bound to use.

Budd et al. (1979) perform experiments for a variety of material in contact with ice close to the pressure melting point (concrete, shale, pebbles, coarse-sawn volcanic rock, and granite). They calculate the coefficient of friction μ, at the limit of sliding, to be in the range 0.2–0.6. With a constant sliding velocity and varying load, the coefficient of friction is much lower. At a velocity of $10\,\mathrm{m\,a^{-1}}$, the concrete slab has a coefficient of friction of 0.09 with a 10 bar load, and 0.04 with a 30 bar load. They find that sliding velocity is proportional to a cube of basal shear stress and inversely proportional to the load. Budd et al. (1979) also report a correlation between a transition from stable to unstable flow and the value of shear stress times sliding velocity, a common equation for estimating friction under glaciers.

It is useful to spend time discussing the work done by Marmo et al. (2005) because of their thorough investigation of the parameter space. This work, reproduced in Figure 4.2, maps μ against temperature and velocity for ice sliding on steel. They find a strong temperature dependence at low temperatures. The nature of the relationship changes with temperature. At $-11.5\,^{\circ}\mathrm{C}$, μ varies as the inverse square root of the velocity. This is consistent with work done by Evans et al. (1976). At lower temperatures, the dependence on velocity is higher as the movement is plastic due to a lack of water at the interface. At higher temperatures, there is less dependence on velocity due to the presence of extra water. This is likely to be the regime I must try to reproduce in the model.

Perhaps one of the more useful experiments for determining subglacial friction is by Cohen et al. (2005). They measure the frictional force experienced by a granite tablet under

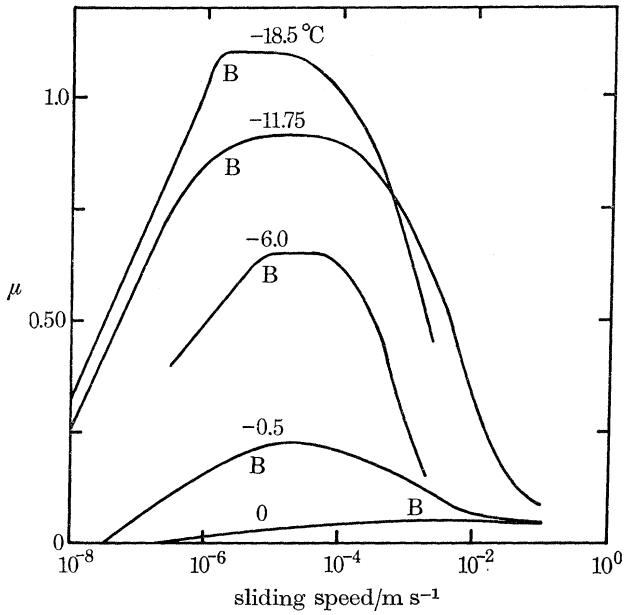

Figure 4.1 Contour plot of the coefficient of friction from ice-on-granite laboratory experiments for a range of temperatures and sliding speeds. The coefficient of friction is highly dependent on speed and temperature, partially because melting ice lubricates the interface. For typical glacier velocities, this graph implies that the coefficient of friction increases with sliding. Results are reproduced from Barnes et al. (1971).

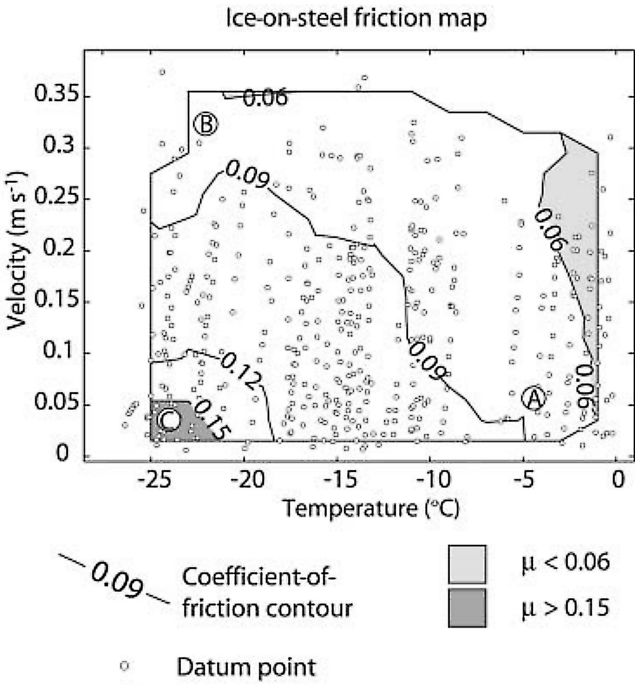

Figure 4.2 A map showing the variation of the coefficient of friction (contours) for a laboratory-based ice-on-steel experiment. In this case the coefficient of friction decreases with increasing sliding. The system is less sensitive to sliding at warmer temperatures. Results are reproduce from Marmo et al. (2005).

Engabreen, a hard-bedded outlet glacier of Svartisen ice cap in northern Norway. One of their key results is that the coefficient of friction is dependent on the size and abundance of debris transported by the glacier, not the properties of ice itself. This agrees with earlier theoretical work by other authors (eg Morland, 1976; Schweizer and Iken, 1992). Cohen et al. (2005) obtain values of μ between 0.05 and 0.08, still an order of magnitude below most solids, despite the influence of the clasts over the granite tablet. Earlier work by Iverson et al. (2003), based on the same data, also suggests that $\mu = 0.05$ appears to be a reasonable for the value bulk-friction at the bed of a glacier.

4.1.4 Coefficient μ values for thesis

Despite the dependence of μ on the material ice is sliding on and the contamination of ice with debris, there is general agreement that the value of μ is an order of magnitude lower than that of everyday materials. This is true for temperatures approaching the melting point of ice where the interface is lubricated[1] . Thus, taking $\mu_{\max} = 0.05$, as calculated by Cohen et al. (2005) for a debris rich hard-bedded glacier, as a standard value seems appropriate. As everything I am doing is an approximation whether, $\mu_{\max}$ is 0.05 or 0.08 has far less impact than getting the order of magnitude correct. In Section 4.4, I determine the sensitivity of the system to $\mu_{\max}$.

The dependence of the coefficient of friction μ on normalised effective pressure[2] $\bar{N}$ also needs to be considered. The simplest relationship is a linear one. I therefore use this as a starting point. However, at $-11.5\,^{\circ}\mathrm{C}$ both Evans et al. (1976) and Marmo et al. (2005) observe an inverse square root relationship.

By scaling μ with $\bar{N}$, which in turn depends on ice velocity due to the meltwater production from frictional heating, I can simulate the reduction of friction that many authors observe with increasing velocity. The nature of the scaling can, to some extent, take into account different regimes of the contact geometry. This contact geometry cannot be simulated directly, at least not without a disproportionate volume of work. Fourier analysis of high resolution bed DEMs may work, but such DEMs do not exist except for individual basins or valley glaciers. A basal slipperiness adjustment parameter t_s is a useful proxy for this instead because of the

[1] Cuffey et al. (1999) observe sliding at $-17\,^{\circ}\mathrm{C}$, but the ice still has a water film present due to the chemical potential of water near debris. In this thesis, this effect is ignored and sliding is only allowed where melting is calculated due to the various heat sources.

[2] I usually refer to normalised effective pressure $\bar{N}$ instead of effective pressure N. This simplifies the equations by scaling N to the dimensionless range $[0, 1]$, where 1 is fully grounded ice.

shape of the response function to a given perturbation at the bed. It can be defined to be more sensitive either when effective pressures are high (sliding starts quickly) or when they are low (lots of basal water is needed for significant sliding). These relationships are shown in Figure 2.3

4.2 Conceptual friction model

The various experiments described in Section 4.1 investigate how the coefficient of friction responds to different parameters. I now use the ideas introduced to describe how I envision the friction under ice sheets to behave.

The holistic discussion, in Section 4.1.1 as to why ice is slippy, links the properties of ice to the presence of water at the contact surface. A common theme of the various studies is that μ is a function of a number of variables. These include: basal ice velocity, temperature, perhaps load, *et cetera*. There is good evidence that this dependency exists because these variables affect the production of meltwater. The meltwater then causes the reduction of μ that is observed. In this conceptual model, I differentiate these two processes and look at the sources of heat separately to how the water affects μ. The first process can be approximated using known physics. How water affects μ is more challenging to determine.

4.2.1 Response of μ to effective pressure

A question is: if μ is a function of $\bar{N}$, then what shape does this function take and why? This affects the dynamic response of the ice. To some extent the answer depends on the nature of the bed; this is something that, for ice sheets, is mostly unknown.

Generally, there are three categories which summarise the response of μ to $\bar{N}$. The simplest is linear, but this is physically unlikely. The other two categories are a quick response when effective pressure is high and the need for the system to have lots of water (low effective pressure) before sliding velocities increase significantly. The topography of the bed and whether the bed is hard or soft may affect which category the response falls under.

Consider a rough undulating hard bed. It stands to reason that this may exhibit a delayed response to an increase of water pressure. A possible physical justification of this is that protrusions are the main source of basal drag. Only when high water pressures are reached do the protrusions begin to decouple from the ice. This idea seems to agree with the inverse

square relationship described by Evans et al. (1976) and Marmo et al. (2005).

Alternatively, a soft bed may respond to a little water pressure and produce a quick response as water pressure begins to increase. If a soft bed is deforming and the ice is rafted then extra heat sources from the shear of the till may need to be considered. GLIMMER-HYDRO does not distinguish between a hard and soft bed so this extra heat term is ignored in this thesis. By scaling friction in the quick response category velocity may respond appropriately but the heat flux calculation does not.

4.2.2 Feedback mechanisms

The reduction of the coefficient of friction has two important effects and a number of secondary ones which lead to various feedback mechanisms. These mechanisms have the potential to stabilize flow in ice sheets and remove the streaming and "flickering" described by numerous authors (eg Hulton and Mineter, 2000; Payne and Baldwin, 2000; Bueler et al., 2005; Jamieson et al., 2008).

As friction decreases, sliding velocities increase for the same driving stress and the heat generated by sliding decreases, for a given velocity. With less heat being generated the melt rate, and therefore the water pressure, cannot be maintained. This may then cause the coefficient of friction to increase again resulting in a higher melt rate. This could lead to both variables adapting around each other to reach a steady state or it could lead to the system oscillating between two states. Figure 2.7 gives a graphical representation of these feedback mechanisms.

In areas where high water pressure is maintained without frictional heat this feedback disappears and the coefficient of friction reduces to a residual value, possibly zero. This is the case in natural hollows where water tends to converge as discussed in Chapter 3. Frictional heat may still be important at the edges of such fast flow features because the water pressure drops in these regions.

4.2.3 Numerical considerations

In light of the conceptual friction model, I want to review the key numerical considerations of its implementation. In this discussion I assume the following to be true:

1. where the bed is frozen, the coefficient of friction is very high;

2. μ is a function of several different and complex variables; and
3. everywhere the effective pressure is zero, the ice is not fully decoupled from the bed due to local variation in the bed causing residual friction.

The frozen bed is not allowed to slide. This means that physically the coefficient of friction is very high but numerically its value does not have to be determined. A logical statement in GLIMMER's code suffices to account for this portion of the conceptual model.

The maximum coefficient of friction, when the ice just reaches pressure melting point but before water pressure has built up, needs to be defined. This is the variable $\mu_{\max}$. Experimentally μ is a function of many variables but numerically it makes sense to only link it to $\mu_{\max}$, effective pressure N and an adjustment parameter γ as in Equation 2.26. The dependencies on temperature, sliding velocity, and load, amongst others, are determined by the effect those variables have on the effective pressure.

Changes in effective pressure affect the sliding velocity. GLIMMER determines sliding velocity using the basal slipperiness parameter t_s. Item 3, above, stops runaway acceleration of the ice as the effective pressure approaches zero. This is done by setting a maximum value for basal slipperiness $t_{s\max}$. μ and t_s should be linked numerically, but in this thesis they are not because the relationship between them has not been investigated. When calculating frictional heat flux the $t_{s\max}$ terms cancel leaving the heat flux as a function of $\mu_{\max}$; conversely, sliding velocities are dependent on $t_{s\max}$ and not $\mu_{\max}$. This must be borne in mind when interpreting the results, especially as $t_{s\max}$ and $\mu_{\max}$ are not directly coupled.

4.3 Frictional heat flux

Before I discuss the friction experiments, I discuss the magnitude of the frictional heat flux term. I compare these values to the geothermal and strain heat flux terms discussed in Section 3.3 to gain an understanding of the relative importance of the terms.

Sliding is dependent on effective pressure and that, in turn, is dependent on the basal melt pattern. How does heat from sliding friction contribute to this pattern? How does this extra heat compare in magnitude and distribution to the heat from internal strain heat flux at the bed?

Section 2.3.1 derived Equation 2.28 for calculating the frictional heat flux H_f from first principles. This section looks at the values of H_f and compare them with the traditional

calculation used in other work.

4.3.1 Order of magnitude

In Chapter 2, I derive a new equation for calculating frictional heat flux that depends on water pressure (Section 2.3.1). I now compare the magnitude of the values obtained from this equation to the values obtained from the more traditionally used equations.

GLIMMER as released calculates frictional heat flux using

$$H_f = \boldsymbol{v}_b \boldsymbol{\tau}_b = \boldsymbol{v}_b \rho_i g h \tan \Theta_s \tag{4.1}$$

where $\tan \Theta_s$ is the surface ice gradient (Rutt et al., 2009). Equation 2.27 modifies this to be

$$H_f = \mu(\bar{N}, \gamma) \boldsymbol{v}_b \rho_i g h \cos \Theta_b \, . \tag{4.2}$$

Both equations are similar and have the same dimensions but there are some notable differences. These have been discussed in Section 2.3.2 . The key difference is the dependence of the friction on the normal force at the bed and not the driving stress. $\cos \Theta_b$ is used because H_f should be a maximum when sliding over a flat bed because the normal force is also a maximum. Both equations produce values of a similar magnitude when the surface gradient is small.

For a small angle Θ in radians, $\Theta \approx \tan \Theta$. For example, a surface gradient of $\Theta_s = 5^\circ = 0.0873$ radians and $\tan 5^\circ = 0.0875$. Conversely for a small angle Θ, $\cos \Theta \approx 1$. As a realistic value for $\mu_{\max}$ seems to be 0.05, $\mu \cos \Theta$ has the same order of magnitude as $\tan \Theta$ when Θ is small. $\boldsymbol{v}_b \rho_i g h$ is the same in both equations. Therefore, the magnitude of both heat fluxes are comparable in most circumstances. However, if Θ gets very small then $\mu \cos \Theta > \tan \Theta$.

The order of magnitude of H_f is $100\,\mathrm{mW\,m^{-2}}$ when typical values[3] for an ice sheet are used which double the typical value for geothermal heat flux ($42\,\mathrm{mW\,m^{-2}}$) often quoted in literature for Greenland (eg Lee, 1969; Greve, 1996; Johnson and Fastook, 2002). It is, however, the same order of magnitude suggested as a maximum value in northern Greenland by Greve and Otsu (2007).

[3] Typical orders of magnitude of variables for an ice sheet: $O(h) = 10^3\,\mathrm{m}$, $O(g) = 10\,\mathrm{m\,s^{-2}}$, $O(\rho_i) = 10^3\,\mathrm{kg\,m^{-3}}$ $O(\mu_{\max}) = 10^{-2}, O(\boldsymbol{v}_b) = 10\,\mathrm{m\,a^{-1}} = 10^{-7}\,\mathrm{m\,s^{-1}}$, $O(\Theta) = 10^{-2}$ radians. $O(h)$, $O(\boldsymbol{v}_b)$ and $O(\Theta)$ may vary affecting $O(H_f)$ accordingly.

Depending on the exact order of magnitude of the parameters the order of H_f may go up or down. Ice tends to speed up near the margin but this is also where the ice gets thinner; ice thickness and velocity counter each other to some extent. Ice flows more quickly where effective pressure is low and so in these regions frictional heat from sliding may stop being a consideration altogether when Equation 4.2 is used. With the traditional method of only considering velocity and driving stress, areas of fast ice are where the frictional heat may be a maximum as there is no dependence on water pressure.

4.4 Eismint experiment

The goal of this experiment is to investigate how frictional heat flux feedbacks potentially affect ice sheets. For this, I use the idealised circular ice sheet defined in the EISMINT-2 experiments (Payne et al., 2000). This section discusses the goals of this experiment (Section 4.4.1) and the experimental set-up (Section 4.4.2) before presenting the results (Section 4.4.3). The processes responsible for the observed behaviour are discussed in Section 4.4.4.

4.4.1 Research questions

This experiment aims to answer the following questions:

1. To what extent does coupling friction with hydrology and sliding affect the evolution and dynamics of ice sheets?
2. How different are the results of the present formulation compared to the commonly-used equations?
3. Are any feedback mechanisms identified? How do the coupled frictional heat flux (H_f), velocity ($\boldsymbol{v}_b$), and melt rate (M) interact?
4. What is the impact of this coupling on basal ice temperatures?
5. Can this approach help improve the numerical and flow instabilities identified by Hulton and Mineter (2000) and Payne and Baldwin (2000)?

4.4.2 Experimental set-up

This experiment is performed in three stages, each building on the previous: EISMINT-2 control run (1), coupling velocity but not frictional heat generation to water pressures (2), and a fully coupled velocity-friction model (3). The three stages are designed to increase the complexity of the runs in a piecemeal fashion with a view to break down the individual components of any potential feedback mechanism. Table 4.2 shows the model runs used in each experiment stage.

Stage 1: Eismint-2 control

The EISMINT-2 experiments are a useful benchmark for testing ice sheet models. The GLIMMER ice sheet model performs well in these tests (Payne et al., 2000). Stage 1 defines a control run, which does not use any of my modifications, against which the runs in Stages 2 and 3 are compared. In the control run, GLIMMER is run independently.

The run (F1) is set-up to use experiment H, defined in Payne et al. (2000) and discussed in Section 2.2.4. This set-up defines a fully thermomechanical ice sheet model with sliding proportional to basal shear stress where the bed is at pressure melting point (Equation 2.10). Instead of a flat bed, I use the trough topography defined for experiment I. Combined, this allows the model to calculate sliding; frictional heating; and, in Stages 2–3, a convergence of water in the trough. This allows us to investigate the full frictional feedbacks on sliding and heat generation both where water converges and where it does not.

The trough topography is 1000 m at its deepest point and has a parabolic cross-section and a linear long-profile (Figure 2.1). Following Jamieson et al. (2008), adding a ± 1 m uniformly distributed random element to the topography reduces the grid dependence of the results. The DEM is 61×61 cells with a grid resolution of 25 km. At this resolution the bed is effectively flat, except for the trough, even with the random undulations. In the Stage 1 control run, GLIMMER is run without any coupling to HYDRO.

The model runs for 200 ka with a 5 a time step starting with no ice. Data are output every 1 ka.

Pressure profile model runs

Stage	Run	Variable	Values
1	F1	—	EISMINT-2 experiment H defaults
2	F2–6	γ	$\gamma \in \{0.1, 0.5, 1.0, 2.0, 10.0\}$
3	F7–41	$\gamma \times \mu_{\max}$	$\mu_{\max} \in \{0.001, 0.005, 0.01., 0.05, 0.1, 0.5, 1.0\}$ $\times$ F2–6

Table 4.2 Summary of the EISMINT friction model runs in this chapter. All runs use the EISMINT-2, experiment H set-up with the trough topography with GLIMMER-HYDRO. Each stage introduces GLIMMER-HYDRO's friction calculation in a piecemeal fashion. Stage 1 is the control run without any HYDRO coupling, Stage 2 adds velocity dependence on HYDRO, Stage 3 is the full velocity–friction coupling. In Stage 3 the runs F7–13 correspond with $\gamma = 0.1$ and so on.

Stage 2: Velocity coupling

The second stage of the experiment begins to introduce the GLIMMER-HYDRO coupling. Here, sliding velocity is defined using effective pressure from HYDRO but the friction calculation is not modified from GLIMMER as released. This enables us to consider the effects of this coupling before the full frictional heat flux is considered. This stage is similar to Jamieson et al.'s (2008) coupling of basal slipperiness t_s to basal melt rate except that there is no direct correlation between basal melt rate and effective pressure $\bar{N}$. Nevertheless, despite the differences in geographical distribution, the smooth scaling of t_s introduced should produce similar response in ice dynamics.

This run is defined as for Stage 1 except that GLIMMER calculates t_s using $\bar{N}$ from HYDRO. HYDRO is set-up to use the same 5 a time step as GLIMMER. The bed in HYDRO is defined as frozen, and so impermeable, where the basal melt rate $M \leqslant 0\,\mathrm{mm\,a^{-1}}$. The same arbitrary efficiency condition of $\bar{N} \leqslant 0.1$ (pressure ratio $p_r > 0.9$) is used for consistency. The efficiency factor ψ is set to 40 because preliminary runs show this to be in the plateau region identified in Figure 3.13.

The coupling (Equation 2.15) is defined using the sliding adjustment parameter $\gamma \in \{0.1, 0.5, 1.0, 2.010.0\}$ (runs F2–6). The maximum basal traction is set to $t_{s_{\max}} = 1 \times 10^{-3}\,\mathrm{m\,a^{-1}\,Pa^{-1}}$ as in Stage 1. The effect of γ on t_s is shown in Figure 2.3. γ controls how quickly the system responds to a change in $\bar{N}$. $\gamma = 0.1$ and 10.0 are likely to be unrealistic but provide a discussion point. $\gamma < 1$ is similar to the inverse square relationship observed experimentally by Evans et al. (1976) and Marmo et al. (2005) where effective pressure has

to be small before a significant drop in the friction is observed.

There is an important, but non-realistic, feedback present at this stage. As effective pressure $\bar{N}$ falls, ice velocity increases but because of the equations used in GLIMMER by default frictional heat increases wherever there is fast ice. This is the case in any study that currently uses GLIMMER or many other ice sheet models. In reality, I suggest that the extra lubrication provided by basal water should begin to limit frictional heat generation. This is the full coupling that the next experiment stage introduces.

Stage 3: Full coupling

The final stage of this experiment considers the full feedback mechanism between friction heat generation, sliding, and basal melt rates. As sliding increases due to increased basal water, the frictional heat generation should decrease which, in turn, should reduce basal melt rates. This reduction in basal melt rate may reduce the effective pressure which may then increase frictional heat generation and melt water production. These feedbacks are complex, and their full interaction cannot be considered conceptually.

This stage adds Equation 2.27 to the coupling in GLIMMER-HYDRO which defines frictional heat flux as a function of normalised effective pressure $\bar{N}$, the sliding adjustment parameter γ, and a maximum coefficient of friction $\mu_{\max}$ defined by the user. Physically, $\mu_{\max}$ defines the maximum bulk-friction of the bed. It measures the friction experienced by the ice over the whole grid square and not the friction experienced by the ice locally. However, as appropriately realistic values of bulk-friction are not known the experiment is loosely based on the values reviewed in Section 4.1, with scope for exploring the parameter space.

This experiment stage uses the same values for γ as Stage 2. For each of these values, $\mu_{\max} = \{0.001, 0.005, 0.01, 0.05, 0.1, 0.5, 1.0\}$ are defined (runs F7–41). $\gamma = 0.1$ with the full range of $\mu_{\max}$ values corresponds to runs F7–13.

4.4.3 Results

The results of experimental Stages 1–3 are now presented in sequence. The key features of the runs are highlighted but the discussion of their implications, and the processes which may be responsible, is left for Section 4.4.4.

In most cases, the final 200 ka time slice is mapped but a few results plot the previous

three times slices to show a sequence. Time dependence is generally displayed using three methods. One, the standard deviation of a variable over the last 75 ka, once the system has reached quasi-equilibrium, is mapped to give an indication of the variability of the system. Two, the evolution of a variable through the full 200 ka is plotted across a transect (cross-section in Figure 2.1) to compare the behaviour of nearby points. Three, four points are plotted through the last 75 ka to provide a detailed view of their behaviour and to enable easier comparison between runs.

The four points used are defined in Table 4.3. These are chosen to represent an area: of high variability, away from the trough (1); near the warm-cold boundary, away from the trough (2); at the head of the trough (3); and near the middle of the trough (4). Points 1 and 2 are defined using runs where the system responds quickly to a given change (sliding adjustment parameter $\gamma = 0.1$) because these runs have a large frozen bed and all the points need to be in a warm-bedded area. The variability and the proximity to the cold bed are not constant of other values of γ.

Stage 1: Control

Stage 1 is the Eismint-2 control run which does not include any coupling with Hydro. Frictional heat flux is calculated by Glimmer as released and sliding is allowed where the bed reaches pressure melting point.

Figure 4.3 maps ice thickness, basal ice temperature, and basal melt rate at the end of the 200 ka run. Figure 4.4 maps the last four time slices of the ice speed and the standard deviation of the speed over the last 75 ka of the run.

Key things to note are that:

1. there is a fast flow feature in the trough;
2. there is "streaming" type behaviour away from the trough with
3. fingers of warm based ice exist next to cold based ice;
4. except for in the trough, the "streaming" flickers; and
5. ice suddenly starts sliding at around $50\,\mathrm{m\,a^{-1}}$; there is no gradual start to the sliding.

Figure 4.5 shows the basal sliding speed for the four points defined in Table 4.3. Point 1 is near the origin of a fast flow feature. This point alternates both warm and cold conditions and this is reflected by an oscillation between fast sliding and no sliding. The other points

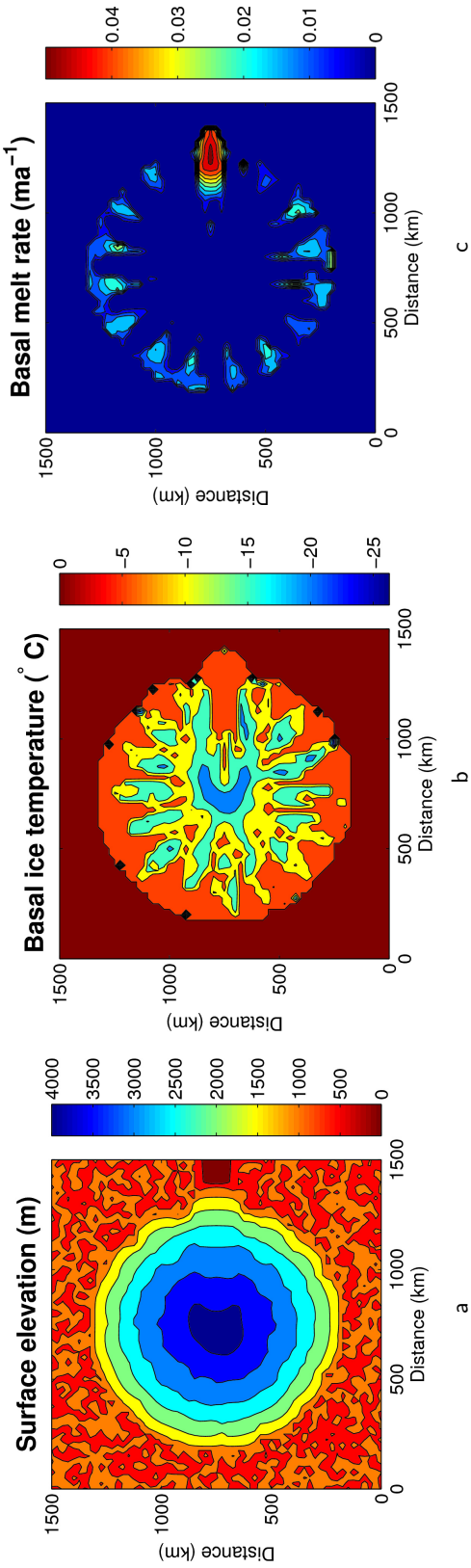

Figure 4.3 Stage 1 EISMINT-2 control (run F1) at end of 200 ka. (a) The surface elevation is irregular and varies with time. There is a dip over the trough, where there is fast-flowing ice. (b) The basal ice temperature shows "fingers" of cold and warm basal conditions. This pattern defines melting and therefore sliding and so explains the irregularities in the ice surface. (c) The basal melt rate is highest in the trough but all fingers have comparatively high melt.

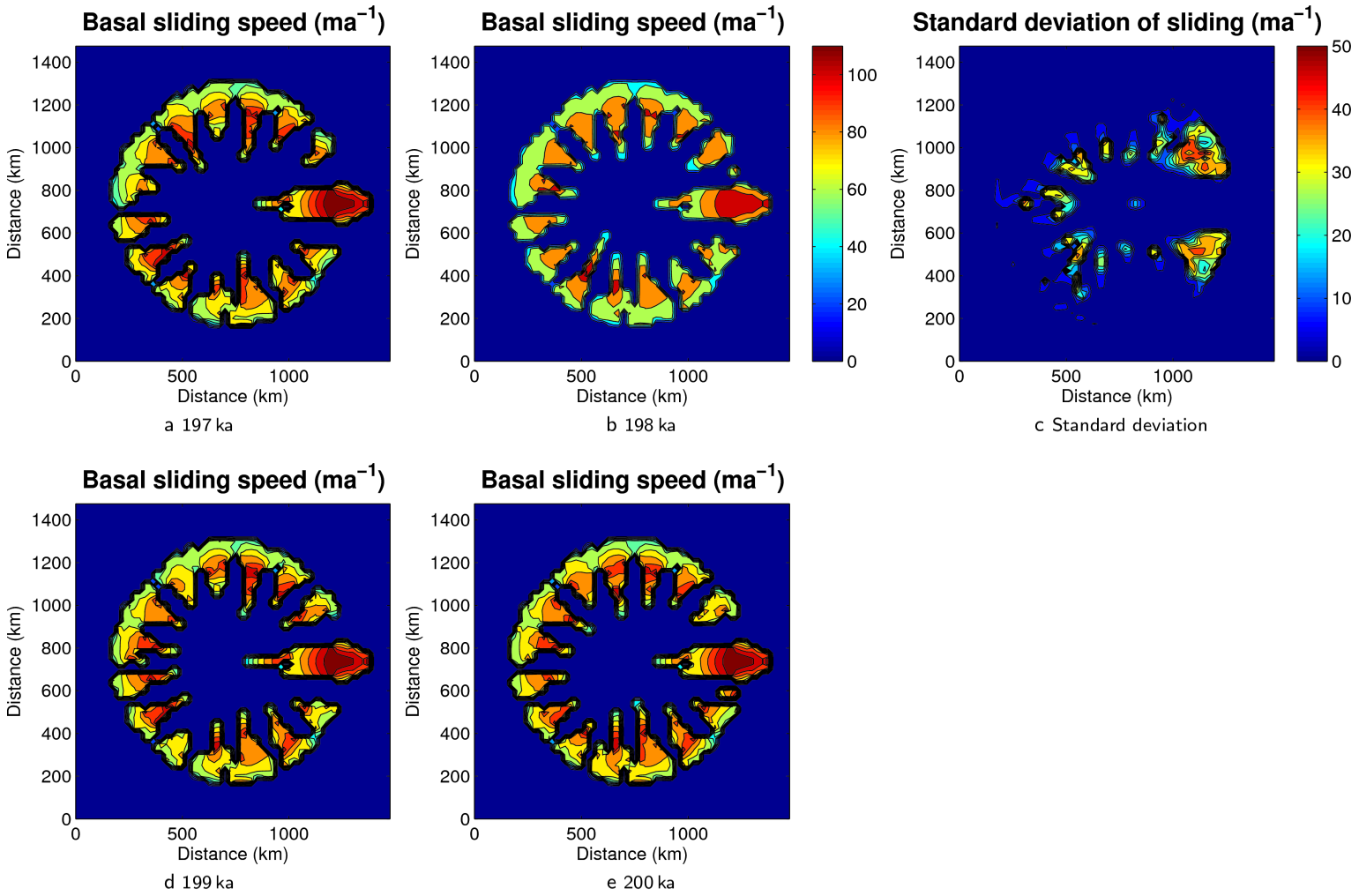

Figure 4.4 Stage 1 EISMINT-2 control (run F1) at end of 200 ka. (a,b,d,e) Basal sliding velocities at 197, 198, 199, 200 ka. Each map is noticeably different because of the stiffness of the system. (c) Standard deviation of basal sliding speed over the last 75 ka of the run show high variability over a large area.

Time series location

Point	Location	Description	Trough
1	$(37, 39)$	High variability	No
2	$(31, 45)$	Near cold-warm bed boundary	No
3	$(36, 31)$	Head of trough	Yes
4	$(47, 31)$	Middle of trough	Yes
5	$(45, 15)$	Stage 3 pulsing	Yes
6	$(45, 25)$	Stage 3 flickering	Yes

Table 4.3 Points 1–4 are used to plot time series from 125–200 ka; Figure 4.6a maps the location of these points. Points 5–6 are defined along a transect and plot the full run in Stage 3; Figure 4.16b shows the location of these along the transect.

The locations shown are the indexes (i, j) with (1,1) defining the south-west corner. The domain is 61×61 cells. Points 1 and 2 are defined using run F2 (Stage 2, $\gamma = 0.1$) because this run has a large frozen bed and all the points need to be in a warm-bedded area for all runs.

show some random flickering. At Point 3, near the origin of the trough, this instability is amplified towards the end of the run. Flickering is also apparent in Figure 4.4. Steeper gradients in the standard deviation plot imply less correlation between the flickering of adjacent points.

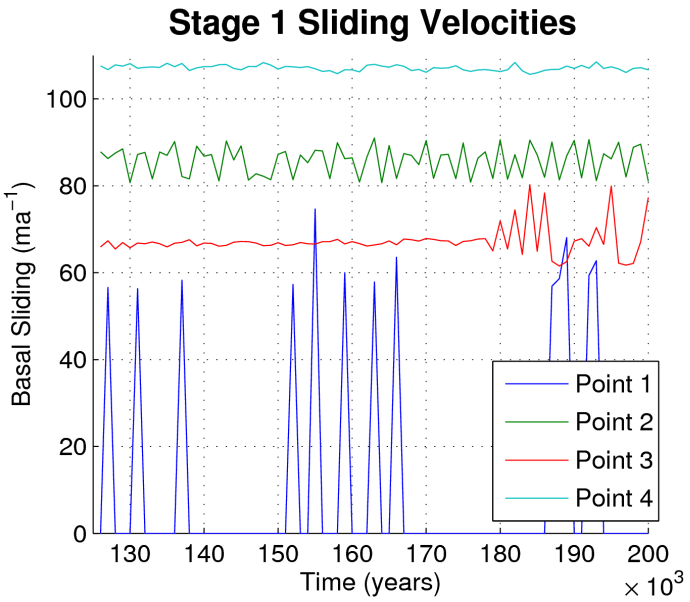

Figure 4.5 The basal sliding speed for the four points defined in Table 4.3. Point 1 is near the origin of a fast flow feature. This point alternates both warm and cold conditions and this is reflected by occasional fast sliding, then no sliding, The other points show a random flickering. For Point 3, this gets amplified near the end of the run, near the origin of one of the fast flow features. Point 4, the most regular of the four points, is the most regular because it is near the middle of the fast flow feature where flow can be maintained.

Stage 2: Velocity coupling

Stage 2 calculates sliding velocity using effective pressure from Hydro. The frictional heat calculation is the same as in Glimmer as released. Runs F2–6 vary the sliding adjustment parameter $\gamma \in \{0.1, 0.5, 1.0, 2.0, 10.0\}$. This section maps the variables that affect the frictional feedbacks: frozen bed, basal melt rate, normalised effective pressure, basal sliding speed, and surface elevation.

Figure 4.6 maps the warm basal area, and so the area which may slide, at the end of the 200 ka run for each γ value. The warm basal area controls where ice may slide. Because the actual temperature in cold regions is not important to this or the frictional feedbacks, I simply plot the cold and warm bed distribution. Smaller γ make the system more sensitive to small changes when there is little water in the system. There is a general increase in the warm basal area, and the system becomes increasingly symmetric, as γ increases. With lower γ there is fingering, although this is less than in the Stage 1 control. Figure 4.6 also plots the frozen basal area against γ to highlight the relation between them. The system is more sensitive to changes in γ when γ is small.

Figure 4.7 maps basal melt rates and effective pressure for the five sliding adjustment parameter γ values. The pattern of melt becomes more circular and symmetric as γ increases. There is an area of melt around $0.015\,\mathrm{mm\,a^{-1}}$ which increase and penetrates towards the centre. There is some grid dependence in the results with peaks in melt rate occurring at the northern, western, and southern margins, away from the trough. In the slowest response system ($\gamma = 10$) the melt at the western margin of the ice sheet is of the same magnitude as in the trough. In all cases, the trough has the highest melt rates. Normalised effective pressure is lowest in the trough. $\gamma = 10$ has the highest effective pressure in the trough. Sliding is calculated from effective pressure and this is one of the main links in the coupling in Glimmer-Hydro.

Figure 4.8 maps the basal sliding speed and standard deviation of the five runs. Except for $\gamma = 10.0$, the speeds in the trough are similar for all runs with a range from $106\,\mathrm{m\,a^{-1}}$ for $\gamma = 0.1$ to $94\,\mathrm{m\,a^{-1}}$ for $\gamma = 2.0$. For $\gamma = 10.0$ the maximum trough speed drops to $40\,\mathrm{m\,a^{-1}}$. The area of high speed in the trough spreads as t_s increases, consistent with the pattern observed in the effective pressure.

Perhaps, the effect of coupling sliding with effective pressure is most apparent by looking

at the surface elevation. Figure 4.9 shows that as the sliding adjustment parameter γ increases the surface becomes increasingly smooth and the ice over the trough loses its curvature (the contours becomes straighter). Figures 4.10 and 4.11 plot ice thickness and sliding speed for Points 2 (flat bed) and 3 (head of trough) for all values of γ and the Stage 1 control (run F1). Ice thickness and sliding speed both depend on the value of γ. All Stage 2 runs are much more stable than the Stage 1 control run. The head of the trough shows more variability than the flat bed. The values pulse with increasing magnitude as γ, except for $\gamma = 10$ which remains frozen at Point 3.

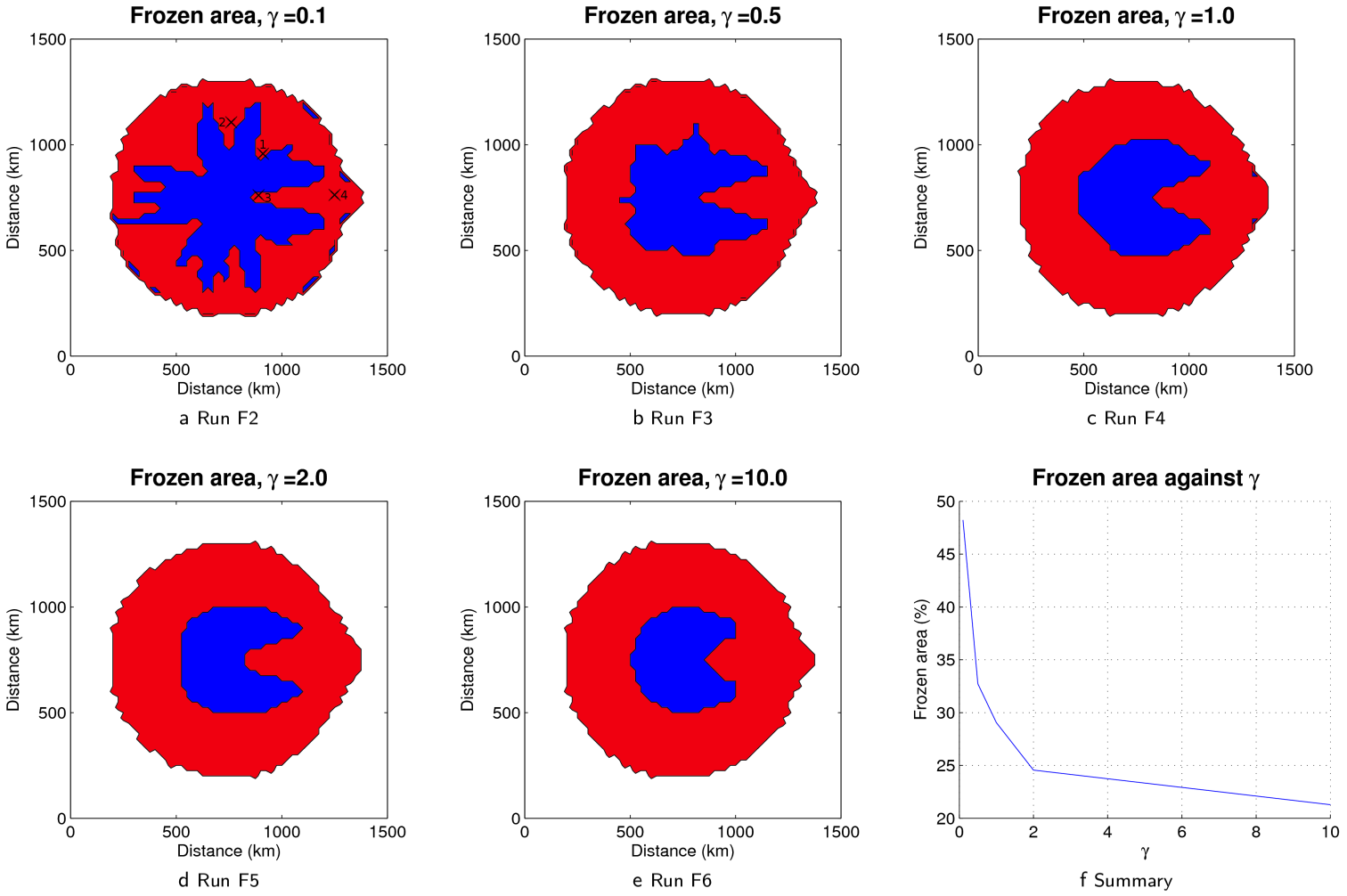

Figure 4.6 (a–e) Maps showing warm (red) and frozen (blue) areas for runs F2–6 varying the basal sliding adjustment parameter γ. As γ increase the basal pattern become more regular and symmetric. (f) Plot of the frozen bed area for runs F2–6 shows that the frozen bed is more sensitive to lower values of the basal sliding adjustment parameter γ.

(a) also shows the four points used for plotting time series (Table 4.3).

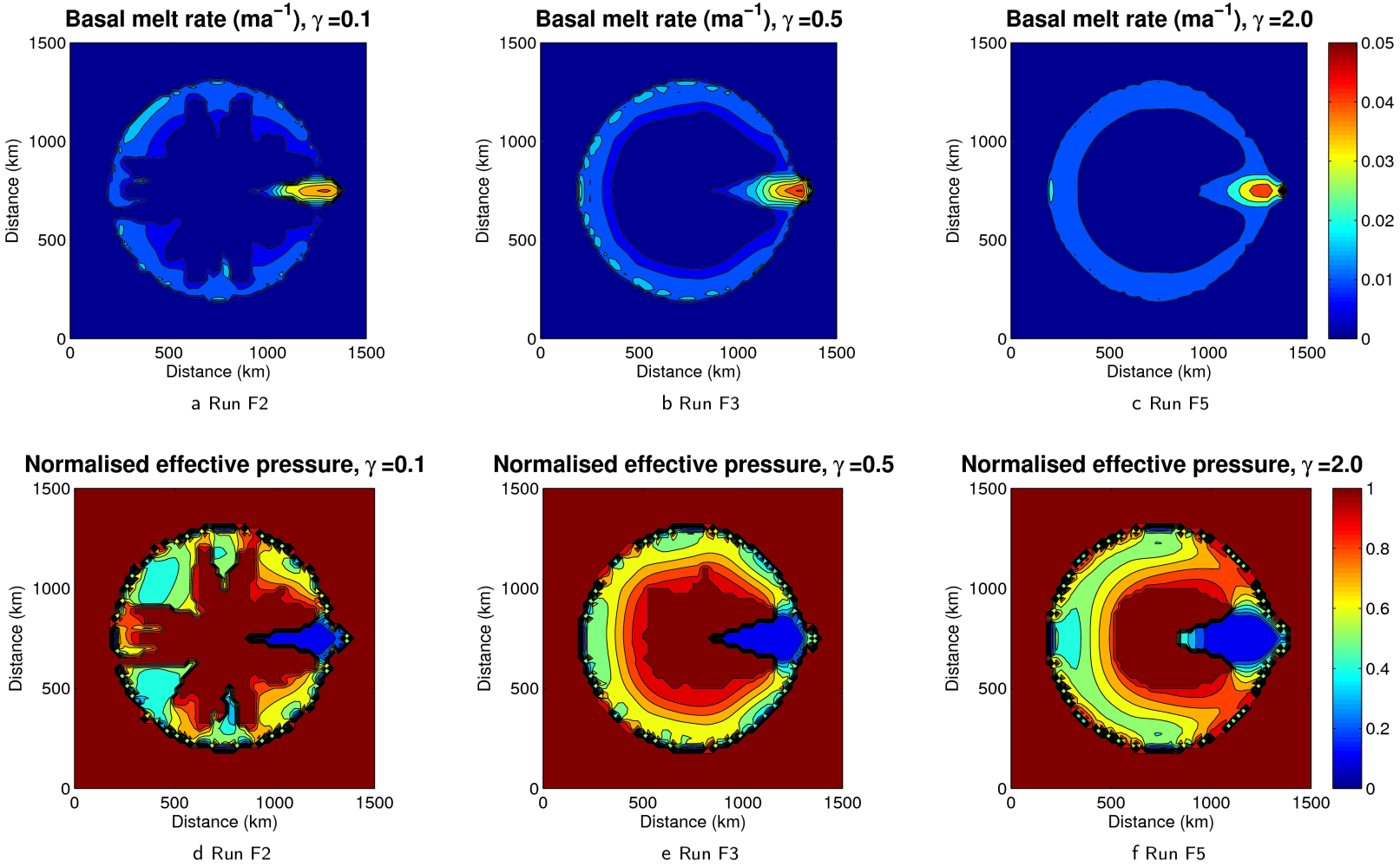

Figure 4.7 Top row: basal melt rate M. Bottom row: normalised effective pressure $\bar{N}$. The columns show, from left to right, runs F2, 3, and 5. Basal melt rates and normalised effective pressure decreases as the sliding adjustment parameter γ increases. There is a slight grid dependence, noticeable to the north, west, and south of the ice sheet. The area of low $\bar{N}$, due to convergence of flow identified in Chapter 3, spreads as γ increases.

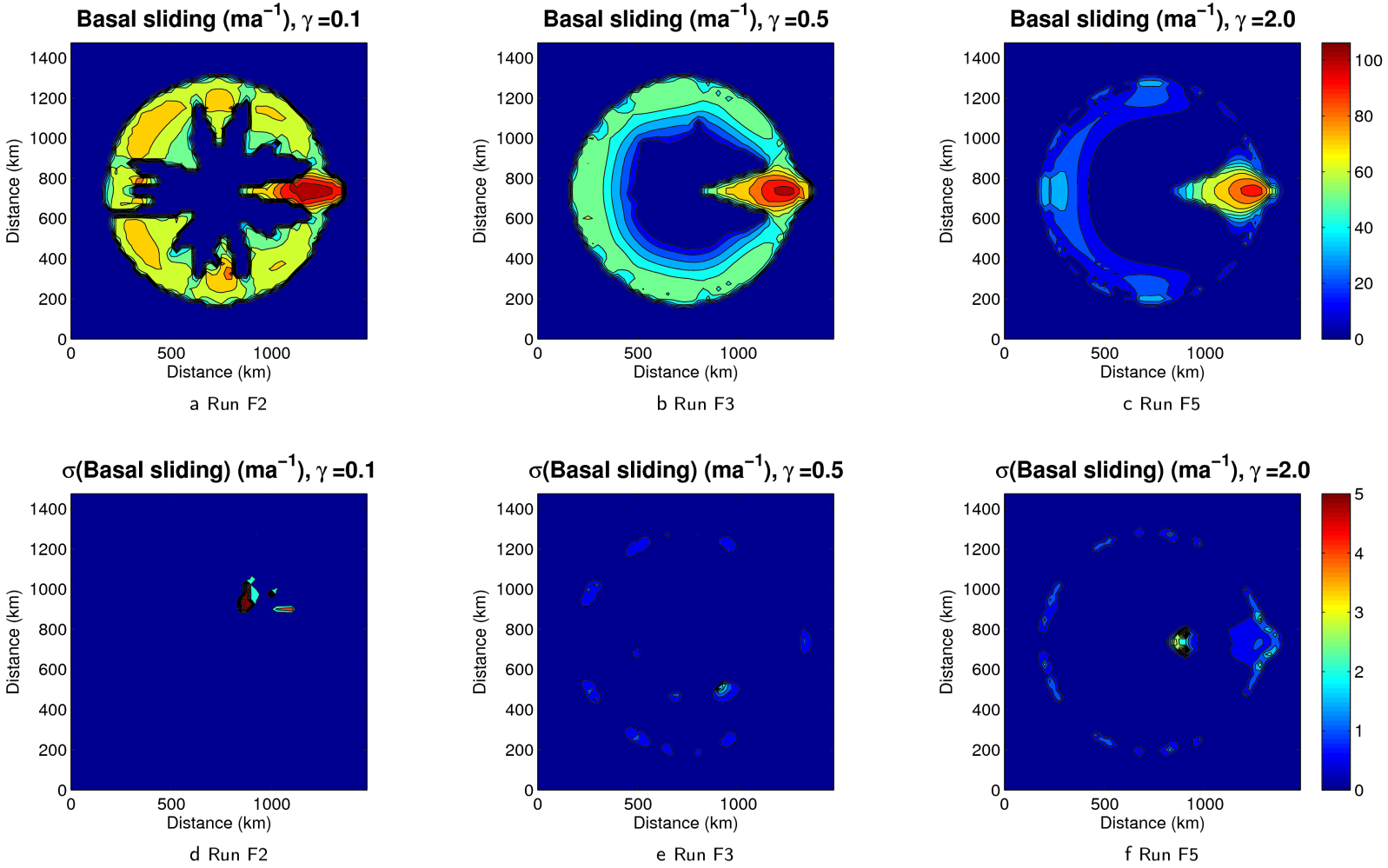

Figure 4.8 Top row: basal sliding speed. Bottom row: Standard deviation of sliding speed. The columns show, from left to right, runs F2, 3, and 5 (Stage 2). Sliding velocities become smaller, away from the trough, as the sliding adjustment parameter γ increases and the system becomes looser. The velocity in the trough stays approximately the same.

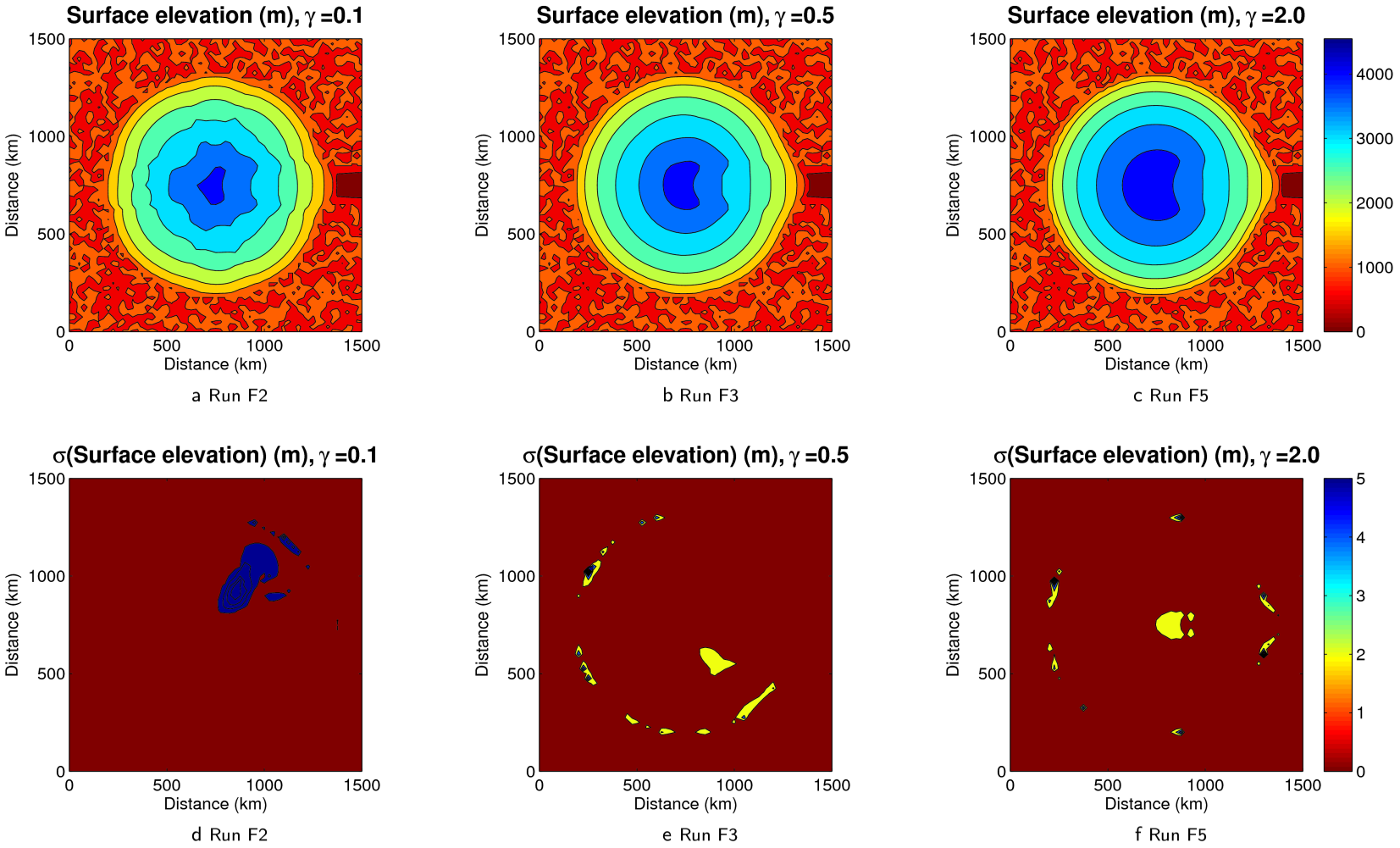

Figure 4.9 Top row: surface elevation. Bottom row: Standard deviation of surface elevation. The columns show, from left to right, runs F2, 3, and 5 (Stage 2). The surface elevation raises as γ increases. The surface also become more regular and the cross section across the trough shows less variation in elevation. The undulating flat surface is at an elevation of 1000 m.

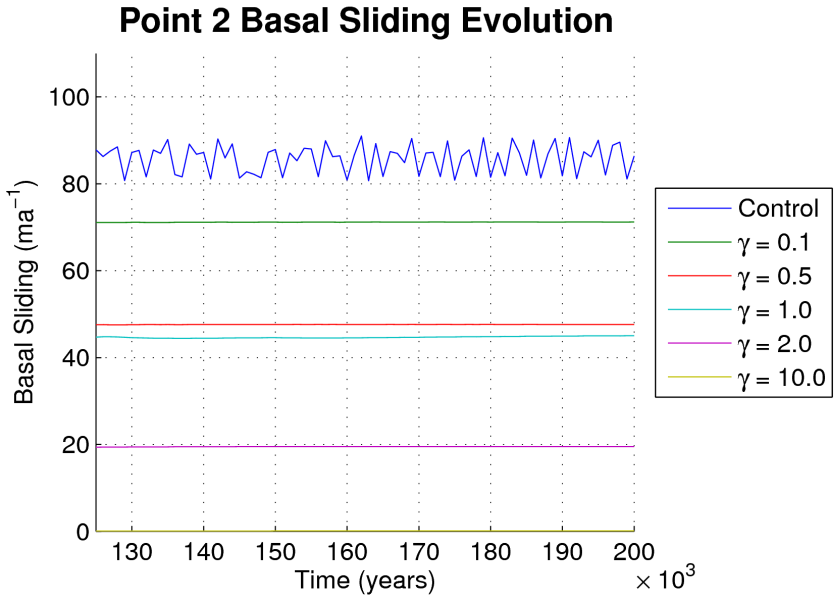

a Point 2 basal sliding

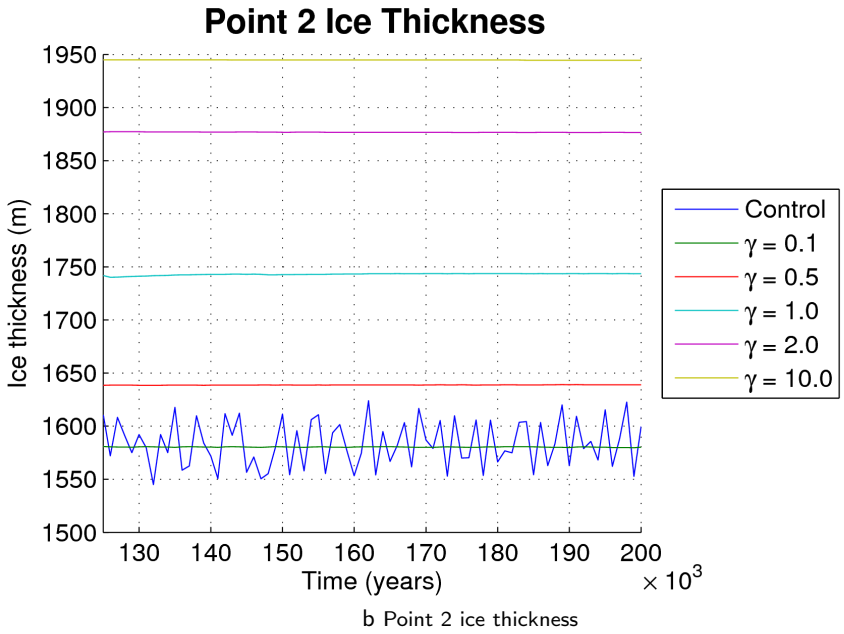

b Point 2 ice thickness

Figure 4.10 Point two is near the north-west margin of the ice sheet. It is away from any cold regions and so variation due to that will be damped. The stage one control run shows lots of variation but the sliding and ice thickness are steady for all the runs in stage two. This figure clearly shows the inverse relationship between sliding and ice thickness.

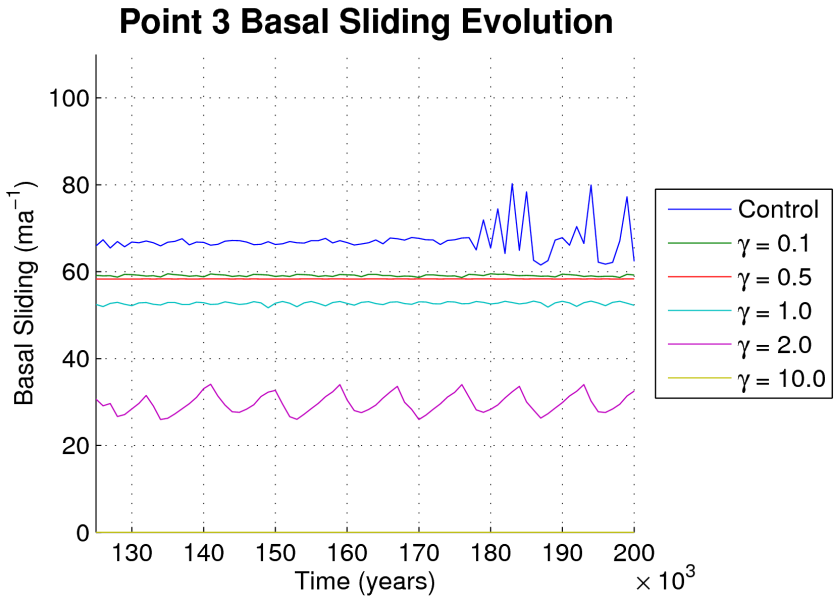

a Point 3 basal sliding

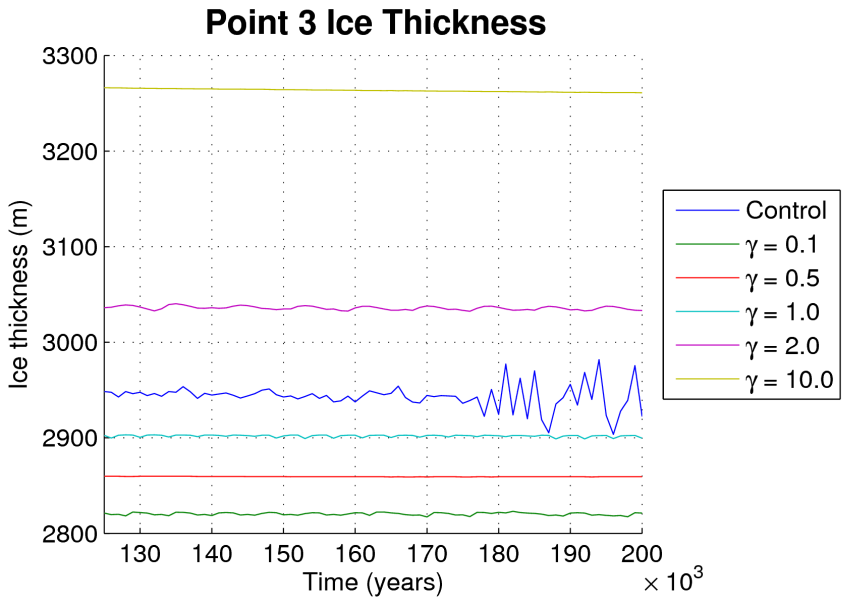

b Point 3 ice thickness

Figure 4.11 Point three is near the head of the trough. Variation in the frozen be pattern and the melt rate cause a regular pulsing behaviour. This is especially apparent for $\gamma = 2.0$. The control run is much more random and fluctuations suddenly increase at 180 ka.

Stage 3: Full coupling

The final stage of this experiment couples frictional heat flux to water pressure. The maximum coefficient of friction $\mu_{\max}$ is added to the experiment set-up. The parameter set used in this experiment becomes basal sliding adjustment parameter $\gamma \in \{0.1, 0.5, 1.0, 2.0, 10.0\}$ and maximum coefficient of friction $\mu_{\max} \in \{0.001, 0.005, 0.01, 0.05, 0.10, 0.5, 1.0\}$. The results resemble the Stage 2 more than the Stage 1 control run. In many cases the only discernible differences are in the time dimension. Introducing μ increases the variability in the run and makes the run more prone to instability.

Figure 4.13 maps the frozen bed for $\gamma \in \{0.1, 0.5, 10.0\} \times \mu_{\max} \in \{0.001, 0.01\}$. The gamma values are chosen to display a representative range of behavior. The model becomes unstable with larger values of $\mu_{\max}$ so two low, reliably stable, values are mapped. The symmetry of the system increases with both increasing γ and $\mu_{\max}$. Figure 4.12 plots the frozen area for all runs in Stage 3.

As in Stage 2, the system is more sensitive to changes when γ is small. This variability decreases as γ increases. To a lesser extent, the variability increases as $\mu_{\max}$ increases. The standard deviation of each variable after equilibrium is a good proxy for the variation at each point. Figure 4.14 maps the variation in frictional heat flux, basal melt rate, basal sliding speeds, and ice thickness. Although there are differences, the patterns shown are very similar. I therefore focus on just one variable: basal sliding velocities. This was one of the two variables used in Stages 1 and 2 so provides a good comparison. Figure 4.18 plots the sliding speed and ice thickness of Point 4 to show the increased variation of the run, compared to run F14 in Stage 2. Note that while, the Stage 3 runs show oscillation, it has a regular behaviour.

Figure 4.15 maps the velocity variation pattern of six runs. The variability decreases with both γ and $\mu_{\max}$. The nature of the variability is also apparent from these figures. Steep gradients in the surface usually imply flickering and shallower, smoother, gradients usually imply pulsing. The difference between what I have qualitatively called *flickering* (quick, random variation) and *pulsing* (slower, more regular variation) is seen in Figures 4.16 and 4.17. Figure 4.16 plots the variation of basal melt rate and frictional heat flux through time across a transect through the trough. Figure 4.17 plots the variation of frictional heat flux at 350 km (flickering) and 625 km (pulsing) across the transect. Note that in both figures

there is an initial pulse which lasts longer than subsequent pulses.

Runs with larger values of γ and $\mu_{\max}$ are more likely to be unstable. Figure 4.19 shows different modes of instability. The reasons for this are discussed in Section 4.4.4.

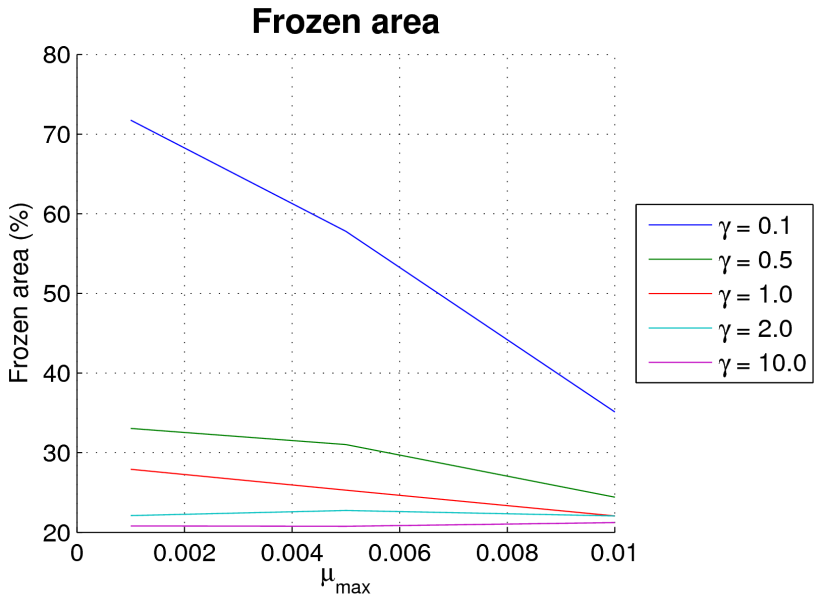

Figure 4.12 The total frozen area depends on γ and $\mu_{\max}$. This graph shows how the frozen area changes with $\mu_{\max}$ for different γ. Where the system responds quickly to velocity, small γ, there is a large dependence of the frozen area on the value of μ. As the response slows the exact values of $\mu_{\max}$ become less important. These data plot $\mu_{\max} \in \{0.001, 0.005, 0.01\}$.

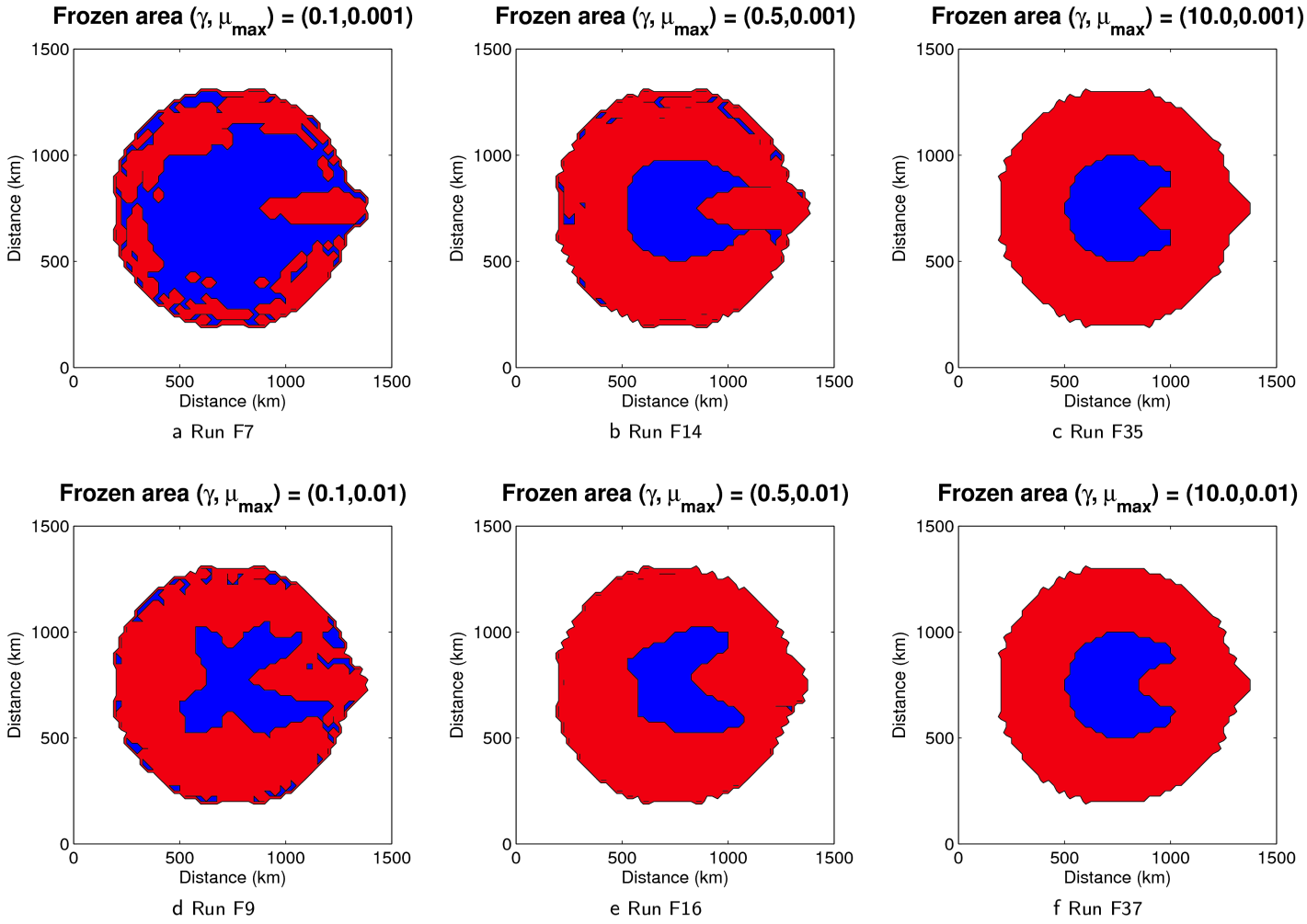

Figure 4.13 Stage 3 basal temperature showing the warm (red) and cold (blue) bed. Rows: Increasing basal sliding adjustment parameter γ. Columns: Increasing maximum friction $\mu_{\max}$. Stage 3 runs are more sensitive and variable than the Stage 2 runs because of the extra frictional feedbacks.

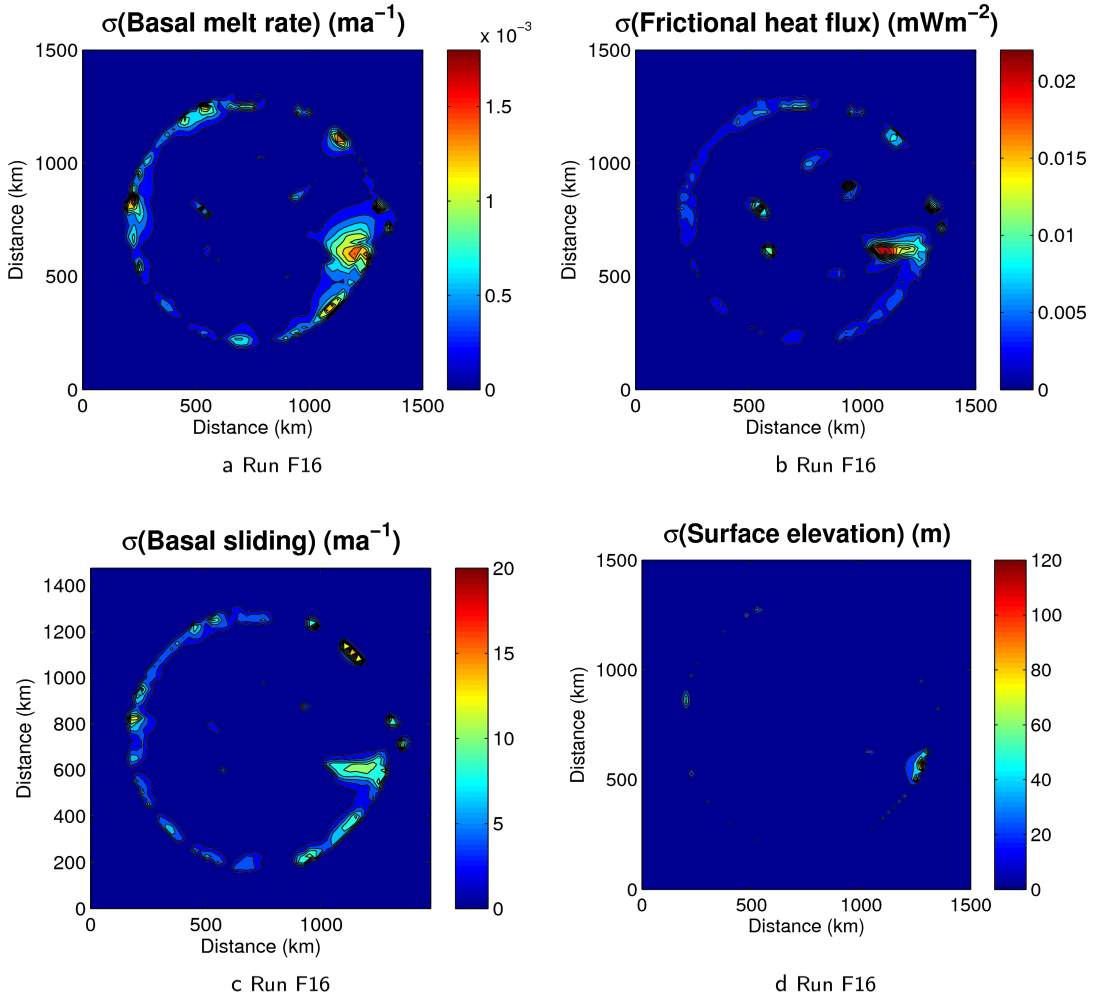

Figure 4.14 Stage 3 runs (full friction coupling) are more variable than Stage 2 (velocity coupling only), but less so than the Stage 1 control (EISMINT control). These maps plot the standard deviation of (a) basal melt rate, (b) frictional heat flux, (c) basal sliding, and (d) surface elevation. The variables of the coupling all continually adapt around each other, with the largest heat flux being at the edge of the trough fast flow feature because this balance moderate flow with increased grounding.

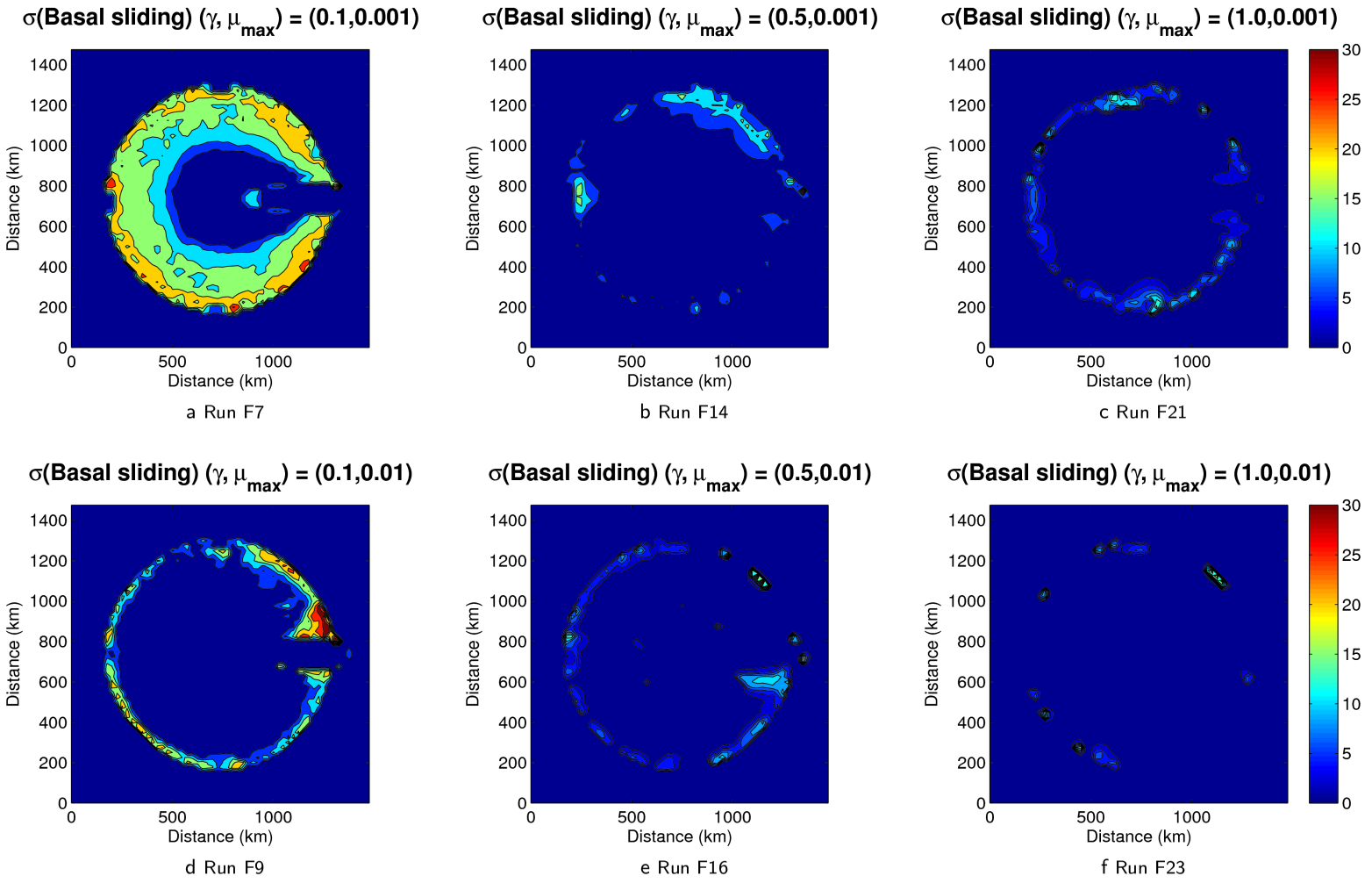

Figure 4.15 Stage 3 standard deviation of sliding velocity. Rows: Increasing basal sliding adjustment parameter γ. Columns: Increasing maximum friction $\mu_{\max}$. Stage 3 runs are more sensitive and variable than the Stage 2 runs because of the extra frictional feedbacks.

As the looseness of the system increases (increasing γ or $\mu_{\max}$) sliding slows down and the run becomes smoother, but this can lead to instability for the higher values (not shown).

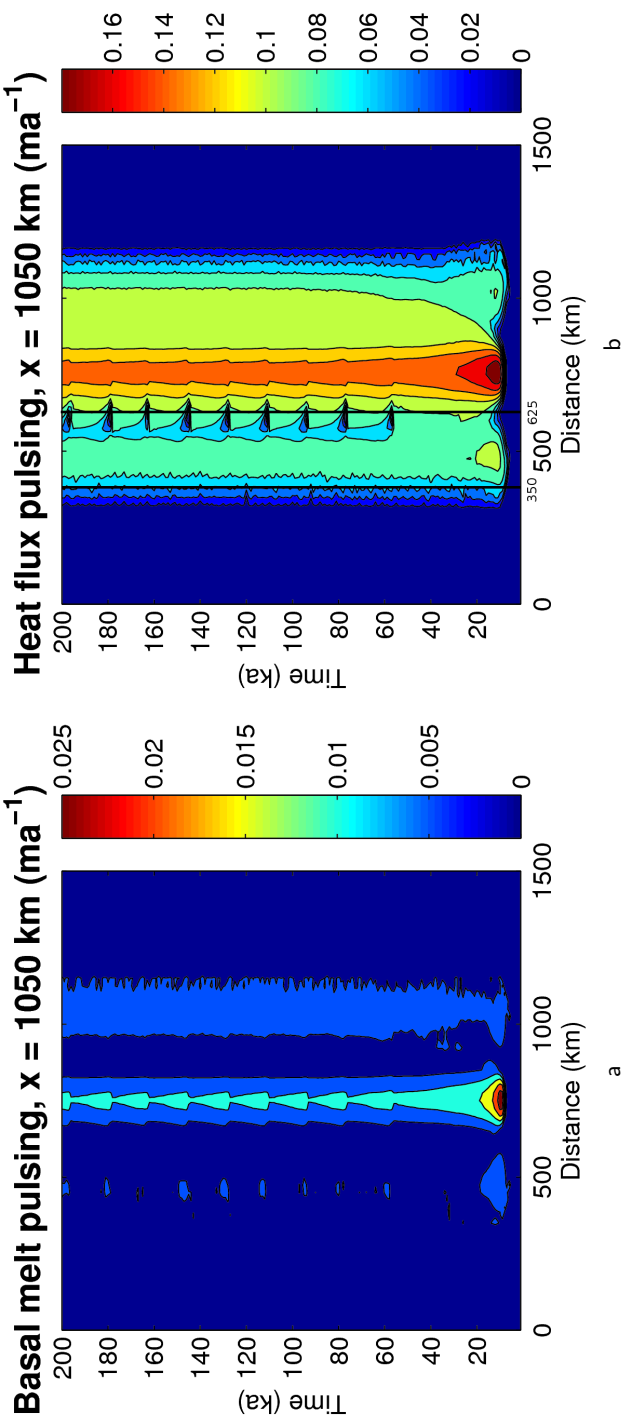

Figure 4.16 Stage 3: Transect through the trough showing the full 200 ka model run. (a) Basal melt rate in $\mathrm{mm\,a^{-1}}$ (b) Frictional heat flux in $\mathrm{W\,m^{-2}}$. The centre of the trough pulses as the coupled variables evolve around each other and periodically switch state. The edge of the trough, where frictional heat flux is largest, flicker where the variables continually adapt without apparent pattern. The variation of two points ($x = 350$ and $x = 626$) along the transect are plotted in Figure 4.17.

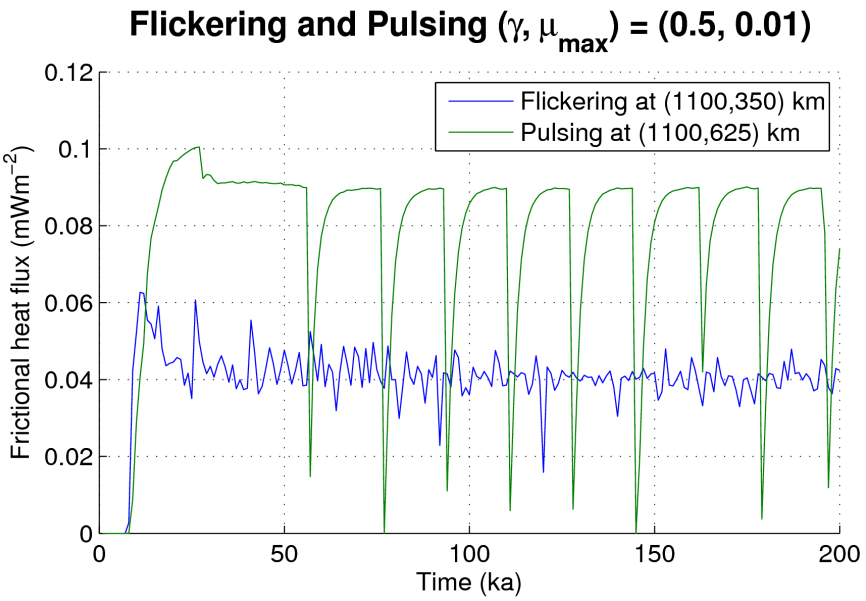

Figure 4.17 This plot shows the frictional heat flux at the two points marked on Figure 4.16: one is near the margin and the other just south of the trough. There is a clear difference between flickering at the margin and pulsing near the trough. Pulsing is regular and predictable while flickering values are more random. Flickering could be a result of sampling the solution every 1 ka if a pulse shorter than this is present. The larger and longer initial pulse is also noticeable.

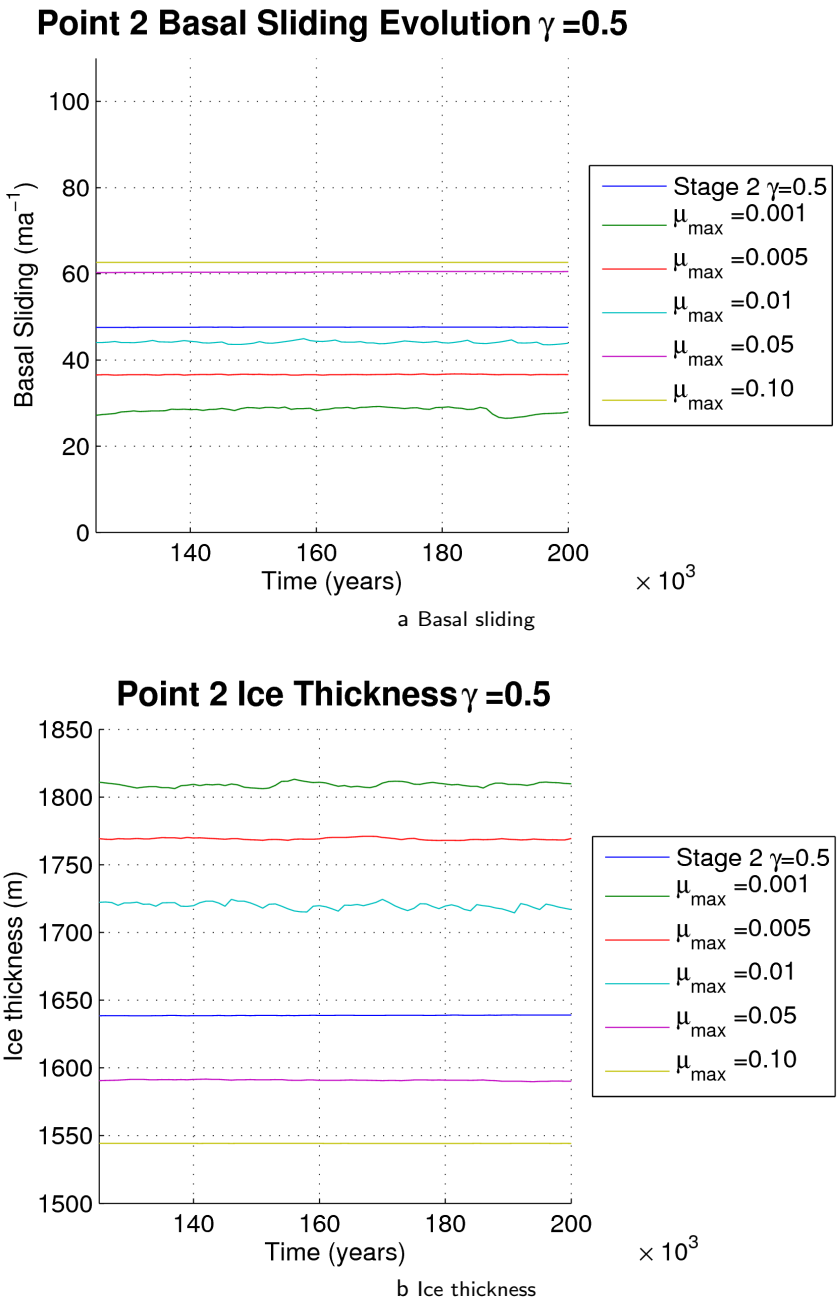

Figure 4.18 Basal sliding speed and ice thickness of runs F14–20 (Stage 3) at Point 2. Point 2 is away from the trough. The runs show more variability than Stage 2 but much less than the Stage 1 control. The inverse relationship between sliding velocity and ice thickness is apparent.

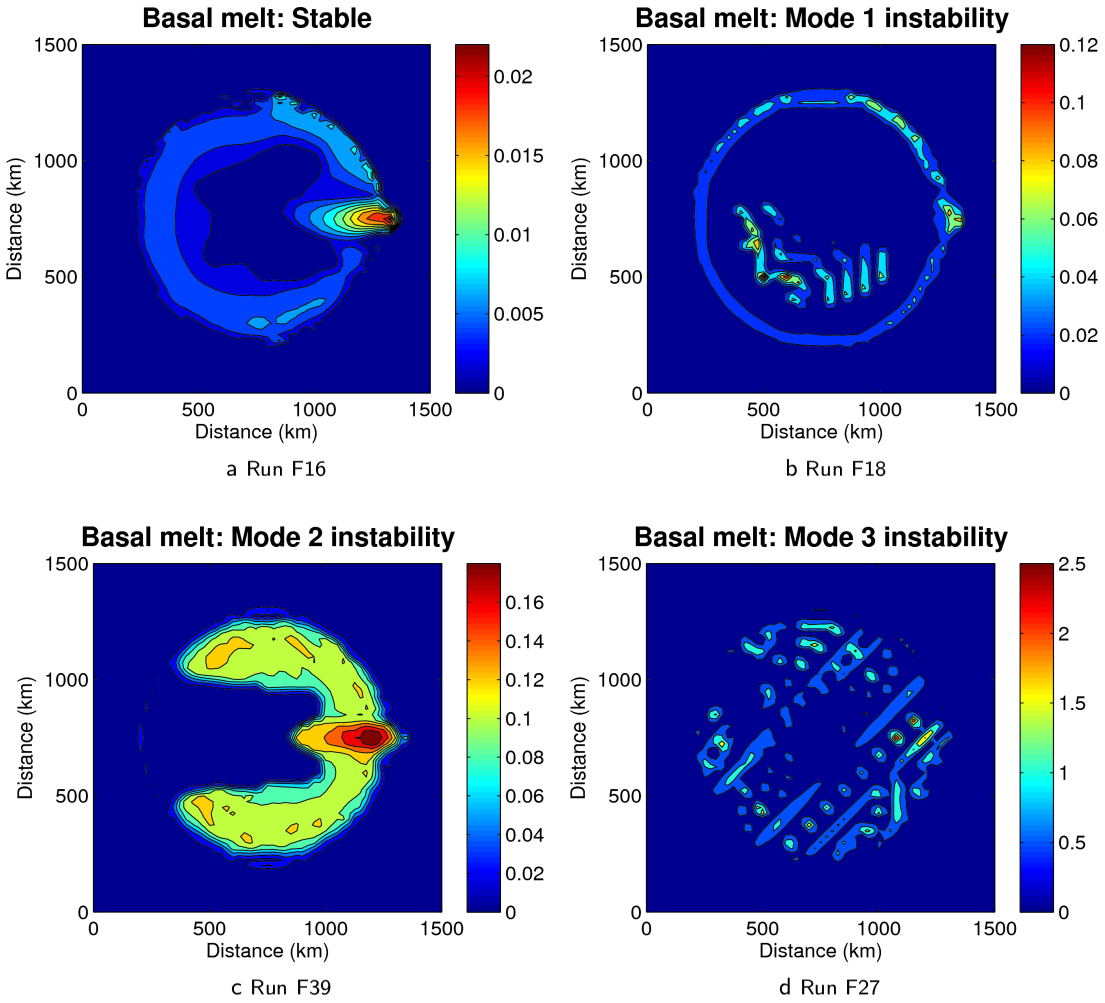

Figure 4.19 Stage 3: modes of instability. Coupling frictional heat flux, sliding, and effective pressure can make the system unstable if inappropriate values for the basal sliding adjustment parameter γ or maximum friction coefficient $\mu_{\max}$ are chosen: (a) stable run example basal melt rate, (b) localised numerical instability, (c) physically-based instability, (d) global numerical instability.

4.4.4 Discussion

I now discuss the possible reasons for the features and behaviour identified in Section 4.4.3. The discussion focuses on processes and combines elements from the three experimental stages as necessary. Broadly speaking, there are five general themes to this discussion: the stiffness of the system; basal temperatures, sliding, and ice thickness; symmetry and its implications; the interaction between the frictional feedback elements; and the stability of the runs.

Stiffness of the system

The stiffness of the system is a measure of how easily and quickly the system responds to a basal perturbation when effective pressure is high (the ice is mostly grounded). When high ice velocities are reached before sliding starts, instead of sliding starting gradually, I define this system as *stiff* and its opposite as *loose*. In my setup, the basal sliding adjustment parameter γ controls the stiffness and smaller values are stiffer (eg $\gamma = 0.1$ in Figure 2.3, Equation 2.15).

The EISMINT-2 control run (Stage 1), especially, is very stiff and this leads to the rough surface topography, basal ice temperature, and the *fingered* melt rate displayed in Figure 4.3. A similar, although not as extreme, situation is present with $\gamma = 0.1$ in Stages two (velocity coupling) and three (full coupling). To initiate sliding, sufficient energy needs to build up to overcome the resistance of the system. When this happens, the energy is released quickly and flow is often fast but cannot be sustained (Payne, 1995). For example, the minimum sliding speed in the interior of the ice sheet is approximately $50\,\mathrm{m\,a^{-1}}$ in Stage 1 and is approximately $30\,\mathrm{m\,a^{-1}}$ in Stage 2 ($\gamma = 0.1$). The resultant fluctuation of basal sliding is apparent in Figures 4.5 and 4.4; all the points oscillate and Point 1 alternates between sliding and not. This is a well-documented situation in ice sheet modelling (eg Hulton and Mineter, 2000; Payne and Baldwin, 2000; Bueler et al., 2005; Jamieson et al., 2008). Parametrising sliding so that it starts gradually reduces the problem. Jamieson et al. (2008) use basal melt rates for this; here, I use effective pressure from HYDRO coupled with the basal slipperiness adjustment parameter γ.

In the Stage 2 and 3 runs, increasing γ increases the looseness of the system. Figure 4.6 (Stage 2) shows the resultant increase in symmetry and resolution in fingering. The Stage 3

case is more complicated because of the extra feedbacks. Increasing both γ and the maximum coefficient of friction $\mu_{\max}$ reduces stiffness and makes the system more symmetric, Figures 4.13 and 4.12. The system appears to be more sensitive to γ than $\mu_{\max}$ because $\mu_{\max}$ only adjusts the scaling of the basal sliding and frictional heat generation whereas γ affects the shape of the function.

The reason for increasing maximum friction increasing the looseness is not necessarily obvious. By increasing the maximum friction, some may say intuitively that the system should become more resistant to flow and not less. The key process here is that $\mu_{\max}$ affects frictional heat generation which in turn affects effective pressure. When the ice begins to slide, basal melt rate increases quicker when $\mu_{\max}$ is larger and so the effective pressure falls which enables a stiff system, as defined by γ in Equation 2.15, to flow quicker than it would do otherwise. Because the system then finds it easier to slide, this makes the system looser overall.

Basal temperatures, sliding, and ice thickness

The stiffness of the system affects the shape and size of the warm bed. This section discusses the impact of this on large-scale ice dynamics. The discussion of the intricate details of the frictional heat coupling are left for later.

When the system is stiff, so the basal sliding adjustment parameter γ is small, fast-flow features (which I've called fingers for convenience) develop, as already discussed. This leads to two effects which are worth mentioning now because they affect both sliding velocity and surface elevation. One, the fingering restricts the divergence of water and this enables water pressures to build up quickly in regions sandwiched between frozen areas. This is especially noticeable in the southern-most finger of the effective pressure map in Figure 4.7d (Stage 2, velocity coupling only). The system is already primed, by being stiff, to flow quickly and this build up of pressure enhances that effect. However, by allowing water pressure to build this reduces basal melting when the full coupling is enabled. Two, sliding affects the ice thickness because of continuity. This lowers the ice surface where the ice is sliding. Because of this, runs which are stiff often have a much more irregular ice surface than looser runs. This is apparent in Figure 4.3 (Stage 1, control) and Figure 4.9 (Stage 2).

Figures 4.10 and 4.11 plot basal sliding speed and ice thickness for all Stage 2 runs and the Stage 1 control run at Points 2 (away from trough) and 3 (head of trough). The coupling

of sliding with effective pressure in Stage 2 significantly stabilises the system. The inverse relationship between sliding speed and ice thickness is also obvious. The full coupling at Stage 3 reduces stability again but the system is still much smoother than the control run (eg Point 2 in Figure 4.18).

Ice thickness affects the pressure melting point and so possibly may affect the resultant basal melt rate for a constant heat flux at the bed. Higher melt rates produce more water, which lowers effective pressure and causes more sliding, which lowers the ice surface. On top of this, the mass balance gradient across the ice in a system with faster sliding is lower so accumulation may also be affected. Combined, these may contribute somewhat to the fingered nature of the stiff runs. As the looseness increases the system becomes more symmetric and these feedbacks become less important. This is all theoretical, however, because in reality topography influences ice sheet significantly, as the presence of the trough demonstrates. However, it is unknown at the moment to what degree troughs are needed to initiate fast flow or to what degree fast-flowing ice can initiate troughs (eg Briner et al., 2008; Swift et al., 2008; Glasser and Ghiglione, 2009).

Symmetry

I now consider the increasing symmetry as the system loosens due to the basal sliding adjustment parameter γ or maximum friction coefficient $\mu_{\max}$ increasing.

Except for the trough in the topography, the equations and domain describing the idealised EISMINT ice sheet are radially symmetric. As demonstrated, in the original EISMINT definition this system is inherently unstable. Flow nucleates around any irregularity, for example the $\pm 1\,\mathrm{m}$ noise applied to the topography or, in its absence, the model grid.

By adding extra physics to the model, which we are reasonably sure actually describes the system at some level (eg Budd et al., 1979; Weertman, 1979), the system is made inherently more stable, resulting in a more symmetric simulation. Instead of fast-flow features adjacent to a cold bed (fingers) there are much larger areas of slower sliding ice which evacuate mass from the system. Indeed in the Stage 2 experiments, the slowest sliding speed is approximately $35\,\mathrm{m\,a^{-1}}$ when $\gamma = 0.1$ and approximately $0.005\,\mathrm{m\,a^{-1}}$ with $\gamma = 0.5$. In the EISMINT-2 control run (Stage 1) the minimum velocity is approximately $50\,\mathrm{m\,a^{-1}}$. The warm area increases proportionally.

A question then is, how representative of a real ice sheet is this? It is difficult to know

and the answer partly depends on the basal conditions of real ice sheets. Because of this, it is likely to vary from location to location, and through time, depending on many variables such as the bed rock or till underneath the ice, the ice thickness, and air temperature. For example a thin ice sheet may remain below pressure melting point everywhere, preserving the pre-glaciated landscape (eg Hall and Sugden, 1987).

Another related point is that even with the extra physics defining the subglacial boundary conditions, there is still a grid dependence in the model runs. Possibly, even, the grid dependence is more apparent because the hydrology smoothes out any irregularities in the bed which would have masked it (this hypothesis is not tested here). However, the hydrology and especially the sliding adjustment parameter γ acts as a buffer between the numerical grid and ice dynamics. While grid dependence is apparent in the calculated basal melt rates and effective pressures (Figure 4.7), it is less apparent in sliding velocity (Figure 4.8) and even less apparent in the ice thickness (Figure 4.9). This smoothness is partly due to the defined diffusive flow of water but also because the system does not have to build a head of steam before sliding can start, as already discussed.

Compensation between variables and switching states

The full frictional feedback mechanism (coupling effective pressure $\bar{N}$, sliding $\boldsymbol{v}_b$, frictional heat flux H_f, and basal melt water production M) introduces complex interactions. The four variables continually adjust their values around each other. This leads to an increase in the variation of these variables, compared to the Stage 2 runs. Figures 4.14 and 4.15 show this increased variability; compare these figures to the Stage 2 standard deviation maps in Figure 4.8. The standard deviation in Figure 4.15 is a similar order of magnitude to the control run (Stage 1) but, except for run F7, the area of high variation is less spatially extensive. Note however that, unlike the control run, the symmetrical shape of the ice sheet is retained.

The coupling between the variables can take a number of forms. One, the variables may be in a relatively stable quasi-equilibrium and therefore not show significant time dependence. Two, the variables may continually flicker and adapt around each other. Three, the variables may oscillate around each other in a more rhythmic manner while switching between two distinct states. Which one happens appears to depend, at least partly, on how stable the background hydraulic pressure profile (BHPP) is at a given location.

Where the bed is flat and there is no significant convergence or divergence of flow in the BHPP, the variables appear to mostly adapt mode one: the relatively stable quasi-equilibrium, Figure 4.18.

Where water converges in a major topographic feature, such as the trough, the values of the sliding adjustment parameter γ and the maximum coefficient of friction $\mu_{\max}$ become more important. When the system is stiff the model run has high variability and the sliding switches on and off so any regular interaction between the coupling variables is lost. If the system is very loose, then the model run is unstable because of physical and numerical instabilities. This is discussed in the next subsection. When the system is only slightly stiff (run F16, $\gamma = 0.1$, $\mu_{\max} = 0.01$) the variables pulsate regularly around each other (in this instance with a 10.4 ± 1.4 ka period, Figure 4.16). This is the system oscillating between the two conceptual end-member states — high friction, low velocity and high velocity, low friction. Given the physics defined in the model, it is reasonable to assume that this is a physical effect that may take place in real glaciers. It is in fact a similar situation to one of the proposed surge mechanisms in valley glaciers (eg Kamb et al., 1985; Kamb, 1987), although the time scales are very different. This pulsing has a noticeable impact on ice dynamics and if it is ignored, and it actually exists, it has the potential to confuse the interpretation of field data. Oscillatory behaviour is documented in ice sheet models and in field data; Payne (1995) reviews these studies.

The final mode of behaviour identified in the coupling is a fast flickering of the variables. This appears to occur at the margin of the convergent features in the BHPP. Here, effective pressures are higher than in the trough but still low enough to enable fast flow, compared to the non-trough topography, and therefore increased frictional heat flux. Due to this combination of variables, these areas are modelled to have the highest frictional heat flux generation in the domain[4]. This leads to the variables continually adapting around each other and so flickering. The 350 km transect in Figure 4.16 displays this behaviour. Figure 4.17 plots both flickering and pulsing to demonstrate the differences between them. Note that the pulsing is more or less predictable through time, but the range of values is much smaller.

An important point to remember is that GLIMMER uses the shallow ice approximation and so ignores longitudinal and other higher-order stresses. These higher-order terms become

[4] It is interesting to note that this increased frictional heating occurs around the same location (upper slopes of a valley) that geothermal heating is least significant because geothermal heat flow converges in valley bottoms (Van der Veen et al., 2007).

important when the glacier is decoupled from its bed, as the effective pressures are suggesting here. Therefore this analysis needs to be reconsidered when higher-order stresses are available. This problem does not invalidate the results, however, because the main elements of the coupling between the terms may be similar. The main differences may be that ice velocities will be affected by flow elsewhere.

4.5 Implications and Summary

This chapter demonstrates that coupling frictional heat generation to effective pressure as well as sliding has a strong influence on ice dynamics. Many current models calculate frictional heat from the product of basal shear stress and sliding velocity, but I suggest that this is incorrect physics which misses out on important feedback mechanisms. Glaciers often slide quickly because they are partially decoupled at the bed because of basal water (Weertman, 1979). The lubrication provided by this water not only allows faster sliding, but also reduces the effective friction at the bed. This chapter uses an equation for frictional heat flux that depends on the bulk-friction of the bed, at the model resolution, and a sliding response adjustment parameter γ. Both sliding and frictional heat generation are coupled to effective pressure through γ.

An important result is that by adding the frictional heat flux to the model, stiffness of the system is reduced and the simulation is less likely to show flow instabilities and develop streaming. Where a real ice sheet is on the stiffness–looseness spectrum is unknown and probably depends on the ice sheet and climate. Coupling water pressure only to sliding greatly enhances the looseness and therefore symmetry of the system. Basal melt rate is sometimes used as a reasonable proxy for this in other models (eg Jamieson, 2008). When the full mechanism is included, more variation is added to the system when compared to the velocity-only coupling. The system, depending on choice of coupling parameter, is still much less stiff than in the standard Eismint experiments.

The full coupling increases variability of sliding velocity, ice thickness, basal melt rate and the other related variables because they have to continually adapt around each other. Where water converged in the trough, effective pressure is low and as a result so is frictional heat generation. This leads to a pulsing behaviour in the trough and flickering at its margin. If this sort of behaviour is present in real ice sheets then it has a number of implications. Let

us temporarily assume, whether correctly or not, that this effect is real. In that case, where pulsing exists the system may never be in equilibrium. To an observer it may always appear that the system is losing or gaining mass for reasons that are non immediately obvious. This situation is similar to the suspected causes of glacier surging (eg Kamb et al., 1985; Kamb, 1987) and may indeed by partially due to the same mechanism although the times scales are very different. Oscillatory behaviour is common in ice sheet modelling and there is evidence from ice and deep-sea cores that real ice sheets may oscillate between states (Payne, 1995). I am not claiming that the effects described in this chapter are a cause of this, but simply demonstrating that oscillatory behaviour is a possible state of the system when frictional heat is coupled to hydrology.

The highest frictional heat fluxes are at the edge of fast flow features instead of the middle. This may subtly change the distribution of water in the background hydraulic pressure profile.

Chapter 5

Dynamic Response to Draining Surface Ponds

> "[T]he velocity of comparatively slow-moving ice increased just after the seasonal onset of drainage of surface melt into the ice sheet [...] Much uncertainty remains, especially related to whether fast-moving glaciers and ice streams are similarly affected."
>
> —*Fourth IPCC Assessment Report 2007, §4.6.3.3*

This thesis has so far only considered basal processes for perturbing basal motion. However, recent studies (eg Zwally et al., 2002; McMillan et al., 2007; Das et al., 2008; Shepherd et al., 2009; Bartholomew et al., 2010) demonstrate that there is an important link between surface and basal hydrology across the Greenland ice sheet. The resulting dynamic feedback, due to seasonal and diurnal effective pressure variation, may increase the sensitivity of the Greenland ice sheet to future climate (Parizek and Alley, 2004). It may also counter any increased accumulation due to a wetter climate, thereby increasing sea-level rise predictions (Shepherd et al., 2009). This study is one of the first to capture the dynamic response of the Greenland ice sheet to a surface melt signal using a basal hydrology model.

Surface ponds appear to be a key component in the link between surface climate and basal boundary conditions. Various studies have observed supraglacial lakes draining in a matter of hours though moulins (eg Box and Ski, 2007; Das et al., 2008), Figure 5.1. Theoretical work suggests that a fracture can only propagate through thick, cold ice if there is sufficient water available to fill the fracture up to the ice surface (Weertman, 1973; Alley et al., 2005b;

Van der Veen, 2007). Once the link is established, the dynamics and surface melt appear to remain coupled for the remainder of the melt season (Shepherd et al., 2009).

This chapter reviews Greenland's climate, surface hydrology and observed seasonal speedup in Section 5.1. Theoretical and observed mechanisms for coupling ice dynamics to surface hydrology, such as hydrofracture, are reviewed in Section 5.2. Section 5.3 reviews current modelling in this field. The ponding and coupling algorithm used with HYDRO is introduced in Section 5.4. This is used for the experiments in Section 5.5 investigating the nature and implications of the dynamic response.

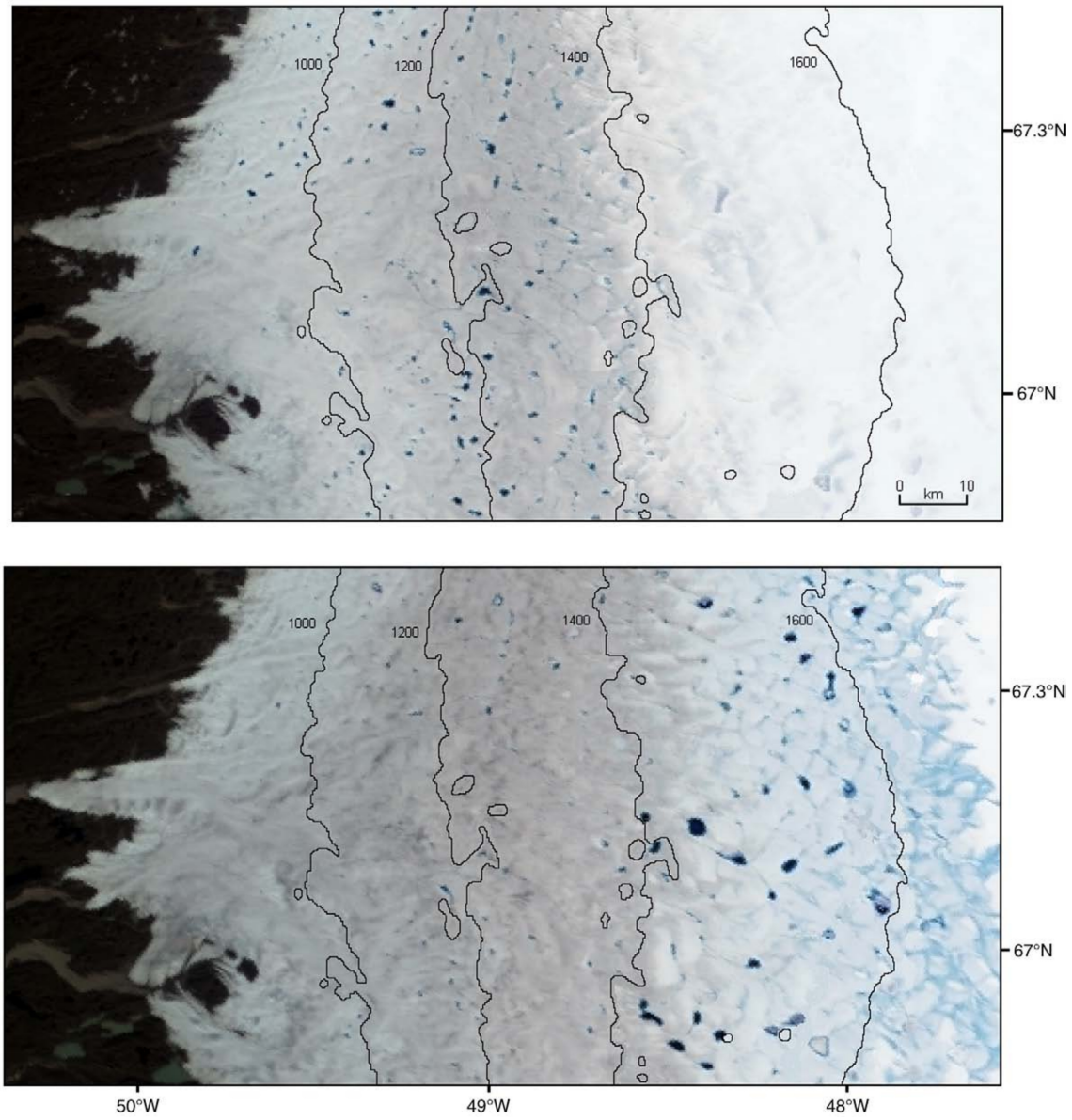

Figure 5.1 Large seasonal lakes form on the surface of the Greenland ice sheet every year. This figure from Sundal et al. (2009) shows two MODIS true-colour images, with surface contours, from day 162 (top) and 199 (bottom) of 2003. Key observations are: lakes form earlier at lower elevations; many of these lakes have drained by day 199 but new, higher lakes have formed; and higher lakes are larger than lower lakes.

5.1 Surface hydrology overview

Seasonal surface ponds form in Greenland's ablation zone every summer and appear to have an impact on the ice dynamics (eg McMillan et al., 2007; Shepherd et al., 2009). This section focuses on the observations of those lakes and the dynamic response. The discussion of how the two systems connect is left for Section 5.2.

5.1.1 Surface ponds

Ponds appear to be a key component in forming a link between the surface and basal systems. Before looking at this link in Section 5.2, it is useful to understand the ponds' physical characteristics. This section focuses on the Greenland-wide distribution and individual properties of ponds. I also discuss their typical evolution as well as the effect they have on the ice surface.

Pond characteristics

Ponds can form anywhere on Greenland's surface which experiences melt; they are concentrated on the western margin, with the majority south of 70 °N (Lüthje et al., 2006). They are relatively less abundant in the south-east, possibly due to steeper surface gradients (Sundal et al., 2009). Surface slope, latitude and altitude appear to be important factors controlling lake distribution. Sundal et al. (2009) find a high negative correlation between surface slope and the likelihood of ponds. Ponds in steeper areas are fewer and are usually smaller. This could be due to the lack of surface back slopes creating dips in the surface (Nienow and Hubbard, 2005) or it could be that faster, warmer ice[1] results in more crevasses through which water drains without ponding (Sundal et al., 2009). McMillan et al. (2007), studying the Swiss Camp area on the western flank of Greenland, observe on 7$^{\text{th}}$ July 2001 that 95% of all lakes are above 750 m, supporting the negative correlation. Sundal et al. (2009) observe lakes up to 1200 m in the north and 1700 m at their south-western study area.

Ponds often form in the same dips in subsequent years (Sneed and Hamilton, 2007; Catania et al., 2008), showing that surface topography is important in their formation. Surface drainage, and drainage outlets, are also important in pond formation (Lüthje et al., 2006; Sundal et al., 2009). Some, but not all, lakes have drainage outlets (Box and Ski, 2007);

[1] Lower, and therefore warmer, ice is often faster due to steeper surface gradients nearer the margin.

Figure 5.2 shows a ASTER image of a surface channel connecting two lakes. This shows that surface flow occurs but, in this example, does not travel far.

Lakes typically cover less than 1% of the ablation zone (Lüthje et al., 2006). Sundal et al. (2009) find 0.68%, 0.81%, and 0.58% coverage at their south-western, north-western, and north-eastern field sites respectively. Box and Ski (2007) report a coverage of 2.7% for their field site and an average lakes area of $3.4 \pm 2.3\,\mathrm{km}^2$.

Typical pond depths and volumes remain statistically unresolved (Box and Ski, 2007), but methods to resolve them remotely are becoming available (Georgiou et al., 2009). Surface ponds are typically shallow. For the western margin of Greenland: McMillan et al. (2007) calculate an average depth of $3.9 \pm 1.1\,\mathrm{m}$; Box and Ski (2007) find an average depth of 4.1 m and a maximum of 12.2 m; and Sneed and Hamilton (2007) find lakes between 1 m and 20 m in crevasses. McMillan et al. (2007) estimate lake volumes by combining degree day modelling with meteorological data. They find a maximum volume of $157 \pm 42 \times 10^6\,\mathrm{m}^3$. Box and Ski (2007) report that most lakes have volumes in the range $1\text{–}100 \times 10^6\,\mathrm{m}^3$, with a mean of $14.3 \pm 8.4 \times 10^6\,\mathrm{m}^3$.

Modelling by Lüthje et al. (2006) suggests that lake areas are predominantly determined by topography and therefore increased warming should not affect the overall area of individual lakes.

Local effects

Supraglacial lakes alter the surface conditions of ice sheets. They lower the surface albedo by reducing scattering and reflectance (Box and Ski, 2007). Box and Ski suggest that this results

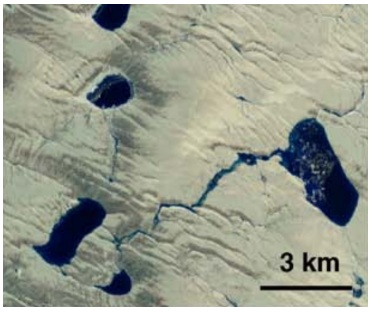

Figure 5.2 ASTER image showing lakes on Greenland's surface, from Sundal et al. (2009). There is drainage between lakes and, in this case, water travels less than 10 km. 10 km is the resolution of the model runs in this chapter.

in a positive feedback mechanism which raises lakes temperatures and therefore expands the lake area. This contrasts with Lüthje et al.'s (2006) modelling study which did not take this feedback into account. Modelling work also suggests that lakes increase the ablation of the ice surface at the their bed by between 110–170% (Lüthje et al., 2006). Lakes result in warmer ice through the winter and spring by keeping their bed at melting point until the entire lake is frozen. This makes it easier for hydrofracturing to occur in subsequent years[2] (Alley et al., 2005b).

Pond evolution

Surface ponds evolve throughout the melt season. The general pattern is that lakes form during the melt season, increase in size and then many of them drain. Figures 5.1 and 5.3, from Sundal et al. (2009) and McMillan et al. (2007), show this sequence of events.

The onset of pond formation varies annually and there appears to be little correlation between early onset at different locations (Sundal et al., 2009). McMillan et al. (2007) find that, around Swiss Camp at approximately 1200 m in western Greenland, lakes mainly form in May and June, peaking at the end of June. On average, the north appears to reach its maximum lake area two to three weeks after the south (Sundal et al., 2009). Lakes primarily drain late in the season, but can drain at any time (McMillan et al., 2007). Maximum lake area, volume, and depth do not always coincide (Box and Ski, 2007; Sundal et al., 2009). Sundal et al. (2009) find that in their three field sites approximately a third of lakes drain before maximum lake area is reached. This implies that lakes can form and drain simultaneously. McMillan et al. (2007) also observe lakes filling and draining at the same time.

There is a clear correlation between surface elevation and lake formation. Lakes at higher elevations form and drain later (Sundal et al., 2009); this is clearly seen in Figure 5.1. McMillan et al. (2007) find that 95% of lakes in their study area are above 750 m on 7th July and above 880 m on 1st August 2001 respectively.

Lake drainage can be rapid. Box and Ski (2007) observe the complete draining of lakes within a day (average flux $31.5 \times 10^6\,m^3\,s^{-1}$) using daily MODIS repeat images while Das et al. (2008) report a lake draining within two hours (average flux $8700\,m^3\,s^{-1}$). McMillan et al. (2007) calculate an average draining flux of $1.3 \pm 0.3\,m^3\,s^{-1}$ for the lakes in their study

[2] Hydrofracturing is discussed in Section 5.2.1.

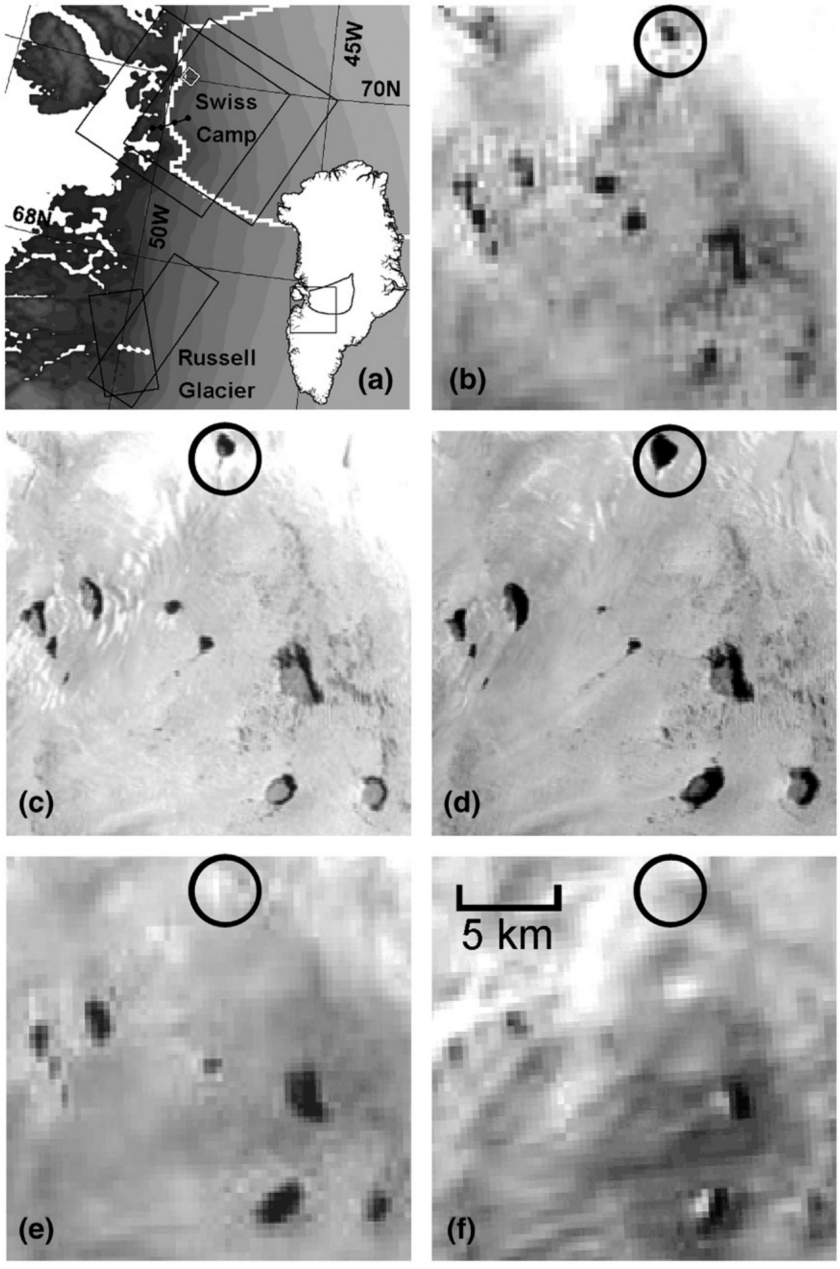

Figure 5.3 This figure from McMillan et al. (2007) shows the evolution of a surface lake at Swiss Camp in 2001 using Landsat images. The circled lake is at approximately 1100 m. It grows in size from (b) 30th June to (d) 1st August. By (e) 8th August the lake has drained. In (d) the lake has an area of 0.69 km^2.

area. Once drained, the connection with the surface can remain open for the remainder of the melt season (Shepherd et al., 2009), enabling subsequent surface melt to quickly reach the bed.

5.1.2 Dynamic response

Draining lakes appear to cause a dynamic response in ice velocity (Zwally et al., 2002; Das et al., 2008; Shepherd et al., 2009). This is the process that this chapter models. Here, I overview field-work studying this dynamic behaviour.

Seasonal signals

Seasonal speedup of glacial velocities have been studied for over a century for Alpine glaciers and over two decades on the Greenland ice sheet (Andreasen, 1985a). Krabill et al. (1999) identify dynamics as the cause for thinning, in excess of ablation rates, on the margin of the ice sheet. This may offset the increased accumulation expected as part of a warmer and wetter climate (Shepherd and Wingham, 2007). Recent studies on the seasonal evolution of ice velocities and hydrological efficiency (Joughin et al., 2008; Van de Wal et al., 2008; Shepherd et al., 2009) show parallels with the established behaviour of Alpine and polythermal valley glaciers (eg Nienow et al., 2005; Bingham et al., 2008). Not all glaciers, however, show a seasonal response; Echelmeyer and Harrison (1990) observe that Jakobshavn Isbræ does not increase its velocity in the summer.

The question of where and why a dynamic response is present is as important as what that response is. I will discuss the former question first. Sole et al. (2008) take Krabill et al.'s (1999) work further by identifying areas either where dynamic or ablation based thinning dominate. They find that, in general, marine-terminating outlet glaciers thin dynamically and that land-terminating glaciers thin due to their mass balance. Jakobshavn Isbræ thins dynamically and this effect reaches up to 120 km inland while Kangerdlugssuaq's and Helheim's dynamic thinning are observed 100 and 95 km inland respectively (Pritchard et al., 2009). Jakobshavn Isbræ's velocity has increased recently and a possible reason for this could be a lack of buttressing as opposed to increased lubrication at the bed (Joughin et al., 2004b) or that the glacier is changing its flow regime and beginning to show a seasonal signal (Luckman and Murray, 2005).

Dynamic response to surface melting is observed on two timescales: seasonal and diurnal. Often, diurnal speedups are also associated with an uplift of the glacier surface, indicating high water pressures. Andreasen (1985a) investigates diurnal velocity variations in western Greenland using a network of stakes for measurements. Horizontal velocity and uplift data correlate well but Andreasen interprets the data as instrumental error due to diurnal changes in atmospheric refraction, not as an actual speedup. This could be due to the accepted belief at the time that water could not penetrate through thick, cold ice (Hodgkins, 1997). Modern techniques, such as GPS measurements and interferometric velocity maps, remove the complication of dealing with atmospheric refraction.

Because of the perceived lack of accuracy of daily data, the next survey was conducted using a 10 day interval. This survey shows a definite response in seasonal velocity change (Andreasen, 1985b). Maximum uplift correlates well with maximum velocity but again this was interpreted as coincidence. Andreasen (1985b) concludes that only changes in basal hydrology, resulting in increased sliding, can explain his results in the ablation zone. One mechanism he proposes is a frozen margin early in the season, which stops water escaping, resulting in back pressure reaching the upper parts of the ablation zone.

In south-east Greenland, Howat et al. (2008) find an average speedup of 10% in summer for 32 outlet glaciers, using a combination of radar interferometry and speckle tracking. Looking at Kangerdlugssuaq and Helheim, Howat et al. (2007) find that large variations in seasonal velocity are possible in subsequent years. The two outlet glaciers doubled their mass loss in less then one year in 2004, before returning to previous rates in 2006. They suggest that this could be due to changes in back-pressure from ice buttressing.

On the west coast, Zwally et al. (2002) show a seasonal velocity increase and uplift near the ELA at Swiss Camp (1200 m elevation) using GPS. Their results span a four-year period and years with higher melt show higher velocities. Joughin et al. (2008) also look at the western margin of Greenland, but they use a combination of interferometry and GPS measurements. They observe a 50 to 100% speedup of areas moving slower than $150\,\mathrm{m\,a^{-1}}$ but only a 15% speedup of the outlet glaciers, defined as flowing faster than $150\,\mathrm{m\,a^{-1}}$. They note that frequent GPS measurements give higher, but shorter lived, speedups than the RADARSAT satellites, due to the satellites' 24 day repeat period.

Diurnal signals

Diurnal speedups are observed by at least three groups. This implies that a rapid connection exists between the surface and the bed in a manner analogous to Alpine glaciers.

Das et al. (2008) investigate the evolution of two supraglacial lakes larger than 2 km in diameter. Using GPS, they report uplift and increases in surface velocity upon the draining of a lake. This motion response is short-lived and velocities return to background levels within 24 hours, suggesting an efficient network of subglacial channels developing rapidly at the bed. The ice through which the water drained was 980 m thick and subfreezing.

Van de Wal et al. (2008) study the seasonal evolution of Russell Glacier on the western flank of the Greenland ice sheet, near the settlement of Kangerdlugssuaq. They use a series of GPS receivers and ablation monitors to obtain both multi-year and daily data sets. Their interannual data shows a seasonal signal, but does not correlate with annual ablation. They note a decrease in annual velocities, with associated reduction in total water pressure and ice motion, in some regions near the margin in response to extra melt. This could be the result of the rapid formation of an efficient drainage network. Further inland, annual ice velocities are more constant.

Van de Wal et al. (2008) argue that this shows that the dynamic positive feedback associated with increased melting may not be as important as believed. More interestingly, their daily data correlates very well with daily ablation rates. They find a response in ice velocities up to 30% over the winter rate. Velocities start to increase at the onset of the melt season in early May; Van de Wal et al. imply that this is before lakes start draining and therefore an alternate, unnamed, mechanism causes the speedup. This could simply be water reaching the bed through thinner, warmer and therefore potentially heavily-crevassed ice, but they do not specify. On top of the variation linked directly to ablation rates, they also have unpredictable speedups later in the season which are interpreted as draining lakes.

Shepherd et al. (2009) report similar findings, but in their case the strong diurnal link with ablation appears only after the lakes begin draining; they still find a gradual increase of velocity at the start of the melt season. Their study uses GPS measurements along the same flow-line transect used by Van de Wal et al. (2008). Figure 5.4 shows Shepherd et al.'s (2009) key result. They observe a seasonal speed up of 55–60%, depending on instrumentation, over the winter average. Maximum velocities are near the margin and there is a gradual

decrease in velocity over the summer, suggesting the drainage becomes efficient. Where the ice thickness is 1000 m, surface melt peaks on a diurnal basis two hours before maximum velocity diurnally. Crucially, the diurnal velocity change is independent of episodic lake drainage. This implies that once a connection forms, it remains open for the remainder of the melt season.

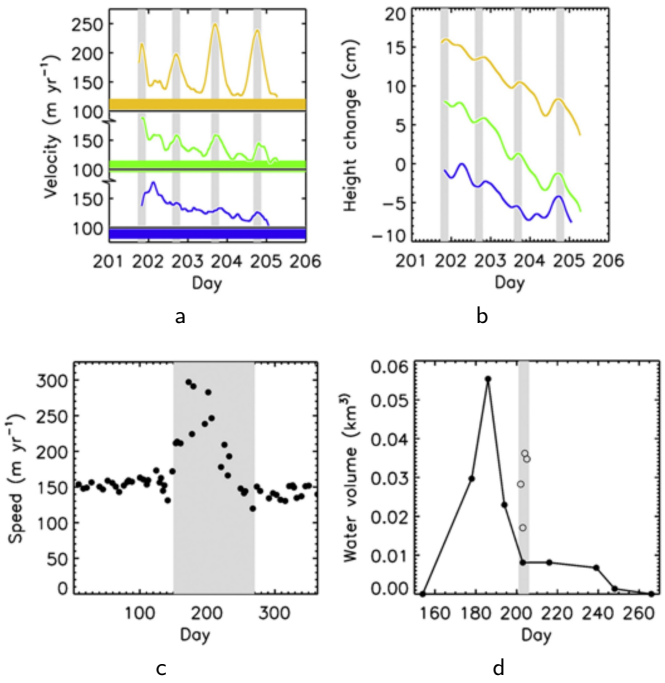

Figure 5.4 Both seasonal and diurnal speedups are observed at three locations on the Russell Glacier, western Greenland (Shepherd et al., 2009). (a) diurnal speedup over the 2006 winter-average velocities (thick lines), (b) corresponding vertical height change, (c) overall seasonal speedup, (d) water volume in supraglacial lakes.

Note that speedup is associated with an increase in surface elevation, implying high water pressure at the bed in response to daily surface melt. The nature of the diurnal response changes further from the margin (blue lines). As lake volumes decrease, the associated uplift also decreases due to the formation of efficient subglacial drainage networks.

5.2 Connection mechanism

A discussion of supra and subglacial hydrological coupling is not complete without considering the nature of the connection between the two systems. This section reviews the theory and field observations of *hydrofracturing* and other possible mechanisms explaining the apparent link between surface melt and ice motion.

5.2.1 Theory

There are three proposed mechanisms for the observed dynamic response to surface melt. Water may reach the bed through hydrofracture (eg Zwally et al., 2002), hydraulic back pressure may provide the extra water (Andreasen, 1985b), or the effect may be due to longitudinal stresses from coupling closer to the margin (Price et al., 2008; Nick et al., 2009).

Hydrofracture is the propagation of a water-filled crevasse due to the stresses at the tip of the crevasse overcoming the deviatoric stresses in the ice. It was first proposed as a possible mechanism by Weertman (1973) for lone crevasses. The theory is extended to crevasse fields by de Q. Robin (1974) and Weertman (1974). The theory is based on the fact that the pressure difference at the tip of a water-filled crevasse is always equal to $(\rho_w - \rho_i)gd_c$, where ρ_w and ρ_i are the densities of water and ice; g is the acceleration due to gravity; and d_c is the crevasse depth (de Q. Robin, 1974). This means that, as long as the crevasse remains water-filled, the pressure difference increases with depth and so the fracture propagates downwards.

Whether this mechanism can work for thick ($> 1000\,\mathrm{m}$), subfreezing ice, as implied by Zwally et al. (2002), has been a matter of debate (eg Price et al., 2008). Echelmeyer and Harrison (1990) comment

> it appears that surface melt water can penetrate to the bed [...] even when the ice is cold at the surface.

Understanding this is key to incorporating the observed dynamic response of Greenland into models. Modelling and field observations are both important for resolving this issue. Section 5.2.2 deals with modelling and Section 5.2.4 with observations supporting hydrofracture.

5.2.2 Hydrofracture connection mechanism

Van der Veen (1998) uses linear elastic fracture mechanics[3] (LEFM), applied to idealised water-filled cracks in ice, to show that Weertman (1973) underestimates the potential for crevasses to reach the bed by a factor of two, thereby making penetration to the bed more likely. This method helps determine key controls (water-filling rate) on final fracture depth and penetration time. Van der Veen (2007) finds that the time taken for the fracture to propagate is independent of the tensile stress in the ice. Tensile stress, however, appears to be important in fracture nucleation (Boon and Sharp, 2003).

Alley et al. (2005b) apply an established magma-filled rock fracture model to the same problem. They calculate the time and potential for water-filled cracks to penetrate thick

[3] Linear elastic fracture mechanics (LEFM) was first proposed by Griffith (1921). It is a method of dealing with the, theoretically, infinite stresses at the tip of an ideal linear crack, in an elastic material, using principles from thermodynamics.

subfreezing ice. This model uses many unconstrained variables, so Alley et al. do not have faith in individual results, but the overall result that crevasses can penetrate to the bed of an ice sheet if filled with water throughout appears consistent.

Both Alley et al. (2005b) and Van der Veen (2007) find that water-filled fractures can potentially reach the bed through thick, subfreezing ice. Both studies emphasize that the crack must remain water-filled throughout. Practically, they point out, this means having a large water reservoir such as a lake. Lakes also increase the likelihood of fracture initiation by keeping the ice warmer throughout the winter, due to the energy it takes to freeze an undrained lake (Alley et al., 2005b).

5.2.3 Other possible connection mechanisms

Two other possible explanations may explain the observed seasonal speedup without relying on passing water through cold, thick ice.

Andreasen (1985b) suggests hydraulic back pressure may account for the observed speedup. His suggested mechanism is that a frozen margin early in the season means that water entering the basal system near the margin cannot escape, so that back pressure builds. This increases ice velocity inland but cannot explain observed diurnal velocity changes. This suggestion was made at a time when hydrofracturing through subfreezing, thick ice was deemed impossible. We now know it is possible, but back pressure may is still worth investigating.

Longitudinal coupling may also cause the observed dynamic response of inland ice without requiring hydrofracture. Nick et al. (2009) model the Helheim glacier with both longitudinal coupling and enhanced melt in turn. They find that outlet glaciers are very sensitive to perturbations at their terminus. For land-terminating ice, Price et al. (2008) argue that near the Greenland margin there is plenty of heavily crevassed, thinner ice where water can more easily reach the bed. They use model results to show that a strong diurnal signal 12 km downstream, where ice is 800 m thick, can account for the weak diurnal acceleration observed by Zwally et al. (2002) though longitudinal stresses. Shepherd et al. (2009) counter this by pointing out that both their data and Zwally et al.'s show uplift of the ice surface during maximum velocity. This implies high basal water pressures. If the response was through longitudinal coupling, a thinning would be expected due to continuity. Indeed, Bartholomew et al. (2010) find that, on the land-terminating Russel Glacier, western Greenland, the

highest surface velocities correspond with the largest uplift and, conversely, when the surface is lowering or stable the surface velocity drops. This suggests that longitudinal coupling is not a primary mechanism.

5.2.4 Observations

Theory suggests that supraglacial lakes are required for water to reach the bed of the Greenland ice sheet through hydrofracturing where ice is thick and cold. Field observations also support this key conclusion. A number of field studies find evidence, both directly and indirectly, of fractures in glacial ice.

Fractures are observed in the field. Boon and Sharp (2003) document the draining of a supraglacier lake after two failed attempts on John Evans Glacier, Ellesmere Island. During the draining event, they hear loud cracking noises which they interpret as fractures opening. They also find evidence of moulins at the bottom of drained surface lakes. Their work suggests that the increase in velocity, associated with the extra water at the bed, is important in maintaining the tensile stresses needed to keep the connection open once hydrofracture is complete.

Fountain et al. (2005) also observe fractures using bore-hole video in Storglaciären, Sweden. Figure 5.5 shows one of their video frames. Their key result is that fractures are the dominant pathway for water to reach the bed of Storglaciären, although their study completely ignores the presence of moulins which are known to be a primary pathway in Alpine glaciers (Nienow and Hubbard, 2005). Fountain et al. (2005) do not observe any evidence of englacial conduits, which have been suggested as an alternate mechanism for water transport inside a glacier without the water reaching the bed (Hooke, 1989).

On Greenland, Das et al. (2008) observe open fractures in 980 m thick ice. These were in known lake locations and a number were actively receiving meltwater. Crucially, they also observe one lake draining in under two hours following hydrofracturing with the subsequent creation of a new moulin. There was increased seismicity half an hour before rapid drainage commenced; Das et al. (2008) tentatively link this to fracture propagation. Catania et al. (2008) also find evidence of lakes draining through moulins using ground-penetrating radar. Their survey was conducted in the vicinity of Swiss Camp and ranged in altitude from approximately 900 to 1400 m in a region where the equilibrium line altitude, ELA, is 1200 m.

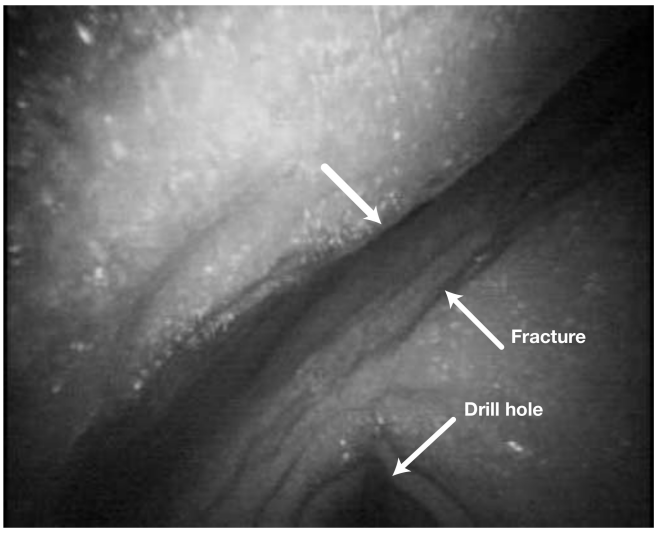

Figure 5.5 Deviatoric stresses at the tip of a water-filled fracture can quickly propagate the fracture through ice. This video still from Fountain et al. (2005) shows an englacial water-filled fracture in Storglaciären, Sweden.

They find numerous water-filled moulins below the ELA. These are loosely correlated with surface lakes and most surface lakes, in their results, are not associated with moulins. The radar survey is sparse compared to its area, but there is correlation between moulin location and bedrock ridges. This suggests that tensile stresses are important in the nucleation of fractures, even in thick ice. An interesting result is that they find no evidence of moulins above the ELA despite the presence of large surface lakes which are known to drain.

5.2.5 Success rate

Hydrofracturing is not always successful. Both theory and observations support this. Weertman (1973) demonstrates that a downward propagating crevasse can pinch off, closing the connection to the surface.

Refrozen water-filled crevasses are commonly observed. Blue-ice bands from refrozen meltwater in icebergs and calving fronts are common (Alley et al., 2005b); Figure 5.6 shows an example from Bamber et al. (2007). Catania et al. (2008) also observe blue-ice surface bumps which they interpret to be refrozen moulins. These observations show that water entering moulins does not necessarily reach the bed. A possible explanation could be that there is not sufficient energy in the water entering the ice to maintain the thermal conditions needed for hydrofracture, or if hydrofracture is successful to maintain the connection (Boon

and Sharp, 2003). Water naturally freezes at the end of the melt season, but if the connection was still open any water entering the moulin would presumably fall all the way to the bed without freezing.

Failed fracture propagation may make subsequent fracture propagation easier. Boon and Sharp (2003) discuss the establishment of the initial connection between the surface and the bed on John Evans Glacier, Ellesmere Island, Canada. They observe two partial drainage events of a lake before a third full drainage event. The third event results in increased surface velocities while the previous events do not. They suggest that the initial events may have warmed the ice to enable the third to succeed. Once the dynamic response begins, the increased longitudinal stresses and frictional heat from meltwater pouring through the moulin help prevent the connection from closing.

As mentioned in Section 5.1.1, Alley et al. (2005b) suggest that lakes may increase the chance of hydrofracture in subsequent years. Lakes often form in the same locations due to surface topography (Sneed and Hamilton, 2007; Catania et al., 2008). If they do not drain, these lakes maintain their beds at melting point until the entire lake freezes. This can result in warmer ice the following year, enabling easier hydrofracturing.

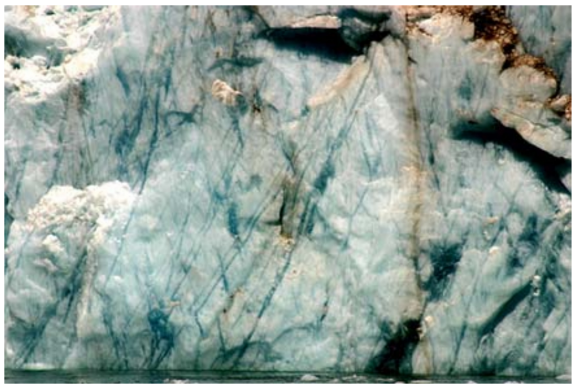

Figure 5.6 Blue-ice bands are evidence of water-filled fractures, where the water has refrozen. This photograph from Bamber et al. (2007) shows blue-ice bands in the calving front of the Kangersuneq qingordleq outlet glacier in southern Greenland. Note that the bands are mostly orientated vertically, implying that these fractures propagate downwards.

5.3 Modelling review

There are three distinct components of the seasonal response that can be modelled: lake formation, hydraulic connection, and dynamic response. This section overviews the current treatment of lake formation and dynamic response in models. The view is to explain the design decisions of my own model in the next section. Section 5.2.1 already discusses the theoretical consideration of the connection mechanisms. Existing subglacial hydrology models are reviewed in Section 2.4 so are not reviewed again except for two studies which specifically attempt to model a dynamic response and are therefore relevant here.

5.3.1 Overview

Section 5.1 establishes the need to include seasonal dynamic response in models. This has not yet been done at an ice sheet scale. Shepherd et al. (2009) conclude their recent paper:

> [...] until the physics associated with the hydrology of Alpine glaciers is incorporated into models of the Greenland ice sheet, projections of its evolution in a warming climate will remain speculative.

The 2007 fourth IPCC assessment report also warns that dynamic effects are not included in its future projections due to a lack of understanding of the processes, despite the importance of them being recognised (Solomon et al., 2007).

As this thesis already describes, the processes involved are complex. While a number of studies show that a direct connection exists between surface conditions and basal sliding

the same studies show that the nature of the coupling depends on the evolving hydraulic configuration of the bed. Truffer et al. (2005) warn that models must account for this when dealing with surface coupling. They use Gulkana Glacier, Alaska as an example. Despite record runoff between May 2004 and May 2005, the glacier has its lowest velocities in its 32 year record, due to sufficient water forming and maintaining efficient drainage.

5.3.2 Supraglacial lakes

Most modelling work on supraglacial lakes concentrates on determining lake volumes using satellite imagery and degree-day models. At least one study takes a more general approach.

Sneed and Hamilton (2007) use ASTER satellite imagery to determine current lake depths and volumes. Obviously, this technique cannot be used for predictions, but is important in constraining these statistics. McMillan et al. (2007) compare area and volume from airborne altimetry to degree-day modelling based on *in situ* meteorological data. Their model accounts for different surface conditions during the seasonal cycle: snow, saturated snow, bare ice etc. They report good agreement between their modelled volumes and satellite derived values. The largest errors come from uncertainties in winter accumulation. Their data are used to predict water fluxes from draining lakes. Sundal et al. (2009) also use a degree-day model. They calculate total runoff and correlate this with total lake area at their field sites. They find high runoff associates with larger lake area, but years with higher accumulation have less runoff in the summer due to increased water retention by surface snow and lower melt rates on snow surface when compared with ice surfaces (Braithwaite, 1995).

At least one model uses a more intricate approach than an degree-day parametrisation. Lüthje et al. (2006) couple an one-dimensional energy balance melt model with a two-dimensional, 100 m resolution drainage model to calculate lake area and volume evolution. The total area of their drainage model is $20 \times 20\,\mathrm{km}^2$. They force their model with two 30-day meteorological and radiation data sets from 1999 and 2001. Their method estimates lake coverage to be around 7% (4% when simple moulins are included); the model overestimates the $< 2.2\%$ coverage they observed in Landsat images. Lüthje et al. suggest that this discrepancy is because they cannot model individual surface channels with a 100 m resolution DEM. Their model does, however, produce lakes where they are observed in the Landsat image.

5.3.3 Dynamic response

This subsection discusses two specific Greenland ice sheet models. These attempt to understand the consequences of a dynamics response to surface melt using contrasting assumptions. Parizek and Alley (2004) assume that surface water reaches the basal system through hydrofracturing. Price et al. (2008) propose that surface water travels on the surface until it is close to the margin where it penetrates to the bed; the resultant longitudinal coupling is observed as a seasonal signal further inland.

Parizek and Alley (2004) use a two-dimensional finite-element, thermomechanical, flow-line model to investigate the consequences of Zwally et al.'s (2002) work. The model is forced using a positive degree-day method. This work uses a simple linear sliding law that is proportional to basal shear stress[4]. The constant of proportionality is then made a linear function of surface input and a figure based on the average ice-flow enhancement, from dynamic response, of the four previous years. The four-yearly averaged figure accounts for the system adapting between efficient and inefficient conditions based on Zwally et al.'s (2002) data. There is no provision for the efficiency to adapt to a sudden flux of surface meltwater. Surface water is calculated by integrating ablation upstream of moulins and it is passed directly to the bed. Surface meltwater reaches the bed as soon as there is ablation. Once a pre-defined threshold of water flux is reached, enhanced sliding is used. The moulin location is fixed before each run. Parizek and Alley's key result is that sliding dependence on surface melt increases the Greenland ice sheet's sensitivity to future climate because dynamic thinning brings a large portion of Greenland into the ablation zone. Truffer et al. (2005) warns that Parizek and Alley's inability to deal with seasonally evolving hydraulic configuration makes their results unreliable. Price et al. (2008) argue that an efficient system may reduce the overall acceleration of the ice and therefore reduce the sensitivity to climate.

Price et al. (2008) also use a two-dimensional flow-line model to simulate Zwally et al.'s findings. They use a finite-volume model with full stress coupling. They hypothesize that water reaching the bed downglacier from Swiss Camp can account for the observed acceleration at Swiss Camp, through longitudinal coupling. Ice 12 km downglacier is 40% thinner, warmer, and crevassed, making it easier for surface water to penetrate. They calculate static solutions of the velocity for a variety of increased sliding scenarios; both the

[4] GLIMMER uses the same principle.

origin and magnitude of enhanced sliding are varied. Price et al. also use a variety of time dependent response functions to look at temporal effects. They find the final acceleration observed at Swiss Camp is not greatly affected by this time function and therefore ignore it. They find their longitudinal coupling hypothesis valid for a wide range of runs. The example they give in their paper is that doubling the velocity 12 km downglacier accounts for Zwally et al.'s observations. Price et al. further state that this will decrease the sensitivity to climate because the acceleration occurs closer to the margin, where the gradients are steeper. This means the associated thinning will not move as much horizontally and so less of the ice sheet will be brought into the ablation zone through dynamic thinning, as argued by Parizek and Alley (2004).

It is interesting to note that Price et al.'s results show a thinning at Swiss Camp at maximum velocity, as expected if longitudinal coupling is the dominant mechanism. Shepherd et al. (2009) point out that Zwally et al.'s data actually shows an uplift at maximum velocity, suggesting high local water pressures, not longitudinal coupling, is the dominant mechanism. However, Price et al. bring a very valid point into the discussion. The longitudinal effects must be taken into account, where possible, when investigating seasonal speedup. This does not, however, automatically rule out hydrofracture through thick, cold ice. The two mechanisms can coexist.

5.4 Model design

I now introduce a new component of the Hydro model that deals with surface melt coupling. This component is designed to incorporate the key points from the reviews in this chapter. Some elements must be ignored and I will explain major assumptions that deviate from known processes. In most cases these are due to scaling.

The driving principles behind the surface hydrology algorithm are:

1. The majority of meltwater leaves the Greenland ice sheet subglacially (Ahlstrøm et al., 2005).

2. Longitudinal coupling is a secondary effect (Price et al., 2008; Shepherd et al., 2009).

3. Hydrofracture is the main supraglacial–subglacial connection (Das et al., 2008; Shepherd et al., 2009).

4. Supraglacial lakes are necessary to initiate hydrofracture (Alley et al., 2005b; Van der Veen, 2007).

5. Supraglacial lakes can form and drain anywhere in the ablation zone (Sundal et al., 2009); the majority of observed moulins are below the ELA (Catania et al., 2008).

6. Some seasonal coupling occurs before lakes begin to drain (Van de Wal et al., 2008; Shepherd et al., 2009).

7. A strong diurnal signal is only observed after lakes start draining (Shepherd et al., 2009). Afterwards, daily velocities correlate well with daily ablation (Van de Wal et al., 2008; Shepherd et al., 2009). However, the relationship between velocity and ablation is not simple, mainly due to evolving basal conditions (Truffer et al., 2005).

8. A signal from a draining lake can last several days. This signal is superimposed over any diurnal or seasonal signal (Shepherd et al., 2009).

9. The seasonal speedup signal is greatest at the margin ($< 30\,\text{km}$) and thereafter diminishes inland (Shepherd et al., 2009; Bartholomew et al., 2010). The hydrological configuration near the margin evolves to cope with increased water (Van de Wal et al., 2008).

10. The diurnal signal diminishes throughout the melt season, probably as an efficient drainage network forms (Shepherd et al., 2009).

11. Lakes which have not drained generally freeze in winter, Figure 5.7 (Lüthje et al., 2006) but some large lakes are known to survive until spring (Nienow and Hubbard, 2005).

5.4.1 Design decisions

The core idea of the new surface hydrology component is to track pond evolution and decide when, where, and how much water to pass to the bed. HYDRO already has the capability to update its hydraulic configuration depending on water pressure. The model can deal with any extra water entering the system without knowing whether it is basal or surface water.

Figure 5.8 shows the algorithm implementing the surface hydrology. Key design decisions are:

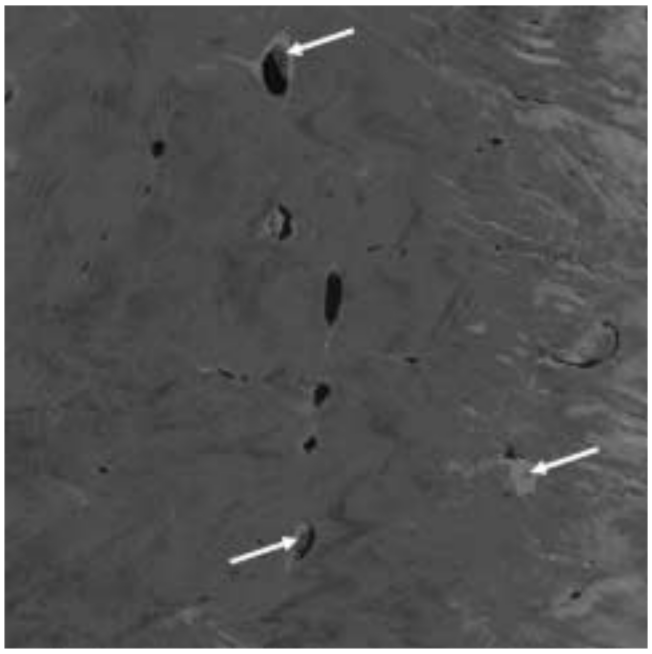

Figure 5.7 Surface lakes which do not drain refreeze over the winter. Generally, lakes completely refreeze, but some can survive until the spring. This $20 \times 20\,\mathrm{km}^2$ Landsat 7 image from 23 August 2007 shows two partially frozen lakes (near centre line) and one lake with an entirely frozen surface (bottom right). The figure is from Lüthje et al. (2006).

- to track pond depth for every cells using the default model resolution;
- to prevent water flow between cells;
- to drain ponds randomly, but couple the probability of draining to pond depth;
- and to pass all surface meltwater to the bed once a pond has drained for the remainder of the melt season.

Figure 5.9 shows a cartoon of the surface–bed connection of a single cell.

Model resolution

DiMarzio et al. (2007) publish a 1 km surface DEM of Greenland but I keep the surface model at the same resolution as GLIMMER-HYDRO for simplicity. GLIMMER-HYDRO uses a 10 km resolution because it is difficult for GLIMMER to maintain stability at a finer resolution due to the shallow ice approximation.

Due to this broad resolution, many modelled processes happen at much smaller scales than the model resolution, as typical in glaciological modelling. For example, within a module cell there may be many lakes, varying surface melt, and varying surface flow. Understanding

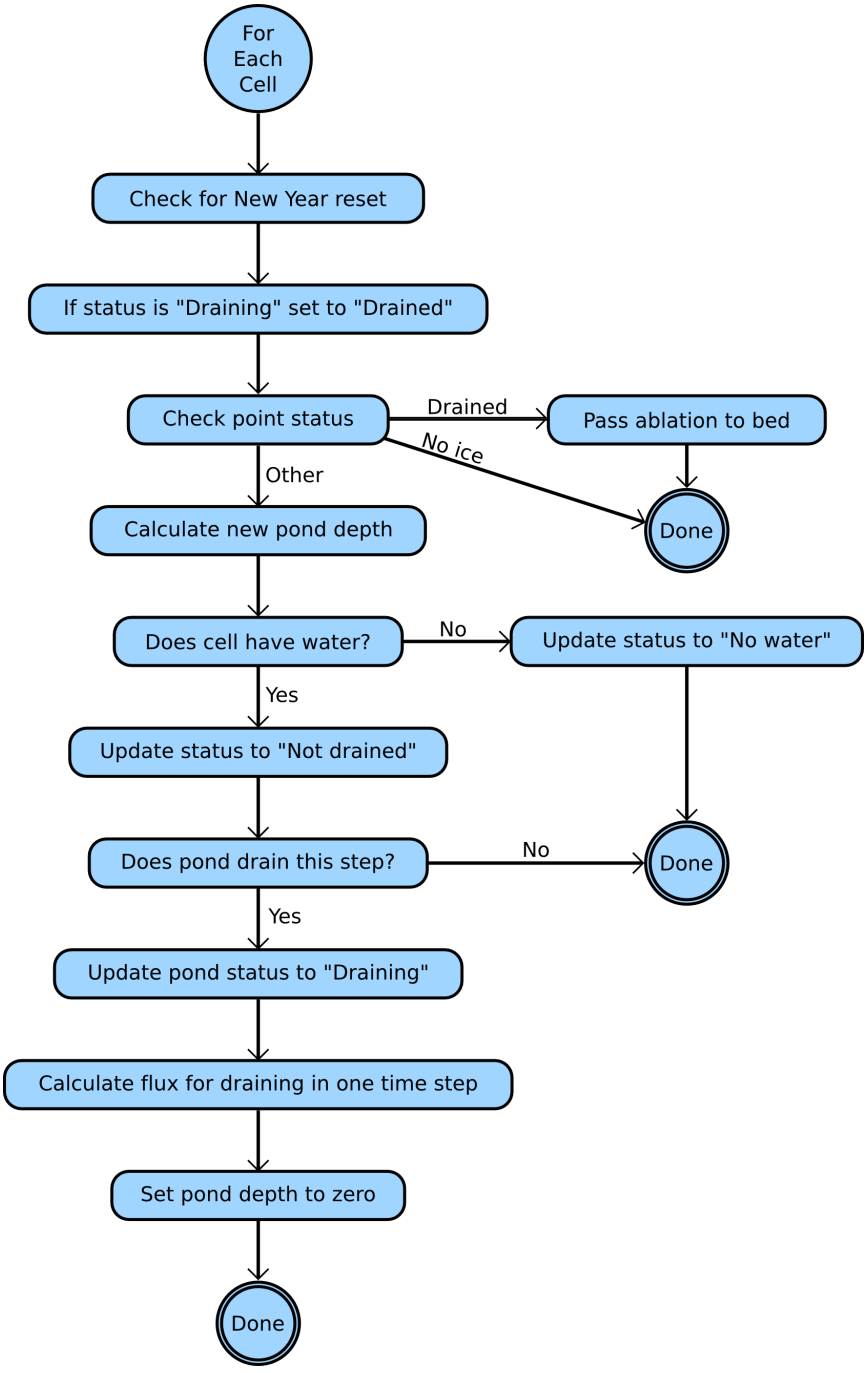

Figure 5.8 Algorithm for tracking surface pond evolution and passing water to the bed. Each cell can have status: no ice, ice but no water, not drained, drained, or draining. All the water in a pond is passed to the bed in a single "draining" time step. Afterwards, any ablation in that cell is passed directly to the bed. At the New Year: open connections are closed, cells reset to "ice but no water", and pond depths reset to zero. Ponds can freeze on their own accord as temperatures drop, hence the need to check for "no water" every time step if the pond has not drained.

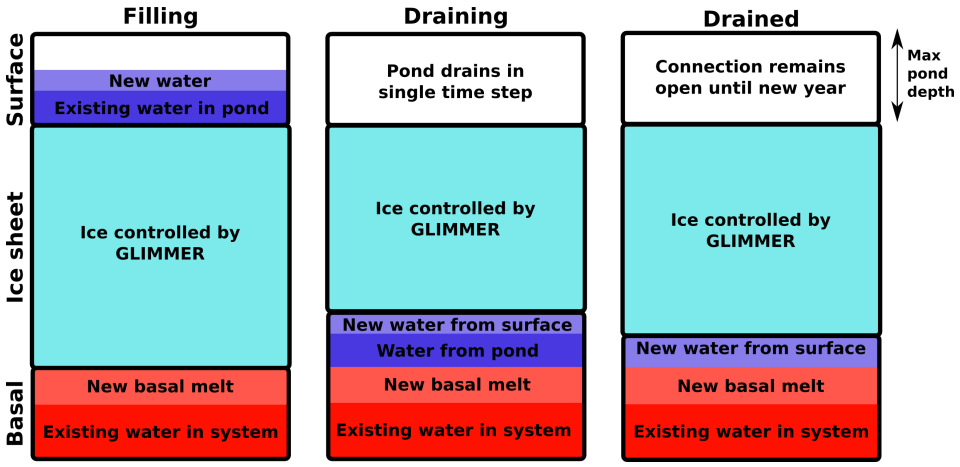

Figure 5.9 The ponding algorithm (Figure 5.8), connecting the surface and the basal systems, works on each model cell individually. These three boxes represent the ice column at different stages of ponding: filling, draining and drained. Each ice column is divided to represent, top to bottom: the surface system, the ice sheet (controlled by GLIMMER), and the basal boundary (controlled by HYDRO). A maximum pond depth is defined at which the cell is guaranteed to drain. As the pond depth approaches this value draining becomes increasingly likely. When the ponded surface water (blue) drains, it adds to the existing water at the bed (red). For the remainder of the melt season any surface water is passed directly to the bed.

surface processes is not the goal of this study. A good understanding is required to suitably deal with the downscaling of data from a 1 km to a 10 km grid when coupling the ponding algorithm with the bed.

If a finer DEM were used, combined with a surface flow model, the ponding algorithm may be able to model the location of lakes more accurately and not necessarily place a lake in every cell which experiences melt. As ponds appear to occur in the same surface hollows each years (eg Lüthje et al., 2006; Sneed and Hamilton, 2007), the long-term impact of these lakes draining from similar positions each year could be assessed.

No surface flow

The ponding algorithm does not calculate any surface flow between cells because at these scales, surface flow may not make much differences as a first approximation. Figure 5.2 shows an ASTER image of an approximately 10 km channel between two ponds. While this is only an example of a single surface channel, it is possible that on average any surface flow will be less than the 10 km model resolution. Adding a surface flow routing greatly increases the complexity of the model. Because of limited initial return at this resolution I do not do this,

but is should be done at a later date, especially if a finer surface DEM is used.

5.4.2 Capabilities before ponding algorithm

GLIMMER-HYDRO's present capabilities can deal with several requirements without modification. HYDRO's ability to evolve the basal efficiency addresses Items 7 and 10. The relationship between ablation and velocity evolves throughout the melt season, Item 7. If the basal conditions require it, areas will become efficient and this should lower velocities, Item 10. GLIMMER calculates surface ablation based on the climate driver. There will naturally be more surface melt near the margin because lapse rate is taken into account. GLIMMER-HYDRO should calculate a larger response closer to the margin (Item 9) due to the combined effects of larger surface gradients resulting in larger basal shear stress (GLIMMER), and increased surface melt at lower elevations affecting the basal boundary conditions (HYDRO). This is further complicated by the evolution of hydraulic efficiency. HYDRO calculates the evolution of effective pressure from water input; therefore, ablation is not linked directly to sliding velocity. Because HYDRO tracks this evolution, it automatically calculates how long a signal lasts and any superimposition, Item 8. Unfortunately, GLIMMER does not currently have the higher-order physics needed for longitudinal stresses. Item 2 cannot be implemented with the present version of GLIMMER-HYDRO This is purely down to the ice sheet model; the surface algorithm and HYDRO can couple with other models or use a newer version of GLIMMER in the future.

5.4.3 Ponding algorithm

The surface hydrology component is based on tracking pond depth and linking this to the draining probability, Item 4. The algorithm, Figure 5.8, tracks the ponding status of every cell which has ice. The four options are: ice but no water; not yet drained, filling; drained earlier in the season; and started draining this time step. The model takes three parameters, set at run time, to determine draining: minimum pond depth, maximum pond depth, and percentage of the signal to pass to the bed. The draining probability is defined to be zero at minimum pond depth and below, unity at maximum pond depth. If a uniformly generated random number is less than the draining probability of the cell, the cell is deemed to drain that time step. By increasing the maximum pond depth, the probability of draining therefore

reduces. Linking the draining to minimum and maximum pond depth, which in turn is linked to ablation and therefore altitude, means that lower ponds are more likely to drain than higher ones, Item 5. Setting the minimum depth to be low, or even zero, opens some connections as soon as there is melt, Item 6; this accounts for the observations by Van de Wal et al. (2008) and Shepherd et al. (2009). This method also allows for some ponds to drain before reaching their maximum area, as observed by McMillan et al. (2007) and Sundal et al. (2009).

A lake is deemed to drain in a single time step. For a monthly time step or longer this is not a problem, but if an hourly time step is used, for example, this may result in unrealistically high, but short-lived, water input rates at the bed[5]. Water is passed vertically downwards; hydrofracture is the assumed mechanism, but no explicit hydrofracture calculations are performed, Item 3. Once a lake has drained the connection remains open; any further ablation in the cell is passed directly to the bed. This follows the observations of Van de Wal et al. (2008) and Shepherd et al. (2009), Item 7. As most water is observed to leave the Greenland ice sheet from its subglacial system, Item 1, passing all ablation to the bed, once connected, is appropriate.

The ponding algorithm takes surface mass balance data as an input, in this case from Glimmer. A positive ice mass balance allows ponds to lose water by freezing, Item 11. This should remove ponds by the end of the year. Nienow and Hubbard (2005) discuss ponds that survive through the winter. As ponds are unlikely to drain in the winter, due to colder temperatures, it is easiest to reset all cells to "ice but no water" and all pond depths to zero every new year. This avoids the added complication of declaring the likelihood of draining based on unknown, changing factors.

5.4.4 Discussion

This section explores some of the design features of the ponding algorithm. All of the principles set out at the start of Section 5.4, except Item 2: longitudinal coupling, are fulfilled. The first focus is the broad scale processes with no surface flow. The second focus is the time step and its consequences. The third focus is the probability of draining. All the improvement suggestions in this section are mentioned for completeness, to enable others to

[5] Das et al. (2008) observe a lake draining within two hours, so perhaps an hourly step will not cause a significant overestimation of the flux reaching the bed.

use the same algorithm.

The ponding algorithm operates on the same scale as Glimmer-Hydro, using grid squares of 100 to 400 km^2. This means that individual ponds cannot be tracked and the pond depth is the average depth over the entire cell. Therefore, pond depths are shallower than field data suggests. At these scales, there is a high likelihood that water will remain in the same model cell. Therefore, as a first approximation, avoiding calculating surface flow is reasonable.

Future developments

Considering possible future improvements to the ponding algorithm is a useful way to highlight the current state of the algorithm. The ideas now discussed are not implemented in this thesis.

Surface streams are known to flow on the ice sheet's surface and to feed moulins (Das et al., 2008). Currently no surface flow is allowed but if this is added then more water may reach the bed nearer to the margin. Water may also reach the bed sooner because higher ponds will not have to drain to deliver water from these cells to the bed. This may affect the observed dynamic velocity response.

Catania et al.'s (2008) data suggests that the draining of ponds are restricted above the ELA. This region includes the wet-snow and percolation zones. A feature could be added to the algorithm to reduce the likelihood of draining above the ELA or simply reduce the likelihood with increasing ice thickness. This, arguably, already occurs because less melt at altitude fills ponds slower which reduces their chance of draining, as draining is a function of pond depth. Adding a feature which allows water to refreeze in the snowpack, as happens in the percolation zone (Parry et al., 2007), will also enable more accurate calculation of pond depths.

Currently, the algorithm does not take the time step into account when calculating the probability for ponds draining. This has two effects. One, ponds are statistically more likely to drain sooner with a shorter time step as the check whether a pond drains is performed more frequently. Two, draining is assumed to occur in a single time step so if a short time step is used then the flux reaching the bed may become unrealistically large. Neither of these are a problem in this thesis because all the runs use a one-month time step but it is an area that can be improved to prevent it becoming a problem in future for, as yet, undefined

experiments.

Adding a drainage frequency variable to the algorithm may be a useful way to control the frequency of draining without affecting pond volumes. Currently, drainage frequency is a function of minimum and maximum pond depths and in order to drain ponds less frequently the maximum pond depth $d_{p\max}$ must be increased. This increases the water flux reaching the bed when a pond does drain unless the surface-to-bed magnification factor ω is reduced accordingly. A drainage frequency variable, if introduced, would remove the need to couple $d_{p\max}$ and ω and keep their values more physically meaningful for describing the system.

5.5 Experiment

The goal of the experiment is to demonstrate a dynamic response to a seasonal signal, including evolving basal efficiency, and to look at possible explanations of Howat et al.'s (2007), Joughin et al.'s (2008), Shepherd et al.'s (2009), and other authors' observations. This body of work describes the seasonal and diurnal response of ice dynamics to surface ablation, bringing the future stability of the Greenland ice sheet into question. The successful modelling of the response on a Greenland-wide scale has yet to be published. Without this modelling, it is impossible to include the observed dynamics in future climate predictions (Solomon et al., 2007).

5.5.1 Research questions

This chapter aims to answer the following questions:

1. Does Glimmer-Hydro, using the surface ponding algorithm, capture a seasonal dynamic response? What are the physical processes which allow this?

2. Does the hydrological system evolve with the climate signal? For example, does the efficient area increase as the season progresses?

3. How long does the signal from a lake draining event last? How sensitive is this to the choice of base diffusivity of the bed?

4. How sensitive is the response to the drainage frequency and magnitude?

5. Is there a response inland from where water reaches the bed?

6. Is there an equal speedup everywhere? More specifically, is the speedup in areas identified as having low effective pressure in Chapter 3 less than areas with higher effective pressure?

7. Does the basal hydrology result in large interannual variation in sliding velocity? If so, what are the processes responsible?

A positive answer to Question 1 is needed to answer the remaining questions. Question 2 has often been ignored by other authors due to the inabilities of their models to evolve basal conditions (eg Parizek and Alley, 2004) but is requested by Truffer et al. (2005). Question 3 looks at the sensitivity of the system to the diffusivity of the bed and other model parameters. Question 4 explores one aspect of the sensitivity of the Greenland ice sheet to a warmer climate. Question 5 looks at whether ponds can affect upstream ice dynamics through hydraulic back pressure at the bed. Question 6 refers to the convergence of water reported in Chapter 3 and the variable speedup reported by Joughin et al. (2008). I demonstrate in Chapter 4 that basal water converges in the troughs under Greenland's outlet glaciers, resulting in low effective pressure. I further hypothesize that these are fast flowing due to the background signal, so the effect of the surface signal will be limited. This may explain the 15% speedup of Jakobshavn Isbræ compared to 50–100% speedup of nearby land terminating glaciers reported by Joughin et al. (2008). Question 7 addresses Howat et al.'s (2007) work. Their results indicate that there is large interannual variation in outlet glacier discharge. This has not yet been satisfactorily explained. Buttressing from the position of the calving front is one possible explanation. This research question looks at whether the hydrological controls may cause a multi-year speedup.

5.5.2 Experimental set-up

The approach to this experiment is to understand behaviour of a characteristic run using the ponding algorithm and then to investigate the processes controlling the identified behaviour by exploring the parameter space. Three pairs of land- and marine-terminating transects are used to analyse data. The control run uses the same set-up as the other model runs except surface melt water input is set to be zero.

Transects

Data are analysed along six transects which provide a reasonable representation of the system. These transects cover the marine-terminating Jakobshavn Isbræ (T1), Helheim (T3), Kangerdlugssuaq (T5) outlet glaciers and land-terminating lines (T2, T4, T6) to the south of each of these. The major outlet glaciers to the north of Greenland, for example Petermann and the NEGIS, are not covered to limit the scope of the work. Figure 5.10 maps and labels these six transects; Table 5.1 gives the start co-ordinates of each transect on the velocity grid and the direction to the next cell.

Jakobshavn Isbræ and Kangerdlugssuaq are two of the fastest flowing outlet glaciers of Greenland and therefore the focus of many studies (eg Howat et al., 2007; Joughin et al., 2008). In the full friction run at the end of Chapter 4, these two glaciers are shown to have different basal regimes in GLIMMER-HYDRO. Jakobshavn Isbræ has a large catchment area with other outlet glaciers in the same region of warm basal ice. By contrast, Kangerdlugssuaq has its own catchment of warm basal ice upstream from it. Both have subglacial troughs, but at the 10 km model scale, Kangerdlugssuaq's is much more distinct in the DEM. Helheim is similar to Jakobshavn Isbræ but with a smaller catchment area and a wider, and therefore more distinct, subglacial trough.

Climate driver

The Edinburgh Ice Sheet, EIS, driver is used in this experiment because it is easy to parametrise a monthly climate signal. The EIS is an equilibrium line altitude, ELA, based

Transects

Label	Description	Margin	Step
T1	Jakobshavn Isbræ	$(38, 125)$	$+1, +0$
T2	South of Jakobshavn Isbræ	$(38, 121)$	$+1, +0$
T3	Helheim	$(86, 79)$	$-1, +1$
T4	South-west of Helheim	$(82, 75)$	$-1, +1$
T5	Kangerdlugssuaq	$(109, 103)$	$-1, +1$
T6	South-west of Kangerdlugssuaq	$(108, 99)$	$-1, +1$

Table 5.1 The start co-ordinates of the four-cell transects used in the data analysis. The coordinates are on GLIMMER's velocity grid; $(1, 1)$ is the south-western corner. T1.A refers to the margin cell (A) of transect T1

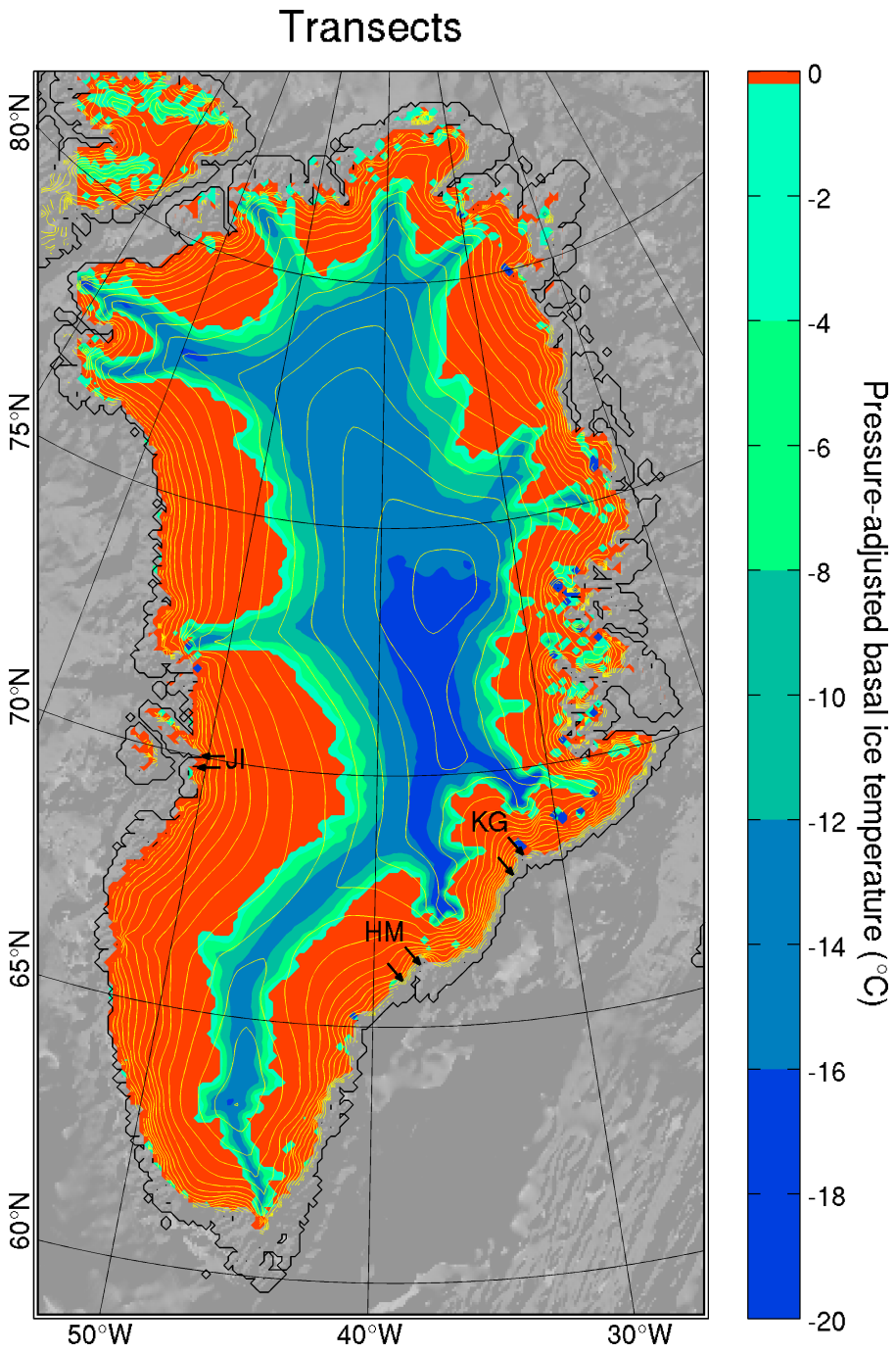

Figure 5.10 Six transects are used in this chapter to investigate the dynamic response to draining surface ponds. These come in land- and marine-terminating pairs covering: Jakobshavn Isbræ (JI), Helheim (HM) and Kangerdlugssuaq (KG). In each case the marine-terminating transect, along the outlet glacier, is to the north of the land-terminating transect. This figure also shows the location of each transect pair in relation to the area of warm bed and the size of the basal-catchment area.

climate driver. The ELA function is defined to vary spatially with latitude and sinusoidally through time.

Spatially, the ELA curve is defined as the best fit quadratic through three points. These points are: 1000 m at 80 °N, 1200 m at 70 °N, and 2200 m at 60 °N The first two are taken directly from Van der Veen (1999) and Zwally et al. (2002). The last ELA point has been raised by 200–400 m from the 1600–1800 m reported by Van der Veen (1999) in the south. This is to improve the melt extent in the south. For simplicity, there is no east-west variation in the ELA prescribed despite there being an east-west gradient in reality.

Seasonal variation is introduced by moving the monthly effective-ELA[6]. While this is not the most realistic situation physically, it is a very quick method to obtain monthly ablation data. As it gives the melt pattern required, it is fine for the purpose of this work. Seasonal variation is defined as a sinusoidal shifting of the ELA from 0 m to 1400 m. Figure 5.11 shows the summer melt extent calculated by the EIS driver; minimal melt is calculated in winter. The melting area is less than the melt extent schematic shown in Figure 1.7 but is similar to the ablation zone shown. This is done to prevent lakes draining high on the ice sheet as the ponding algorithm takes neither ice thickness nor percolation into account.

Model set-up

The experiment uses the 10 km DEM from Chapter 3. The model spins up using a monthly time step for 5000 years with the ponding algorithm running throughout so the basal conditions approximate an equilibrium solution. The model run then outputs data every month for ten years to investigate the seasonal signal.

The base run is the same as used in Chapter 3 (runs G3 and H107) with uniform geothermal heat flux $H_g = 42\,\mathrm{mW\,m^{-2}}$ except that it is coupled to HYDRO using the surface ponding algorithm and $\gamma = 0.5$ and $\mu_{\max} = 0.01$. These values are chosen because they make the system slightly loose without creating instabilities. This set-up provides friction heat flux coupled to effective pressure, an evolving basal hydrology, and climatic feedback.

Each parameter is varied, one at a time, by approximately $\pm 10\%$ to investigate the processes controlling the behaviour of the base run. The values of the parameters used for the base run and their variation are summarised in Table 5.2. Each model run is given a

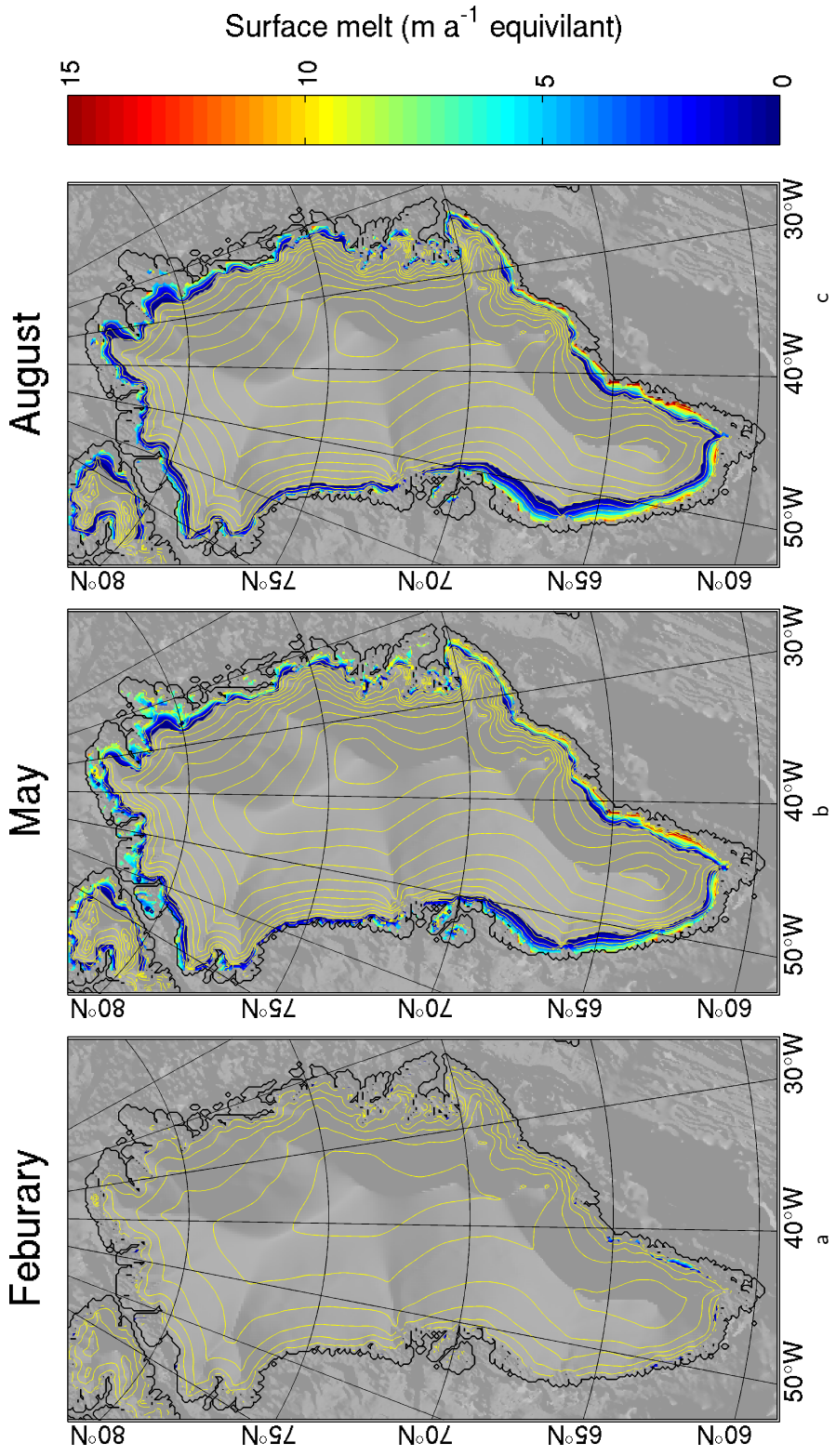

Figure 5.11 Summer melt extents, used for model forcing. These are calculated by the ERA driver based on a prescribed time- and latitude-based ELA function. Shown are (a) winter, (b) spring, (c) summer. Compare with the maximum observed extents in Figure 1.7. The maximum summer melt extent with surface melt is defined to approximate areas with surface lakes. This prevents lakes forming and draining in areas which are in the percolation zone and which are not observed to drain.

Ponding model runs

Run	Variable	Value (Run P1)	Min	Max
P2–3	κ	$3.0 \times 10^{-3}\,\mathrm{m\,s^{-1}}$	2.7	3.3
P4–5	c_T	$2.0 \times 10^{-7}\,\mathrm{Pa^{-1}}$	1.8	2.2
P6–7	d	10 m	9	11
P8–9	$\mu_{\max}$	0.010	0.009	0.011
P10–11	$t_{s_{\max}}$	$1.0 \times 10^{-3}\,\mathrm{m\,a^{-1}\,Pa^{-1}}$	0.9	1.1
P12–13	γ	0.5	0.4	0.6
P14–15	p_{limit}	0.9	0.8	1.0
P16–17	ψ	$\times 100$	90	110
P18	Efficient bed	Yes	No	—
P19	$d_{p_{\max}}$	0.1 m	—	1.0
P20–21	ω	$\times 10$	5	10
P22–31	Seed	Constant	Random	
P32–33	Ponding	On	No-signal	Straight-to-bed
P34	Basal sliding	On, f($\bar{N}$)	Off	

Table 5.2 This table summarizes the model set-up for the main run (P1) in this chapter. It also gives the range of values used when exploring the parameter space.

Only one variable is changed at a time when deviating from run P1. The minimum and maximum are usually approximately ±10% of the base run value; only the leading coefficient is shown. The random series (P22–31) of runs uses $d_{p\max} = 1.0\,\mathrm{m}$, $\omega = 1$ as there is very little randomness in lake draining with $d_{p\max} = 0.1\,\mathrm{m}$. This is because the primary controls when $d_{p\max}$ is small are surface elevation and latitude. Run P32, with no surface signal, is the control run.

letter code for easy referencing in the discussion.

The three ponding algorithm parameters are: minimum pond depth $d_{p_{\min}} = 0\,\mathrm{m}$, maximum pond depth $d_{p_{\max}} = 0.1\,\mathrm{m}$, and 1000% of the surface signal is passed to the bed. $d_{p_{\min}} = 0\,\mathrm{m}$ allows water to be passed to the bed early in the melt season as suggested by field observations (eg Sundal et al., 2009). The maximum pond depth is the average lake depth over a $100\,\mathrm{km}^2$ cell based on Box and Ski (2007) and Sneed and Hamilton (2007). The water passed to the bed is magnified by a factor of ten to overcome scale issues; these are discussed in Section 5.5.3.

In most cases, the same random seed[7] is used for all experiments. This allows for a degree of consistency between runs. For an individual run, the auto-generated number determining

[6] The Eis driver accepts three time-based forcing files: the ELA, the surface temperature gradient from the ELA, and the sea-level rise. These are discussed further in Section 2.2.4.

[7] A random seed determines the apparently random sequence of numbers from the random number generator. If the random seed is the same then the same sequence of pseudo-random numbers are generated in different model runs.

whether the cell drains will appear random. However, the sequence of random numbers are identical in a different run. Other factors, such as surface melt and elevation, influence whether a given cell drains. Because of this lakes are not guaranteed to drain at the same time in different runs even with an identical random sequence of numbers. Varying random seeds are used to investigate Question 7; these runs (P22–31) each use a different sequence of random numbers and therefore investigate the sensitivity of the system to its stochastic nature.

5.5.3 Model scale

Glimmer-Hydro, with a surface ponding algorithm, does not capture a dynamic response of the ice because of scaling issues, when lake depths are realistic ($d_{p\max} = 0.1\,\mathrm{m}$ averaged over cell) and 100% of the surface water is passed to the bed ($\omega = 1$). Water volumes are too small to affect effective pressure when averaged over a $100\,\mathrm{km}^2$ cell. Glimmer-Hydro operates on a 10 km grid, but dynamic effects due to draining lakes are known to occur over much smaller scales as moulins inject water into a small basal area. Therefore, in reality the surface signal is concentrated into a small area.

To compensate for this in the model, I artificially magnify the volume of water as it is passed to the bed by a factor of $\omega = 10$ in the base run. The pond depth is kept the same so the stochastic draining is not affected. When this is done, a seasonal signal is present in the model output. The magnitude of the resultant speedups are smaller than observations suggest. Bearing this in mind, meaningful insight into the system can still be gained. Some effort must go to understanding which modelled effects are due to physical processes and which ones are due to the 10 km model scale or to the magnification factor ω.

5.5.4 Results

This section presents the results for the base run (P1) which are then discussed in Sections 5.5.5 and 5.5.6. Data from other runs are presented as required in the discussion. Maps and global figures are presented first to give an overall picture, followed by velocity transects and then Fourier transform transects.

Maps and global efficiency

Figure 5.12 plots the pond status early in the season (February), near the start of the melt season (May) and late in the season (August) in the first year of model output. All the other runs which use $d_{p\max} = 0.1\,\mathrm{m}$ have a very similar pattern because for small $d_{p\max}$, surface elevation and latitude, not randomness, are the primary controls on lake drainage. Figure 5.13 maps the basal sliding speed to show the typical distribution. The speedup is small, compared to absolute velocities, and is therefore difficult to see on the map so only August is mapped. Figures 5.14 and 5.15 plot the *relative*[8] basal sliding speed and normalised effective pressure for February, May, and August. The normalised effective pressure map highlights efficient cells in blue. Figure 5.16 plots the total efficient area under the ice through time.

Relative velocity transects

Figures 5.17–5.22 plot the six relative velocity transects for the main model run. The data are discussed in Sections 5.5.5 and 5.5.6. These transect plots show each cell from the margin (a) towards the interior (d). The left-hand axis shows the relative speedup of basal sliding $\bar{v}$ (blue). The right-hand axis shows the normalised effective pressure $\bar{N}$ (red). Grey background shading denotes the status of the surface pond (no water, filling, draining, drained). The bottom of each cell's plot is shaded pink if the cell is efficient. Each plot also annotates the average and standard deviation of the velocity over the ten-year period.

Fourier transform transects

Fourier analysis enables periodic behaviour to be distinguished from random variation in a signal. It is useful in this context to identify the strength of any seasonal or multi-annual variation in relative velocity.

Frequency analysis is performed in MATLAB® using its inbuilt Fast Fourier Transform function. This function is based on the open source FFTW library (Frigo and Johnson, 2005). The Fourier transform of real numbers results in complex numbers. Therefore, the absolute values of the transforms are plotted. Each figure plots a land- and marine-terminating transect pair.

[8] Relative speedup is calculated as the velocity divided by the average velocity, minus one.

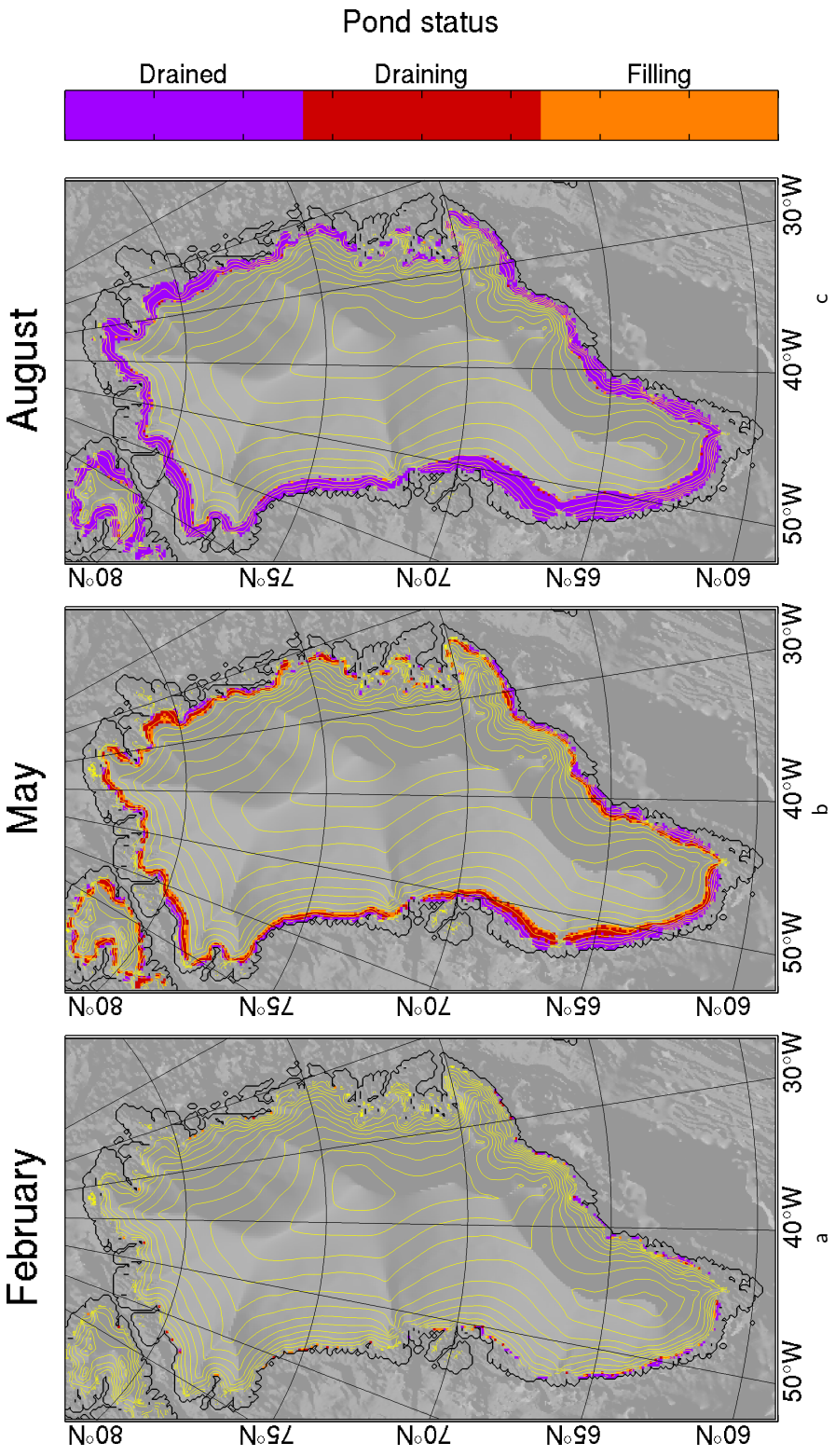

Figure 5.12 In all runs (P1 shown) there is some early draining due to the ELA definition and the low $d_{pmax} = 0.1$ m value used. As the season progresses, the model captures lakes filling and draining by increasing elevation band. At the highest elevations, there are some lakes which do not drain and subsequently refreeze. In the south lakes reach 2000 m and around Jakobshavn Isbræ they reach 1500 m. This agrees with pond elevations shown in Figure 5.1. The surface elevation contours are 500 m apart.

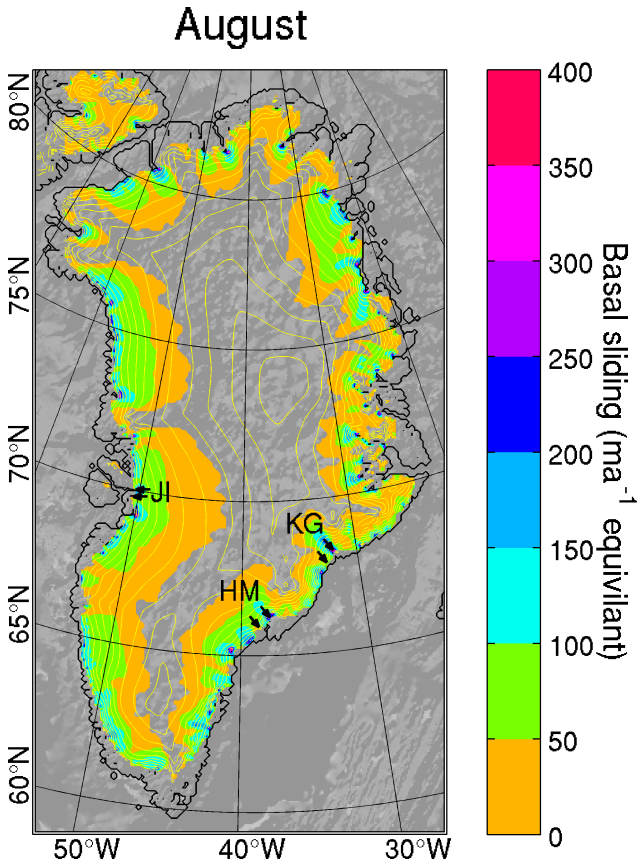

Figure 5.13 Basal sliding speeds for run P1. Note that the fastest speeds correspond with the locations of outlet glaciers. The frozen bed is shown as the transparent central region. The run shows a seasonal variation, but this is small compared to absolute velocities and so is difficult to map. Therefore, only one time-slice is shown. Figure 5.14 maps the relative speed to demonstrate the speedup.

To establish a baseline for comparison and to understand any effects from the monthly sampling of ten-year data, Figure 5.23 plots the Fourier transform of $\bar{v} = \sin(2\pi t)/4$, where t is in years. $\bar{v}$ has a one-year period and is sampled monthly, the same as the model output. The amplitude of a quarter approximates the range of the relative velocities in the margin cells in Figures 5.17–5.22. Key points of Figure 5.23 are:

- There is a distinct peak at 1 a which corresponds to the prescribed seasonal signal.
- The 1 a peak is broad due to the large sampling interval.
- There are no significant peaks with a longer period than 1 a which may have resulted due to the sampling
- The frequencies smaller then 1 a are noisy; this is due to the coarse sampling.

For actual model output, it is therefore likely that any significant features on top of those

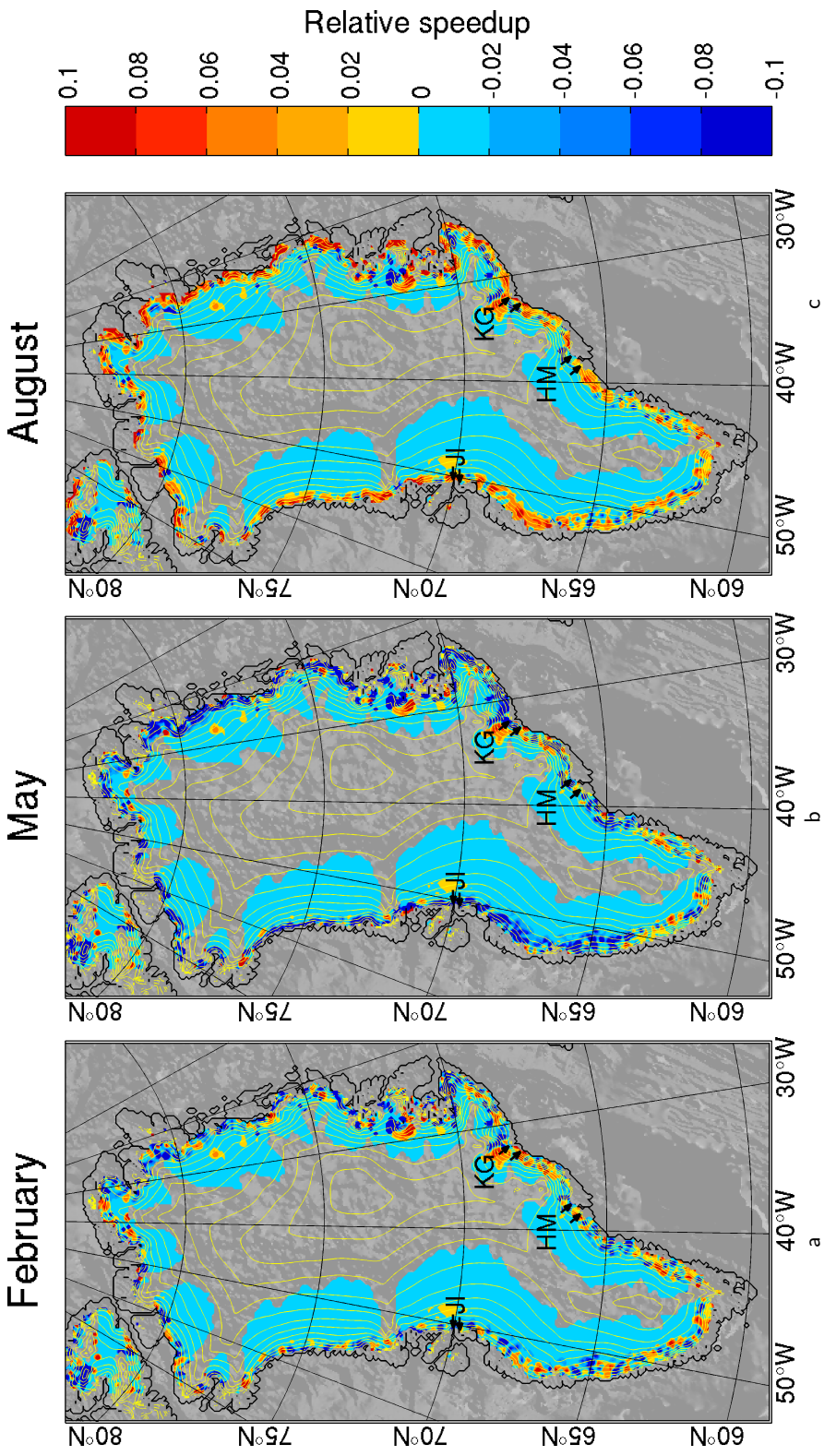

Figure 5.14 Relative speedup maps for (a) February, (b) May, and (c) August. In all runs (P1 shown) the sliding velocity in the interior of the ice sheet is constant throughout the run. These regions are controlled primarily by the basal melting and not a surface signal. Near the margin, run P1 shows a seasonal increase in sliding velocity as surface ponds drain.

The relative velocity shows a dip in May. This is because the velocities continually fall throughout winter. In May, when most lakes are beginning to drain, the velocities do rise, but are lower than February's values. By August, the velocities and efficiency are usually at their maximum. Transect plots (Figures 5.17–5.22) make this clearer.

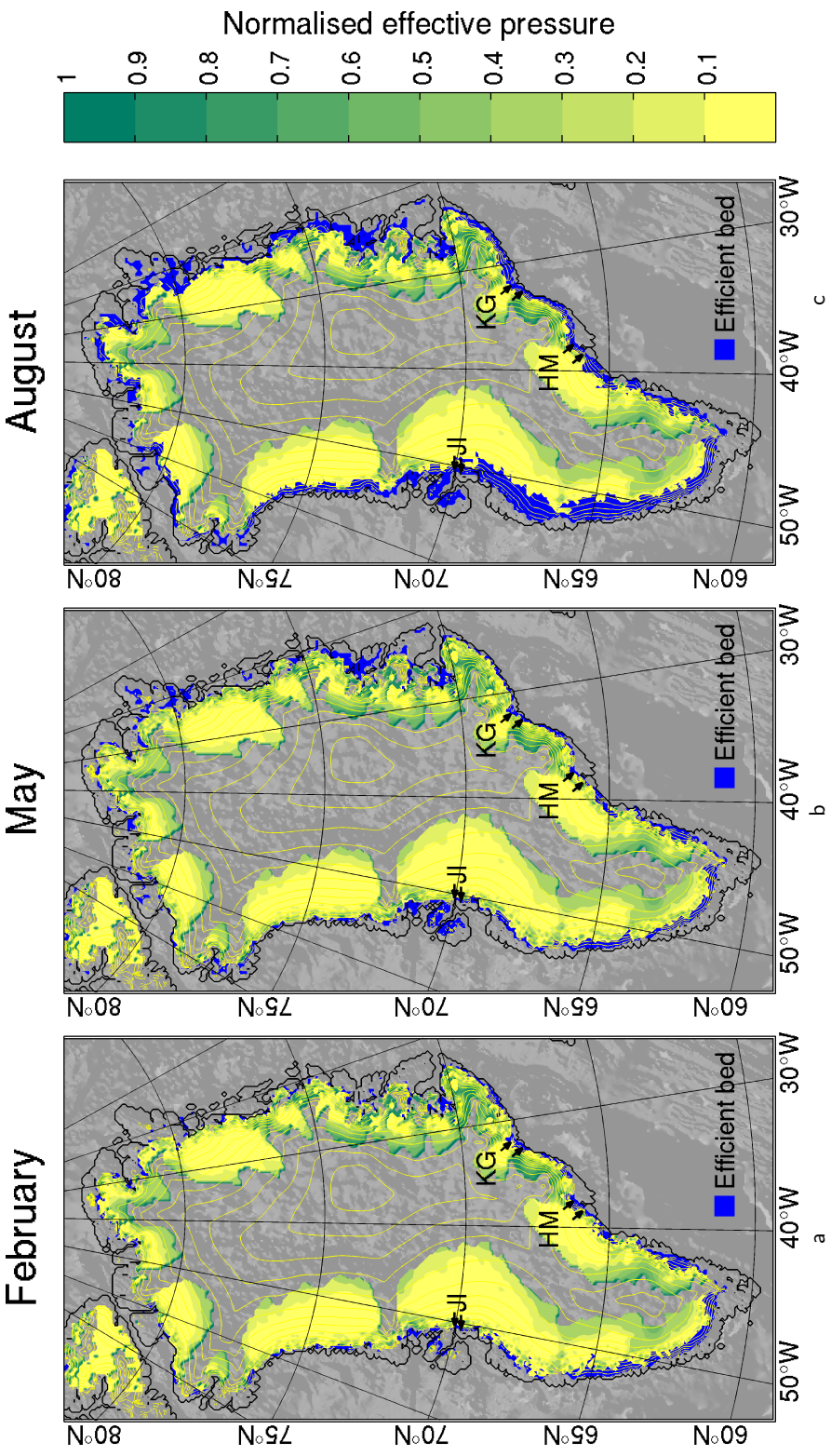

Figure 5.15 Normalised effective pressures reduce near the margin throughout the melt season, due to extra water from draining ponds. Efficient areas (blue) form which further complicates the pressure signal. Inland, the effective pressure is at equilibrium with basal melt. Effective pressures are shown in velocity transects (Figures 5.17–5.22) for run P1.

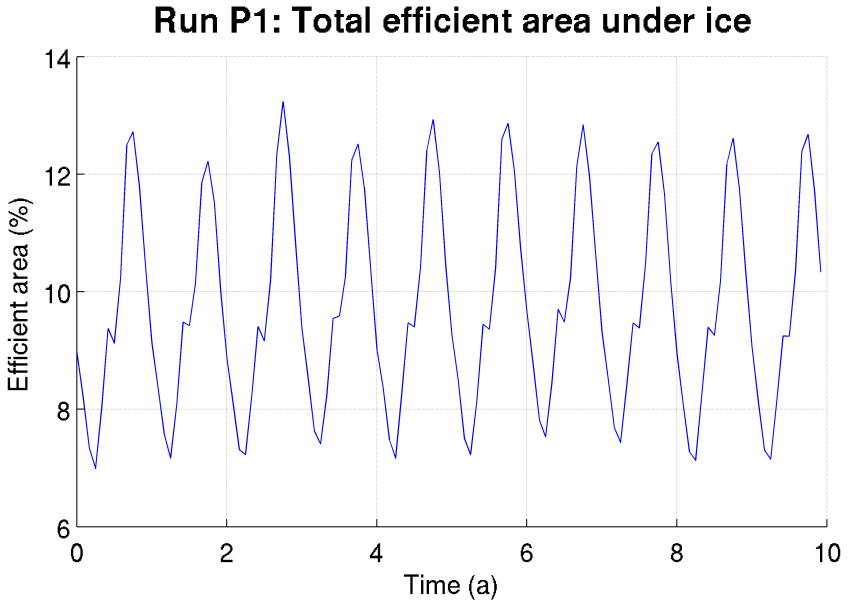

Figure 5.16 The model shows a cyclic behaviour in the total efficient area of the bed. The minor peaks each year around 9.5% efficient area are due to the loss of seasonal ice around the margin. The switching on and off of efficiency in a single location is usually less regular; this is shown in the transect plots in Figures 5.17–5.22.

described here are genuine and not an artifact of the sampling.

Figures 5.24–5.26 plot the Fourier transform of the three transect pairs of the base run. Data are discussed in Sections 5.5.5 and 5.5.6.

Surface transects

So far only basal sliding data are presented as this is the interface between the basal hydrology and ice sheet models. However, in the field, only surface velocity data are readily available. This section presents surface velocity data for the Jakobshavn Isbræ transect pair (Figures 5.27 and 5.28) and their Fourier transform transect (Figure 5.29).

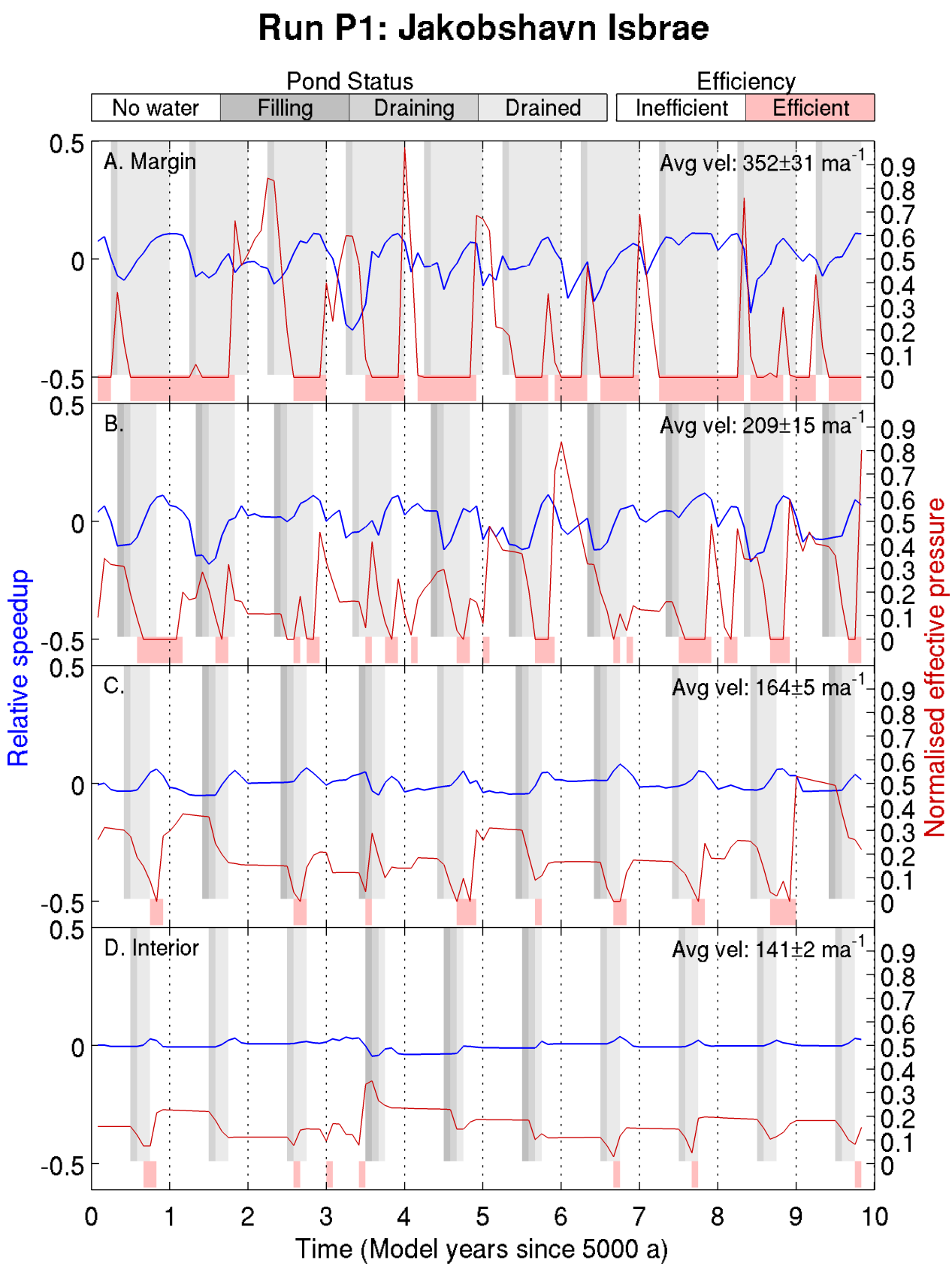

Figure 5.17 Run P1, Transect 1: Jakobshavn Isbræ (marine-terminating). Relative basal speedup (blue line), showing pond draining (grey background), normalised effective pressure (red lines), and efficient bed (red background).

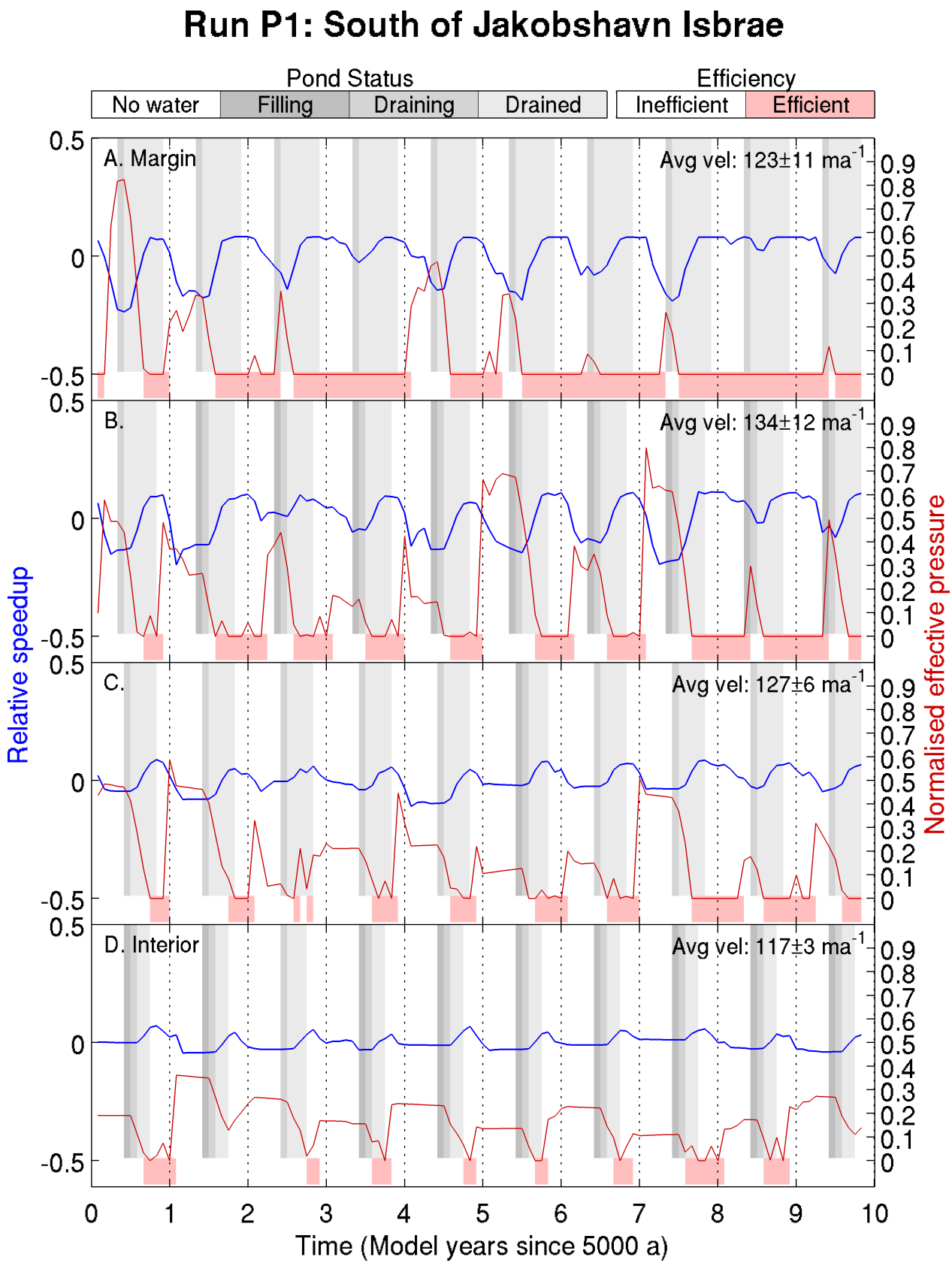

Figure 5.18 Run P1, Transect 2: South of Jakobshavn Isbræ (land-terminating). Relative basal speedup (blue line), showing pond draining (grey background), normalised effective pressure (red lines), and efficient bed (red background).

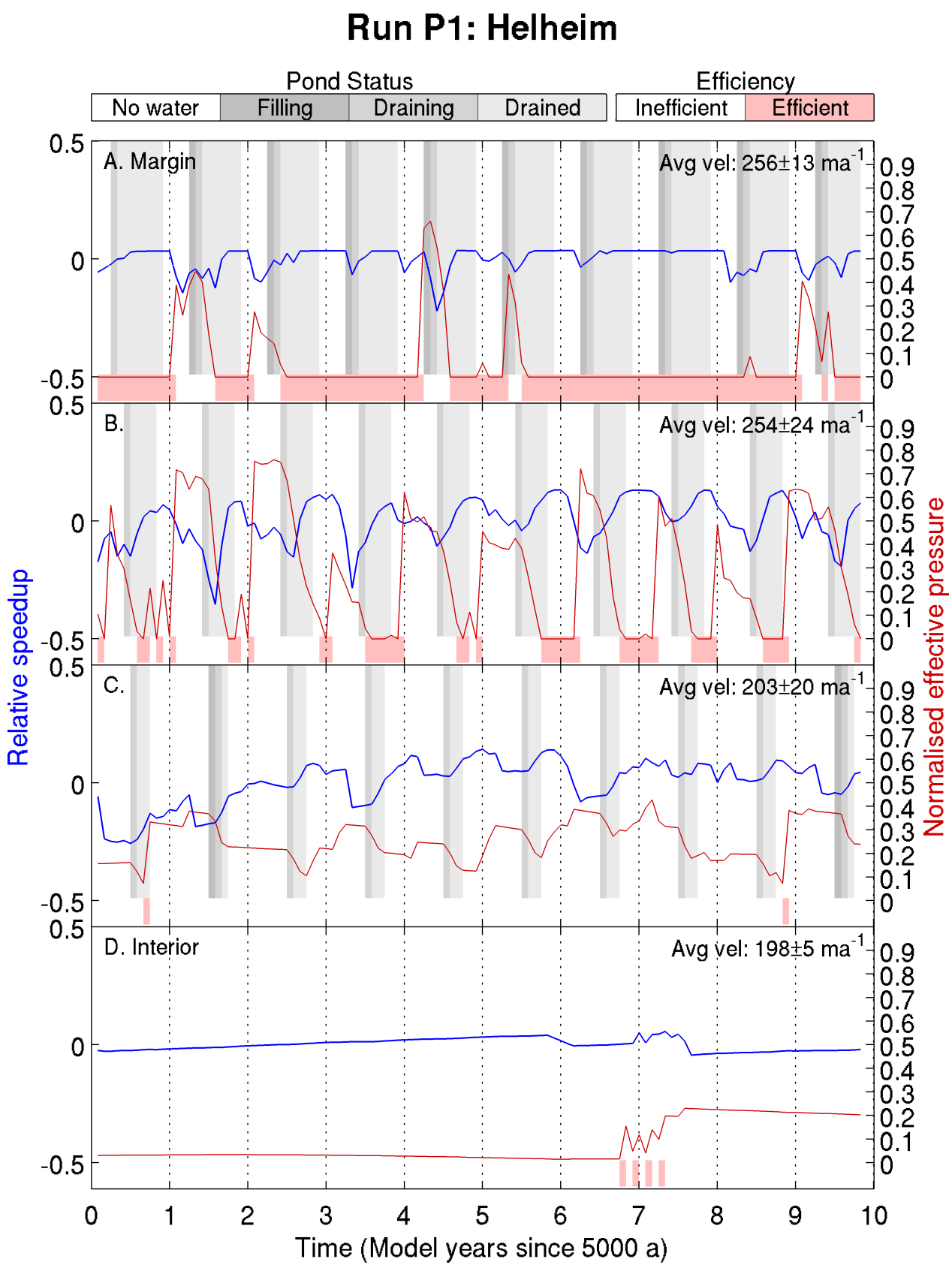

Figure 5.19 Run P1, Transect 3: Helheim (marine-terminating). Relative basal speedup (blue line), showing pond draining (grey background), normalised effective pressure (red lines), and efficient bed (red background).

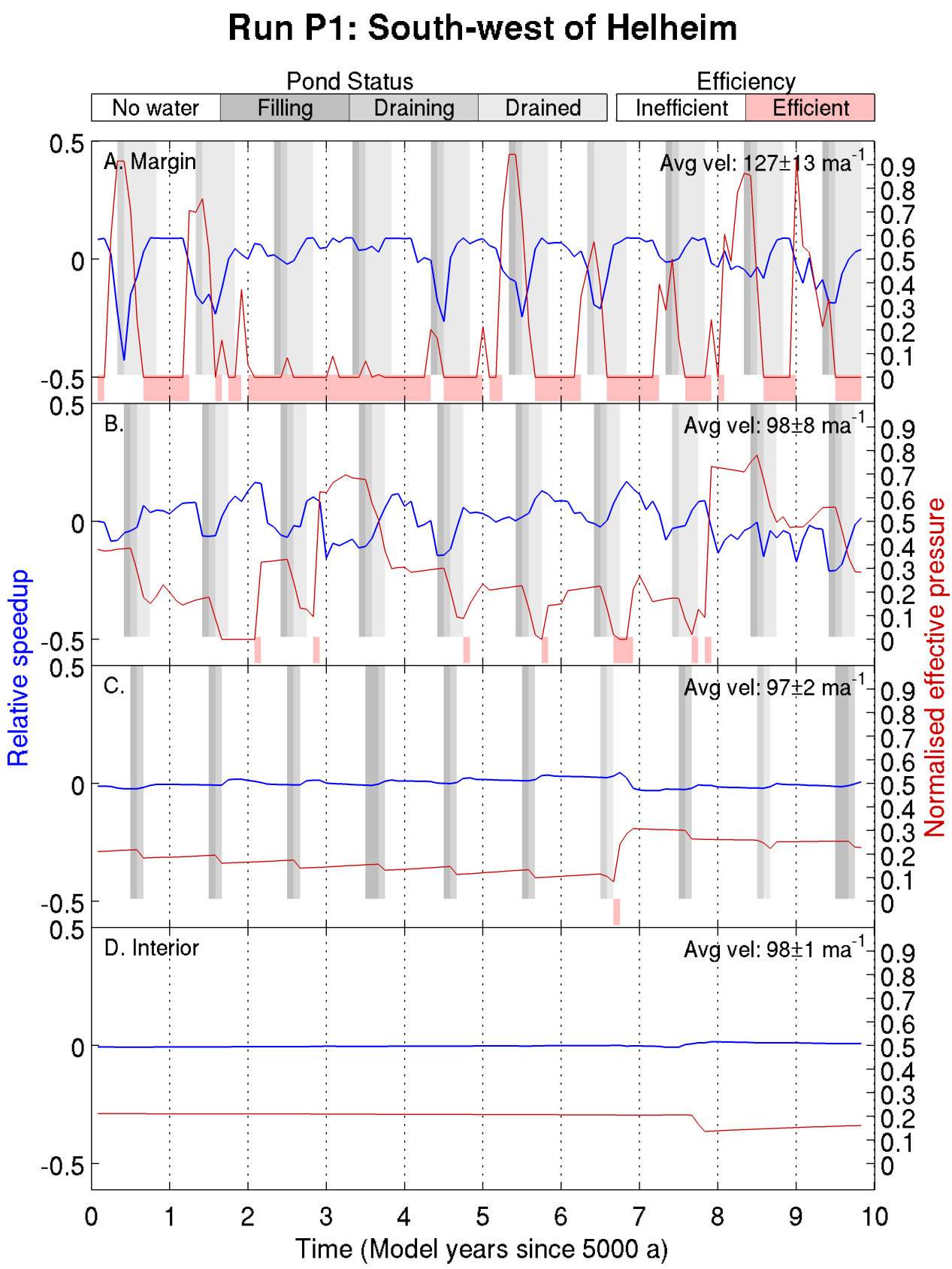

Figure 5.20 Run P1, Transect 4: South-west of Helheim (land-terminating). Relative basal speedup (blue line), showing pond draining (grey background), normalised effective pressure (red lines), and efficient bed (red background).

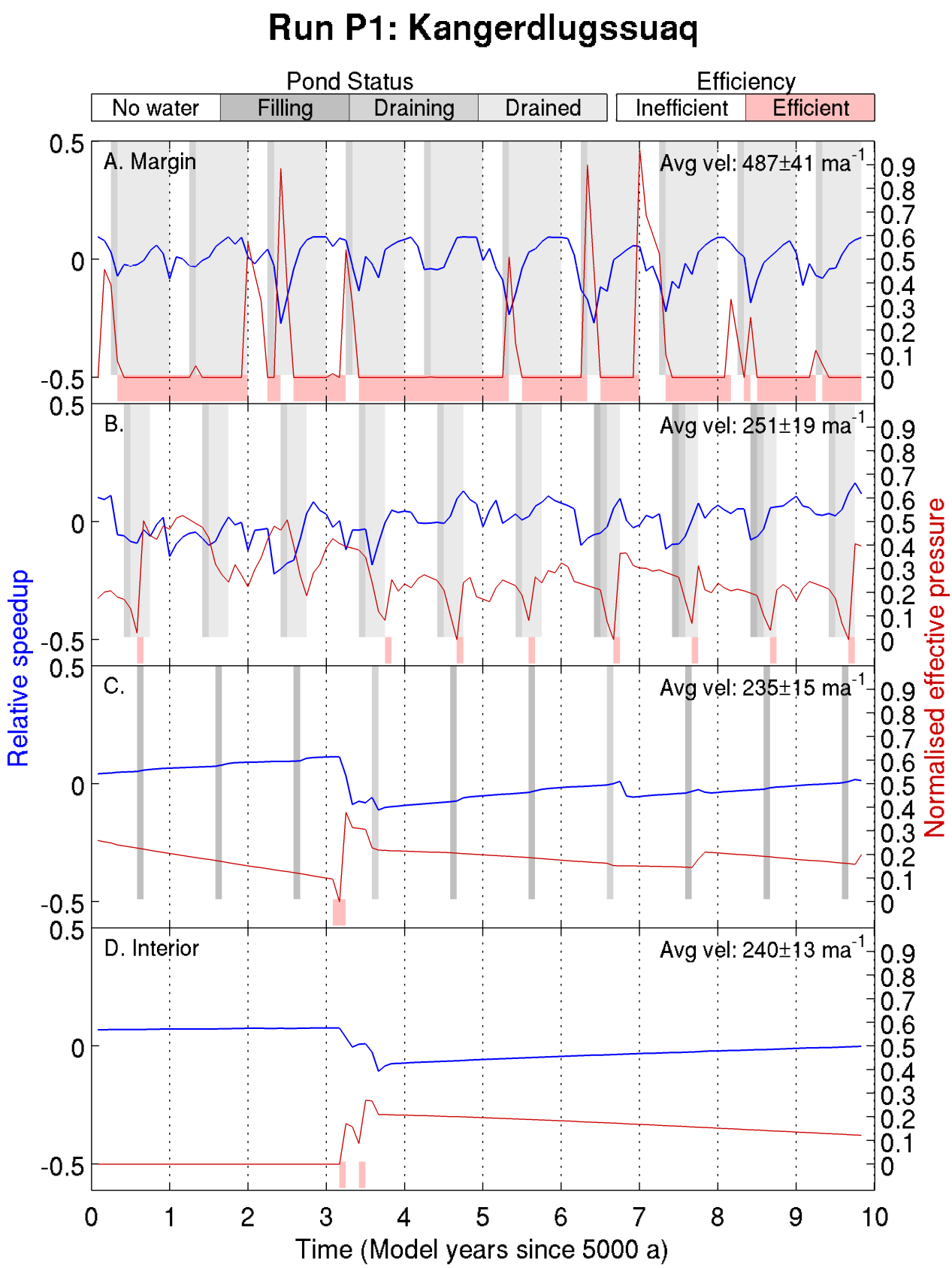

Figure 5.21 Run P1, Transect 5: Kangerdlugssuaq (marine-terminating). Relative basal speedup (blue line), showing pond draining (grey background), normalised effective pressure (red lines), and efficient bed (red background).

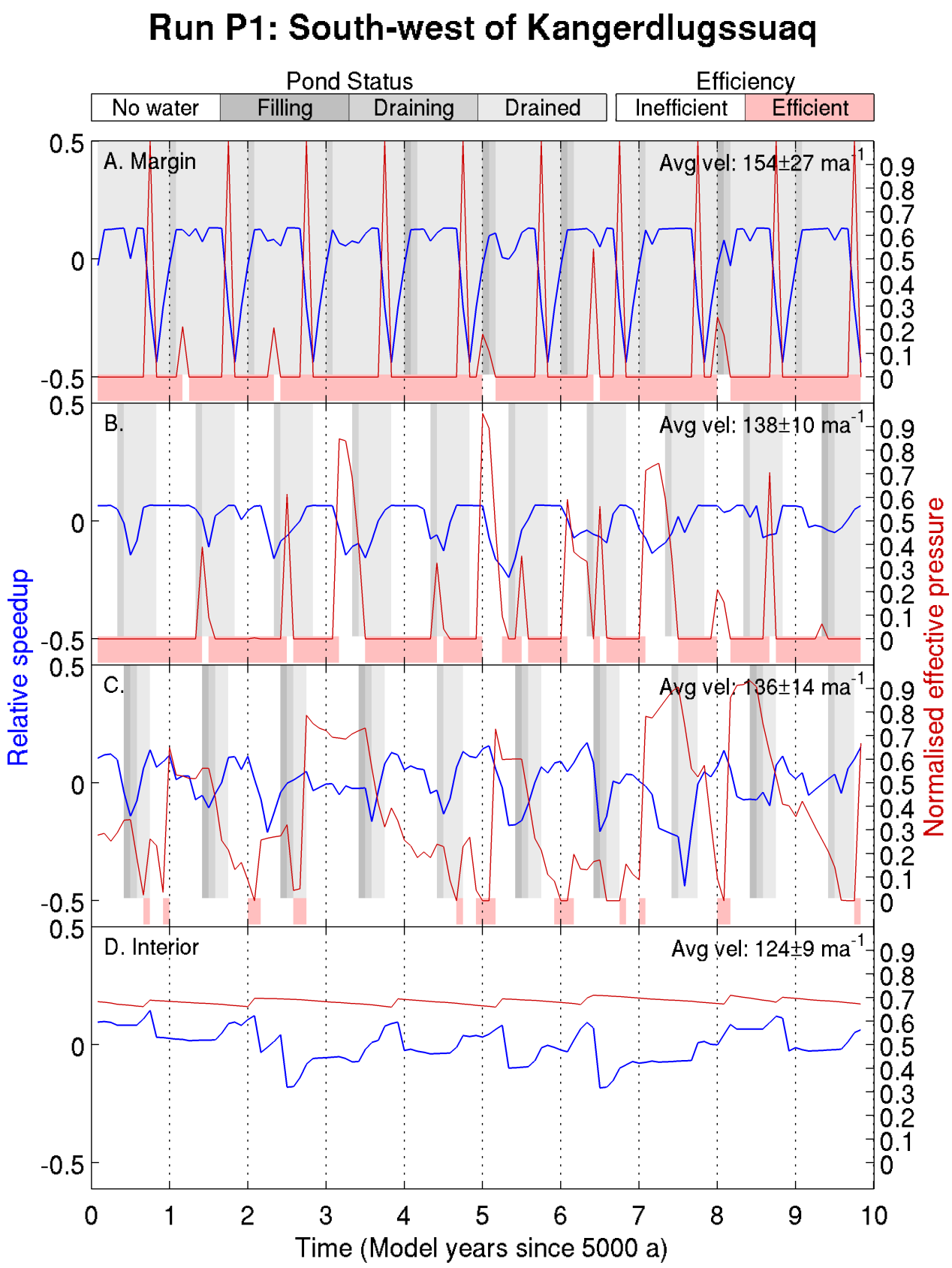

Figure 5.22 Run P1, Transect 6: South-west of Kangerdlugssuaq (land-terminating). Relative basal speedup (blue line), showing pond draining (grey background), normalised effective pressure (red lines), and efficient bed (red background).

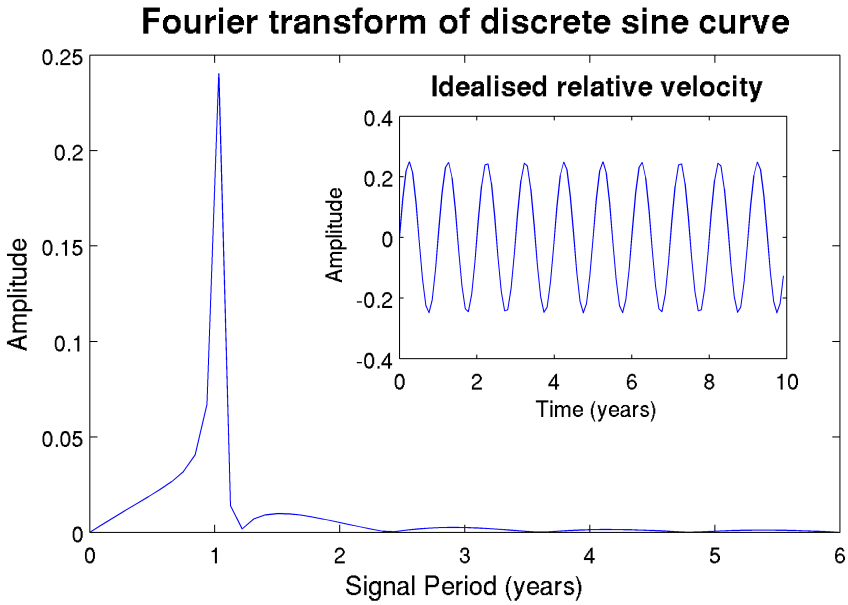

Figure 5.23 Discrete Fourier transforms of relative velocity data are used to analyse results. This plot shows the Fourier transform of a sine curve ($y = 0.25\sin(2\pi t)$, inset) in order to understand the inherent features of the idealised system. Sinusoidal data are sampled monthly over a ten-year period. Note that the Fourier transform has a distinct peak at 1 a which corresponds to the input signal's period. There are no other significant peaks, but the signal is broad due to the coarse, discrete sampling and there is noise for periods shorter than 1 a. The amplitude of the transform corresponds to the amplitude of the inital signal.

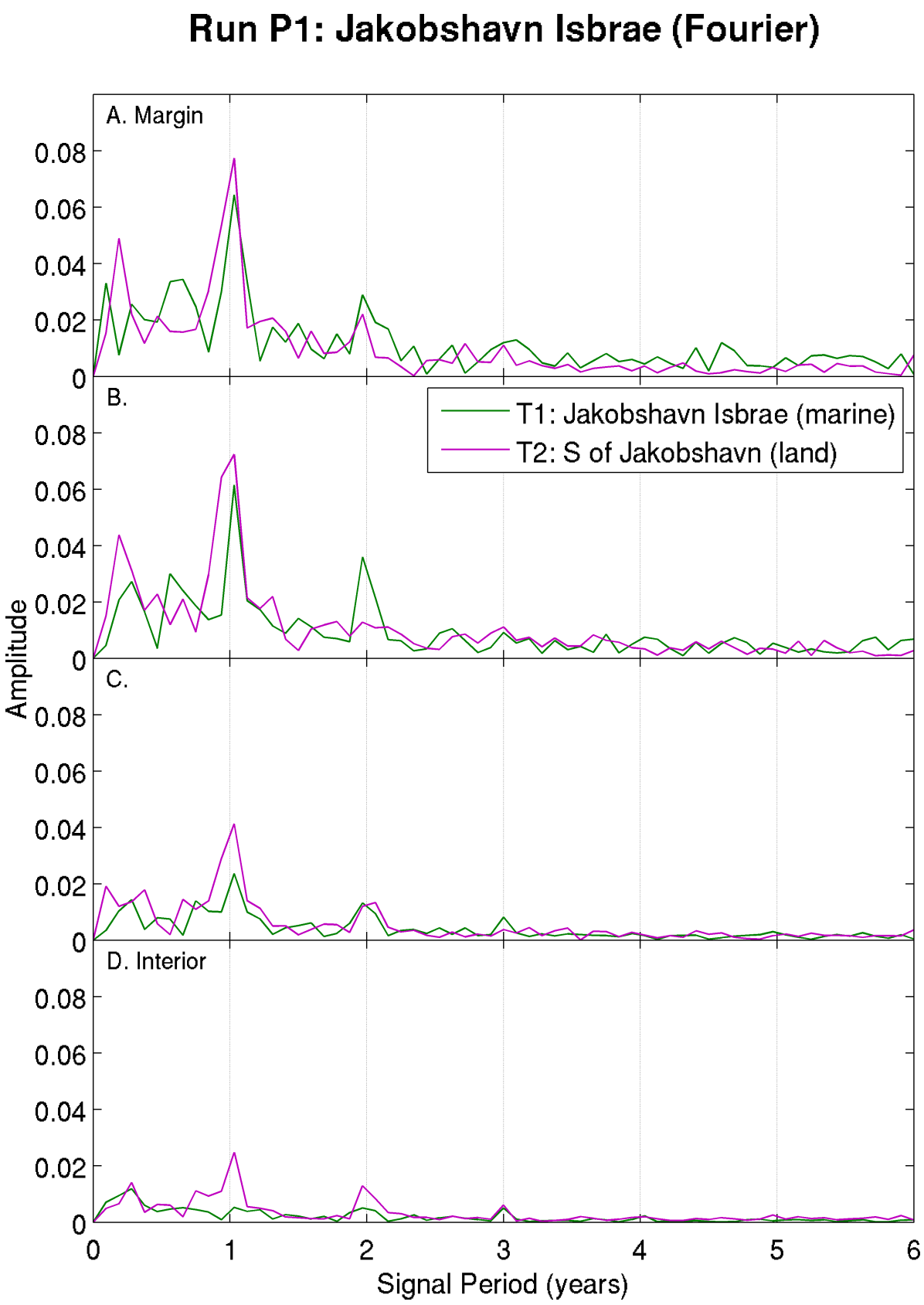

Figure 5.24 Run P1, Transects 1 and 2: Fourier-transform plots for Jakobshavn Isbræ transect pair. The amplitude of the transform gives the strength of each period. There is a strong 1 a seasonal signal which gets weaker further inland.

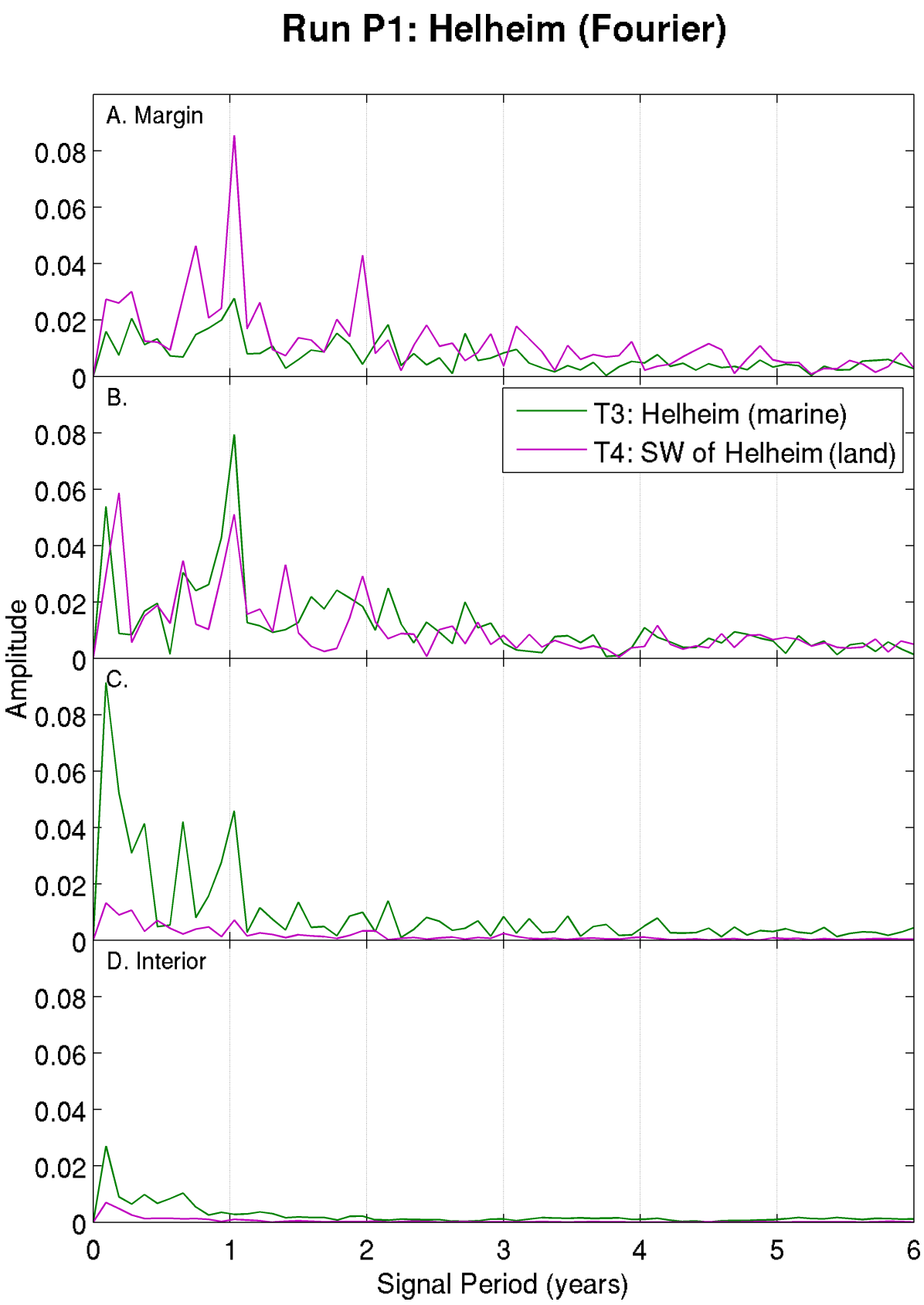

Figure 5.25 Run P1, Transects 3 and 4: Fourier-transform plots for Helheim transect pair. See Figure 5.24 for explanation.

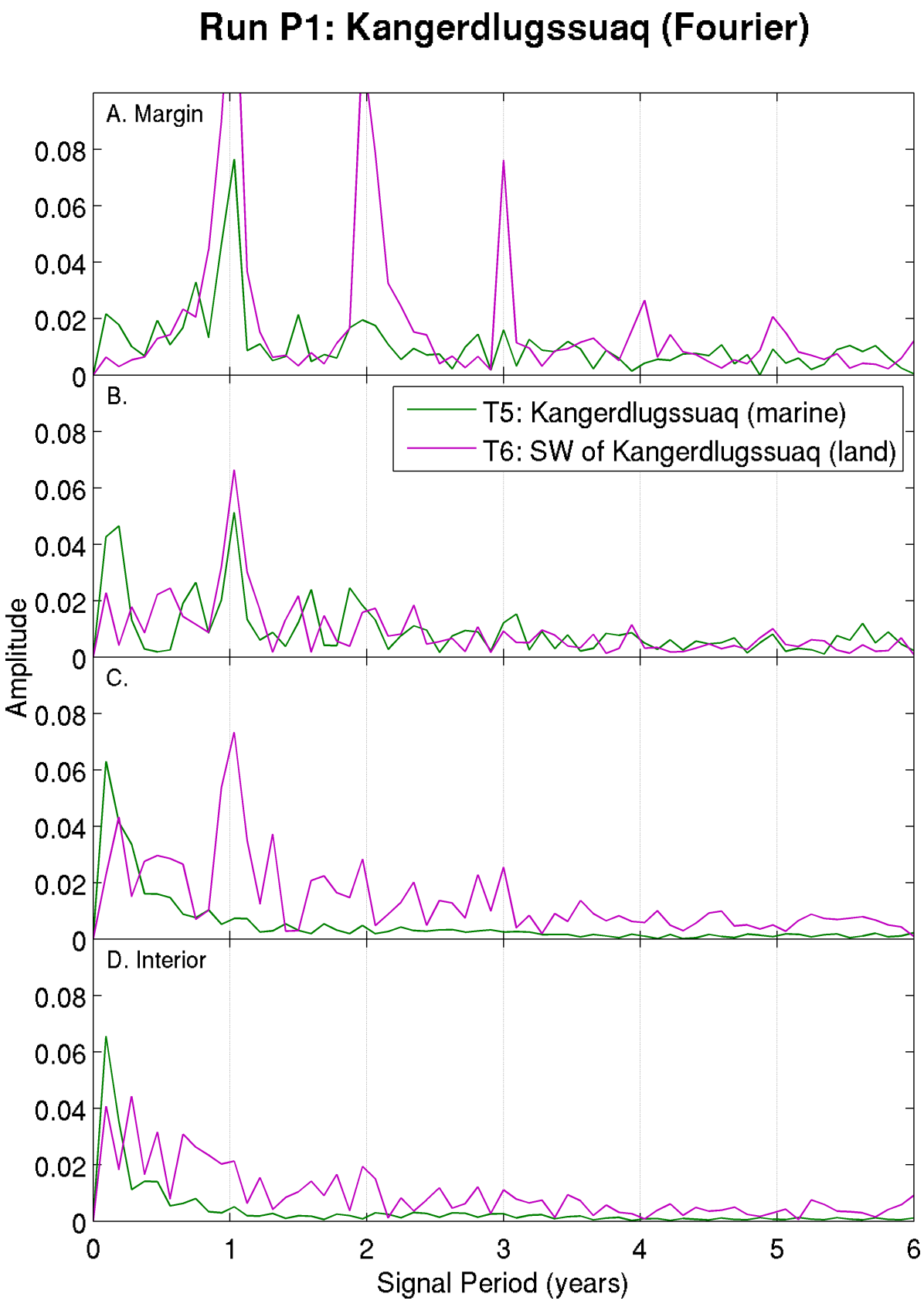

Figure 5.26 Run P1, Transects 5 and 6: Fourier-transform plots for Kangerdlugssuaq transect pair. See Figure 5.24 for explanation. There is a lack of a 1 a seasonal signal for the marine-terminating glacier away from the margin; this signal is still present for the land-terminating glacier cells A–C.

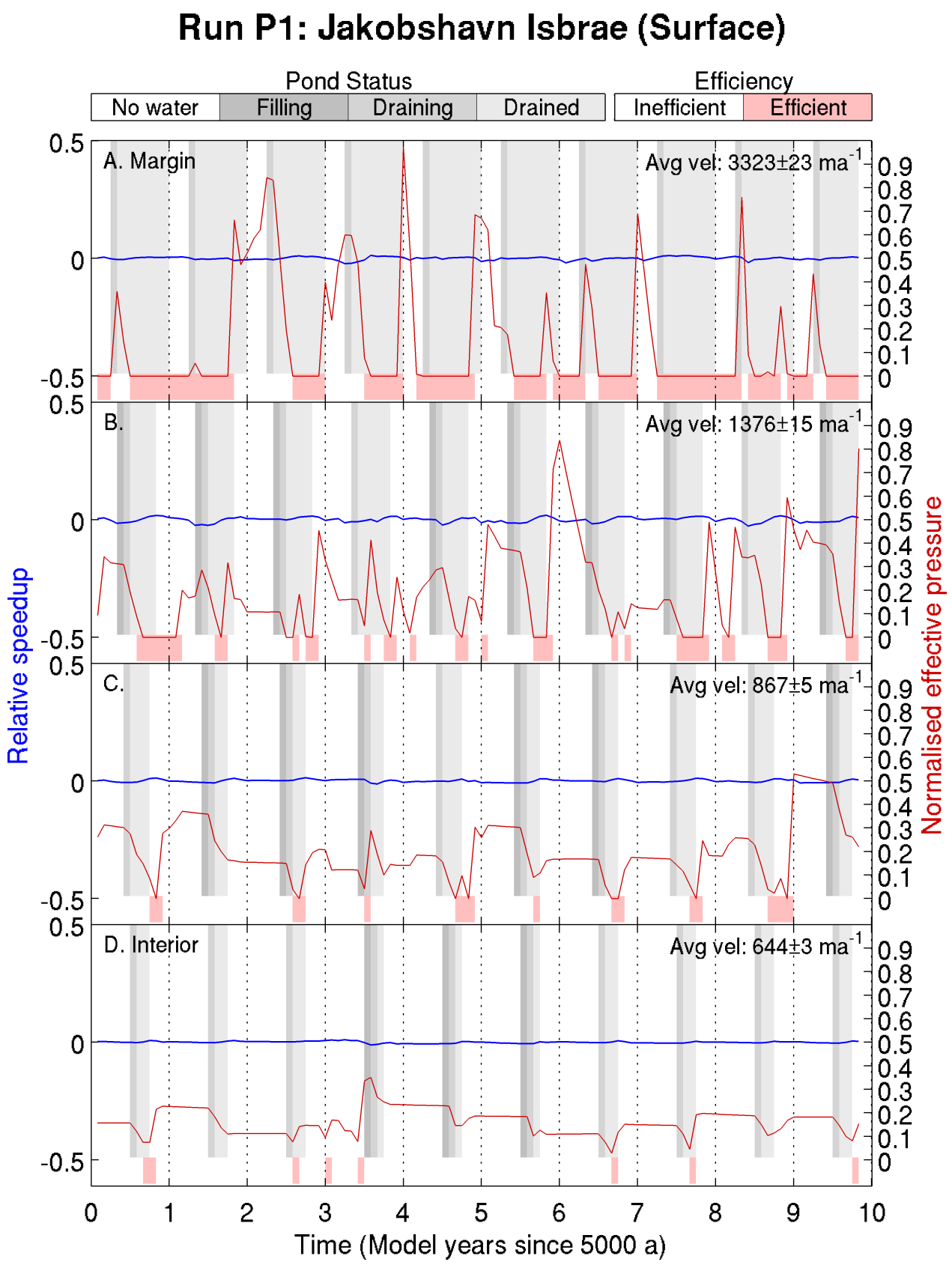

Figure 5.27 Run P1, Surface Transect 1: Jakobshavn Isbræ (marine-terminating). Relative surface speedup (blue line), showing pond draining (grey background), normalised effective pressure (red lines), and efficient bed (red background).

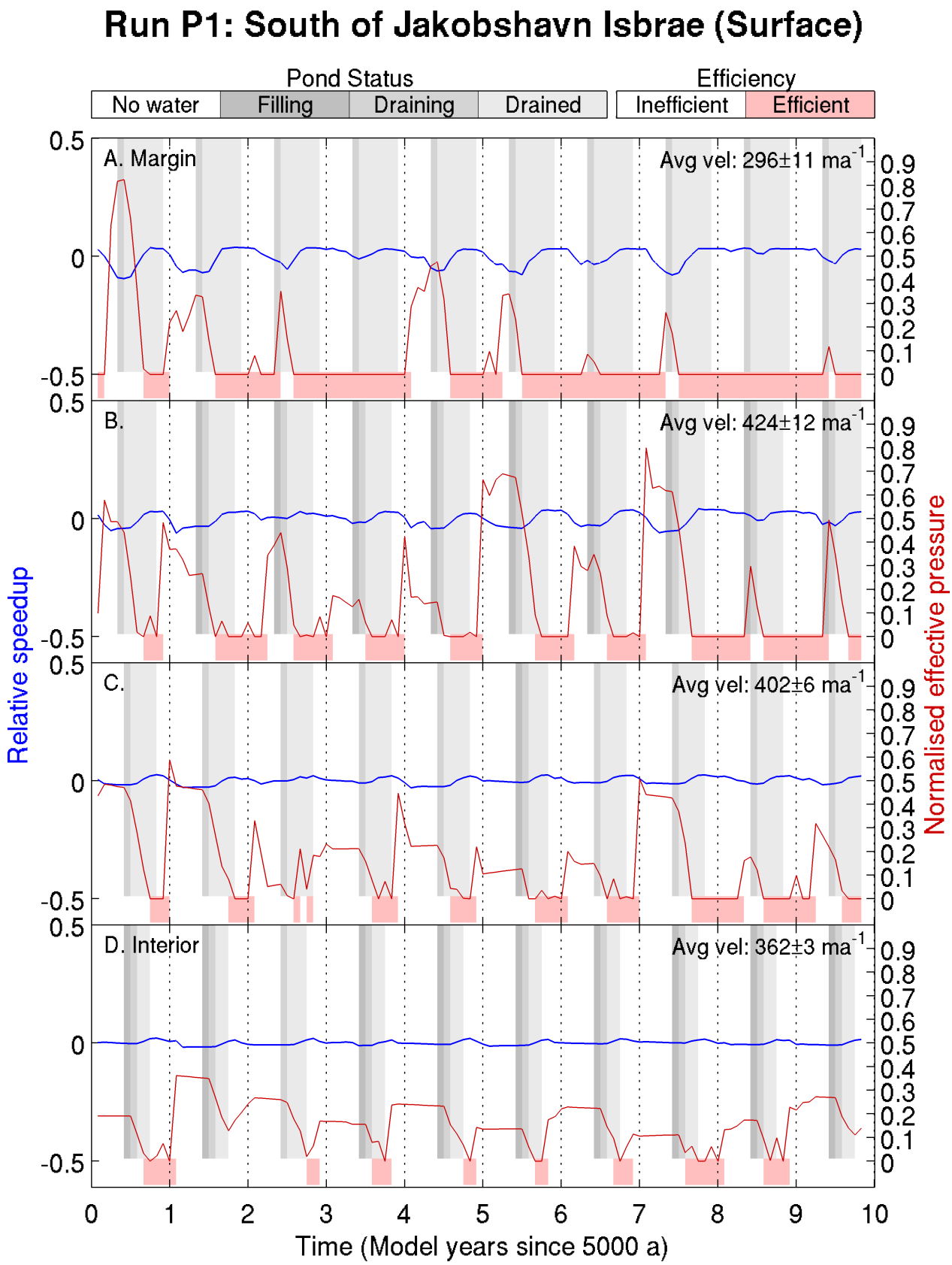

Figure 5.28 Run P1, Surface Transect 2: South of Jakobshavn Isbræ (land-terminating). See Figure 5.27 for explanation.

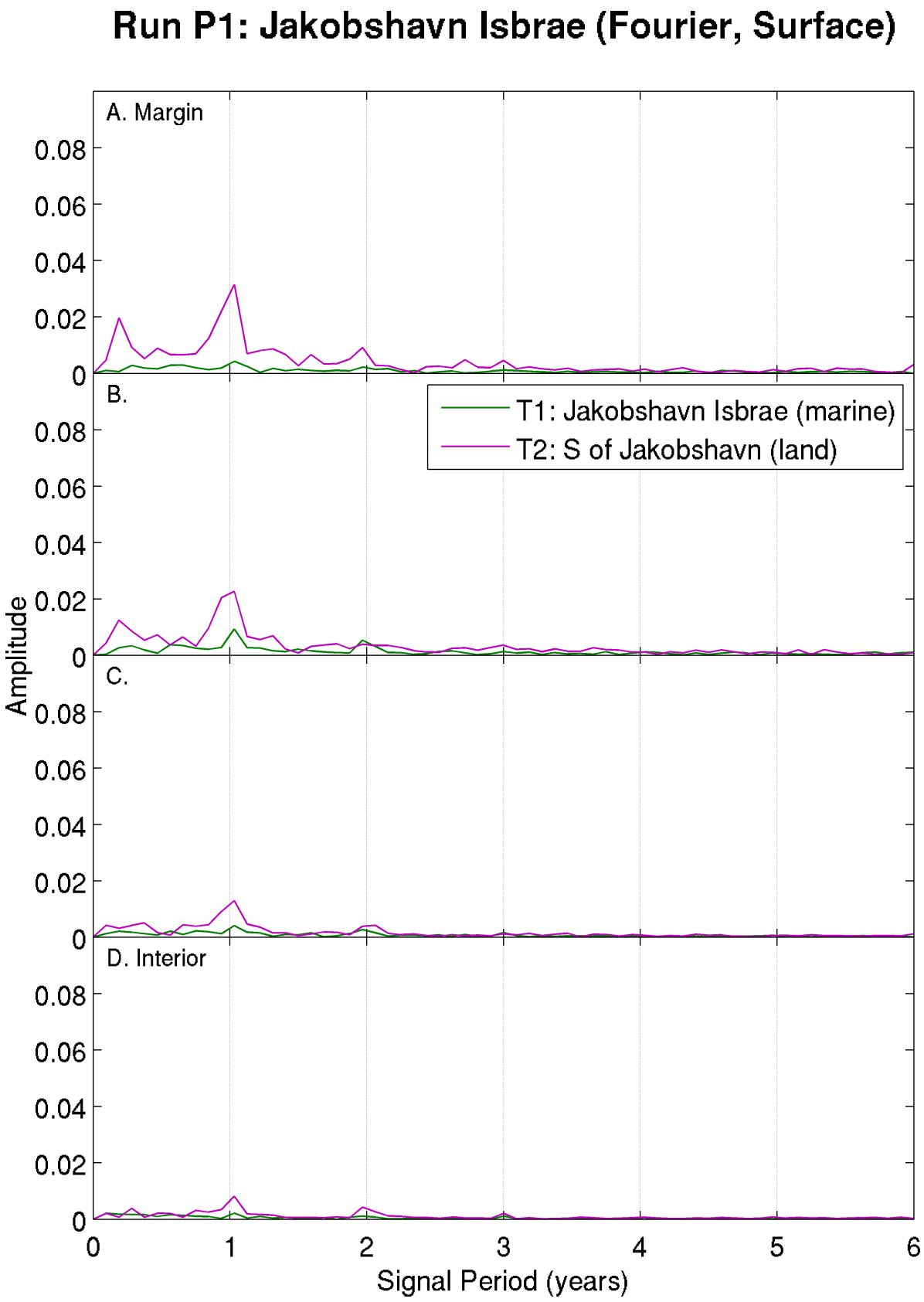

Figure 5.29 Run P1, Transects 1 and 2: surface Fourier-transform plots for the Jakobshavn Isbræ transect pair. The amplitude of the transform gives the strength of each period. Note that the 1 a is much more distinct that the equivalent basal speedup plot (Figure 5.24).

5.5.5 Discussion

This section discusses the main features of the data presented in Section 5.5.4. The processes responsible for these features are discussed in more detail in Section 5.5.6.

The first result is that a seasonal signal is captured when the surface-to-bed magnification factor $\omega = 10$ is used; all further discussion relies on the presence of this seasonal signal. The behaviour of the model shows distinct behaviour as one travels up each transect, due to a variety of factors including less surface water and thicker ice. The key result is that land- and marine-terminating glaciers are modelled to behave differently and, within the constraint of the scaling issues, appear to support observations. To date, no sufficient explanation for this disparity in behaviour between land- and marine-terminating has been proposed.

Seasonal signal

The model, with the artificial $\times 10$ scaling factor, captures a seasonal signal. The maps plotting relative basal speedup in Figure 5.14 as well as the velocity and Fourier transect plots support this. The nature of the signal varies from reasonably smooth (T2.A, T3.B) to more irregular (T5.A), to capped by effective pressure and basal shear stresses (T6.A–B). This is also seen in the Fourier plots by additional noise for the more irregular ones, but each transect shows a 1 a peak, indicating a seasonal signal. As the transects are traversed upglacier, the seasonal signal becomes less pronounced. Occasionally cell B appears more seasonal visually than cell A. For example, compare the relative velocity plots of T3.A and T3.B (Figure 5.19). This is due to overall lower effective pressure nearer the margin due to thinner ice.

Basal hydraulic efficiency evolves on a seasonal basis as well. The maps in Figure 5.15 show the minimum and maximum efficiency in a typical model year. Figure 5.16 plots the total efficient area under the ice over the last ten years of the model run. The efficient area reaches its minimum in March and it maximum in September. The decline seems to take an unrealistically long time given that surface water flux stops reaching the bed in November but the minimum is in March. This may indicate that the treatment of bulk-diffusivity in HYDRO needs improvement. When an area is efficient water should escape quickly, but the model set-up perhaps does not allow this to happen quickly enough. Possible improvements to the model are discussed in Chapter 6.

There is a minor peak in the efficient area every year during May. Disappearing seasonal ice is responsible for this. Because seasonal ice is very thin, it does not take much water for the efficiency condition to be reached. Therefore most of the seasonal ice becomes efficient rapidly and when it disappears in June there is a temporary drop in total efficient area under the ice.

It is worth noting that the run P32, without any surface melt input, also displays a seasonal change in basal efficiency, Figure 5.30. This is due to the yearly formation and melt of margin ice as already discussed. To a lesser extent, thinning of ice may also help trigger the efficiency condition due to it affecting the effective pressure. The shape of the curve is spiky instead of sinusoidal due to the differing primary control on efficiency.

Transects

The nature of the seasonal signal changes as transects are traversed inland. The winter-average velocity begins to dominate while the summer speedup becomes short-lived (eg T2.D); the signal becomes noisy (eg T3.C) or loses the seasonality altogether (eg T5.C). There is no evidence of a seasonal speedup where no ponds drain in a given cell (eg T3.D, T4.D, T5.D). By contrast, T6.D shows strong variability in velocity, though not seasonal, for no obvious reason. This lack of seasonal speedup shows that, within the model set-up (including run P21 with surface-to-bed magnification factor $\omega = 20$), inland cells are not affected by draining ponds (Question 5).

The smaller signal uptransect is due to a shorter melt season, which greatly reduces the water reaching the bed because the melt rate and duration are less. The system transmits these smaller perturbations downglacier without much difficulty and returns to its initial state.

This lack of response upglacier from a draining lake is due to the relatively small volumes of water reaching the bed. This means that the overall pressure gradient towards the margin is maintained and back-pressure is not a problem. At smaller scales, this effect may become more apparent but at the 10 km scale there is no evidence.

There are two modes to the seasonal development of efficiency along a transect. One, efficiency progresses upstream through the melt season, for example years 1 to 3 on Transect T2 (Figure 5.18). Two, much of the transect becomes efficient at the same time, for example years 6 to 8 on Transect T1, (Figure 5.17). Mode one is caused by lakes draining in increasingly

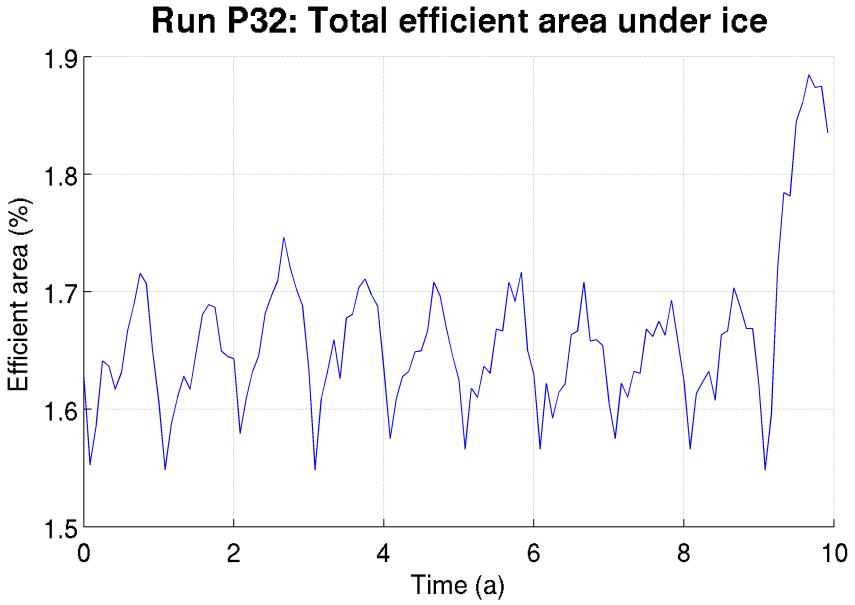

Figure 5.30 Without any surface water reaching the bed, the model still displays a cyclic pattern in total efficient area. In run P32, the model is set up as for the full-friction run at the end of Chapter 4 and forced with the ELA definition used in this chapter. The resulting change in ice area, the temperature diffusing through to the bed near the margin, and the friction feedback already discussed all contribute to the observed signal.

In some regions, an efficient bed does not form every year as there is insufficient basal water. These regions become primed over a number of years and then become efficient. This is the reason for the large increase in efficiency at the end of the run.

higher elevation bands throughout the melt season and therefore water injection further upglacier triggering the efficiency condition. Mode two occurs when the cell pressurises upglacier before the downstream cell connects to the efficient network. Only cells connected to a downstream efficient network are allowed to become efficient due to the model set-up. When the downstream cell does become efficient it releases the pressure in a number of upstream cells simultaneously.

Land- and marine-terminating comparison

I now compare land- and marine-terminating transects. As discussed in Section 3.2, this terminology is adopted for ease of language. The feature driving the physics is the deep subglacial trough under the marine-terminating outlet glaciers. This trough may be there because of fjord-creating feedbacks, which in turn may depend on the fact that the glacier is marine-terminating. The physics in this discussion are only dependent on the fact that the

water converges in the trough as identified in Chapter 3.

As hypothesised, based on Chapter 3, land- and marine-terminating glaciers respond differently to a seasonal signal. This may provide an explanation to the behaviour commented on by Echelmeyer and Harrison (1990) and Hughes (2009) for Jakobshavn Isbræ and by Howat et al. (2007) for Helheim and Kangerdlugssuaq.

While the magnitude of the basal sliding speedup appears similar in the run P1, the seasonality of each transect does not. The Fourier transects show this well. In Figure 5.24, the land-terminating glacier (T2) has a clear 1 a peak for all cells, while Jakobshavn Isbræ (T1) only has a strong 1 a peak in cells A and B. For all cells, the land-terminating glacier has a higher amplitude speedup than Jakobshavn Isbræ. The relative velocity plots also support this with T1 (Figure 5.17) showing a visually noisier and less seasonal signal than T2 (Figure 5.18). As expected, the amplitude of the seasonal signal diminished inland, but on Jakobshavn Isbræ this decay is stronger.

This polarity in behaviour is even stronger for Kangerdlugssuaq. The Fourier transect (Figure 5.26) shows a large 1 a peak for the land-terminating glacier (T6.A–C) while only the margin cell of the marine-terminating glacier (T5.A) has a 1 a peak. Upglacier from this, short lived noise dominates the T5 signal. Again, this is also apparent from Figures 5.21 and 5.22, where the land-terminating transect shows a more seasonal signal. The situation is slightly complicated by the fact that T5.C–D do not have regular draining lakes, however T5.B does and this cell does not have a 1 a peak in the Fourier plot negating the T5.C–D issue. The 2 and 3 a peaks for T6.A are due to the top-hat nature of the velocity function[9].

Surface velocities (Figures 5.27–5.29) make this even clearer, because the internal deformation of the ice magnifies the signal because the shallow ice approximation treats the bed as grounded. While this is incorrect physics, it helps, for the moment, to interpret the results. In order to help this analysis, I define the *polarity of speedup* Υ as the land speedup amplitude divided by the marine speedup amplitude. Numbers greater than one show that land-terminating ice has a larger relative speedup than neighbouring marine-terminating ice. The *average polarity* $\bar{\Upsilon}$ is the mean of the polarity of all cells on a transect. Table 5.3 shows the average polarity for the surface and basal speedup of the three transect pairs.

While the average basal sliding speedup polarity $\bar{\Upsilon}$ ranges from 0.9 to 2.3 for Helheim

[9] The Fourier transform of a pure top-hat function ($y = 1$ if $|x| < 0.5$, 0 otherwise) is the sinc function $(\sin(2\pi x)/\pi x)$. For a periodic top-hat function, which T6.A approximates, this gives a diminishing peak on the whole-year signal periods.

Run P1 transect polarity ($\bar{\Upsilon}$)

Region	Surface $\bar{\Upsilon}$	Basal $\bar{\Upsilon}$
Jakobshavn Isbræ	3.8	1.4
Helheim	5.3	0.9
Kangerdlugssuaq	13.8	2.3

Table 5.3 The average polarity of each transect pair shows a much stronger modelled seasonal speedup for land-terminating ice than marine-terminating ice. While this is apparent for basal sliding speedup, it is especially noticeable for the surface velocity speedup.

and Kangerdlugssuaq, the average surface speedup polarity ranges from 3.8 (Jakobshavn Isbræ) to 13.8 (Kangerdlugssuaq), showing a very distinct surface speedup for ice adjacent to outlet glaciers. The maximum polarity Υ (cell A, margin) reaches 34.0 for Helheim and 35.0 Kangerdlugssuaq. The role of the ice column in amplifying this signal is discussed in the Ice Rheology subsection of Section 5.5.6.

The key point here is that due to the water convergence demonstrated in Chapter 3 in the subglacial trough of outlet glaciers and due to the ice rheology, outlet glaciers show a muted response to surface water reaching the bed. This is partially due to the already lower effective pressures in these regions. It is also due to, at least in Glimmer-Hydro, converging water arriving with a delay from lakes draining upstream which causes the speedup to be noisier. The ice column removes this noise, but amplifies the surface speedup, to make the land-marine polarity even clearer.

The significance of marine-terminating glaciers showing a limited response to surface melting is that, in effect, this mechanism caps, or at least reduces, the increase of dynamic ice loss from Greenland for a given increase of surface melt water reaching the bed. Greenland loses approximately two-thirds of its ice dynamically through its outlet glaciers (Rignot and Kanagaratnam, 2006). The remainder of the mass is lost through surface melt. If outlet glaciers show a reduced dynamic response to draining surface lakes, as observations and this work suggest, then the future of the ice sheet appears more secure. A warmer climate may still increase dynamic ice loss, by affecting the rheology of ice for example or by increasing the area of fast ice, but perhaps it will have a lesser effect than previously thought on the basal boundary conditions of outlet glaciers which are already flowing quickly. Long term sensitivity studies incorporating this process are needed.

Due to Glimmer-Hydro's large scale and lack of higher order physics it is impossible to

fully simulate the dynamics of fast-flowing ice. It is difficult to say what effect longitudinal stresses will have on the observed polarity between land- and marine-terminating ice but the essential idea should remain the same. The basal boundary condition is unaffected by higher-order ice physics, except for some melting feedbacks, and therefore the basal slipperiness t_s parameter, calculated from effective pressure $\bar{N}$, is also unaffected. Basal shear stress, the other variable used to calculate sliding velocity, is affected as is the transfer of any basal speedup to the surface through the ice column. However, ignoring these effects gives a reasonable approximation to the behaviour I am interested in. When the ice sheet model incorporates better physics the experiment can be re-run to understand its effects.

Further evidence of land-marine polarity is discussed in Section 5.5.6.

Interannual

There is no substantial evidence that interannual speedup is a result of hydrology (Question 7). My hypothesis was that water may take longer than a single melt season to evacuate, perhaps because efficient basal conditions do not form annually, leading to increased winter velocities in some years. An example of this may possibly be seen between 2–4 a of T4.A in Figure 5.20 but this is inconclusive. In this example, there appears to be enough water over two winters to sustain efficient hydraulic flow.

5.5.6 Processes

The base run, with a surface-to-bed magnification factor of $\omega = 10$, shows a clear seasonal speedup and evolution of efficiency. Marine-terminating outlet glaciers show less seasonality than their land-terminating counterparts. This section explores the sensitivity of the system to model parameters and looks at the physical processes responsible for the modelled speedup.

Three main factors control the behaviour of the modelled speedup: diffusivity, hydraulic efficiency, and frictional heat generation. Each of these are affected by a number of the model parameters but the key to understanding the behaviour of the system are the general processes. It is also necessary to understand the complexities added by the ice column to interpreting surface velocity data. The nature of the ponding, as long as it is present, does not greatly affect the model behaviour when maximum pond depths are constrained realistically.

Ponding

The nature of the ponding does not have a large effect on modelled behaviour because of the small pond volumes before draining. I test this using three methods: a control run without any ponds; passing all surface melt directly to the bed without ponding; and changing the surface-to-bed magnification factor ω.

Control: No surface water

Without any ponding (run P32) there is a very slight seasonal basal speedup. For example, cell A of the Jakobshavn Isbræ Fourier-transect has a 1 a amplitude of 0.0013, compared with 0.078 when surface water is included (run P1). The speedup is a result of monthly temperature changes affecting ice rheology, shear stress, and basal temperatures and therefore basal melt rate. The warm summer climate reduces ice thickness which affects shear stresses and, possibly more importantly, the pressure melting point at the ice bed as well as effective pressure calculations. Where the ice is thin, surface heat can also diffuse to the bed of the ice sheet. These processes combine to provide a low-magnitude speedup of ice in the summer.

Interestingly, without a surface signal Hydro does not form an efficient bed each year as there is not sufficient water. One of the model set-up conditions is that for an efficient network to form the efficient area must connect to the margin. This lets the system become primed to become efficient over much larger areas than experienced with a surface signal. Sufficient water builds up over time and the trigger is reached simultaneously for a number of cells (final year, Figure 5.30).

The seasonal speedup, when there is no surface signal, is very small and any surface melt water that passes to the bed overrides it.

Straight to bed

Conceptually, ponding may affect ice dynamics because it allows a larger water flux to reach the bed compared to passing water directly to the bed in the model without ponding first. This may cause a more significant response in Hydro. In practice, with the maximum pond depth $d_{p\max} = 0.1$ m used in the base run, ponding does not play a significant role. Physically, of course, ponds are very important because they are key to opening the connection from the surface to the bed (eg Alley et al., 2005b; Van der Veen, 2007).

Run P33 passes all surface melt straight to the bed without ponding but the model output is very similar to the base run. This is due to a number of interconnected reasons:

1. Because the maximum pond depth is small in the base run, water only ponds for one or two months before draining. The summer melt season, especially nearer the margin, lasts for longer than this so maximum surface melt is after the pond has drained. Therefore the ponding, in the modelled case, does not bring significantly more melt water to the bed than will happen later in the season.

2. Because the ponds drain two or three months into the melt season, the bed only misses out on one or two months of surface melt when ponding is allowed. The system takes time to diffuse the new water downstream so a one month delay in receiving the water does not significantly affect the basal conditions.

3. The model scale of $100\,\mathrm{km}^2$ grid squares diffuses any effect of the ponds. The magnification factor of $\omega = 10$ attempts to compensate for this, but this parameter was chosen to show a response, not for a more robust reason. In reality, or if the model operated on a smaller scale, then the increased delivery from ponding may have a larger effect locally. Currently any such effect is averaged out over a large cell.

Drainage magnitude

Varying the surface-to-bed magnification factor ω helps understand local effects which may get masked by the scaling. It also gives an indication to the importance of the volume of water reaching the bed from the surface. The purpose of these runs is not realism, but to look at how significant water volumes are likely to be when applied to a small area.

Figure 5.31 plots the relative speedup and its Fourier transform for cell A of the Jakobshavn Isbræ transect pair for $\omega \in \{5, 10\}$. Key things to note are that as ω increases: the variability of the system increases and the system becomes less smooth, and marine-terminating ice exhibits a smaller speedup while land-terminating ice exhibits a larger speedup. The increased variability is caused by extra water causing more frequent fluctuations in hydraulic efficiency.

Table 5.4 gives the basal speedup factors for cell A of the six transects for $\omega \in \{5, 10, 20\}$. For $\omega = 5$ marine-terminating glaciers show a larger speedup at the margin than land terminating glaciers (polarity[10] $\Upsilon < 1$ for Jakobshavn Isbræ and Kangerdlugssuaq). As ω

[10] *Polarity of speedup* is defined in Section 5.5.5 as the land-terminating ice speedup 1 a amplitude divided by the marine-terminating ice speedup 1 a amplitude. Numbers greater than one show that land-terminating ice has a larger relative speedup than neighbouring marine-terminating ice.

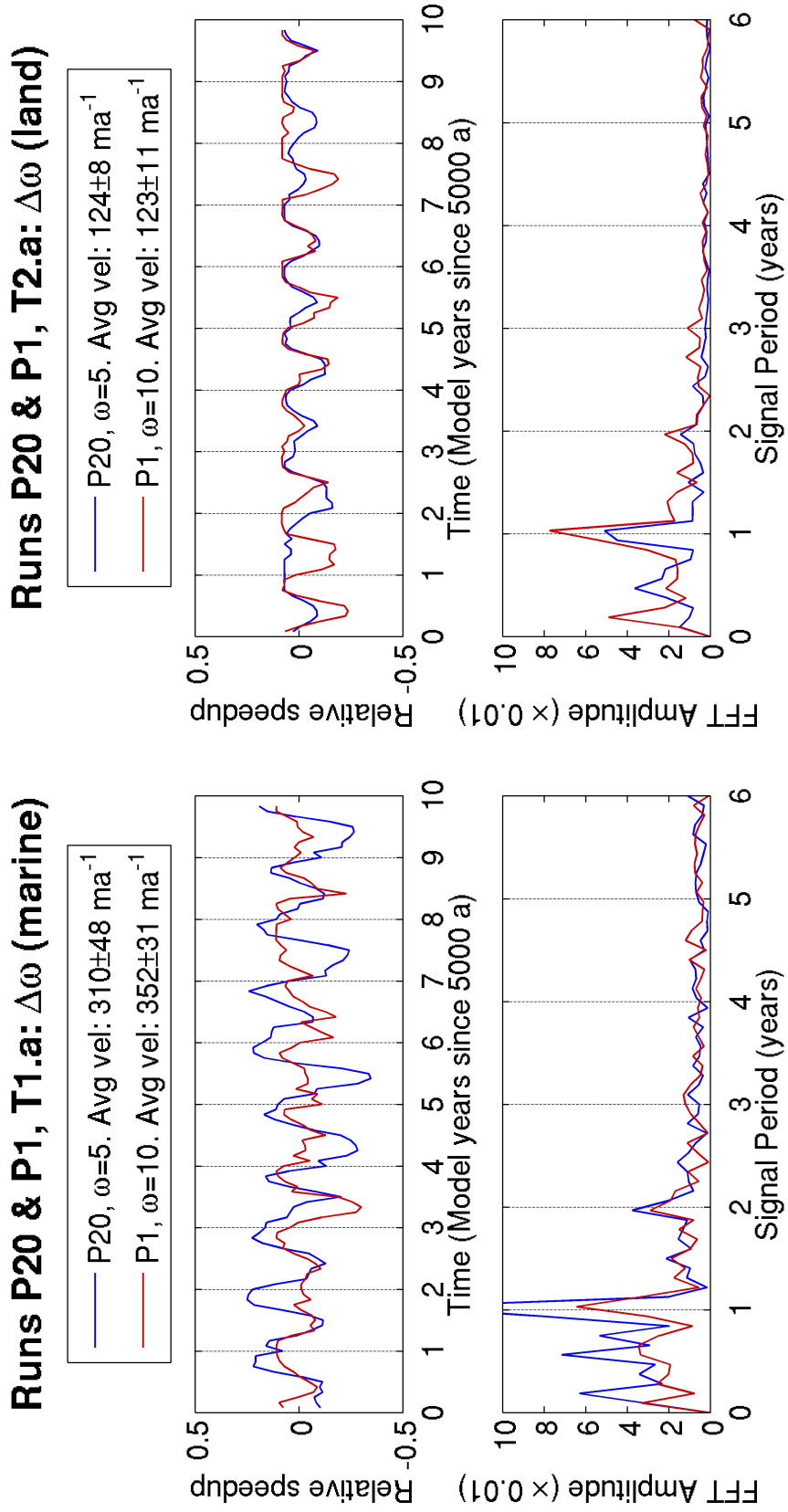

Figure 5.31 The system is sensitive to the surface-to-bed magnification factor ω. This plot compares Cell A of the Jakobshavn Isbræ transect pair for $\omega \in \{5, 10\}$. Note that the signal is smoother with $\omega = 5$. As ω increases, the 1 a peak decreases for marine-terminating ice, but increases for land-terminating ice.

1 a Speedup Amplitude

ω	Marine	Land	Polarity
	Jakobshavn Isbræ		
5	0.150	0.051	0.34
10	0.064	0.077	1.20
20	0.047	0.035	0.74
	Helheim		
5	0.069	0.161	2.35
10	0.028	0.085	3.08
20	0.027	0.033	1.25
	Kangerdlugssuaq		
5	0.110	0.052	0.47
10	0.077	0.155	2.03
20	0.032	0.160	5.01

Table 5.4 The 1 a period Fourier speedup amplitudes are shown for cell A of the three transect pairs for surface-to-bed magnification factors $\omega \in \{5, 10, 20\}$. The polarity between land- and marine-terminating glaciers is defined here as the land speedup amplitude divided by the marine speedup amplitude.

increases ($\omega = 10$), more water enters the system from the surface. This leads to an increase in the land speedup but a decrease in the marine speedup ($\Upsilon > 1$ for all transect pairs). This is further evidence that the convergence of water under outlet glaciers is the process responsible for the polarity of speedup.

As ω increases further to presumably unrealistic volumes ($\omega = 20$), water overwhelms the system. At this point, land-terminating ice begins to behave more like marine-terminating ice and the speedup amplitude drops for Jakobshavn Isbræ ($\Upsilon < 1$) and Helheim ($\Upsilon > 1$). Kangerdlugssuaq, due to its enclosed catchment area, is less affected and its speedup amplitude continues to increase for land-terminating ice and decrease for marine-terminating ice. This leads to a large increase in its polarity ($\Upsilon = 5$).

The change in behaviour towards a marine-terminating system with $\omega = 20$ shows that water entering from the surface is significant. This implies that, on smaller scales, ponds are likely to have a greater effect. Models which attempt to understand these processes are probably better working on a basin-scale instead of the Greenland-wide scale.

Summary

As a process ponds are key for opening the connection, but do not affect ice dynamics in themselves, at least in this study. They are therefore not one of the physical processes that

determine the modelled behaviour. When no surface signal is present a seasonal speedup is observed, but this is much smaller than the one in the base run. The basal hydrology, especially the hydraulic efficiency evolution, behaves very differently. The volume of water reaching the bed is a key control on the dynamics of the system. A corollary of this is that model scale is also an important factor determining the dynamics of the system.

Ice rheology

Ice rheology amplifies the effects of seasonal speedup through the ice column. I have so far focused on basal sliding velocities to remove this extra complexity. However, it cannot be ignored completely as surface velocities are the data collected in field studies. This section, therefore, focuses on how the ice column modifies the seasonal basal sliding speedup.

Surface velocity is an integration of ice deformation through the ice column plus the sliding velocity[11]. Deformation is greatest near the bed. GLIMMER calculates high surface velocities for outlet glaciers, implying that these regions have much higher deformation than land-terminating ice. Figure 5.32 maps the surface velocities when no basal sliding is allowed (run P34). The maximum surface velocities of Jakobshavn Isbræ and Kangerdlugssuaq are in excess of $4\,\mathrm{km\,a^{-1}}$ and $12\,\mathrm{km\,a^{-1}}$ respectively.

Even when no basal sliding is allowed in the model run, there is still a seasonal surface speedup due to the climatic forcing. Figure 5.33 plots the surface speedup Fourier transform for the Kangerdlugssuaq transect pair. This pair shows the strongest seasonal signal for all transects. It is relatively weak, but it is very clear. The amplitude of the 1 a peak for marine-terminating ice is less than that of land-terminating ice. This is due to the high surface velocities of these regions making an absolute speedup proportionally less. Field studies often report seasonal speedup as a percentage of average velocity (eg Howat et al., 2007; Shepherd et al., 2009), so this analysis approach is valid.

This analysis shows that the observed variable speedup of land- and marine-terminating ice are not purely due to basal boundary conditions. However, Section 5.5.5 demonstrated that there is a difference in the basal boundary conditions for these two types of ice leading to varying behaviour for each region. The observed surface speedup is therefore a combination of the two processes. So far the analysis of the experiment has focused on basal sliding data. Figures 5.27–5.29 plot the relative surface speedup and Fourier transects for the

[11] Surface velocity also includes a deforming sediment component, but this is not modelled.

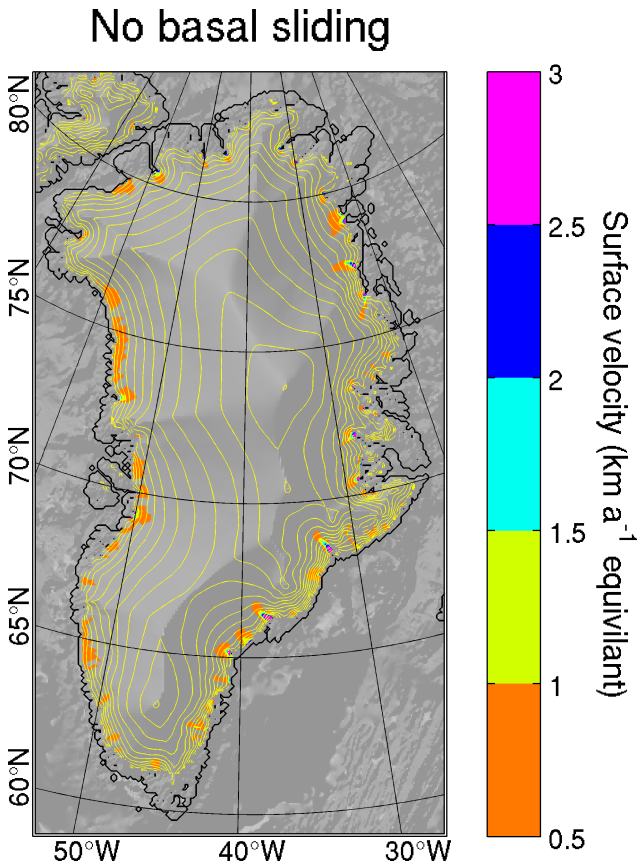

Figure 5.32 GLIMMER calculates high surface velocities ($> 12\,\mathrm{km\,a^{-1}}$ for Kangerdlugssuaq), from internal ice deformation, for marine-terminating ice even when there is no basal sliding allowed. This map plots surface velocities greater than $500\,\mathrm{m\,a^{-1}}$.

The consequence of high surface velocities is that any basal sliding speedup in the main runs become proportionally less distinct for marine-terminating ice. This is not the only reason for the lack of a strong seasonal signal in marine-terminating ice: the basal sliding velocities also show a less distinct speedup in these regions, compounding the effect.

Jakobshavn Isbræ transect pair for the main model run (P1). The primary result is that the land-marine polarity is amplified and now very clear. Noise at the bed is lost through the ice column, compared to the relative basal sliding speedup, leaving a relatively smaller, but clearer signal. Figure 5.29 shows a much more distinct 1 a peak for land-terminating than marine-terminating ice. The secondary result is that the seasonal signal is much larger and noisier than the no sliding case showing both processes do indeed occur simultaneously.

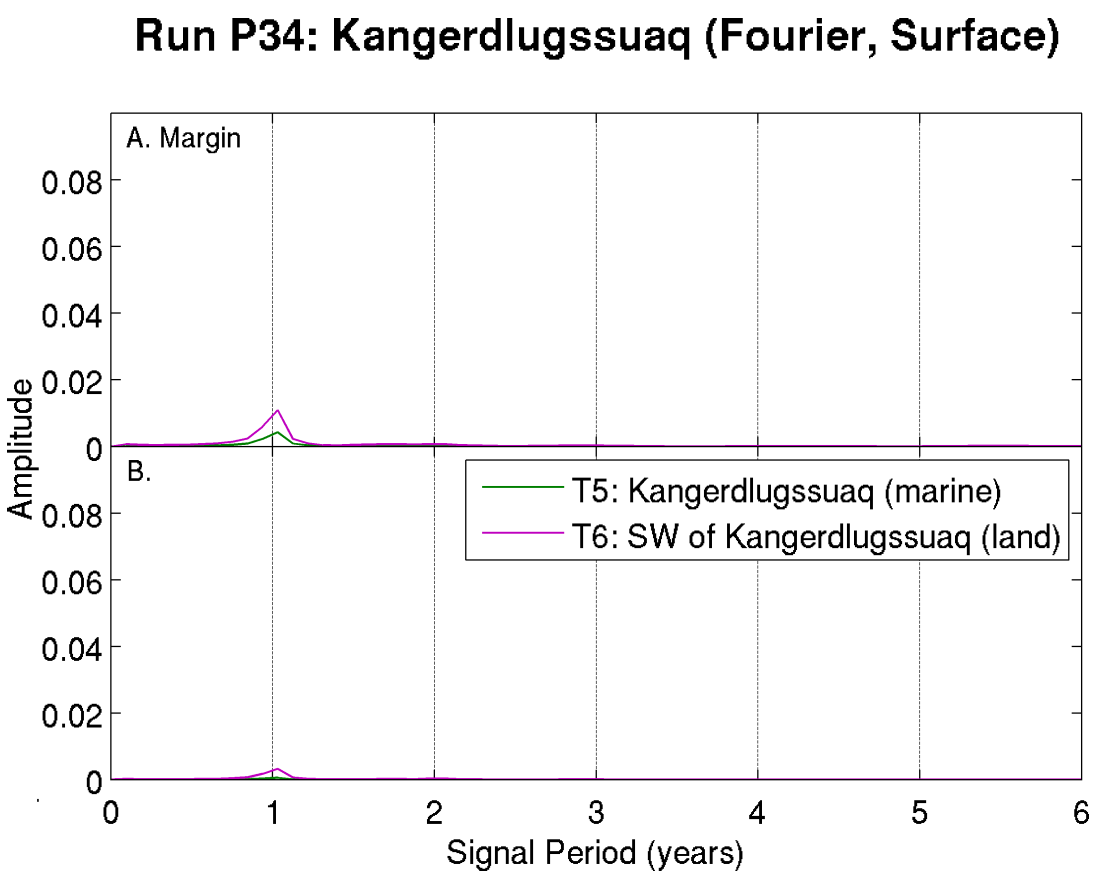

Figure 5.33 Run P34, Transects 5 and 6: surface Fourier-transform plots for the Kangerdlugssuaq transect pair with no basal sliding. Note that there is still a small, but distinct, 1 a peak. Land-terminating ice has a larger peak than marine-terminating ice. All transect pairs show a 1 a peak, but the Kangerdlugssuaq pair's amplitude (0.0110) is twice as large as the Jakobshavn Isbræ (0.0045) and Helheim (0.0052) transect pairs.

Diffusion

As the value of the bulk-diffusivity D increases, the system becomes more responsive because the water finds it easier to flow through the system. This makes the behaviour of the system less seasonal. A given perturbation is dealt with more quickly by water diffusing downstream, but then each cell gets a signal that is a more complex integration of what is happening upstream at the bed. This means that any seasonality, due to the surface signal, becomes increasingly overwhelmed by shorter frequency noise making any annual variation less distinct.

Diffusivity is affected by a number of model parameters including transmissivity $\mathcal{T}$, compressibility c_T, and aquifer depth d. Equation 2.37 shows this relationship: $D =$

$\mathcal{T}/c_T\rho_w gd$. As the individual values vary, it is only the diffusivity that affects water flow in the model set-up because the equation governing HYDRO is reduced to Equation 2.46,

$$\frac{\partial p^*}{\partial t} = D\boldsymbol{\nabla}\dot{\kappa}\cdot\boldsymbol{\nabla}p_t + \phi\ .$$

The source term is $\phi = M/(dc_T)$.

Figure 5.34 compares runs P2 and P3, the Jakobshavn Isbræ region transect pair. In these runs only the transmissivity is varied, but varying the other parameters has the same effect. As D increases, both land- and marine-terminating ice lose seasonality to the point that neither may show any at all, eg Jakobshavn Isbræ. Higher D also introduces more variation to cells that are not connected to the surface (eg T5.D). This may be due to less resistance to back pressure or a more complex signal arriving from upstream.

As D decreases, the polarity between land- and marine-terminating ice increases, with marine-terminating ice showing a weaker speedup. This shows that polarity is indeed due to water flow as there is more water present in the system, especially under the outlet glaciers, when the system is more resistant to flow. All transect pairs in runs which vary diffusivity (P2–7) show this effect. Figure 5.35 shows cell B for the Kangerdlugssuaq transect pair (runs P2–3, vary κ). Varying c_T and d (runs P4–7) produce more complex behaviour because these variables define properties of the aquifer beyond diffusivity through the source term ϕ; this is discussed at the end of Section 5.5.6.

Efficiency

Hydraulic efficiency is very important for the system. Chapter 3 demonstrated that if the bed is not allowed to become efficient then the system is overwhelmed; most temperate regions of the bed reach ice overburden pressure ($\bar{N} = 0$). In that experiment the source term was a constant basal melt rate with no surface signal or temporal variability. Run P18 introduces both of these while not allowing an efficient bed. The result is the same.

Two parameters in HYDRO are responsible for controlling efficiency: the limit p_{limit} at which the condition is triggered, and the efficiency factor ψ which controls the degree of efficiency. Section 3.4.3 demonstrates, for a constant signal, that as ψ increases, an asymptotical limit in its influence is reached. Figure 5.36b plots a cell from runs P16 and P17 (10% change in ψ) showing that this is the case with a seasonal signal as well. The runs

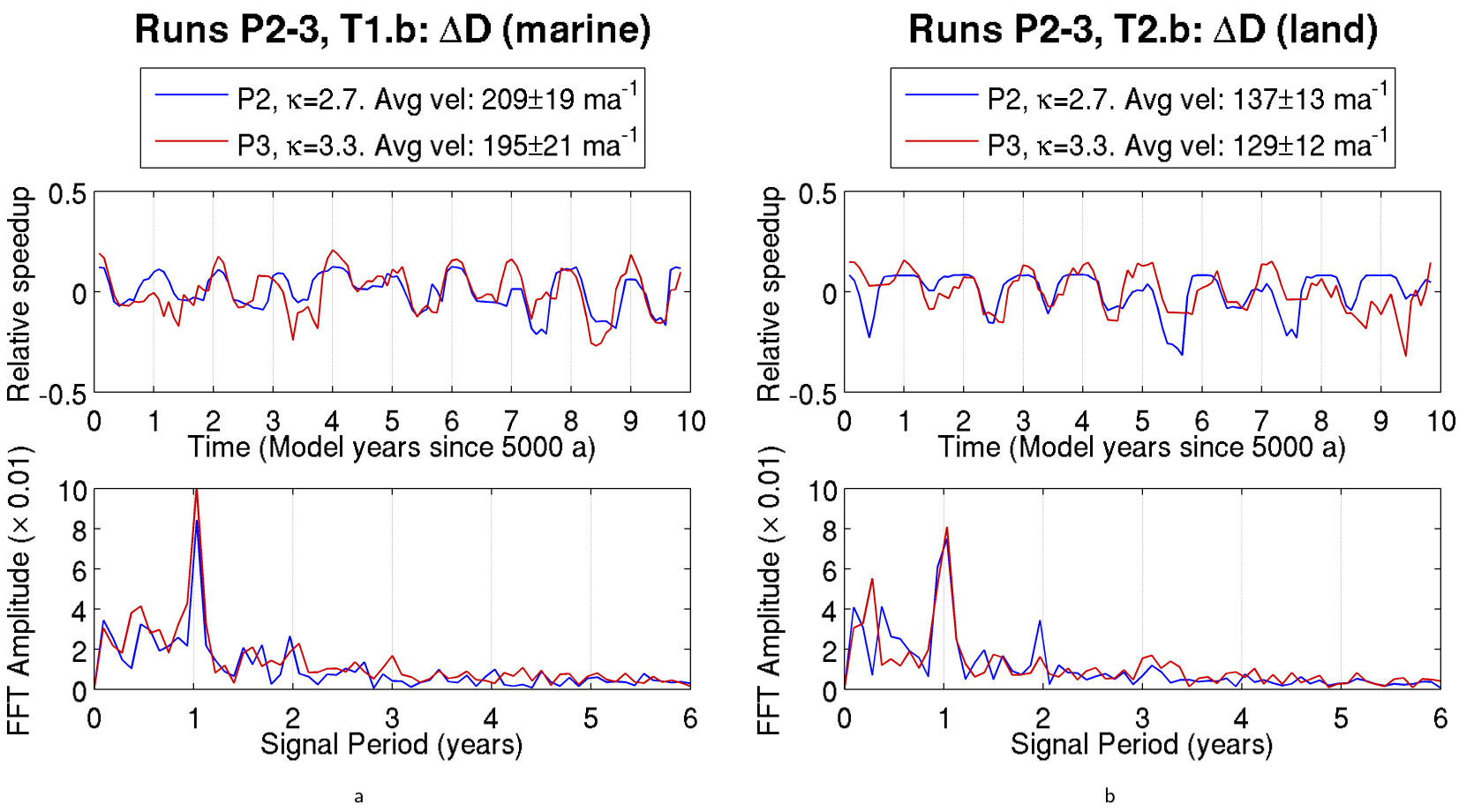

Figure 5.34 The system is sensitive to the bulk-diffusivity D of the bed, a function of hydraulic conductivity κ. Other variables that affect diffusivity (c_T and D, runs P4–P7) produce similar results.

As D decreases (blue), the summer speedup becomes smoother and less noisy for both marine- (a) and land-terminating ice. The winter variability is less affected and this results in short period (< 1 a) noise in the Fourier plots. The amplitude of the speed decreases as D decreases for marine-terminating ice, but the amplitude is not affected for land-terminating ice.

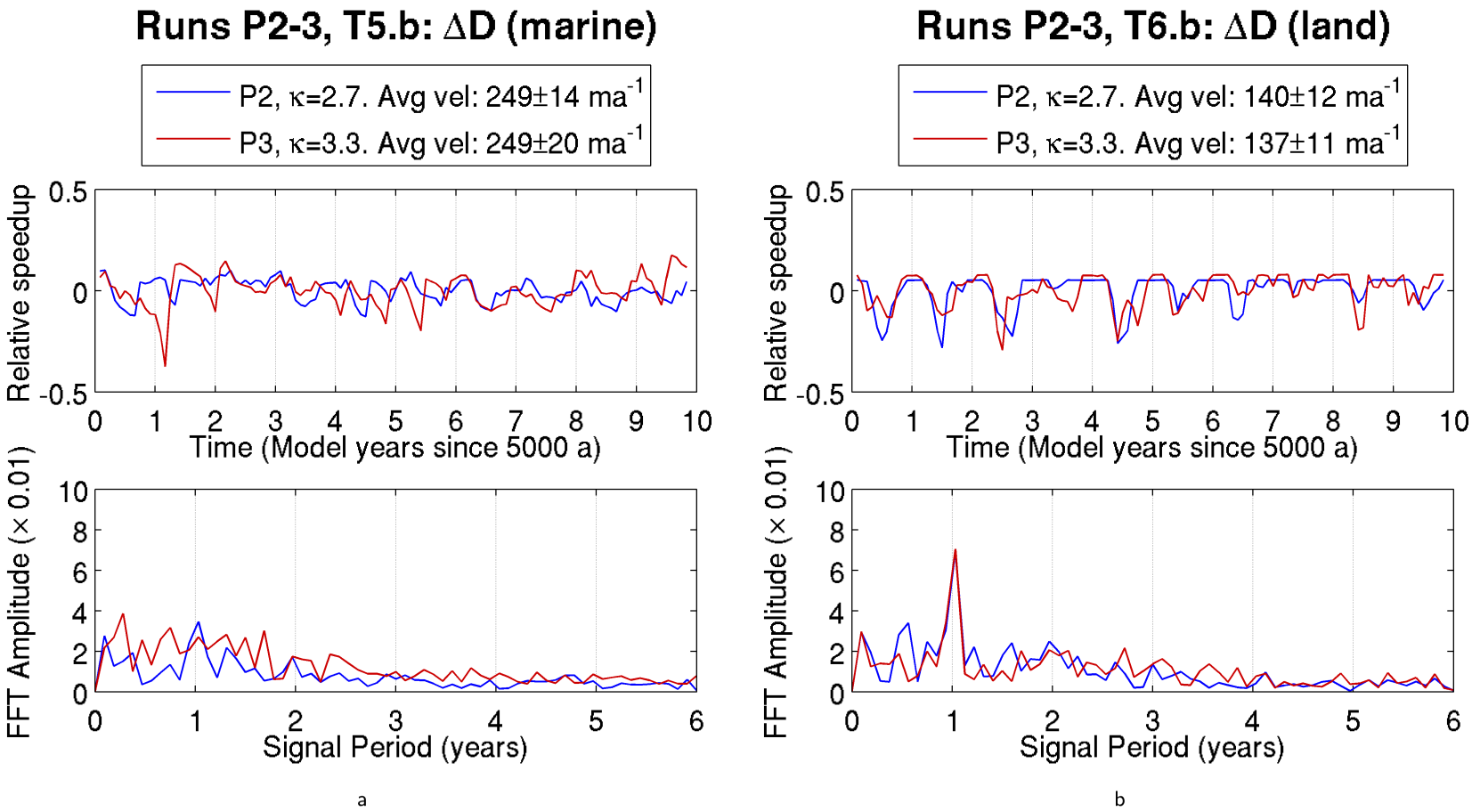

Figure 5.35 The system is sensitive to the bulk-diffusivity D of the bed, a function of hydraulic conductivity κ. This plot shows cell B of the Kangerdlugssuaq transect pair. Note that the amplitude of the seasonal 1 a peak decreases for marine-terminating ice (a) as diffusivity decreases, but there is no such effect for land-terminating ice (b). In both cases, the marine ice signal is more noisy than the land ice due to the convergence of water in the subglacial trough.

are not identical but the behaviour of the system cannot be distinguished between the runs. The Fourier plot shows this well: the signals are different, but the amount of noise and the amplitude of the major peaks are too similar for the system to be behaving differently[12].

By contrast to ψ, p_{limit} does have a large influence on the system. As it increases, efficient areas become harder to form and less of the bed becomes efficient. The seasonality of the signal decreases (smaller 1 a peak) but so does the noise, giving a smoother signal to the remaining seasonality. This is because the effective pressure $\bar{N}$ shows a strong response to efficiency (Figure 5.36a, runs P14–15), as the model was designed. This means velocity $\boldsymbol{v}_b$ also shows a strong response to efficiency. For example, in Transect T5.B (Figure 5.21), just after the bed becomes efficient, $\bar{N}$ increases and $\boldsymbol{v}_b$ decreases. When more of the bed becomes efficient, or a cell becomes efficient more often (lower p_{limit}), the noise in the signal increases.

Frictional heat

As the frictional heat flux H_f becomes more sensitive to a given change, the system becomes less seasonal and more noisy because H_f affects basal melt rate and therefore effective pressure. Figure 5.37 shows increased and decreased seasonality due to a low and high H_f sensitivity respectively for Jakobshavn Isbræ.

The processes responsible for this are discussed in Chapter 4. To summarise, as effective pressure decreases ice flows faster leading to more basal melt due to increased frictional heating. Increased basal lubrication, from increased melt, has a two-fold effect: effective pressures drop resulting in even faster ice, and frictional heat production drops due to increased lubrication. This, in turn, provides a cap on an otherwise potential runaway feedback mechanism. Chapter 4 looked at how coupling effective pressure to H_f reduces the variability and flickering of the system by allowing the system to respond gradually to changes in the basal conditions. Before this change the system had to build up sufficient potential energy to overcome a threshold to start fast flow; this led to the flickering. One result from Chapter 4 is that low effective pressure in subglacial troughs means that these areas produce very little frictional heat, as does slow moving land-terminating ice, but the feedback mechanism switches between states near the edges of fast-flowing ice.

[12] The difference between the runs is not down to stochastic variation because when a single run is repeated using a different sequence of random numbers (no run code) the runs are identical. This is because $d_{p\max}$ is small and so lakes drain quickly, without having time to be a function of the random element.

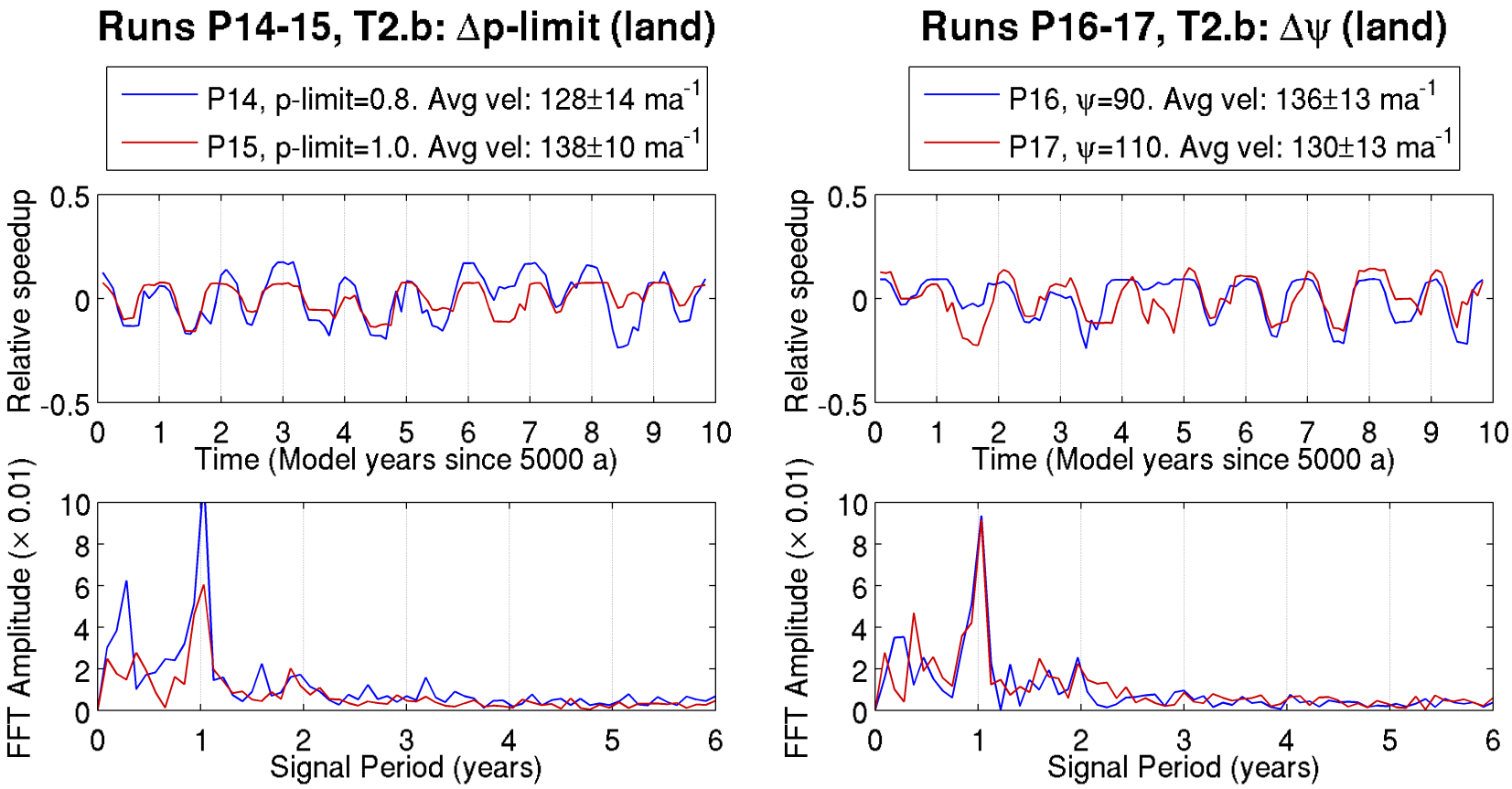

a Efficiency condition, p_{limit}

b Efficiency factor, ψ

Figure 5.36 The variables used in prescribing hydraulic efficiency, p_{limit} (a) and ψ (b), may affect the modelled system. As shown in Chapter 3, varying ψ does not have an effect on the system if ψ is large enough. The velocity in (b) is no more or less smooth or seasonal as ψ varies. The similarity of the two signals is also seen by the similarity of the Fourier transform plots. The system is sensitive to p_{limit} (a). As it increases, and efficient areas become harder to form, the seasonality of the signal decreases but so does the noise (Fourier amplitude < 1 a).

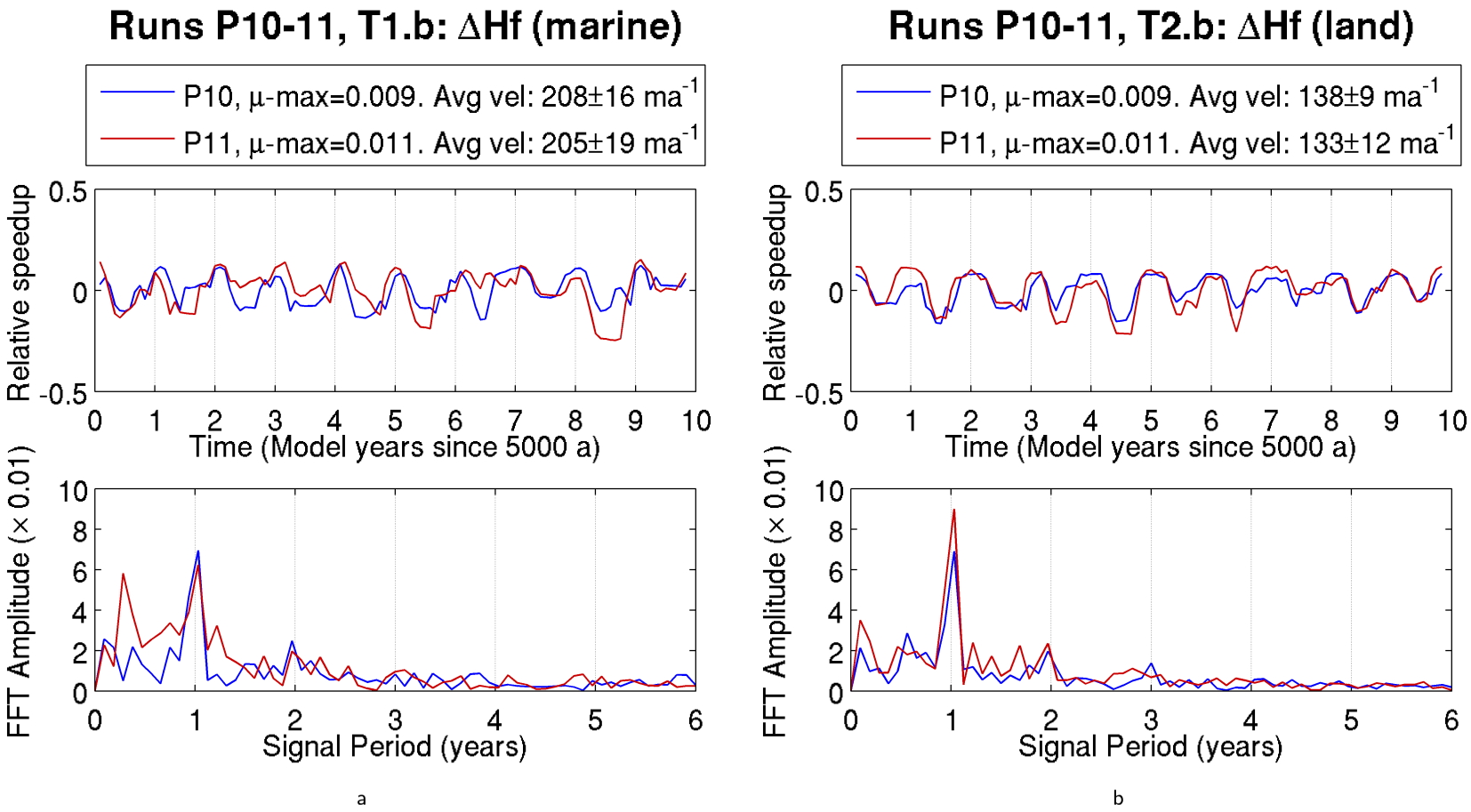

Figure 5.37 The system is sensitive to changes in frictional heat flux H_f because this affects fluctuations in basal melt rate and therefore effective pressure, as discussed in Chapter 4. In these plots H_f is varied via a 10% change in $\mu_{\max}$. The plots show the effect of this for marine- (a) and land-terminating ice. The system becomes less seasonal and more noisy as $\mu_{\max}$ increases in both cases. For land-terminating ice, the amplitude of the summer speedup increases as $\mu_{\max}$ increases; this is not noticeable for marine-terminating ice. Varying $t_{s\max}$ and γ (runs P10–P13), the other variables which control H_f, has a similar effect.

Chapter 4 investigated this using a wide range of values to control frictional heat flux H_f. Run P1 already uses $\mu_{\max} = 0.01$, $\gamma = 0.5$, $t_{s_{\max}} = 1.0 \times 10^{-3}\,\mathrm{m\,a^{-1}\,Pa^{-1}}$ which results in a smooth response to changing basal boundary conditions, when compared to GLIMMER as released. Here, I apply an approximately 10% change to these values. Figure 5.37 presents runs P8–9, varying $\mu_{\max}$. The results for varying γ and $t_{s_{\max}}$ (runs P10–P13) are very similar and are therefore not presented.

As the frictional heat becomes more sensitive, for example by increasing $\mu_{\max}$, the sensitivity of the whole system increases and the signal becomes less seasonal. The amplitude of the 1 a peak in the Fourier plot is not affected for marine-terminating ice, but there is increased low period (< 1 a) noise as sensitivity increases. Land-terminating ice also shows an increase in low period noise, but in this case the amplitude of the 1 a signal also increases as sensitivity increases.

The reason for this different response between land- and marine-terminating ice is the build up water pressure under marine ice. As demonstrated in Chapter 4, subglacial troughs reduce frictional heat output and are therefore less affected by its changes. The increased noise is due to the edges of the trough where a strong flickering was demonstrated. This water diffuses into the trough contributing to a slightly more irregular signal. Under land-terminating ice, where effective pressures are not as low, friction is more important. As the ice undergoes its summer speedup, increased velocity leads to increased basal melt which further increases velocity resulting in a higher amplitude 1 a peak. The seasonal nature of the speedup dominates and once surface water no longer reaches the bed frictional heat feedback slows down.

Secondary effects

There are two secondary effects which also affect the modelled seasonal response. These are changes to the source term ϕ of HYDRO and changes in basal slipperiness t_s.

Source term

The source term in Equation 2.39, which accounts for water entering each cell from basal and surface melt, is dependent on aquifer depth d and compressibility c_T. These factors are needed to convert melt rate entering a cell into a change in pressure. As the aquifer depth and compressibility, which measures the dilation of till for a given pressure, change how

accommodating the system is to new water this controls the response in effective pressure $\bar{N}$ for a given melt water input. Both of these variables also affect the diffusivity discussed previously. By making the system better able to cope with incoming water (increasing d or c_T) the system becomes slightly more seasonal. When the system is less able to cope (decreasing parameters) it reacts to a given change quicker producing more variability in the signal and therefore a less seasonal signal.

While in this model these parameters are constant for the entire model domain, in reality both compressibility and aquifer depth will change from region to region. Therefore the nature of the observed seasonal response in Greenland may be different depending on the location chosen. If the aquifer depth is taken literally, and not as a proxy as I have used in this thesis, then basins which have a larger warm-based bed may accumulate more till as it converges from a wider catchment area. This may mean areas with a large erosive catchment may behave differently to surface water input than areas which are on bed rock or with less sediment. Erosion and sediment transport under glaciers and ice sheets is an active area of research (eg Jamieson et al., 2008) that I do not consider in this thesis but the Glimmer-Hydro model developed, with the erosion model developed by Jamieson et al. (2008), may be able to help investigate fjord-creating feedbacks in future.

Basal slipperiness

Varying the parameters $t_{s\max}$ and γ, which control frictional heat flux H_f, by their nature, also affects basal slipperiness t_s. This, in turn, affects how the sliding velocity responds to effective pressure and therefore affects the seasonality of the signal.

$\mu_{\max}$ only affects frictional heat flux H_f and not basal slipperiness t_s. The data from varying $t_{s\max}$, γ, and $\mu_{\max}$ are very similar, showing that changes in H_f is the dominant process determining the seasonality of the system.

5.6 Summary

This chapter successfully models the seasonal response of the Greenland ice sheet to draining surface lakes using the Glimmer-Hydro model with a surface ponding algorithm. This response is well documented in the literature. A surface ponding algorithm is developed to agree with field observations of lake formation and hydrofracture. The 10 km model scale limits the effectiveness of the model unless water volumes are artificially magnified

as they pass to the bed. This compensates for the effect of draining ponds being averaged over a 100 km^2 grid cell. Within this set-up, the dynamic response is then calculated by Glimmer-Hydro using a physically based model evolving effective pressure, and not simply as proxy of lake drainage, as has been done to date by other studies (eg Parizek and Alley, 2004; Nick et al., 2009).

Key results are:

1. Seasonal dynamic response, and seasonally evolving hydraulic efficiency, are modelled.
2. In general, land-terminating glaciers show a much larger response to a surface signal than marine-terminating glaciers because of the subglacial trough associated with them.
3. Frictional heat flux is a key physical process controlling the sensitivity of the system to draining lakes.
4. The bulk-diffusivity of the bed is a key model parameter controlling the sensitivity of the system to draining lakes.

Result 1 is important because the modelled dynamic response is due to the evolving physics of the model and not a proxy. Although an artificial magnification factor is applied to overcome scale issues, there is no proxy used to determine the response. Field studies (eg Shepherd et al., 2009) suggest that the evolving hydraulic configuration of the bed is important in determining the response of the system. This is captured as an integral part of Glimmer-Hydro. While the mechanism by which this is implemented can be improved, even with its current complexity some behaviour that has not been possible to model before is present, such as the response to a surface signal changing as the melt season progresses.

The key contribution of this chapter is Result 2. This reproduces, and suggests a mechanism for, hitherto unexplained observations from the Greenland ice sheet. Echelmeyer and Harrison (1990), Solomon et al. (2007), and Hughes (2009) all comment that outlet glaciers, such as Jakobshavn Isbræ, show a muted seasonal acceleration when compared with neighbouring land-terminating ice but that the reason for this is unknown. Understanding the consequences of this is vital if the future mass loss of the Greenland ice sheet is to be predicted as Greenland loses two-thirds of its mass through outlet glaciers (Rignot and Kanagaratnam, 2006).

Finally, this chapter builds upon Chapter 4 and the work of Hulton and Mineter (2000) and Jamieson et al. (2008) in understanding the frictional heat, velocity, and effective pressure feedback mechanism (Results 3 and 4). Even when the model is allowed to start sliding gradually, by coupling effective pressure to basal slipperiness, small perturbations in frictional heat flux still have a large effect in the smooth evolution of the system. Small-magnitude changes in frictional heat flux, set up to include smooth switch-on of sliding, control the seasonality displayed by the system.

Chapter 6

Conclusions

This thesis has investigated the basal boundary conditions of the Greenland ice sheet and modelled a dynamic response to surface draining lakes. Recent work increasingly shows the importance of surface lakes and the impact they have on basal dynamics. Despite this, there are relatively few models which are able to model basal conditions physically and so discover behaviour which is not simply a consequence of the model parametrisation. Lipscomb et al. (2008) highlight basal hydrology as one of the key processes missing from the current generation of ice sheet models. This thesis has attempted to address this by creating the subglacial hydrology model Hydro and coupling it to the existing Glimmer ice sheet model. This new coupled model was used for the majority of the work.

The main objectives of the thesis were to:

- Understand the relative importance of heat sources in ice sheets and relate this to the basal hydraulic pressure profile (bhpp) underneath the Greenland ice sheet.
- Understand how the basal boundary condition of the Greenland ice sheet is controlled by basal hydrology.
- Investigate the consequences of coupling frictional heat flux from sliding to water pressure.
- Investigate the dynamic response of the Greenland ice sheet to draining surface lakes.

This chapter critically assesses the main contributions of this thesis and discusses to what extent each of these objectives were met. First, Section 6.1 examines the contributions and

puts them into context with each other and the thesis overall. The assumptions and setup of the subglacial hydrology model are also reviewed as the conclusions must be interpreted within the bounds of the model definition. Section 6.2 discusses the implications of the results and possible counter arguments. Finally, Section 6.3 aims to direct future work, both from general glaciological and specific modelling perspectives.

6.1 Summary of contributions

The main contributions of this work are that:

1. A new, physically-based, ice-sheet scale, subglacial hydrology model (Hydro) has been developed; Hydro is coupled with Glimmer, an existing ice sheet model, which is modified to enable it to use effective pressure data available from Hydro;

2. An assessment of the relative importance of heat sources (strain, frictional, and geothermal) and their impact on basal melt rates is performed; this assessment also establishes how basal melt rates affect the bhpp, which any surface melt water injection must perturb. A low, but spatially extensive, basal melt rate is found to converge in subglacial troughs and significantly lower effective pressures in these regions;

3. A modelling analysis of the frictional heat flux feedbacks, using the coupled Glimmer-Hydro model, has been performed; water pressures are found to limit melt water generation where the bhpp is low, leading to smoother, more stable, numerics within the ice sheet model;

4. The dynamic response of the Greenland ice sheet to draining surface lakes is captured using the physics built into Hydro and a surface-to-bed magnification factor to overcome scaling issues; the basal conditions (diffusivity, frictional heat generation) are found to control the degree and smoothness of the modelled speedup; the speedup of areas with subglacial troughs (ie marine-terminating outlet glaciers) are found to be much smaller than areas without subglacial troughs (ie land-terminating ice).

Item 1 is discussed in Section 6.1.1 and the remainder are discussed in Section 6.2 along with their implications.

6.1.1 The Glimmer-Hydro model

The discussion must start with the GLIMMER-HYDRO model because all interpretation of the results must be in the context of its assumptions. The key abilities of the model and suggested future improvements are then discussed.

Model assumptions

The base of the Greenland ice sheet is largely inaccessible and so the basis of the HYDRO model is to couple two conservation laws (momentum and mass) that must, in some form, hold. The resulting time- and spatially-dependent diffusion equation is solved by assuming diffusivity to simply be a proxy of how easily water flows along the bed. No explicit assumption of whether the bed is an aquifer of till or hard bedrock is made, but the origins of the conservation of momentum equation used (Darcy's law) is defined for aquifers.

Hydraulic efficiency determines how water pressures respond to a given water flux through the system (Kamb, 1987) and therefore are very important to include in subglacial hydraulic modelling (Truffer et al., 2005). Many contemporary models have thus far tended to not include the effects of efficiency (eg Flowers et al., 2005; Brocq et al., 2009), but this results in important behaviour not being modelled. The approach in HYDRO is to treat bulk-diffusivity as a proxy for efficiency and thereby allow the model to dynamically determine where the bed should be efficient.

The model is defined to prevent water flow where the bed is frozen. The frozen bed is determined by GLIMMER's temperature calculations.

GLIMMER uses the shallow ice approximation (SIA) which limits its ability to model fast-flowing ice and also limits the DEM resolution used (the model is unstable with $< 10\,\text{km}$ grid cells). The SIA causes GLIMMER to over-predict strain rates in outlet glaciers and to model incorrect ice physics where the ice is predicted to decouple from the bed as a result of HYDRO's calculations.

When surface ponding is allowed, water is assumed not to flow on the surface and draining of the lakes is assumed to take one time step (1 month). This is based on the observations and theory of hydrofracturing (eg Alley et al., 2005b; Das et al., 2008) as well as the density of lakes and moulines on the surface of the ice sheet (eg McMillan et al., 2007; Sundal et al., 2009).

Model scale is found to be a limiting factor, and a response to draining surface lakes is only found when an artificial surface-to-bed magnification factor is added. This is because on a $10 \times 10\,\mathrm{km}^2$ grid square any draining water is averaged over the entire cell. By using the surface-to-bed magnification the model can simulate, crudely, what happens on a smaller scale when a lake drains. This factor especially must be remembered when discussing the different response of marine- and land-terminating[1] glaciers to surface draining.

Key abilities of Glimmer-Hydro

The coupled Glimmer-Hydro model provides features not available in other contemporary ice sheet or basal hydrology models. Effective pressure is the main output of Hydro and basal melt rate and surface water input are the main inputs from Glimmer.

The key abilities of the coupled Glimmer-Hydro model are to:

1. fully solve the heat equation for ice sheets (existing ability in Glimmer),
2. explicitly predict water pressures based on physical conservation law while incorporating the effects of evolving hydraulic efficiency,
3. link basal sliding to water pressure,
4. link frictional heat generation from sliding to water pressure, and
5. simulate surface melt-water pond drainage using a stochastic ponding algorithm.

Item 1 is not a new feature, but is very important for accurately calculating the basal melt rate that Hydro relies on. Items 2 to 5 are only possible because of the new Hydro model developed. Items 2 and 5 are handled by Hydro while items 3 and 4 are new abilities added to Glimmer that use effective pressure data from Hydro. Combined, this allows Glimmer-Hydro to calculate basal conditions based on the defined physics instead of relying on proxies to simulate response to surface melt water input (eg Parizek and Alley, 2004; Nick et al., 2009). This is an important step towards creating the next generation of ice sheet models (Lipscomb et al., 2008).

[1] The key difference between these two regimes is the subglacial trough associated with outlet glaciers, not the fact that the glacier is land- or marine-terminating. This is discussed in Section 3.2.

Suggested improvements

The nature of modelling means that there will always be possible improvements to any model. This thesis has highlighted a number of these areas for GLIMMER-HYDRO already. This section now discusses suggested improvements to the model some of which, with hindsight, would have been incorporated from the beginning. This section may provide experience-based guidance to others who are developing a similar model.

Outlet glaciers are important to model correctly if the future stability of the Greenland ice sheet is to be assessed. GLIMMER's current use of the shallow ice approximation misses important components of the system. For example, longitudinal stresses should begin to dominate when effective pressures become low. Adding higher-order physics to GLIMMER is one of the current goals of the GLIMMER community. HYDRO will be able to couple with this improved model when it is available, improving the accuracy of studies of this nature.

Efficiency handling

Perhaps the largest area for improvement of the HYDRO model is its handling of an efficient bed. Efficiency is a primary control on ice dynamics as it has a large impact on effective pressures and so sliding velocities. Without it, the modelled system over-pressurises (Chapter 3). Currently the bed is made efficient, as a binary switch, if water pressures reach a sufficient level. The efficiency factor ψ is set as large as possible without affecting the model stability. When conditions are no longer met, the bed becomes inefficient again.

While some may argue that modelling an efficient system using maths describing diffusive, and therefore inherently inefficient, flow is not a valid approach, increasing the diffusivity does reduce overall water pressure in an analogous way to the efficient regime described by Kamb (1987). Also, within a grid cell a true channel will only take minimal space and the rest of the cell will still be inefficient. The average pressure in the cell, not the channel, is the important value. The approach used in this thesis is simply a method for estimating that value. Even with these limitations HYDRO uses physics which are not considered by most other hydrology models, with Arnold and Sharp (2002) being the exception. Within this setup, the model has a tendency to over-pressurise because of the limitations of the proxy method, if not careful, because the system did not lose water as easily or as quickly as it would with true channels. The model as defined can still investigate possible basal processes but, as always, if the system is more realistic then other processes may become apparent. I

therefore suggest the following improvements for handling efficiency at ice-sheet scales:

- Only allow efficient areas where the ice is slow. Fast areas, such as Jakobshavn Isbræ, are unlikely to be able to sustain efficient areas. This may affect the dynamics of the ice, possibly by raising water pressure, further enhancing the effects of any convergence.
- Scale efficiency smoothly with $\bar{N}$ instead of using a binary switch.
- Make the efficiency condition a function of water flux, not pressure. Water pressure is a good first approximation because in an inefficient system it increases proportionally to water flux, and has the desired effect of lowering water pressures once triggered.
- Have a mechanism by which efficiency is lost gradually. If there is no longer sufficient flow to maintain channels, then these channels take time to disappear under the creep of ice (Röthlisberger, 1972). Meanwhile, any small volume of water that enters the system flows through the shrinking channels and so does not affect sliding.
- Possibly add advection to efficient cells to aid water flow downstream. Diffusion alone, by its very nature and as currently used in Hydro, may not remove water in the quantities suggested by field work.
- An alternative approach to dealing with efficiency may be to artificially lower the water pressures in a cell directly instead of relying on there being less water. I did consider this approach initially but rejected it on the grounds that it is less physical, and it adds complication to tracking basal water volumes.

Limiting water pressure to ice overburden pressure in areas that are likely to have crevasses may help relieve over-pressurisation as well. Water can escape to the surface in these areas through the crevasses, reducing pressure. This will have an impact on the maximum pressure reached in the interior of the ice sheet.

Surface ponding

If the approach to surface ponding is deemed satisfactory for future studies, then I suggest that a surface flow component is added to the algorithm. This will enable the model to fill lower ponds sooner and to pass water from undrained cells into moulins in lower cells. Both of these will increase water reaching the bed, which I have shown to be an important control in ice dynamics.

Higher resolution data sets (1 km, Bamber et al., 2001a) are available for the Greenland ice surface. This may open the possibility of using different model resolutions for different processes. HYDRO is stable at a finer resolution than GLIMMER. Using a 5 km bed DEM and 1 km surface DEM may capture processes in more detail, but this effect may also get overridden when the data are averaged to GLIMMER's 10 km scale. This is an area of possible further development, which if successful method is found, would go someway to incorporating the processes which are lost due to the coarse resolution used by GLIMMER-HYDRO.

6.2 Implications

I now discuss further details of the main contributions of this work and their implications.

6.2.1 Heat terms and the background pressure profile

The magnitudes of strain, frictional, and geothermal heat flux terms overlap. Understanding where each term dominates is therefore important. After recognising that geothermal heat flux varies spatially underneath the Greenland ice sheet, this thesis used a constant value of $42\,\mathrm{mW\,m^{-2}}$, following many other studies (eg Lee, 1969; Huybrechts and Payne, 1996; Johnsen et al., 2002), because it is difficult to know how it varies.

Heat fluxes

Geothermal heat flux is found to be the dominant term in the interior of ice sheets, with strain and frictional heat fluxes becoming dominant near the margin. Strain heat flux is found to be an order of magnitude larger than geothermal heat flux near the margin of the ice sheet, away from fast-flowing outlet glaciers. At the outlet glaciers, strain heating is calculated to be two orders of magnitude larger than geothermal heat flux. This calculation is analytical and takes basal ice temperature, surface gradient and ice thickness into account. Velocity is not taken into account because the setup of the analytical equation assumes high basal stresses and therefore effectively a frozen bed. This situation is unrealistic under outlet glaciers so basal strain heat flux may not be as dominant in these regions as suggested. This work ignores the effects of strain heating from lateral shear and other higher-order terms. Frictional heat flux, when the fully-coupled model is run, is found to be highest at the edges

of fast-flowing ice due to high water pressures in the subglacial troughs lowering sliding friction.

An interesting outcome of the strain heat flux analysis in Chapter 3 is finding the sensitivity of the basal strain heat flux on surface ice temperature. The surface temperature dependence is partly a result of the model setup; the true dependence is found to be the temperature in the ice column. Small changes, integrated through the column are found to affect basal strain heat flux, and therefore basal melting if the bed is at pressure melting point, much more than large changes in the ice column close to the bed. The main implication of this is that basal melt rates and ice deformation strongly depend on the past temperature history of the ice. Thermal equilibrium in ice sheets is a 100 ka process (Hindmarsh, 1990) and so model spin-up may affect basal melt rates, which affect the BHPP, and therefore any potential dynamic response to draining surface lakes. While this may not be so important in sensitivity studies or studies focusing on processes, it will need to be considered when attempting to predict the future stability and evolution of the Greenland ice sheet.

Background profile

The melt rate pattern is found to depend on the frictional and strain heat fluxes near the margin. In the interior of the ice sheet geothermal heat flux is the primary control on the low, but spatially extensive, basal melt rates and the size of the central frozen area. Both the low basal melt rates and the size of the frozen area are found to be primary controls on the BHPP because, combined, they control the volume of basal water entering the system (Chapter 3).

In the BHPP, water is found to converge in subglacial troughs due to the hydrostatic surface (function of ice overburden pressure and basal topography) driving the flow. This agrees with the drainage basin analysis by Lewis and Smith (2009). Arnold and Sharp (2002) and Brocq et al. (2009) also report a convergence of flow. What no other study so far has discussed is the implication of this convergence, which is potentially a major one. The convergence allows water pressure to build (effective pressure to drop) in subglacial troughs (which presumably through fjord-creating feedback are associated with marine-terminating outlet glaciers[2]). An important contribution of this thesis is that this background profile

[2] These feedback are beyond the scope of this thesis although the work in this thesis may help model the feedbacks in future.

appears to limit the dynamic response of outlet glaciers to draining surface lakes. The potential significance of this is now discussed.

6.2.2 Dynamic response to draining lakes

This thesis has modelled, with the help of an artificial surface-to-bed water magnification factor, a dynamic response to draining surface lakes that is due to the physics of the system and not a proxy. The surface-to-bed magnification is a method to overcome scaling issues, but as it is applied uniformly it does not bias the physics or act as a proxy; it simply magnifies the effects to compensate for the model scale.

Overview

This is one of the first studies to model a seasonal dynamic response of the Greenland ice sheet to draining surface lakes using a physically-based hydrology model (Chapter 5). Furthermore, this thesis also models the evolution of a hydraulically efficient network in response to seasonally draining surface lakes. Again, this is one of the first studies to do so. Some might argue that the parametrisation of efficiency was over-simplistic. As discussed in Section 6.1.1, the system still captures the expected drop in effective pressure and so ice velocity and is therefore a reasonable first approximation of these processes in an ice-sheet scale model.

Impact of the bhpp on dynamic response

The BHPP is found to have low effective pressure in the troughs under outlet glaciers and this is found to have a large impact on the dynamic response of these regions. While convergence of flow has already been reported by other authors, the potential significance of this, to my knowledge, is overlooked. A low effective pressure helps account for the fast flow of these glaciers by decoupling them from the bed. As this decoupling is largely due, by the analysis in Chapter 3, to the low basal melt rate integrated over a large area, it is present throughout the year. This means that surface draining lakes in these regions have a limited impact on ice dynamics because the extra basal water injection cannot decouple the system much further. The relative lack of seasonal speedup of Greenland's outlet glaciers, compared to nearby land-terminating ice where the BHPP has higher effective pressure, is well documented

(eg Echelmeyer and Harrison, 1990; Joughin et al., 2008) but until this thesis no possible explanation had been provided (Hughes, 2009).

The significance of this result is that this may be a capping mechanism which limits the dynamic ice loss from the Greenland ice sheet. Conceptually, this may make the Greenland ice sheet more stable in response to global warming but more stability studies, incorporating these newly identified processes, are needed. Nevertheless, Greenland is losing an increasing volume of ice though dynamic thinning (eg Rignot and Kanagaratnam, 2006; Velicogna, 2009). Its outlet glaciers appear to be speeding up (eg Joughin et al., 2004a) and thinning (eg Rignot and Thomas, 2002) so what is driving this if it is not draining surface lakes? If my conclusions are valid, this implies the dynamic mass loss of the Greenland ice sheet is more a function of buttressing and potentially calving (eg Howat et al., 2008; Joughin et al., 2008; Nick et al., 2009) as well as ocean interaction (eg Holland et al., 2008; Thomas et al., 2009). This agrees with Thomas et al.'s (2009) conclusion that "[...] basal lubrication as a result of increased surface melting has only a marginal impact on Greenland outlet-glacier acceleration". I therefore believe that one of the next steps is to better understand these processes to enable them to be modelled so the future of the Greenland ice sheet can be better ascertained.

An interesting logical outcome of the dependence on the BHPP is that the dynamic response may depend on the past temperature history, and therefore climate, of the ice sheet. Chapter 3 demonstrated that strain heating rates, and therefore basal melt rates, depend on the temperature of the entire ice column. The sensitivity study appeared to show that basal strain heat flux is more sensitive to small changes in temperature over the majority of the ice column rather than large changes in temperature in a small region close to the bed.

6.2.3 Frictional feedbacks and stability

This work furthers the efforts of Hulton and Mineter (2000), Payne and Baldwin (2000), and Jamieson et al. (2008) in reducing numerical flow-instability in ice sheet models (Chapter 4). These instabilities occur when modelling fast-flowing ice with rigid basal boundary conditions. The system has to build up a large surface gradient for ice flow to initiate. Once started, motion contributes to further heating of the ice leading to instabilities and a fast switching on and off of flow. This results in flickering "fingers" of warm and cold ice which, when a

flat bed is used, align with the numerical grid.

Often ice sheet models use a binary switch for switching on flow. Replacing this with a gradual increase in basal slipperiness, for example by coupling to basal melt rate, alleviates some of the problem (Jamieson et al., 2008). In Chapter 4, I take this approach but coupled sliding to effective pressure to better approximate a Budd-type sliding law. Furthermore, I couple frictional heat flux to effective pressure so the melt rate does not purely depend on sliding velocity and basal shear stress, as most other models do. The first step, coupling sliding to effective pressure, greatly increases the stability of the system. In a circular ice sheet, the system increases its radial symmetry, except around the subglacial trough defined in the topography, resulting in more mathematically natural behaviour. The second step, adding frictional heating feedbacks, destabilises the system slightly but overall the system is still significantly more stable than before. Frictional feedbacks introduce compensatory behaviour between friction, melt rate, and water pressure. This behaviour appears to be most significant at the edge of fast-flow features. Once suitable values for the coefficient of friction and the sliding response parameter are determined, small variations in these variables affect the smoothness and seasonality of the response to draining surface lakes (Chapter 5).

6.3 Research direction

This thesis goes some way in answering the objectives set out in the introduction. I now look at where this research should lead and both discuss general glaciology and suggest future modelling studies.

A key contribution of this work is the suggested explanation for why marine-terminating ice shows a less distinct speedup and seasonality, compared to its land-terminating neighbour. I believe this is a real effect and that it, and the processes responsible, need more investigation as it has a large impact on the future stability of the Greenland ice sheet and therefore global climate. Both further modelling and new field studies are needed.

I propose that, if practical, basal water pressure variation under an outlet glacier and its neighbouring land-terminating ice should be logged over at least one summer season. Ideally, a similar data sets could be collected for both subglacial troughs, and non-trough transects during the same season. If at all practical, this would be a method to test the hypothesis put forward in this thesis that the outlet glaciers are not showing a strong seasonal dynamic

response to draining surface lakes because of convergence of water already in the subglacial system from basal melt.

The importance of this effect also needs further attention by running long-duration simulations of the Greenland ice sheet under various warming scenarios. Current similar studies do not include dynamic response and therefore do not even consider treating the speedup of land- and marine-terminating ice separately. Conceptually, if outlet glaciers do show a muted response to a surface signal then the future of the ice sheet may be more secure than currently thought. Buttressing and ocean interaction, in this case, become increasingly important and so improving the treatment of these in models must be a priority.

The specific localised effects of draining ponds are also of great interest. This thesis has not been able to answer specific questions about these effects due to the large-scale approach taken. I therefore call for basin-scale studies which model these effects, while taking into account the complex water flow at the bed of the ice sheet. Due to the convergence of water under outlet glaciers, I do not believe flow-line models on their own are enough, although they are definitely an important step in the right direction. I have demonstrated the importance of the two-dimensional movement of water so perhaps some way could be found to couple a model such as HYDRO with a detailed flow-line ice model.

Fjord evolution is an active area of research (eg Briner et al., 2008; Swift et al., 2008; Glasser and Ghiglione, 2009) which is important for understanding the thermal regime underneath past ice sheets, for linking erosion from climate change to off shore sediments, and for understanding landscape evolution over successive glacial cycles (Swift et al., 2008). Fjords are created by glacial erosion, which in turn is strongly linked to basal water (Jamieson, 2008). The ability to calculate basal water pressure should therefore greatly enhance glacial erosion models (eg Jamieson, 2008; Jamieson et al., 2008).

I suggest that frictional heat should be coupled to basal sliding using a more complex formulation than simply making it proportional to $\boldsymbol{v}_b \cdot \boldsymbol{\tau}_b$ as is the case in most current models[3] (eg Arnold and Sharp, 2002; Rutt et al., 2009). In this thesis, I did this with effective pressure and demonstrated that this stabilises the numerics, affects basal melt rates, and changes the overall dynamics of the idealised system. While the effect is not as large when bed topography and climate are more complex, it still has an effect by changing the

[3] The problem here is equating basal shear stress with driving stress, which the model assumes because of the shallow ice approximation. In a higher-order model, the basal shear stress will be lower than the driving stress and so the frictional heat calculation will compensate accordingly.

distribution of basal heat sources. Increasing basal melting simply because ice is flowing fast is incorrect physics and should be avoided. Even if effective pressure data are not available some proxy should be found, and become commonly used, to account for a lowering of frictional heat as the bed becomes decoupled.

This thesis also highlights the problems of modelling draining ponds at the ice-sheet scale, which by their nature are a small-scale process. These issues were to an extent overcome, but I need to highlight this issue for other modellers. Either a better method to handle the scaling issue is needed, or models need to use two different scaled grids when operating at the ice sheet scale and attempting to resolve a more realistic dynamic response. The other alternative is to focus more on basin studies and then incorporate the net-effect of any key behaviour into a future generation of ice sheet models.

6.4 Summary

By considering basal hydrology at the ice-sheet scale this study highlighted a number of interesting feedback mechanisms. There is potential for the basal boundary conditions of the Greenland ice sheet to be preconditioned by the ice sheet's thermal history, which may affect how different regions of the ice sheet respond to surface and climatic forcing. The study considered the interaction between frictional heat generation on the large scale and hydrology and demonstrated how this may lead to oscillatory behaviour of ice sheets in general. This study also suggested that ponding may be an important process in controlling how the basal system evolves with an open surface-to-bed connection because the delivery of large volumes of water may be necessary to enable efficient conditions to form over a large area. Combined, this study provides insight towards how the basal hydraulic system may operate at ice-sheet scales.

References

W. Abdalati and K. Steffen. Greenland ice sheet melt extent: 1979–1999. *J Geophys Res Atmos*, 106:33,983–33,988, 2001. ISSN 0148-0227. DOI 10.1029/2001JD900181.

A. P. Ahlstrøm, J. J. Mohr, N. Reeh, E. L. Christensen, and R. LeB. Hooke. Controls on the basal water pressure in subglacial channels near the margin of the Greenland ice sheet. *J Glaciol*, 51:443–450, 2005. ISSN 0022-1430. DOI 10.3189/172756505781829214.

R. B. Alley. Towards a hydrological model for computerized ice-sheet simulations. *Hydrol Process*, 10:649–660, 1996. ISSN 0885-6087.

R. B. Alley. Wally was right: Predictive ability of the North Atlantic "Conveyor belt" hypothesis for abrupt climate change. *Annu Rev Earth Planet Sci*, 35:241–272, 2007. ISSN 0084-6597. DOI 10.1146/annurev.earth.35.081006.131524.

R. B. Alley, P. U. Clark, P. Huybrechts, and I. Joughin. Ice-sheet and sea-level changes. *Science*, 310:456–460, 2005a. ISSN 0036-8075. DOI 10.1126/science.1114613.

R. B. Alley, T. K. Dupont, B. R. Parizek, and S. Anandakrishnan. Access of surface meltwater to beds of sub-freezing glaciers: preliminary insights. *Ann Glaciol*, 40:8–14, 2005b. ISSN 0260-3055. DOI 10.3189/172756405781813483.

R. B. Alley, M. Fahnestock, and I. Joughin. Understanding glacier flow in changing times. *Science*, 322:1061–1062, 2008. ISSN 0036-8075.

D. E. Anderson. Younger Dryas research and its implications for understanding abrupt climatic change. *Prog Phys Geog*, 21:230–249, 1997. ISSN 0309-1333. DOI 10.1177/030913339702100203.

R. S. Anderson, S. P. Anderson, K. R. MacGregor, E. D. Waddington, S. O'Neel, C. A. Riihimaki, and M. G. Loso. Strong feedbacks between hydrology and sliding of a small alpine glacier. *J Geophys Res Earth Surf*, 109:F03005, 2004. ISSN 0148-0227. DOI 10.1029/2004JF000120.

J. O. Andreasen. Apparent short-term glacier velocity variations. *J Glaciol*, 31:49–53, 1985a. ISSN 0022-1430.

J. O. Andreasen. Seasonal surface-velocity variations on a sub-polar glacier in West Greenland. *J Glaciol*, 31:319–323, 1985b. ISSN 0022-1430.

N. Arnold and M. Sharp. Influence of glacier hydrology on the dynamics of a large Quaternary ice sheet. *J Quaternary Sci*, 7:109–124, 1992. ISSN 0267-8179. DOI 10.1002/jqs.3390070204.

N. Arnold and M. Sharp. Flow variability in the Scandinavian ice sheet: modelling the coupling between ice sheet flow and hydrology. *Quat Sci Rev*, 21:485–502, 2002. ISSN 0277-3791. DOI 10.1016/S0277-3791(01)00059-2.

N. Arnold, K. Richards, I. Willis, and M. Sharp. Initial results from a distributed, physically based model of glacier hydrology. *Hydrol Process*, 12:191–220, 1998. ISSN 0885-6087. DOI 10.1002/(SICI)1099-1085(199802)12:2<191::AID-HYP571>3.0.CO;2-C.

AWWA. *Groundwater*. American Water Works Association, 3rd edition, 2003. ISBN 978-1-58321-188-5fdsadfsfdfs.

J. L. Bamber, R. J. Hardy, P. Huybrechts, and I. Joughin. A comparison of balance velocities, measured velocities and thermomechanically modelled velocities for the Greenland ice sheet. *Ann Glaciol*, 30:211–216, 2000. ISSN 0260-3055. DOI 10.3189/172756400781820589.

J. L. Bamber, S. Ekholm, and W. B. Krabill. A new, high-resolution digital elevation model of Greenland fully validated with airborne laser altimeter data. *J Geophys Res Solid Earth*, 106:6733–6746, 2001a. ISSN 0148-0227. DOI 10.1029/2000JB900365.

J. L. Bamber, R. L. Layberry, and S. P. Gogineni. A new ice thickness and bed data set for the Greenland ice sheet 1. Measurement, data reduction, and errors. *J Geophys Res Atmos*, 106:33,718–33,780, 2001b. ISSN 0148-0227. DOI 10.1029/2001JD900054.

J. L. Bamber, R. B. Alley, and I. Joughin. Rapid response of modern day ice sheets to external forcing. *Earth Planet Sci Lett*, 257:1–13, 2007. ISSN 0012-821X. DOI 10.1016/j.epsl.2007.03.005.

Jonathan L. Bamber and Anthony J. Payne, editors. *Mass Balance of the Cryosphear*. Cambridge University Press, 1st edition, 2004.

P. Barnes, D. Tabor, and J. C. F. Walker. The friction and creep of polycrystalline ice. *Proc R Soc London A*, 324:127–155, 1971. ISSN 0080-4630.

I. Bartholomew, P. Nienow, D. Mair, A. Hubbard, M. A. King, and A. Sole. Seasonal evolution of subglacial drainage and acceleration in a Greenland outlet glacier. *Nat Geosci*, 3:408–411, 2010. ISSN 1752-0894. DOI 10.1038/ngeo863.

BBC. 'Cryo-egg' to predict sea levels. `http://news.bbc.co.uk/1/hi/england/bristol/8407978.stm`, 2009. This is a NERC-funded project that is just starting.

Jacob Bear. *Dynamics of Fluids in Porous Media*. Dover, 1988.

D. I. Benn and D. J. A. Evans. *Glaciers & Glaciation*. Hodder Arnold, 2010. ISBN 978-0-340-90579-1.

D. I. Benn, C. R. Warren, and R. H. Mottram. Calving processes and the dynamics of calving glaciers. *Earth-Sci Rev*, 82:143–179, 2007. ISSN 0012-8252. DOI 10.1016/j.earscirev.2007.02.002.

C. S. Benson. *Stratigraphic studies in the snow and firn of the Greenland ice sheet*. PhD thesis, California Institute of Technology, 1960.

R. Bindschadler. The importance of pressurized subglacial water in separation and sliding at the glacier bed. *J Glaciol*, 29:3–19, 1983. ISSN 0022-1430.

R. G. Bingham, A. L. Hubbard, P. W. Nienow, and M. J. Sharp. An investigation into the mechanisms controlling seasonal speedup events at a High Arctic glacier. *J Geophys Res Earth Surf*, 113:F02006, 2008. ISSN 0148-0227. DOI 10.1029/2007JF000832.

S. Boon and M. Sharp. The role of hydrologically-driven ice fracture in drainage system evolution on an Arctic glacier. *Geophys Res Lett*, 30:18, 2003. ISSN 0094-8276. DOI 10.1029/2003GL018034.

G. Boulton and S. Zatsepin. Hydraulic impacts of glacier advance over a sediment bed. *J Glaciol*, 52:497–527, 2006. ISSN 0022-1430. DOI 10.3189/172756506781828403.

G. S. Boulton. The origin of till sequences by subglacial sediment deformation beneath mid-latitude ice sheets. *Ann Glaciol*, 22:75–84, 1996a. ISSN 0260-3055.

G. S. Boulton. Theory of glacial erosion, transport and deposition as a consequence of subglacial sediment deformation. *J Glaciol*, 42:43–62, 1996b. ISSN 0022-1430.

G. S. Boulton, P. E. Caban, and K. van Gijssel. Groundwater flow beneath ice sheets: Part I — Large scale patterns. *Quat Sci Rev*, 14:545–562, 1995a. ISSN 0277-3791. DOI 10.1016/0277-3791(95)00039-R.

G. S. Boulton, N. R. J. Hulton, and M. Vautravers. Ice-sheet models as tools for palaeoclimatic analysis: the example of the European ice sheet through the last glacial cycle. *Ann Glaciol*, 21:103–110, 1995b. ISSN 0260-3055.

G. S. Boulton, P. E. Caban, K. van Gijssel, A. Leijnse, M. Punkari, and F. H. A. van Weert. The impact of glaciation on the groundwater regime of Northwest Europe. *Global Planet Change*, 12:397–413, 1996. ISSN 0921-8181. DOI 10.1016/0921-8181(95)00030-5.

G.S. Boulton, R. Lunn, P. Vidstrand, and S. Zatsepin. Subglacial drainage by groundwater-channel coupling, and the origin of esker systems: Part 1—glaciological observations. *Quat Sci Rev*, 26:1067–1090, 2007. DOI 10.1016/j.quascirev.2007.01.007.

F. P. Bowden. Friction on snow and ice. *Proc R Soc London A*, 217:462–478, 1953. ISSN 0080-4630.

F. P. Bowden and T. P. Hughes. The mechanism of sliding on ice and snow. *Proc R Soc London A*, 172:280–298, 1939. ISSN 0080-4630.

J. E. Box and K. Ski. Remote sounding of Greenland supraglacial melt lakes: implications for subglacial hydraulics. *J Glaciol*, 53:257–265, 2007. ISSN 0022-1430. DOI 10.3189/172756507782202883.

J. E. Box, D. H. Bromwich, B. A. Veenhuis, L. S. Bai, J. C. Stroeve, J. C. Rogers, K. Steffen, T. Haran, and S. H. Wang. Greenland ice sheet surface mass balance variability (1988–2004) from calibrated Polar MM5 output. *J Climate*, 19:2783–2800, 2006. ISSN 0894-8755. DOI 10.1175/JCLI3738.1.

J. E. Box, L. Yang, D. H. Bromwich, and L. S. Bai. Greenland ice sheet surface air temperature variability: 1840–2007. *J Climate*, 22:4029–4049, 2009. ISSN 0894-8755. DOI 10.1175/2009JCLI2816.1.

R. J. Braithwaite. Positive degree-day factors for ablation of the Greenland ice-sheet studied by energy-balance modeling. *J Glaciol*, 41:153–160, 1995. ISSN 0022-1430.

C. W. Breemer, P. U. Clark, and R. Haggerty. Modeling the subglacial hydrology of the late Pleistocene Lake Michigan Lobe, Laurentide Ice Sheet. *Geol Soc Am Bull*, 114:665–674, 2002. ISSN 0016-7606. DOI 10.1130/0016-7606(2002)114<0665:MTSHOT>2.0.CO;2.

J. P. Briner, G. H. Miller, R. Finkel, and D. P. Hess. Glacial erosion at the fjord onset zone and implications for the organization of ice flow on Baffin Island, Arctic Canada. *Geomorphology*, 97:126–134, 2008. ISSN 0169-555X. DOI 10.1016/j.geomorph.2007.02.039.

A. M. Le Brocq, A. J. Payne, M. J. Siegert, and R. B. Alley. A subglacial water-flow model for West Antarctica. *J Glaciol*, 193:879–887, 2009. ISSN 0022-1430. DOI 10.3189/002214309790152564.

W. S. Broecker. Was the Younger Dryas triggered by a flood? *Science*, 312:1146–1148, 2006. ISSN 0036-8075. DOI 10.1126/science.1123253.

S. L. Buchardt and D. Dahl-Jensen. Estimating the basal melt rate at NorthGRIP using a Monte Carlo technique. In Clarke, GKC and Smellie, J, editor, *Annals of Glaciology, Vol 45, 2007*, volume 45 of *ANNALS OF GLACIOLOGY*, pages 137–142, 2007. ISBN 978-0-946417-40-7.

W. F. Budd and T. H. Jacka. A review of ice rheology for ice sheet modelling. *Cold Reg Sci Technol*, 16:107–144, 1989. ISSN 0165-232X. DOI 10.1016/0165-232X(89)90014-1.

W. F. Budd and D. Jenssen. Numerical modelling of the large-scale basal water flux under the West Antarctic ice sheet. In C. J. van der Veen and J. Oerlemans, editors, *Dynamics of the West Antarctic Ice Sheet*. D. Reidel Publishing Company, 1987.

W. F. Budd, P. L. Keage, and N. A. Blundy. Empirical studies of ice sliding. *J Glaciol*, 23: 159–170, 1979. ISSN 0022-1430.

E. Bueler, J. A. Kallen-Brown, and C. S. Lingle. Exact solutions and the verification of numerical models for isothermal ice sheets. *Geophys Res Abstr*, 7:05241, 2005. ISSN 1029-7006. DOI 10.3189/172756505781829449.

S. P. Carter, D. D. Blankenship, D. A. Young, and J. W. Holt. Using radar-sounding data to identify the distribution and sources of subglacial water: application to Dome C, East Antarctica. *J Glaciol*, 55:1025–1040, 2009. ISSN 0022-1430. DOI 10.3189/002214309790794931.

G. A. Catania, T. A. Neumann, and S. F. Price. Characterizing englacial drainage in the ablation zone of the Greenland ice sheet. *J Glaciol*, 54:567–578, 2008. ISSN 0022-1430. DOI 10.3189/002214308786570854.

P. U. Clark, R. B. Alley, and D. Pollard. Northern hemisphere ice-sheet influences on global climate change. *Science*, 286:1104–1111, 1999. ISSN 1095-9203. DOI 10.1126/science.286.5442.1104.

G. K. C. Clarke. Lumped-element analysis of subglacial hydraulic circuits. *J Geophys Res Solid Earth*, 101:17,547–17,559, 1996. ISSN 0148-0227.

D. Cohen, N. R. Iverson, T. S. Hooyer, U. H. Fischer, M. Jackson, and P. L. Moore. Debris-bed friction of hard-bedded glaciers. *J Geophys Res Earth Surf*, 110:F02007, 2005. ISSN 0148-0227. DOI 10.1029/2004JF000228.

J. Colinge and H. Blatter. Stress and velocity fields in glaciers: Part i. Finite-difference schemes for higher-order glacier models. *J Glaciol*, 44:448–456, 1998. ISSN 0022-1430.

L. Copland, M. J. Sharp, and P. W. Nienow. Links between short-term velocity variations and the subglacial hydrology of a predominantly cold polythermal glacier. *J Glaciol*, 49: 337–348, 2003. ISSN 0022-1430. DOI 10.3189/172756503781830656.

H. F. J. Corr and D. G. Vaughan. A recent volcanic eruption beneath the West Antarctic ice sheet. *Nat Geosci*, 1:AOP, 2008. ISSN 1752-0894. DOI 10.1038/ngeo106.

K. M. Cuffey, H. Conway, B. Hallet, A. M. Gades, and C. F. Raymond. Interfacial water in polar glaciers and glacier sliding at -17°c. *Geophys Res Lett*, 26:751–754, 1999. ISSN 0094-8276. DOI 10.1029/1999GL900096.

D. Dahl-Jensen and S. J. Johnsen. Palaeotemperatures still exist in the Greenland ice sheet. *Nature*, 320:250–252, 1986. ISSN 0028-0836. DOI 10.1038/320250a0.

D. Dahl-Jensen, K. Mosegaard, N. Gundestrup, G. D. Clow, S. J. Johnsen, A. W. Hansen, and N. Balling. Past temperatures directly from the Greenland ice sheet. *Science*, 282: 268–271, 1998. ISSN 0036-8075. DOI 10.1126/science.282.5387.268.

S. B. Das, I. Joughin, M. D. Behn, I. M. Howat, M. A. King, D. Lizarralde, and M. P. Bhatia. Fracture propagation to the base of the Greenland ice sheet during supraglacial lake drainage. *Science*, 320:778–780, 2008. ISSN 0036-8075. DOI 10.1126/science.1153360.

C. H. Davis, Y. Li, J. R. McConnell, M. M. Frey, and E. Hanna. Snowfall-driven growth in East Antarctic ice sheet mitigates recent sea-level rise. *Science*, 308:1898–1901, 2005. ISSN 1095-9203. DOI 10.1126/science.1110662.

H. De Angelis and P. Skvarca. Glacier surge after ice shelf collapse. *Science*, 299:1560–1562, 2003. ISSN 1095-9203. DOI 10.1126/science.1077987.

G. de Q. Robin. Depth of water-filled crevasses that are closely spaced (Correspondence). *J Glaciol*, 13:543, 1974. ISSN 0022-1430.

K. Dethloff, W. Dorn, A. Rinke, K. Fraedrich, M. Junge, E. Roeckner, V. Gayler, U. Cubasch, and J. H. Christensen. The impact of Greenland's deglaciation on the Arctic circulation. *Geophys Res Lett*, 31:L19201, 2004. ISSN 0094-8276. DOI 10.1029/2004GL020714.

J. DiMarzio, A. Brenner, R. Schutz, C. A. Shuman, and H. J. Zwally. GLAS/ICESat 1 km laser altimetry digital elevation model of Greenland. Digital media, 2007. Boulder, Colorado USA: National Snow and Ice Data Center.

C. S. M. Doake and E. W. Wolff. Flow law for ice in polar ice sheets. *Nature*, 314:255–257, 1985. ISSN 0028-0836. DOI 10.1038/314255a0.

E. Driesschaert, T. Fichefet, H. Goosse, P. Huybrechts, I. Janssens, A. Mouchet, G. Munhoven, V. Brovkin, and S. L. Weber. Modeling the influence of Greenland ice sheet melting on the Atlantic meridional overturning circulation during the next millennia. *Geophys Res Lett*, 34:L10707, 2007. ISSN 0094-8276. DOI 10.1029/2007GL029516.

T. K. Dupont and R. B. Alley. Assessment of the importance of ice-shelf buttressing to ice-sheet flow. *Geophys Res Lett*, 32:L04503, 2005. ISSN 0094-8276. DOI 10.1029/2004GL022024.

K. Echelmeyer and W. D. Harrison. Jakobshavns Isbræ, West Greenland: seasonal variations in velocity — or lack thereof. *J Glaciol*, 36:82–88, 1990. ISSN 0022-1430.

H. Engelhardt, N. Humphrey, B. Kamb, and M. Fahnestock. Physical conditions at the base of a fast moving Antarctic ice stream. *Science*, 248:57–59, 1990. ISSN 0036-8075. DOI 10.1126/science.248.4951.57.

D. C. B. Evans, J. F. Nye, and K. J. Cheeseman. The kinetic friction of ice. *Proc R Soc London A*, 347:493–512, 1976. ISSN 0080-4630.

M. Fahnestock, W. Abdalati, I. Joughin, J. Brozena, and P. Gogineni. High geothermal heat flow, basal melt, and the origin of rapid ice flow in central Greenland. *Science*, 294: 2338–2342, 2001. ISSN 0036-8075. DOI 10.1126/science.1065370.

R. S. Fausto, A. P. Ahlstrøm, D Van As, C. E. Bøggild, and S. J. Johnsen. A new present-day temperature parameterization for Greenland. *J Glaciol*, 55:95–105, 2009. ISSN 0022-1430. DOI 0.3189/002214309788608985.

B. Felzer, R. J. Oglesby, T. Webb III, and D. E. Hyman. Sensitivity of a general circulation model to changes in northern hemisphere ice sheets. *J Geophys Res Atmos*, 101:19,077–19,092, 1996. ISSN 0148-0227. DOI 10.1029/96JD01219.

T. Fichefet, C. Poncin, H. Goosse, P. Huyrechts, I. Janssens, and H. Le Treut. Implications of changes in freshwater flux from the Greenland ice sheet for the climate of the 21st century. *Geophys Res Lett*, 30:1991–1995, 2003. ISSN 0094-8276. DOI 10.1029/2003GL017826.

G. E. Flowers. *A multicomponent coupled model of glacier hydrology*. PhD thesis, University of Colorado, 1994.

G. E. Flowers and G. K. C. Clarke. A multicomponent coupled model of glacier hydrology — 1. Theory and synthetic examples. *J Geophys Res Solid Earth*, 107:2287, 2002a. ISSN 0148-0227. DOI 10.1029/2001JB001122.

G. E. Flowers and G. K. C. Clarke. A multicomponent coupled model of glacier hydrology — 2. Application to Trapridge Glacier, Yukon, Canada. *J Geophys Res Solid Earth*, 107: 2288, 2002b. ISSN 0148-0227. DOI 10.1029/2001JB001124.

G. E. Flowers, S. J. Marshall, H. Björnsson, and G. K. C. Clarke. Sensitivity of Vatnajökull ice cap hydrology and dynamics to climate warming over the next 2 centuries. *J Geophys Res Earth Surf*, 110:F02011, 2005. ISSN 0148-0227. DOI 10.1029/2004JF000200.

A. G. Fountain and J. S. Walder. Water flow through temperate glaciers. *Rev Geophys*, 36: 299–328, 1998. ISSN 8755-1209.

A. G. Fountain, R. W. Jacobel, R. Schlichting, and P. Jansson. Fractures as the main pathways of water flow in temperate glaciers. *Nature*, 433:618–621, 2005. ISSN 0028-0836. DOI 10.1038/nature03296.

A. C. Fowler and D. A. Larson. On the flow of polythermal glaciers: II. Surface wave analysis. *Proc R Soc London A*, 370:155–171, 1980. ISSN 0080-4630. DOI 10.1098/rspa.1980.0027.

Free Software Foundation. Gnu general public license, 1991.

M. Frigo and S. G. Johnson. The design and implementation of FFTW3. *Proceedings of the IEEE*, 93:216–231, 2005. ISSN 0018-9219. DOI 10.1109/JPROC.2004.840301. Special issue on "Program Generation, Optimization, and Platform Adaptation".

O. Gagliardini, G. Durand, T. Zwinger, R. C. A. Hindmarsh, and E. Le Meur. Coupling of ice-shelf melting and buttressing is a key process in ice-sheet dynamics. *Geophys Res Lett*, 37:L14501, 2010. ISSN 0094-8276. DOI 10.1029/2010GL043334.

S. Georgiou, A. Shepherd, M. McMillan, and P. Nienow. Determining the depth of supra-glacial lakes by their remotely sensed reflectance. *Ann Glaciol*, 50:95–100, 2009. ISSN 0260-3055. DOI 10.3189/172756409789624328.

R. M. Gladstone, A. J. Payne, and S. L. Cornford. Parameterising the grounding line in ice sheet models. *Cryosphere Discuss*, 4:1063–1105, 2010. ISSN 1994-0432. DOI 10.5194/tcd-4-1063-2010.

N. F. Glasser and M. C. Ghiglione. Structural, tectonic and glaciological controls on the evolution of fjord landscapes. *Geomorphology*, 105:291–302, 2009. ISSN 0169-555X. DOI 10.1016/j.geomorph.2008.10.007.

J. W. Glen. Experiments on the deformation of ice. *J Glaciol*, 2:111–114, 1952. ISSN 0022-1430.

J. W. Glen. The creep of polycrystalline ice. *Proc R Soc London A*, 228:519–538, 1955. ISSN 0080-4630.

S. Gordon, M. Sharp, B. Hubbard, C. Smart, B. Ketterling, and I. Willis. Seasonal reorganization of subglacial drainage inferred from measurements in boreholes. *Hydrol Process*, 12: 105–133, 1998. ISSN 0885-6087.

J. M. Gregory, P. Huybrechts, and S. C. B. Rape. Threatened loss of the Greenland ice-sheet. *Nature*, 428:616, 2004. ISSN 0028-0836. DOI 10.1038/428616a.

R. Greve. Application of a polythermal three-dimensional ice sheet model to the Greenland ice sheet: response to steady-state and transient climate scenarios. *J Climate*, 10:901–918, 1996. ISSN 0894-8755. DOI 10.1175/1520-0442(1997)010<0901:AOAPTD>2.0.CO;2.

R. Greve. On the response of the Greenland ice sheet to greenhouse climate change. *Climatic Change*, 46:289–303, 2000. ISSN 0165-0009. DOI 10.1023/A:1005647226590.

R. Greve and S. Otsu. The effect of the north-east ice stream on the Greenland ice sheet in changing climates. *Cryosphere Discuss*, 1:41–76, 2007. ISSN 1994-0432. DOI 10.5194/tcd-1-41-2007.

A. A. Griffith. The phenomena of rupture and flow in solids. *Philos T R Soc Lond*, A221: 163–198, 1921. ISSN 0264-3952.

D.V. Griffiths and I.M. Smith. *Numerical Methods for Engineers: A programming approach*. Blackwell Scientific Publications, 1991.

M. Hagdorn, I. Rutt, T. Payne, and F. Hebeler. *GLIMMER 1.0.0 Documentation*, 2007.

M. K. M. Hagdorn. *Reconstruction of the past and forecast of the future European and British ice sheets and associated sea-level change*. PhD thesis, The University of Edinburgh, 2003. URL `http://hdl.handle.net/1842/433`.

A. M. Hall and D. E. Sugden. Limited modification of mid-latitude landscapes by ice sheets: The case of northeast Scotland. *Earth Surf Processes Landf*, 12:531–542, 1987. ISSN 0197-9337. DOI 10.1002/esp.3290120510.

E. Hanna, P. Huybrechts, I. Janssens, J. Cappelen, K. Steffen, and A. Stephens. Runoff and mass balance of the Greenland ice sheet: 1958–2003. *J Geophys Res Atmos*, 110:D13108, 2005. ISSN 0148-0227. DOI 10.1029/2004JD005641.

P.C. Heigold, R.H. Gilkeson, K. Cartwright, and P.C. Reed. Aquifer transmissivity from surficial electrical methods. *Ground Water*, 17:338–345, 1979. ISSN 0017-467X. DOI 0.1111/j.1745-6584.1979.tb03326.x.

R. C. A. Hindmarsh. Time-scales and degrees of freedom operating in the evolution of continental ice-sheets. *Trans R Soc Edin*, 81:371–384, 1990. ISSN 0263-5933.

R. Hodgkins. Glacial hydrology in Svalbard, Norwegian High Arctic. *Quat Sci Rev*, 16: 957–973, 1997. ISSN 0277-3791. DOI 10.1016/S0277-3791(97)00032-2.

D. M. Holland, R. H. Thomas, B. de Young, M. H. Ribergaard, and B. Lyberth. Acceleration of Jakobshavn Isbrætriggered by warm subsurface ocean water. *Nat Geosci*, 1:659–664, 2008. ISSN 1752-0894. DOI 10.1038/ngeo316.

R. LeB. Hooke. Basal temperatures in polar ice sheets: a qualitative review. *Quat Res*, 7: 1–13, 1977. ISSN 0033-5894.

R. LeB. Hooke. Flow law for polycrystalline ice in glaciers: comparison of theoretical predictions, laboratory data, and field measurements. *Rev Geophys Space Phys*, 19: 664–672, 1981. ISSN 8755-1209. DOI 10.1029/RG019i004p00664.

R. LeB. Hooke. Englacial and subglacial hydrology — a qualitative review. *Arctic Alpine Res*, 21:221–233, 1989. ISSN 0004-0851.

Roger LeB Hooke. *Principles of Glacier Mechanics*. Cambridge University Press, 2005.

B. J. Hoskins and P. J. Valdes. On the existence of storm-tracks. *J Atmos Sci*, 47:1854–1864, 1990. ISSN 0022-4928. DOI 10.1175/1520-0469(1990)047<1854:OTEOST>2.0.CO;2.

I. M. Howat, I. Joughin, and T. A. Scambos. Rapid changes in ice discharge from Greenland outlet glaciers. *Science*, 315:1559–1561, 2007. ISSN 0036-8075. DOI 10.1126/science.1138478.

I. M. Howat, I. Joughin, M. Fahnestock, B. E. Smith, and T. A. Scambos. Synchronous retreat and acceleration of southeast Greenland outlet glaciers 2000–06: ice dynamics and coupling to climate. *J Glaciol*, 54:646–661, 2008. ISSN 0022-1430. DOI 10.3189/002214308786570908.

A. X. Hu, G. A. Meehl, W. M. Washington, and A. Dai. Response of the Atlantic thermohaline circulation to increased atmospheric CO_2 in a coupled model. *J Climate*, 17:4267–4279, 2004. ISSN 0894-8755. DOI 10.1175/JCLI3208.1.

B. Hubbard and P. Nienow. Alpine subglacial hydrology. *Quat Sci Rev*, 16:939–955, 1997. ISSN 0277-3791.

B. P. Hubbard, M. J. Sharp, I. C. Willis, M. K. Nielsen, and C. C. Smart. Borehole water-level variations and the structure of the subglacial hydrological system of Haut Glacier d'Arolla, Valais, Switzerland. *J Glaciol*, 41:572–583, 1995. ISSN 0022-1430.

T. Hughes. Thermal convection and the origin of ice streams. *J Glaciol*, 55:524–536, 2009. ISSN 0022-1430. DOI 10.3189/002214309788816722.

N. Hulton and M. Mineter. Modelling self-organization in ice streams. *Ann Glaciol*, 30: 127–136, 2000. ISSN 0260-3055. DOI 10.3189/172756400781820561.

N. R. J. Hulton and D. Sugden. Modelling mass balance on former maritime ice caps: a Patagonian example. *Ann Glaciol*, 21:304–310, 1995. ISSN 0260-3055.

N. R. J. Hulton and D. Sugden. Dynamics of mountain ice caps during glacial cycles: the case of Patagonia. *Ann Glaciol*, 24:81–89, 1997. ISSN 0260-3055.

K. Hutter. A mathematical-model of polythermal glaciers and ice sheets. *Geophys Astro Fluid*, 21:201–224, 1982. ISSN 0309-1929. DOI 10.1080/03091928208209013.

K. Hutter. *Theoretical glaciology: materials science of ice and the mechanics of glaciers and ice sheets*. Dordrecht, 1983.

P. Huybrechts. A three-dimensional time-dependent numerical model for polar ice sheets: Some basic testing with a stable and efficient finite difference schemes. Technical report, Geogr. Inst. Vrije Univ. Brussels, Belgium, 1986.

P. Huybrechts. Basal temperature conditions of the Greenland ice sheet during the glacial cycles. *Ann Glaciol*, 23:226–236, 1996. ISSN 0260-3055.

P. Huybrechts and J. de Wolde. The dynamic response of the Greenland and Antarctic ice sheets to multiple-century climatic warming. *J Climate*, 12:2169–2188, 1999. ISSN 0894-8755. DOI 10.1175/1520-0442(1999)012<2169:TDROTG>2.0.CO;2.

P. Huybrechts and T. Payne. The EISMINT benchmarks for testing ice-sheet models. *Ann Glaciol*, 23:1–12, 1996. ISSN 0260-3055.

P. Huybrechts, A. Letréguilly, and N. Reeh. The Greenland Ice Sheet and greenhouse warming. *Global Planet Change*, 3:399–412, 1991. ISSN 0921-8181. DOI 10.1016/0921-8181(91)90119-H.

P. Huybrechts, I. Janssens, C. Poncin, and T. Fichefet. The response of the Greenland ice sheet to climate changes in the 21st century by interactive coupling of an AOGCM with a thermomechanical ice-sheet model. *Ann Glaciol*, 35:409–415, 2002. ISSN 0260-3055. DOI 10.3189/172756402781816537.

P. Huybrechts, J. Gregory, I. Janssens, and M. Wild. Modelling Antarctic and Greenland volume changes during the 20th and 21st centuries forced by GCM time slice integrations. *Global Planet Change*, 42:83–105, 2004. ISSN 0921-8181. DOI doi:10.1016/j.gloplacha.2003.11.011.

A. Iken. The effect of the subglacial water pressure on the sliding velocity of a glacier in an idealized numerical model. *J Glaciol*, 27:407–421, 1981. ISSN 0022-1430.

A. Iken and M. Truffer. The relationship between subglacial water pressure and velocity of Findelengletscher, Switzerland, during its advance and retreat. *J Glaciol*, 43:328–338, 1997. ISSN 0022-1430.

V. Ivanovic, J. Deur, M. Kostelac, Z. Herold, M. Troulis, C. Miano, D. Hrovat, J. Asgari, D. Higgins, J. Blackford, and V. Koutsos. Experimental identification of dynamic tire friction potential on ice surfaces. *Vehicle Syst Dyn*, 44:93–103, 2006. ISSN 0042-3114. DOI 10.1080/00423110600869230.

N. R. Iverson, D. Cohen, T. S. Hooyer, U. H. Fischer, M. Jackson, P. L. Moore, G. Lappegard, and J. Kohler. Effects of basal debris on glacier flow. *Science*, 301:81–84, 2003. ISSN 0036-8075. DOI 10.1126/science.1083086.

S. S. R. Jamieson. *Modelling landscape evolution under ice sheets*. PhD thesis, University of Edinburgh, 2008.

S. S. R. Jamieson, N. R. J. Hulton, and M. Hagdorn. Modelling landscape evolution under ice sheets. *Geomorphology*, 97:91–108, 2008. ISSN 0169-555X.

S. S. R. Jamieson, D. E. Sugden, and N. R. J. Hulton. The evolution of the subglacial landscape of Antarctica. *Earth Planet Sci Lett*, 293:1–27, 2010. ISSN 0012-821X. DOI 10.1016/j.epsl.2010.02.012.

D. Jenssen. A three-dimensional polar ice-sheet model. *J Glaciol*, 18:373–389, 1977. ISSN 0022-1430.

S. J. Johnsen, D. Dahl-Jensenwilli Dansgaard, and N. Gundestrup. Greenland palaeotemperatures derived from GRIP bore hole temperature and ice core isotope profiles. *Tellus B*, 47:624–629, 2002. ISSN 0280-6509. DOI 10.1034/j.1600-0889.47.issue5.9.x.

J. Johnson and J. L. Fastook. Northern Hemisphere glaciation and its sensitivity to basal melt water. *Quaternary International*, 95–96:65–74, 2002. ISSN 1040-6182. DOI 10.1016/S1040-6182(02)00028-9.

J. V. Johnson. *A basal water model for ice sheets*. PhD thesis, The University of Maine, 2002.

I. Joughin, S. Tulaczyk, M. Fahnestock, and R. Kwok. A mini-surge on the Ryder Glacier, Greenland, observed by satellite radar interferometry. *Science*, 274:228–230, 1996. ISSN 1095-9203. DOI 10.1126/science.274.5285.228.

I. Joughin, W. Abdalati, and M. Fahnestock. Large fluctuations in speed on Greenland's Jakobshavn Isbræglacier. *Nature*, 432:608–610, 2004a. ISSN 0028-0836. DOI 10.1038/nature03130.

I. Joughin, S. Tulaczyk, D. R. MacAyeal, and H. Engelhardt. Melting and freezing beneath the Ross ice streams, Antarctica. *J Glaciol*, 50:96–108, 2004b. ISSN 0022-1430. DOI 10.3189/172756504781830295.

I. Joughin, S. B. Das, M. A. King, B. E. Smith, I. M. Howat, and T. Moon. Seasonal speedup along the western flank of the Greenland ice sheet. *Science*, 320:781–783, 2008. ISSN 0036-8075. DOI 10.1126/science.1153288.

M. M. Junge, R. Blender, K. Fraedrich, V. Gayler, U. Luksch, and F. Lunkeit. A world without Greenland: impacts on the northern hemisphere winter circulation in low- and high-resolution models. *Climate Dyn*, 24:297–307, 2005. ISSN 1432-0894. DOI 10.1007/s00382-004-0501-2.

M. Kageyama, P. J. Valdes, G. Ramstein, C. Hewit, and U. Wyputta. Northern hemisphere storm tracks in present day and last glacial maximum climate simulations: A comparison of the European PMIP models. *J Climate*, 12:742–760, 1999. ISSN 0894-8755. DOI 10.1175/1520-0442(1999)012<0742:NHSTIP>2.0.CO;2.

B. Kamb. Glacier surge mechanism based on linked cavity configuration of the basal water conduit system. *J Geophys Res Solid Earth*, 92:9083–9100, 1987. ISSN 0148-0227. DOI 10.1029/JB092iB09p09083.

B. Kamb, C. F. Raymond, W. D. Harrision, H. Engelhardt, K. A. Echelmeyer, N. Humphrey, M. M. Brugman, and T. Pfeffer. Glacier surge mechanism: 1982–1983 surge of Variegated glacier, Alaska. *Science*, 227:469–479, 1985. ISSN 0036-8075. DOI 10.1126/science.227.4686.469.

A.-M. Kietzig, S. G. Hatzikiriakos, and P. Englezos. Ice friction: the effect of thermal conductivity. *J Glaciol*, 56:473–479, 2010. ISSN 0022-1430.

W. Krabill, E. Frederick, S. Manizade, C. Martin, J. Sonntag, R. Swift, R. Thomas, W. Wright, and J. Yungel. Rapid thinning of parts of the southern Greenland ice sheet. *Science*, 283: 1522–1524, 1999. ISSN 0036-8075. DOI 10.1126/science.283.5407.1522.

J. E. Kristjansson and H. McInnes. The impact of Greenland on cyclone evolution in the North Atlantic. *Quat J Roy Meteor Soc*, 125:2819–2834, 1999. ISSN 0035-9009. DOI 10.1002/qj.49712556003.

W. H. K. Lee. On the global variations of terrestrial heat flow. *Phys Earth Planet Inter*, 2: 332–341, 1969. ISSN 0031-9201. DOI 10.1016/0031-9201(69)90026-0.

A. Letréguilly, N. Reeh, and P. Huybrechts. The Greenland ice sheet through the last glacial-interglacial cycle. *Global Planet Change*, 4:385–394, 1991. ISSN 0921-8181. DOI 0.1016/0921-8181(91)90004-G.

S. M. Lewis and L. C. Smith. Hydrologic drainage of the Greenland Ice Sheet. *Hydrol Process*, 23:2004–2011, 2009. ISSN 1099-1085. DOI 10.1002/hyp.7343.

H. Liang, J. M. Martin, and T. L. Mogne. Experimental investigation of friction on low-temperature ice. *Acta Mater*, 51:2639–2646, 2003. ISSN 1359-6454. DOI 10.1016/S1359-6454(03)00061-2.

D. R. Lide. *CRC handbook of chemistry and physics: a ready-reference book of chemical and physical data*. CRC Press, 85$^{\text{th}}$ edition, 2004.

C. S. Lingle and T. J. Brown. A subglacial aquifer bed model and water pressure dependent basal sliding relationship for a West Antarctic Ice Stream. In C. J. van der Veen and J. Oerlemans, editors, *Dynamics of the West Antarctic Ice Sheet*. D. Reidel Publishing Company, 1987.

W. Lipscomb, E. Bueler, D. Holland, J. Johnson, and S. Price. Building a next-generation Community Ice Sheet Model, 2008. URL `http://www.clivar.org/organization/southern/CISM_Workshop_Report.pdf`. Report on a workshop held at Los Alamos National Laboratory, 18–20 August 2008.

M.-F. Loutre. Greenland ice sheet over the next 5000 years. *Geophys Res Lett*, 22:783–786, 1995. ISSN 0094-8276. DOI 10.1029/95GL00362.

A. Luckman and T. Murray. Seasonal variation in velocity before retreat of Jakobshavn Isbræ, Greenland. *Geophys Res Lett*, 32:L08501, 2005. ISSN 0094-8276. DOI 10.1029/2005GL022519.

M. Lüthje, L. T. Pedersen, N. Reeh, and W. Greuell. Modelling the evolution of supraglacial lakes on the West Greenland ice-sheet margin. *J Glaciol*, 52:608–618, 2006. ISSN 0022-1430. DOI 10.3189/172756506781828386.

M. B. Lythe, D. G. Vaughan, and the BEDMAP Consortium. *BEDMAP — Bed topography of the Antarctic. 1:10,000,000 scale map.* British Antarctic Survey, 2000. URL `http://www.antarctica.ac.uk/bas_research/data/access/bedmap/`.

D. R. MacAyeal, C. L. Hulbe, P. Huybrechts, V. Rommelaere, J. Determann, and C. Ritz. An ice-shelf model test based on Ross Ice Shelf, Antarctica. *Ann Glaciol*, 23:46–51, 1996. ISSN 0260-3055.

D. Mair, P. Nienow, M. J. Sharp, T. Wohlleben, and I. Willis. Influence of subglacial drainage system evolution on glacier surface motion: Haut Glacier d'Arolla, Switzerland. *J Geophys Res Solid Earth*, 107:2175, 2002. ISSN 0148-0227. DOI 10.1029/2001JB000514.

D. Mair, I. Willis, U. H. Fischer, B. Hubbard, P. Nienow, and A. Hubbard. Hydrological controls on patterns of surface, internal and basal motion during three "spring events": Haut Glacier d'Arolla, Switzerland. *J Glaciol*, 49:555–567, 2003. ISSN 0022-1430. DOI 10.3189/172756503781830467.

B. A. Marmo, J. R. Blackford, and C. E. Jeffree. Ice friction, wear features and their dependence on sliding velocity and temperature. *J Glaciol*, 51:391–398, 2005. ISSN 0022-1430. DOI 10.3189/172756505781829304.

S. J. Marshall. Recent advances in understanding ice sheet dynamics. *Earth Planet Sci Lett*, 240:191–204, 2005. ISSN 0012-821X. DOI doi:10.1016/j.epsl.2005.08.016.

S. J. Marshall, H. Björnsson, G. E. Flowers, and G. K. C. Clarke. Simulation of Vatnajökull ice cap dynamics. *J Geophys Res Earth Surf*, 110:F03009, 2005. ISSN 0148-0227. DOI 10.1029/2004JF000262.

M. McMillan, P. Nienow, A. Shepherd, T. Benham, and A. Sole. Seasonal evolution of supra-glacial lakes on the Greenland ice sheet. *Earth Planet Sci Lett*, 262:484–492, 2007. ISSN 0012-821X. DOI 10.1016/j.epsl.2007.08.002.

M. F. Meier and A. Post. Fast tidewater glaciers. *J Geophys Res*, 92:9051–9058, 1987. ISSN 0148-0227. DOI 10.1029/JB092iB09p09051.

U. Mikolajewicz, M. Vizcaíno, J. Jungclaus, and G. Schurgers. Effect of ice sheet interactions in anthropogenic climate change simulations. *J Geophys Res*, 34:L18706, 2007. ISSN 0148-0227. DOI 10.1029/2007GL031173.

A. Mills. The coefficient of friction, particularly of ice. *Phys Edu*, 43:392–395, 2008. ISSN 0031-9120. DOI 10.1088/0031-9120/43/4/006.

L. W. Morland. Glacier sliding down an inclined wavy bed with friction. *J Glaciol*, 17: 463–477, 1976. ISSN 0022-1430.

T. L. Mote. Greenland surface melt trends 1973–2007: evidence of a large increase in 2007. *Geophys Res Lett*, 34:L22507, 2007. ISSN 0094-8276. DOI 10.1029/2007GL031976.

L. Mu, D. X. Wu, and X. Chen. Changes in Atlantic thermohaline circulation under different atmospheric CO_2 scenarios in a climate model. *J China Univ Geosci*, 17:326–331, 2006. ISSN 1002-0705. DOI 10.1016/S1002-0705(07)60006-5.

F. M. Nick, A. Vieli, I. M. Howat, and I. Joughin. Large-scale changes in Greenland outlet glacier dynamics triggered at the terminus. *Nat Geosci*, 2:110–114, 2009. ISSN 1752-0894. DOI 10.1038/ngeo394.

P. Nienow and B. Hubbard. Surface and englacial drainage of glaciers and ice sheets. In M. G. Anderson, editor, *Encyclopedia of Hydrological Sciences Part 14. Snow and Glacier Hydrology*, chapter 166, pages 2575–2586. John Wiley and Sons, 2005. DOI 10.1002/0470848944.hsa172.

P. Nienow, M. Sharp, and I. Willis. Seasonal changes in the morphology of the subglacial drainage system, Haut Glacier d'Arolla, Switzerland. *Earth Surf Processes Landf*, 23: 825–843, 1998. ISSN 0197-9337. DOI 10.1002/(SICI)1096-9837(199809)23:9<825::AID-ESP893>3.0.CO;2-2.

P. W. Nienow, A. L. Hubbard, B. P. Hubbard, D. M. Chandler, D. W. F. Mair, M. J. Sharp, and I. C. Willis. Hydrological controls on diurnal ice flow variability in valley glaciers. *J Geophys Res Earth Surf*, 110:F04002, 2005. ISSN 0148-0227. DOI 10.1029/2003JF000112.

NOAA. U.S. Department of Commerce, National Oceanic and Atmospheric Administration, National Geophysical Data Center. 2-minute Gridded Global Relief Data (ETOPO2v2). `http://www.ngdc.noaa.gov/mgg/fliers/06mgg01.html`, 2006.

D. Notz. The future of ice sheets and sea ice: Between reversible retreat and unstoppable loss. *P Natl Acad Sci USA*, 106:20590–20595, 2009. ISSN 0027-8424. DOI 10.1073/pnas.0902356106.

J. F. Nye. The flow law of ice from measurements in glacier tunnels, laboratory experiments and the Jungfraufirn borehole experiment. *Proc R Soc London A*, 219:477–489, 1953. ISSN 0080-4630.

J. F. Nye. The distribution of stress and velocity in glaciers and ice-sheets. *Proc R Soc London A*, 239:113–133, 1957. ISSN 0080-4630.

J. F. Nye. Water flow in glaciers: jokulhlaups, tunnels and veins. *J Glaciol*, 17:181–207, 1976. ISSN 0022-1430.

G. K. A. Oswald and S. P. Gogineni. Recovery of subglacial water extent from Greenland radar survey data. *J Glaciol*, 54:94–106, 2008. ISSN 0022-1430. DOI 10.3189/002214308784409107.

B R. Parizek and R. B. Alley. Implications of increased Greenland surface melt under global-warming scenarios: ice-sheet simulations. *Quat Sci Rev*, 23:1013–1027, 2004. ISSN 0277-3791. DOI 10.1016/j.quascirev.2003.12.024.

V. Parry, P. Nienow, D. Mair, J. Scott, B. Hubbard, K. Steffen, and D. Wingham. Investigations of meltwater refreezing and density variations in the snowpack and firn within the percolation zone of the Greenland ice sheet. *Ann Glaciol*, 46:61–68, 2007. ISSN 0260-3055. DOI 10.3189/172756407782871332.

W. S. B. Paterson. *The Physics of Glaciers*. Pergamon, 3rd edition, 1994. ISBN 0-7506-4742-6.

F. Pattyn. A new three-dimensional higher-order thermomechanical ice sheet model: Basic sensitivity, ice stream development, and ice flow across subglacial lakes. *J Geophys Res*, 108:2382, 2003. ISSN 0148-0227. DOI 10.1029/2002JB002329.

F. Pattyn. GRANTISM: An Excel™ model for Greenland and Antarctic ice-sheet response to climate changes. *Comput Geosci*, 32:316–325, 2006. ISSN 0098-3004. DOI doi:10.1016/j.cageo.2005.06.020.

F. Pattyn, L. Perichon, A. Aschwanden, B. Breuer, B. de Smedt, O. Gagliardini, G. H. Gudmundsson, R. C. A. Hindmarsh, A. Hubbard, J. V. Johnson, T. Kleiner, Y. Konovalov, C. Martin, A. J. Payne, D. Pollard, S. Price, M. Rückamp, F. Saito, O. Souček, S. Sugiyama, and T. Zwinger. Benchmark experiments for higher-order and full-Stokes ice sheet models (ISMIPHOM). *Cryosphere*, 2:95–108, 2008. ISSN 1994-0432. DOI 10.5194/tc-2-95-2008.

A. J. Payne. Limit cycles in the basal thermal regime of ice sheets. *J Geophys Res Solid Earth*, 100:4249–4263, 1995. ISSN 0148-0227. DOI 10.1029/94JB02778.

A. J. Payne and P. W. Dongelmans. Self-organisation in the flow of ice sheets. *J Geophys Res Solid Earth*, 102:12,219–12,233, 1997. ISSN 0148-0227.

A. J. Payne, P. Huybrechts, A. Abe-Ouchi, R. Calov, J. L. Fastook, R. Greve, S. J. Marshall, I. Marsiat, C. Ritz, L. Tarasov, and M. P. A. Thomassen. Results from the EISMINT model intercomparison: the effects of thermomechanical coupling. *J Glaciol*, 46:227–238, 2000. ISSN 0022-1430.

J. J. Payne and D. J. Baldwin. Analysis of ice-flow instabilities identified in the EISMINT intercomparison exercise. *Ann Glaciol*, 30:204–210, 2000. ISSN 0260-3055. DOI 10.3189/172756400781820534.

G. N. Petersen, J. E. Kristjansoon, and H. Olafsson. Numerical simulations of Greenland's impact on the northern hemisphere winter circulation. *Tellus A*, 56:102–111, 2004. ISSN 0280-6495. DOI 10.1111/j.1600-0870.2004.00047.x.

J. A. Piotrowski and S. Tulaczyk. Subglacial conditions under the last ice sheet in northwest Germany: ice-bed separation and enhanced basal sliding? *Quat Sci Rev*, 18(6):737–751, 1999. ISSN 0277-3791. DOI 10.1016/S0277-3791(98)00042-0.

A. J. Pitman and R. J. Stouffer. Abrupt change in climate and climate models. *Hydrol Earth Syst Sc*, 10:903–912, 2006. ISSN 1027-5606. DOI 10.5194/hess-10-903-2006.

H. N. Pollack, S. J. Hurter, and J. R. Johnson. Heat flow from the Earth's interior: analysis of the global data set. *Rev Geophys*, 31:267–280, 1993. ISSN 8755-1209. DOI 10.1029/93RG01249.

D. Pollard and R. M. DeConto. Modelling West Antarctic ice sheet growth and collapse through the past five million years. *Nature*, 458:329–332, 2009. ISSN 0028-0836. DOI 10.1038/nature07809.

William H. Press, Brian P. Flannery, Saul A. Teukolsky, and William T. Vetterling. *Numerical Recipes in Fortran 77: The Art of Scientific Computing*. Cambridge University Press, 1992.

S. F. Price, A. J. Payne, G. A. Catania, and T. A. Neumann. Seasonal acceleration of inland ice via longitudinal coupling to marginal ice. *J Glaciol*, 54:213–220, 2008. ISSN 0022-1430. DOI 10.3189/002214308784886117.

H. Pritchard, T. Murray, A. Luckman, T. Strozzi, and S. Barr. Glacier surge dynamics of Sortebræ, east Greenland, from synthetic aperture radar feature tracking. *J Geophys Res Earth Surf*, 110:F03005, 2005. ISSN 0148-0227. DOI 10.1029/2004JF000233.

H. D. Pritchard, R. J. Arthern, D. G. Vaughan, and L. A. Edwards. Extensive dynamic thinning on the margins of the Greenland and Antarctic ice sheets. *Nature*, 461:971–975, 2009. ISSN 0028-0836. DOI 10.1038/nature08471.

S. Rahmstorf, M. Crucifix, A. Ganopolski, H. Goosse, I. Kamenkovich, R. Knutti, G. Lohmann, R. Marsh, L. A. Mysak, Z. M. Wang, and A. J. Weaver. Thermohaline circulation hysteresis: A model intercomparison. *Geophys Res Lett*, 32:L23605, 2005. ISSN 0094-8276. DOI 10.1029/2005GL023655.

C. F. Raymond. Deformation in the vicinity of ice divides. *J Glaciol*, 29:357–373, 1983. ISSN 0022-1430.

N. Reeh. A flow-line model for calculating the surface profile and the velocity, strain-rate, and stress-fields in an ice-sheet. *J Glaciol*, 34:46–54, 1988. ISSN 0022-1430.

N. Reeh, H. H. Thomsen, A. K. Higgins, and A.. Weidick. Sea ice and the stability of north and northeast Greenland floating glaciers. *Ann Glaciol*, 33:474–480, 2001. ISSN 0260-3055. DOI 10.3189/172756401781818554.

J. K. Ridley, P. Huybrechts, J. M. Gregory, and J. A. Lowe. Elimination of the Greenland ice sheet in a high CO_2 climate. *J Climate*, 18:3409–3427, 2005. ISSN 0894-8755. DOI 10.1175/JCLI3482.1.

E. Rignot and P. Kanagaratnam. Changes in the velocity structure of the Greenland ice sheet. *Science*, 311:986–990, 2006. ISSN 0036-8075. DOI 10.1126/science.1121381.

E. Rignot and R. H. Thomas. Mass balance of polar ice sheets. *Science*, 297:1502–1506, 2002. ISSN 0036-8075. DOI 10.1126/science.1073888.

(Coordinator) C. Ritz. EISMINT intercomparison experiment: comparison of existing Greenland models. http://homepages.vub.ac.be/~phuybrec/eismint/green-descr.pdf, February 1997.

R. Rosenberg. Why is ice slippery. *Phys Today*, 58:50–55, 2005. ISSN 0031-9228.

H. Röthlisberger. Water pressure in intra- and subglacial channels. *J Glaciol*, 11:177–203, 1972. ISSN 0022-1430.

H. Röthlisberger and H. Lang. *Glacial Hydrology*, chapter 10, pages 207–284. John Wiley & Sons Ltd, 1987.

I. C. Rutt, M. Hagdorn, N. R. J. Hulton, and A. J. Payne. The Glimmer community ice sheet model. *J Geophys Res Earth Surf*, 114:F02004, 2009. ISSN 0148-0227. DOI 10.1029/2008JF001015.

C. Schoof. Ice sheet grounding line dynamics: Steady states, stability, and hysteresis. *J Geophys Res Earth Surf*, 112:F03S28, 2007. ISSN 0148-0227. DOI 10.1029/2006JF000664.

J. Schweizer and A. Iken. The role of bed separation and friction in sliding over an undeformable bed. *J Glaciol*, 38:77–92, 1992. ISSN 0022-1430.

A. Shepherd and D. Wingham. Recent sea-level contributions of the Antarctic and Greenland ice sheets. *Science*, 315:1529–1532, 2007. ISSN 0036-8075. DOI 10.1126/science.1136776.

A. Shepherd, A. Hubbard, P. Nienow, M. King, M. McMillan, and I. Joughin. Greenland ice sheet motion coupled with daily melting in late summer. *Geophys Res Lett*, 36:L01501, 2009. ISSN 0094-8276. DOI 10.1029/2008GL035758.

E. M. Shoemaker. Subglacial hydrolgoy for an ice sheet resting on a deformable aquifer. *J Glaciol*, 32:20–30, 1986. ISSN 0022-1430.

R. L. Shreve. Movement of water in glaciers. *J Glaciol*, 11:205–214, 1972. ISSN 0022-1430.

D. Slotfeldt-Ellingsen and L. Torgersen. Water in ice: influence on friction. *J Phys D: Appl Phys*, 16:1715–1719, 1983. ISSN 0022-3727. DOI 10.1088/0022-3727/16/9/017.

A. M. Smith. Basal conditions on Rutford Ice Stream, West Antarctica, from seismic observations. *J Geophys Res Solid Earth*, 102:543–552, 1997. ISSN 0148-0227. DOI 10.1029/96JB02933.

W. A. Sneed and G. S. Hamilton. Evolution of melt pond volume on the surface of the Greenland ice sheet. *Geophys Res Lett*, 34:L03501, 2007. ISSN 0094-8276. DOI 10.1029/2006GL028697.

A. Sole, T. Payne, J. Bamber, P. Nienow, and W. Krabill. Testing hypotheses of the cause of peripheral thinning of the Greenland ice sheet: is land-terminating ice thinning at anomolously high rates? *Cryosphere*, 2:205–218, 2008. ISSN 1994-0432. DOI 10.5194/tc-2-205-2008.

S. Solomon, D. Qin, M. Manning, Z. Chen, M. Marquis, K. B. Avery, M. Tignor, and H. L. Miller, editors. *Climate Change 2007 — The Physical Science Basis: Contribution of Working Group I to the Fourth Assessment Reoprt of the IPCC*. Cambridge University Press, 2007.

P. H. Stauffer. Flux flummoxed: a proposal for consistent usage. *Ground Water*, 44:125–128, 2006. ISSN 0017-467X. DOI 10.1111/j.1745-6584.2006.00197.x.

K. Steffen and J. Box. Surface climatology of the Greenland ice sheet: Greenland Climate Network 1995-1999. *J Geophys Res Atmos*, 106:33,951–33,964, 2001. ISSN 0148-0227.

K. Steffen, S. V. Nghiem, R. Huff, and G. Neumann. The melt anomaly of 2002 on the Greenland ice sheet from active and passive microwave satellite observations. *Geophys Res Lett*, 31:L20402, 2004. ISSN 0094-8276. DOI 10.1029/2004GL020444.

T. F. Stocker. Abrupt climate changes: from the past to the future — a review. *Int J Earth Sci*, 68:365–374, 1999. ISSN 1437-3254. DOI 10.1007/s005310050271.

R. J. Stouffer, J. Yin, J. M. Gregory, K. W. Dixon, M. J. Spelman, W. Hurlin, A. J. Weaver, M. Eby, G. M. Flato, H. Hasumi, A. Hu, J. H. Jungclaus, I. V. Kamenkovich, A. Levermann, M. Montoya, S. Murakami, S. Nawrath, A. Oka, W. R. Peltier, D. Y. Robitaille, A. Sokolov, G. Vettoretti, and S. L. Weber. Investigating the causes of the response of the thermohaline circulation to past and future climate changes. *J Climate*, 19:1365–1387, 2006. ISSN 0894-8755. DOI 10.1175/JCLI3689.1.

D. E. Sugden, D. R. Marchant, and G. H. Denton. The case for a stable East Antarctic ice sheet: the background. *Geogr Ann*, 75A:151–154, 1993. ISSN 0435-3676.

A. V. Sundal, A. Shepherd, P. Nienow, E. Hanna, S. Palmer, and P. Huybrechts. Evolution of supra-glacial lakes across the Greenland ice sheet. *Remote Sens Environ*, 113:2164–2171, 2009. ISSN 0034-4257.

D. A. Swift, P. W. Nienow, T. B. Hoey, and D. W. F. Mair. Seasonal evolution of runoff from Haut Glacier d'Arolla, Switzerland and implications for glacial geomorphic processes. *J Hydrol*, 309:133–148, 2005. ISSN 0022-1694.

D. A. Swift, C. Persano, F. M. Stuart, K. Gallagher, and A. Whithamd. A reassessment of the role of ice sheet glaciation in the long-term evolution of the East Greenland fjord region. *Geomorphology*, 97:109–125, 2008. ISSN 0169-555X. DOI 10.1016/j.geomorph.2007.02.048.

M. Tedesco, M. Serreze, and X. Fettweis. Diagnosing the extreme surface melt event over southwestern Greenland in 2007. *Cryosphere*, 2:159–166, 2008. ISSN 1994-0432. DOI 10.5194/tc-2-159-2008.

R. Thomas, E. Frederick, W. Krabill, S. Manizade, and C. Martin. Recent changes on Greenland outlet glaciers. *J Glaciol*, 55:147–162, 2009. ISSN 0022-1430. DOI 10.3189/002214309788608958.

D. J. R. Thornalley, I. N. McCave, and H. Elderfield. Freshwater input and abrupt deglacial climate change in the North Atlantic. *Paleoceanography*, 25:PA1201, 2010. ISSN 0883-8305. DOI 10.1029/2009PA001772.

T. Toniazzo, J. M. Gregory, and P. Huybrechts. Climatic impact of a Greenland deglaciation and its possible irreversibility. *J Climate*, 17:21–33, 2004. ISSN 0894-8755. DOI 10.1175/1520-0442(2004)017<0021:CIOAGD>2.0.CO;2.

M. Truffer, W. D. Harrison, and R. S. March. Record negative glacier balances and low velocities during the 2004 heatwave in Alaska, USA: implications for the interpretation of observations by Zwally and others in Greenland (Correspondence). *J Glaciol*, 51:663–664, 2005. ISSN 0022-1430. DOI 10.3189/172756505781829016.

D. L. Turcotte and G. Schubert. *Geodynamics*. Cambridge University Press, 2002.

R. S. W. Van de Wal, W. Boot, M. R. van den Broeke, and C. J. P. P. Smeets. Large and rapid melt-induced velocity changes in the ablation zone of the Greenland ice sheet. *Science*, 321:111–113, 2008. ISSN 0036-8075. DOI 10.1126/science.1158540.

C. J. Van der Veen. Fracture mechanics approach to penetration of surface crevasses on glaciers. *Cold Reg Sci Technol*, 27:31–47, 1998. ISSN 0165-232X. DOI 10.1016/S0165-232X(97)00022-0.

C. J. Van der Veen. *Fundamentals of Glacier Dynamics*. A. A. Balkema, 1999. ISBN 90-5410-470-8.

C. J. Van der Veen. Calving glaciers. *Prog Phys Geog*, 26:96–122, 2002. ISSN 0309-1333. DOI 10.1191/0309133302pp327ra.

C. J. Van der Veen. Fracture propagation as means of rapidly transferring surface meltwater to the base of glaciers. *Geophys Res Lett*, 34:L01501, 2007. ISSN 0094-8276. DOI 10.1029/2006GL028385.

C. J. Van der Veen and J. Oerlemans. *Ice Sheets and Climate*. Springer, 1984. ISBN 90-277-1709-5.

C. J. Van der Veen and I. M. Whillans. Flow laws for glacier ice: comparison of numerical predictions and field measurements. *J Glaciol*, 36:324–339, 1990. ISSN 0022-1430.

C. J. Van der Veen, T. Leftwich, R. von Frese, B. M. Csatho, and J. Li. Subglacial topography and geothermal heat flux: potential interactions with drainage of the Greenland ice sheet. *Geophys Res Lett*, 34:L12501, 2007. ISSN 0094-8276. DOI 10.1029/2007GL030046.

I. Velicogna. Increasing rates of ice mass loss from the Greenland and Antarctic ice sheets revealed by GRACE. *Geophys Res Lett*, 36:L19503, 2009. ISSN 0094-8276. DOI 10.1029/2009GL040222.

A. Vieli and A. J. Payne. Assessing the ability of numerical ice sheet models to simulate grounding line migration. *J Geophys Res Earth Surf*, 110:F01003, 2005. ISSN 0148-0227. DOI 10.1029/2004JF000202.

E. D. Waddington. Geothermal heat flux beneath ice sheets. In E. D. Waddington and J. S. Walder, editors, *The Physical Basis of Ice Sheet Modelling*, pages 217–226. International Association of Hydrological Sciences, 1987.

R. T. Walker and D. M. Holland. A two-dimensional coupled model for ice shelfocean interaction. *Ocean Modelling*, 17:123–139, 2007. ISSN 1463-5003. DOI 10.1016/j.ocemod.2007.01.001.

J. Weertman. Comparison between measured and theoretical temperature profiles of the Camp Century, Greenland, borehole. *J Geophys Res*, 73:2691–2700, 1968. ISSN 0148-0227. DOI 10.1029/JB073i008p02691.

J. Weertman. Can a water-filled crevasse reach the bottom surface of a glacier? *Int Assoc Hydrol Sci*, 95:139–145, 1973. ISSN 0262-6667.

J. Weertman. Depth of water-filled crevasses that are closely spaced (Correspondence). *J Glaciol*, 13:545, 1974. ISSN 0022-1430.

J. Weertman. The unsolved general glacier sliding problem. *J Glaciol*, 23:97–115, 1979. ISSN 0022-1430.

J. Weertman and G. E. Birchfield. Basal water film, basal water pressure, and velocity of traveling waves on glaciers. *J Glaciol*, 29:20–26, 1983. ISSN 0022-1430.

J. G. Dash.and J. S. Wettlaufer. The physics of premelted ice and its geophysical consequences. *Rev Mod Phys*, 78:695–741, 2006. ISSN 0034-6861. DOI 10.1103/RevModPhys.78.695.

D. P. Winebrenner, B. E. Smith, G. A. Catania, H. B. Conway, and C. F. Raymond. Radio-frequency attenuation beneath Siple Dome, West Antarctica, from wide-angle and profiling radar observations. *Ann Glaciol*, 37:226–232, 2003. ISSN 0260-3055. DOI 10.3189/172756403781815483.

Wolfram Research, Inc. *Mathematica Edition: Version 7.0*. Wolfram Research, Inc., 2008.

H. J. Zwally, W. Abdalati, T. Herring, K. Larson, J. Saba, and K. Steffen. Surface melt-induced acceleration of Greenland ice-sheet flow. *Science*, 297:218–222, 2002. ISSN 0036-8075. DOI 10.1126/science.1072708.